# VIBRATION ASSISTED DRILLING OF CARBON FIBER REINFORCED POLYMER AND TITANIUM ALLOY FOR AEROSPACE APPLICATION

# Vibration Assisted Drilling of Carbon Fiber Reinforced Polymer and Titanium Alloy for Aerospace Application

By

Ramy Hussein, B.Sc., M.Sc.

A Thesis

Submitted to the School of Graduate Studies in Partial Fulfillment of the Requirements for the Degree Doctor of Philosophy

McMaster University

DOCTOR OF PHILOSOPHY (2019) McMaster University

(Mechanical Engineering) Hamilton, Ontario

| | |
|---|---|
| TITLE: | Vibration Assisted Drilling of Carbon Fiber Reinforced Polymer and Titanium Alloy for Aerospace Application. |
| AUTHOR: | Ramy Hussein |
| | B.Sc. in Mechanical Engineering (Military Technical College) |
| | M.Sc. in Mechanical Engineering (Military Technical College) |
| SUPERVISOR: | Dr. M. A. Elbestawi |
| NUMBER OF PAGES: | 256 |

# Preface

This manuscript is the integrated article thesis, known as a sandwich thesis, of **Ramy Hussein**, the sole author. The author uses **Ramy Hussein** as his formal name in publications. The manuscript consists of eight chapters and presents the experimental and analytical work performed by the author at McMaster University from 2016 to 2019. The author received his B.Sc. in Mechanical Engineering from the Military Technical College, Cairo, Egypt in 2007. He obtained his M.Sc. from the same college in 2014.

The thesis contributes to advanced manufacturing of two selected aerospace materials: CFRP, and Ti-6Al-4V using the vibration assisted dilling technique. The comprehensive experimental investigation was concerned with the drilling of each material separately as well as the stacks technique of CFRP/ Ti-6Al-4V. It is a compilation of six peer-reviewed journal articles, written in accordance with the regulation stipulated by the School of Graduate Studies at McMaster University. All experimental procedures and analyses have been done by the sole author. Advice, guidance, and revision have been provided by the academic supervisor, Dr. M. A. Elbestawi.

Chapter 1 provides an introduction, motivation, and research objectives; Chapters 2-7 are reprinted from six journal papers, and Chapter 8 presents conclusions and closing remarks.

I *declare* that this thesis has been composed solely by myself and that no part of this thesis has been submitted for a higher degree at any other institution.

Ramy Hussein

June 2019

# Abstract

The physical and mechanical characteristics of carbon fiber reinforced polymers (CFRP) and Ti6Al4V make them widely used in the aerospace industry. The hybrid structure of CFRP/ Ti6Al4V material has been used in the new generation of aircraft manufacturing. The drilling process of these materials is often associated with unfavorable machining defects such as delamination, burr formation, reduced surface integrity, and tensile residual stresses. These machining defects are attributed to high thermal load, continuous chip morphology, and poor chips evacuation efficiency. Vibration-assisted drilling (VAD) uses an intermittent cutting process to control the uncut chip thickness and chip morphology. VAD has potential advantages include low thermal load, high chips evacuation effectiveness, and longer tool life.

This thesis presents an experimental investigation into the effect of VAD machining parameters on the cutting energy, CFRP delamination, surface integrity, geometrical geometry, Ti6Al4V burr formation, induced residual stresses, and tool wear during the drilling process of CFRP, Ti6Al4V, and CFRP/Ti6Al4V stacked materials. Moreover, a kinematics model is developed to link the observed results to the independent machining parameters (i.e., cutting speed, feed rate, modulation amplitude, and modulation frequency). The experimental work covers a wide range of machining parameters using four levels of frequencies (83.3, 125, 1500, and 2150 Hz).

The VAD results show up to 56 % reduction in the cutting temperature with a significant enhancement in the CFRP entry and exit delamination, geometrical accuracy, surface integrity, and burr formation. The use of VAD also generates compressive stresses, hence improving the part fatigue life.

# Acknowledgments

I am very grateful to my supervisor, Dr. Mo Elbestawi, for his continuous support. I would like to thank him for being always available to provide answers, encouragement, research guidance, and discussions throughout this critical time. Nothing can describe how it feels to know that I have him as a mentor and adviser. Thanks for being so understanding as I worked through critical time requirements. Your excessive support, teaching, and encouragement are appreciated more than you know.

I would like to express my sincere gratitude to Dr. Helmi Attia and Dr. Ahmad Sadek for invaluable scientific support and guidance. Also, I want to thank the National Research Council Canada (NRC), Aerospace Manufacturing Technologies Centre (AMTC), for hosting all the experimental study in the Aerospace Advanced Material Removal Processes lab. Thanks for all the provided facilities and assistance.

I would also like to thank Dr. Philip Koshy for all what I learned from his valuable " Manufacturing Processes" course. I can definitely say that this research wouldn't have been started without his support and knowledge. I am so proud to be one of your students and will always be thankful for you.

Special thanks to Dr. Mostafa Yakout, Mohamed Balbaa, and Dalia Mahmoud for always being there for me with advice, guidance, and endless support on the scientific and various aspect of my life. I am blessed to have friends like you.

I would like to express my indebtedness to my parents for their prayers, inspiration, support, and blessed wishes. Words cannot express my gratitude to my wife Maiada Ahmed and my son Yassin for all the patience, love, and endless support.

# Contents

# List of Figures

# List of Tables

# List of Abbreviations

| | |
|---|---|
| VAD | Vibration-assisted drilling |
| LF-VAD | Low frequency-vibration assisted drilling |
| HF-VAD | High frequency-vibration assisted drilling |
| CD | Conventional drilling |
| WC | Tungsten carbide |
| ASB | Adiabatic Shear Band |
| SB | Shear Band |
| SD | Segment degree |
| GC | Gross Crack |
| MC | Micro Crack |
| CFRP | Carbon fibre reinforced polymers |
| SPD | Severe plastic deformation |
| MQL | Minimum quantity lubrication |
| ANOVA | Analysis of variance |
| RS | Residual Stress |
| HSS | High-speed steel |
| BUE | Built-up edge |
| A | Initial wear region |
| B | Steady wear region |
| C | Severe wear region |
| CER | Cutting edge radius |
| VB | Average flank wear land |

# List of Nomenclature

| | |
|---|---|
| $N$ | Cutting speed [m/min] |
| $f$ | Feed rate [mm/rev] |
| $A_m$ | Modulation amplitude [mm] |
| $F$ | Frequency [oscillation/rev] |
| $W_f$ | Modulation frequency [oscillation/rev] |
| $t_o$ | Uncut chip thickness [mm] |
| $\theta$ | Chip radian [°] |
| $\gamma$ | Tool rotational angle [°] |
| $t_D$ | Duty cycle (ms) |
| $t_C$ | Cooling cycle (ms) |
| $Z$ | Axial cutting edge position (mm) |
| $Z_k(\gamma)$ | Maximum height of the previous rotation |
| $h_{max}$ | Maximum saw-tooth height [µm] |
| $h_{min}$ | Minimum saw-tooth height [µm] |
| Lc | Deformed chip length [µm] |
| $S_d$ | Sliding distance [µm] |
| $Ø_d$ | Delamination factor [%] |

# Chapter 1

## Introduction and Background

## 1.1 Literature Review

### 1.1.1 Introduction

The use of lightweight materials with superior physical and mechanical characteristics such as carbon fiber-reinforced polymers (CFRP), titanium, and aluminum alloys in the aerospace industry has been steadily growing. In the new generation of aircraft, these materials present about 75% of the new structures total weight [1, 2]. High specific strength and stiffness, low coefficient of thermal expansion, and fatigue resistance are of the main advantages of CFRP materials [3-5]. However, the anisotropic mechanical characteristics, abrasion, and severe sensitivity to cutting temperature lead these materials to be classified as hard to cut materials [6-8]. The machining-induced mechanical and thermal damages, such as delamination, and fiber breakout may result in as much as 60% of the total parts rejection [9].

High strength to weight ratio, high fatigue and creep resistance, and excellent corrosion resistance promotes the use of Ti6Al4V alloy for the aircraft load carrying structure [10, 11]. However, high cutting temperature, poor chip evacuation mechanism, and burr formation are significant challenges during the machining process of the Ti-based alloys [11-13]. These challenges contribute to the low thermal conductivity, continuous chip morphology, and high chemical affinity of titanium alloys to chemically react with the tool material [14].

The drilling process of CFRP and Ti6Al4V is an essential process prior to the assembly process. Despite, efforts to optimize machining process of both materials, significant challenges still exist related to production time, cost, and assembly. Drilling of the CFRP and Ti6Al4V materials in-situ, known as stacked drilling, shows considerable benefits to overcome separate drilling issues [15-19].

This chapter summarizes the main contributions as well as the state of the art of a rather large research effort that have been focussed on improving the drilling process performance. The discussion presents various methods used to enhance the conventional process, as well as introducing non-conventional drilling. Moreover, the discussion provides a special focus on the in-site drilling of CFRP/Ti-6Al-4V stacks material.

### 1.1.2 Machining process of CFRP

The drilling process of laminated composites is found to be more vulnerable to the inter-laminar crack propagation in a phenomenon known as delamination, thus deteriorating its mechanical properties, and lowering fatigue life [9, 20, 21]. Entry and exit delaminations are the typical forms of delamination during conventional drilling [22-25]. Entry delamination due to laminate peel-up resulting in separation damage at the entry surface. While, exit delamination forms when the uncut laminate thickness underneath the chisel edge suffers the machining axial load (thrust force) that resulted in uncut layer separation at the exit surface, as illustrated in Figure 1-1. Delamination defect was attributed mainly to high thrust forces and cutting temperatures [21], consequently, limiting the machining process.

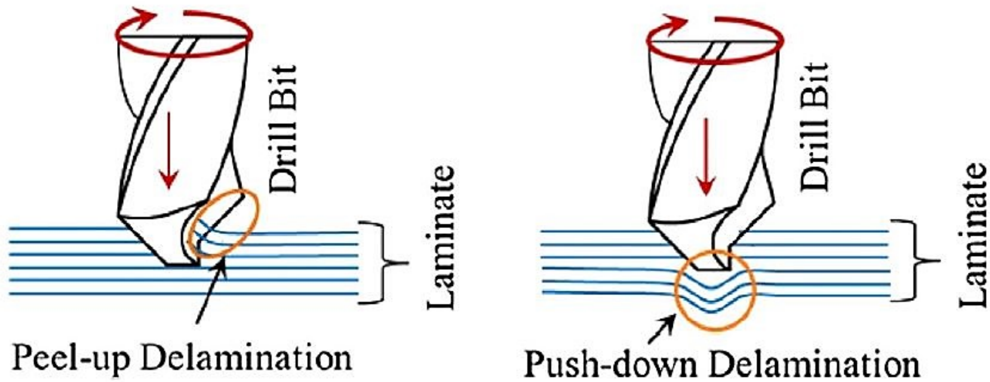


**Figure 1-1:** Delamination forms during the machining process of composite materials [26].

*1.1.2.1 Delamination measurement methodology*

A proper measurement methodology for delamination damage is important for the aerospace industry [3, 23, 27, 28]. One typical method is the one-dimensional formula, shown in Figure 1-2 (b), proposed by Chen et al, [23] and presented in equation (1.1) which is widely used to identify delamination [4, 23, 27, 28].

$$\varphi_d = \frac{[D_{maximum} - D_{nominal}]}{D_{nominal}} \tag{1.1}$$

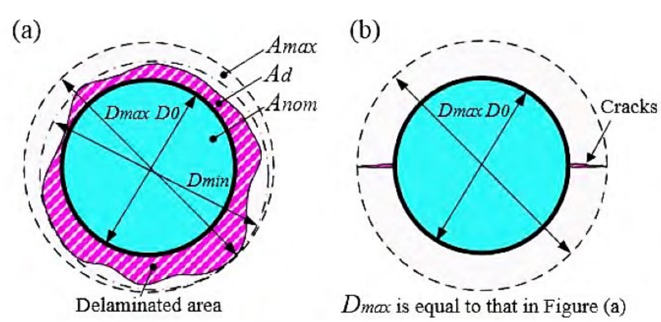


**Figure 1-2:** Schematic diagram of delamination damage (a) uniform damage, (b) cracks [29].

Based on the literature, and for a delamination free machining process the following topics are investigated.

1. The selection of machining parameters aimed at overcoming the produced hole quality, especially the delamination issue [3, 30-33].
2. The effect of drill bit material and geometry on the machining process [34-37].
3. The effect of back-up support on the hole quality and delamination damage [38, 39].
4. Alternative drilling methods [4, 8, 40].

#### *1.1.2.2 Conventional machining process*

The comprehensive study of CFRP machining parameters showed a high correlation between the drilling thrust force and delamination damage [23, 41]. The thrust force threshold at the onset of delamination damage has been pointed out through an extensive experimental investigation [4, 42]. Based on an extensive experimental investigation of a wide range machining conditions design of experiment, Davim et al, [42, 43] develop a statistical model and calculate the delamination factor. Feed rate showed dominance in controlling delamination compared to the cutting speed [23], hence, encouraging the use of low feed rate machining.

Good machining quality could be obtained with low feed rates and high cutting speeds. A study using 12,000 to 20,000 rpm cutting speed, and 0.01 to 0.3 mm/rev feed rates, reported a significant reduction in the thrust force at the high-speed range [44]. However, this reduction found to be associated with high delamination damage due to the high thermal load.

#### *1.1.2.3 Drill bit material and geometry*

Tool chisel edge and progressive tool wear showed a negative effect on the CFRP machining performance. Appropriate selection and design of tool material and geometry could increase the critical feed rate for exit delamination, as reported in [36, 37, 45]. Based on these investigations, the Core drill and Candlestick drill types showed the most improvement of 60% and 47 %, respectively compared to conventional drilling.

To reduce the drawback of the chisel edge, step core drill geometries were tested [46, 47]. It was found that a 0.74 diameter ratio resulted in the least delamination. Despite the significant enhancement of special drill bits, the cost adds more limitations for mass manufacturing. Alternatively, a properly sized pilot hole could reduce the chisel edge effect by 65% [48]. In addition, a 118° point angle showed the least thrust force at 3200 rpm cutting speed and 50.8 mm/min feed [49].

Selection of drill bit material and coating is essential for proper tool-CFRP interaction and low tool wear mechanism. Tungsten carbide (WC) showed a better machining performance compared to the high-speed steel material (HSS) [41-43] due to the higher WC hardness that resulted in a low tool wear progress (mainly abrasion for CFRP) [50]. WC tools showed machined high surface integrity over a wide feed rate range (0.03 to 0.4 mm/rev) [6]. Interestingly, coated WC tools showed little improvement compared to uncoated ones [51].

#### *1.1.2.4 Back up support*

The use of back up support is seen as a possible solution to the delamination issue [39], by reducing the thrust force effect. The exit damage is related to the thrust force and the high material spring-back movement [38]. Therefore, a back up support is relevant to overcome movement. This encouraged a drilling process of stacks such as CFRP/Al, CFRP/Ti6Al4V, AL/CFRP/Ti6Al4V, and glass aluminum reinforced epoxy (GLARE).

Despite the apparent benefits of stack drilling in reducing thrust forces effect, the thermal load posed a problem for exit delamination. Therefore, highlighting the need for an alternative drilling process.

#### *1.1.2.5 Alternative drilling methods*

Superimposing a harmonic motion in the axial direction, over the conventional tool feed movement, is an advanced machining technique that used to control the tool engaging and retracting mechanism about the mean path motion, known as Vibration-assisted drilling (VAD). The instantaneous cutting-edge position defines the chip geometry in terms of the maximum uncut chip thickness and the cutting duration. Controlling the chip geometry has a direct impact on the cutting energy.

Vibration-assisted drilling (VAD) was used to overcome the conventional machining challenges [52] by lowering the mechanical and thermal loads through intermittent cutting [8, 50].

Several studies have approached the optimization of LF-VAD (vibration frequency lower than 1 KHz) machining parameters [8, 26, 50]. LF-VAD with a frequency range of 100 – 300 Hz and high cutting speed (22,000 rpm) showed up to 30% reduction on the thrust force [50]. LF-VAD also showed up to 15% increase in the thrust force and a 15% reduction in the delamination factor [26]. Another study observed a significant reduction of 50% for the cutting temperature, and 40% for the thrust force [8]. This study examined 30-60 Hz frequency range, 800 μm amplitude, and a delamination-free process was achieved at 0.025 mm/rev feed.

In contrast to LF-VAD, the UAD (frequency is higher than 18 KHz ) of CFRP resulted in a significant reduction of the thrust force [53-57] due to a lower coefficient of friction. Moreover, exit delamination and geometrical accuracy, showed slight improvements during the UAD [54, 56, 57].

A comprehensive study of VAD with a wide range of machining parameters is a necessity to understand the effect of each machining condition. Although, the use of back-up support resulted in a great benefit towards delamination damage, its effect during the VAD machining process is not investigated yet.

### 1.1.3 Machining process of titanium alloys (Ti6Al4V).

Titanium alloys are widely used in the aerospace industry due to their high strength to weight ratio, corrosion resistance, and excellent fatigue life [10]. Mainly Ti6Al4V (grade 5) is used representing more than 50 % of the titanium grades [58]. However, these alloys are considered difficult to machine materials [59, 60]. Their poor machinability is attributed to low thermal conductivity, relatively low modulus of elasticity, high chemical affinity to react with the tool material. Machining challenges can be summarized as follows:

- High chemical reactivity with the majority of drill bits materials resulting in the tool-chip welding. Subsequently, rapid tool wear and poor machining performance could be observed.
- The low thermal conductivity leads to a high cutting temperature facilitating the adhesion tool wear mechanism, exit burr formation, and machining-induced tensile residual stresses.

- Poor chip evacuation efficiency of a continuous chip morphology triggers chip-flute accumulation and tool-chip welding.
- The tool-chip friction resulted in higher machining forces and temperature, having a negative effect on the machining quality and productivity [10, 61].

##### *1.1.3.1 Conventional machining parameters*

Optimizing the drilling machine parameters (cutting speed and feed rate) was the first approach to achieve an effective drilling process of Ti6Al4V. Based on the experimental study reported in [62], low surface roughness was observed at low feed and high cutting speed. The thrust force increased with increasing the feed rate or lowering the cutting speed. Moreover, increasing the feed rate resulted in a higher chip stiffness; as a consequence, a discontinuous chip morphology could be achieved, which is preferable for chip evacuation efficiency and machining performance. The effect of machining parameters was also investigated using the high and ultra-high speed range, as presented in [63-65], which resulted in an extremely high cutting temperature (1210° C) leading to rapid tool wear.

As the drilling bit approaches the exit surface, the low thickness material under the chisel edge starts to deform rather than being cut, resulting in protrusion of the material in a phenomenon known as a burr [12]. The drilling thrust force and cutting temperature showed a significant effect on burr height and type. Increasing the cutting speed and feed rate resulted in a higher thermal load, and consequently, a higher burr was observed [12].

##### *1.1.3.2 Coolant condition*

Thermal load is a critical issue during the drilling process of Ti6Al4V. Dry drilling resulted in an extremely high cutting temperature (~ 1100°C) [41]. Therefore, the utilization of a coolant medium was investigated to lower the cutting temperature, the friction coefficient, and to enhance the chip evacuation effectiveness. Cantero et al. [61], presented the benefits of using compressed air after each drilled hole which increased the tool life three folds. More studies highlighted the effect of advanced cooling and lubricant strategies such as Minimal Quantity of Lubricant (MQL) and Cryogenic cooling ($LN_2$) to minimize the machining cost. Zeilmann et al. [66], investigated the effect of the different coolant condition (dry, emulsion, and MQL) and coolant position on the cutting temperature. The lower cutting temperature was observed during the internal emulsion supply rather than MQL, due to the chip evacuation effectiveness. The utilization of LN2 cooling showed also reduced cutting temperature [67, 68]. However, the cutting forces, surface roughness, and hole quality showed contradicting results. This is reverted to the negative effect of LN2 on the material brittleness. On the other hand, the low tool wear and proper chip evacuation were achieved.

#### *1.1.3.3 Tool material and coating*

The low thermal conductivity of titanium alloys resulted in the concentration of more than 80% of the generated heat on the cutting tool [69]. Consequently, the careful selection of tool material, coating, and geometry could enhance machining performance. Based on the literature [69-72], the following material properties are highly recommended to reduce the tool wear:

- Maintaining high hardness characteristics at the elevated temperature to resist the high mechanical load.
- Chemical inertness with titanium alloys, to overcome the titanium chemical affinity.

- High compressive and shear strength, to maintain chip segmentation process and the resulting tensile and shear stresses.
- High thermal conductivity to dissipate the generated thermal gradient.

Tungsten carbide material (WC), particularly uncoated tools, showed high wear and deformation resistance compared to the other tool material [66, 73-75]. Based on the comprehensive study reported in [76], the straight grade cemented carbide (WC-CO) showed the most resistance to crater wear rate, flank wear land, and depth of the cut notch. Other tools such as cubic boron nitride (CBN) [76], and polycrystalline diamond (PCD) [73] proved adds more limiting due to their higher cost.

*1.1.3.4 Alternative drilling methods*

Advanced techniques mainly target a low cutting temperature, proper chip evacuation and reduction of tool wear. Intermittent drilling process such as orbital drilling and VAD are excellent candidates to overcome such issues [77, 78]. VAD results in chip segmentation through the axial tool oscillation. The VAD techniques are typically classified as follows:

- Low-frequency high amplitude, vibration-assisted drilling (LF-VAD): where the generated frequency is lower than 1000 Hz combined with a relatively high amplitude (close to the feed rate) [4].
- High-frequency low amplitude, vibration-assisted drilling (HF-VAD)($\geq$ 1000 Hz) [79, 80].

Chip geometry and evacuation mechanism can be controlled using LF-VAD technique [81], where the necessary conditions to achieve the chip breaking criteria were presented. The relationship between normalized frequency and amplitude showed a direct impact on the chip morphology and thrust force profile [82]. Consequently, enhancing machining performance [83].

A kinematic model was proposed to study the effect of using 1.5 oscillation/rev frequency module on the chip radian, effective cutting time, and tool impact velocity [84]. The proper selection of modulation amplitude resulted in low chip radian and reduced the effective cutting time. This achievement enhanced chip evacuation efficiency and reduced the cutting temperature [85].

The effect of high-frequency vibration assisted drilling was investigated [10, 13, 57]. Based on the investigated ranges, HF-VAD showed a significant reduction in the actual uncut chip thickness, cutting forces, cutting temperature, and enhanced the chip evacuation efficiency. Furthermore, the hole dimensions error, burr height, and surface roughness were reducing by 50%, 85%, and 25%, respectively.

Despite the improvement with VAD, wide modulation frequencies are not investigated yet. The LF-VAD was only presented using 1.5 cycle/rev, while the HF-VAD started from 17KHz. Moreover, the effect of VAD on the machining-induced residual stresses is also not investigated, which is critical for part life special in the aerospace industry.

### 1.1.4 Machining process of CFRP/ Ti6Al4V stack material.

The use of stack material was the logical choice to combine the benefits of both CFRP and Ti5Al4V [15-17], which explains their steady growth in the aerospace industry. The hybrid structure of CFRP/ Ti coupling (CFRP/Ti, CFRP/Ti/CFRP, and Ti/CFRP/Ti) has been identified as the common selection in the new generation of aircraft [86, 87].

Single process drilling of the CFRP and Ti6Al4V materials in-situ, also known as stacked drilling, shows considerable benefits to overcome separate drilling issues [15-19].

However, the optimal machining parameters of each material are conflicting [86]. For example, the accumulation of high-temperature titanium chips inside the limited evacuation space (drill flutes), results in CFRP thermal damage, high exit delamination, and chips-tool adhesion. Additionally, entry delamination increased by six folds [87]. Also, the surface roughness during stack drilling was double that for separate drilling [88]. This negative effect was attributed to the adhesion effect of titanium on the cutting edge. Additionally, increasing the cutting temperature during the drilling process of Ti6Al4V resulted in a high adhesion rate that leads to BUE formation [64, 86, 89, 90].

Conversely, entry delamination showed a clear reduction during the CFRP/Ti6Al4V stack drilling [88]. Moreover, the utilization of titanium plate as a backing material for CFRP would result in a clear reduction of exit delamination. In addition, stack drilling reduced the surface roughness of the CFRP, while the Ti6Al4V was rougher than separate drilling [90]. Moreover, the tool life increased three times compared to the separate drilling of titanium material [91].

In summary, machining challenges in stack drilling are as follows:

- The complexity of controlling the tool-material interaction at the CFRP-Ti6Al4V interface surface.
- The poor chip evacuation efficiency of a continuous titanium chip morphology that resulted in a severe degradation on the CFRP machined surface.
- The low thermal conductivity of Ti-alloys.
- The high-temperature sensitivity of composite materials (CFRP).

#### *1.1.4.1 Conventional drilling process of CFRP/Ti6Al4V stack material.*

Conventional drilling of Ti6Al4V /CFRP stacking resulted in a low CFRP surface roughness [92] due to the absence of Ti chip abrasion during the evacuation mechanism, however, the CFRP exit delamination was increased. Consequently, the CFRP/Ti6Al4V was typically utilized in the aerospace industry [86]. This stacking sequence showed a proper machining performance of CFRP due to the following reasons:

1- The drilling process of CFRP conducted at low-temperature drill condition to avoid any thermal damage.

2- The beneficial use of Ti6Al4V plate as back-up support that reduced the CFRP exit delamination.

To overcome such difficulties a few approaches were implemented such as [16, 93, 94], two-step drilling process [15], and the utilization of an advanced lubricant and tool coating to reduce the chip-tool friction [95]. Cutting speed showed a direct effect on surface integrity, delamination, and hole quality [18]. At a high cutting speed, the diameter accuracy showed a 30 μm error due to tool instability [87]. Additionally, the thermal load increased drastically, which negatively impacted the tool geometry and the machined surface quality, specifically the composite layer.

Consequently, most of the experimental studies were conducted using distinct machining parameters for each layer [87, 88, 90, 93, 96-100], which are summarized in Table 1-1.

**Table 1-1:** Workpiece material, tool diameter and material, and cutting conditions used during the drilling process of CFRP/Ti6Al4V stack material.

| Reference | Workpiece material | Tool diameter & material | Cutting conditions | CFRP | Ti |
|---|---|---|---|---|---|
| Park et al. [87] | CFRR /Ti6Al4V | • φ = 9.525 mm<br>• WC | *N:*<br>*f:* | 2000, 6000<br>0.0762 | 400, 800<br>0.0508 |
| Ghassemieh et al.[90] | CFRR /Ti6Al4V | • φ = 6 mm<br>• Carbide (C7) coating | *N:*<br>*f:* | 4500<br>0.1016 | 1400<br>0.0828 |
| Isbilir et al. [88] | CFRR /Ti6Al4V | • φ = 8 mm<br>• Carbide (AlTiN) coating | *N:*<br>*f:* | 4500<br>0.1016 | 1400<br>0.0828 |
| Alonso et al. [101] | CFRR /Ti6Al4V | • φ = 5.87 mm<br>• WC (2, 3 flute No.) | *N:*<br>*f:* | 796<br>0.04, 0.06 | |
| Krishnerej et al. [102] | CFRR /Ti6Al4V | • φ = 5 mm<br>• WC (K 20) | *N:*<br>*f:* | 1000<br>0.02, 0.05, 0.1, and 0.2 | |

Despite the various machining parameters used, the main challenges of stack drilling such as; chip evacuation efficiency, CFRP surface integrity, and adhesion tool wear mechanism were not addressed.

*1.1.4.2 Tool material and coating*

To avoid any react between the tool material and multi-material stack, sharp and high hot hardness tool material are highly recommended [103]. In a comprehensive study of drilling composite and titanium structure using HSS, HSS-Co, and carbide drill bits, the tool life significantly increased by using the carbide drill bit, which successfully drilled 30 holes with an acceptable flank wear. The high hot hardness of carbide drill bit maintained the cutting edge sharpness and proper shearing of the machined material, thus resulting in a low burr height and proper surface topography. The drilling process using high cutting speed resulted in an increased thermal load, which has a critical impact on the tool geometry and the machined surface quality, specifically the composite layer.

Consequently, the utilization of higher mechanical characteristics drills is highly recommended to avoid geometrical tool deformation [17, 90, 94].

#### *1.1.4.3 Alternative drilling methods*

The experimental investigation of Low-frequency vibration assisted drilling (LF-VAD) of CFRP/Ti6Al4V showed promising results compared to the conventional drilling (CD) [85, 104, 105]. The utilization of 1.5 cycle/rev frequency with minimum quantity lubrication (MQL), resulted in a 43% reduction on the cutting temperature with improved surface integrity [85]. This reduction was attributed to the proper chip evacuation and cooling efficiency. Furthermore, the use of LF-VAD resulted in a significant decrease in the tool wear, compared to the CD. In another study, using LF-VAD with 1.5 cycle/rev frequency and 0.2 mm amplitude resulted in a 48 % reduction in the cutting temperature compared to the CD [104]. Also, this reduction was increased to 52 % by using forced air-cooling condition. Same as LF-VAD, studying the effect of the ultrasonic-assisted drilling (UAD) is very limited. The impact of UAD was investigated using 39 KHz frequency and 5.7 μm amplitude during the drilling process of CFRP/Ti6Al4V stack material with different cutting speeds [106]. The study highlighted UAD as a promising solution for the tool wear challenge. Tool wear was reduced by up to 60% at the low cutting speed.

## 1.2 Motivation

Studying the influence of Vibration Assisted Drilling (VAD) process on the cutting forces, cutting temperature, and drilled hole integrity including hole accuracy, surface roughness, as well as residual stresses on the aerospace materials (CFRP, Ti6Al4V, and CFRP/Ti6Al4V stack material) are the main goals of this thesis.

## 1.3 Research Objectives

The main objective of the current thesis is to identify the optimum vibration-assisted drilling machining condition necessary to process each of these materials for aerospace.

This thesis provides a better understanding of:

1. The effect of VAD Kinematics on the chip formation, mechanical and thermal load.
2. Changes in the chip formation mechanism, morphology, and geometry that occurs during the VAD process.
3. The effect of VAD Kinematics on the Ti6Al4V residual stresses, microstructure, and surface integrity.
4. Delamination damage and geometrical accuracy associated with VAD process.
5. Assessment and comparison between LF-VAD and HF-VAD during the drilling process of CFRP/Ti6Al4V stack material.
6. Tool wear progression under VAD and the subsequent effect on the machined surface.

## 1.4 Thesis Outline

Overall, the *main* results of this thesis have been published in *six* journal articles, four of which are already published, and the others are submitted to journals for peer-review.

Chapter 1 introduces the literature review, background, and motivation of the current research as well as the thesis objectives and main contributions. It presents the research gaps in vibration-assisted drilling and how this thesis addresses them.

Chapter 2 investigates the effect of LF-VAD Kinematics on the Ti6Al4V subsurface microstructure, chip morphology, and surface integrity. The effect of LF-VAD on the induced residual stress on the surface and in-depth profile that has a significant impact on the part fatigue life.

Chapter 3 identifies and examines the dominant chip formation mechanisms that occurs during VAD. Moreover, this chapter presents the effect of VAD kinematics on chip morphology with extensive metallurgical analysis. Also, the study presents the influence of VAD on the tool wear mechanisms through the composition analysis of the chips machined surface using Energy Dispersion X-ray Spectroscopy (EDS).

Chapter 4 investigates the exit delamination and geometrical accuracy for LF-VAD and HF-VAD. The VAD kinematics are used to investigate the relationship between the input machining parameters and the uncut chip thickness. Exit delamination and geometrical accuracy are then evaluated in terms of mechanical and thermal loads.

Chapter 5 explains the effect of LF-VAD Kinematics on the CFRP/Ti6Al4V stacked drilling performance. The effects on hole quality and surface roughness are also presented. Moreover, the optimum process window is determined based on the subsurface microstructures, residual stress, delamination, and geometrical accuracy.

Chapter 6 presents an experimental investigation relating the high-frequency vibration assisted drilling (HF-VAD) machining parameters to the Ti6Al4V burr formation and induced residual stresses, as well as CFRP delamination during the drilling of CFRP/Ti6Al4V staked material. Additionally, an assessment and comparison between HF-VAD and LF-VAD of CFRP/Ti6Al4V hybrid structure is presented.

Chapter 7 investigates the effect of VAD machining parameters on the tool wear mechanism and progress based on the selected process window. The effect of tool wear progress on the drilled hole quality is described by CFRP entry and exit delamination, and hole accuracy.

Chapter 8 summarizes the main contributions of this thesis.

## References

[1] E. Brinksmeier and R. Janssen, "Drilling of Multi-Layer Composite Materials consisting of Carbon Fiber Reinforced Plastics (CFRP), Titanium and Aluminum Alloys," *CIRP Annals - Manufacturing Technology,* vol. 51, pp. 87-90, 2002/01/01/ 2002.

[2] S. L. Soo, A. M. Abdelhafeez, M. Li, R. Hood, and C. M. Lim, "The drilling of carbon fibre composite–aluminium stacks and its effect on hole quality and integrity," *Proceedings of the Institution of Mechanical Engineers, Part B: Journal of Engineering Manufacture,* p. 0954405417728312, 2017.

[3] J. Xu, C. Li, S. Mi, Q. An, and M. Chen, "Study of drilling-induced defects for CFRP composites using new criteria," *Composite Structures,* vol. 201, pp. 1076-1087, 2018/10/01/ 2018.

[4] A. Sadek, "Vibration Assisted Drilling of Multidirectional Fiber Reinforced Polymer Laminates," Ph.D. Thesis, McGill University Libraries, 2014.

[5] D. Liu, Y. Tang, and W. L. Cong, "A review of mechanical drilling for composite laminates," *Composite Structures,* vol. 94, pp. 1265-1279, 2012/03/01/ 2012.

[6] S. Malhotra, "Some studies on drilling of fibrous composites," *Journal of Materials Processing Technology,* vol. 24, pp. 291-300, 1990.

[7] S. Lin and I. Chen, "Drilling carbon fiber-reinforced composite material at high speed," *Wear,* vol. 194, pp. 156-162, 1996.

[8] A. Sadek, M. Attia, M. Meshreki, and B. Shi, "Characterization and optimization of vibration-assisted drilling of fibre reinforced epoxy laminates," *CIRP Annals-Manufacturing Technology,* vol. 62, pp. 91-94, 2013.

[9] R. Stone and K. Krishnamurthy, "A neural network thrust force controller to minimize delamination during drilling of graphite-epoxy laminates," *International Journal of Machine Tools and Manufacture,* vol. 36, pp. 985-1003, 1996.

[10] Z. Li, D. Zhang, X. Jiang, W. Qin, and D. Geng, "Study on rotary ultrasonic-assisted drilling of titanium alloys (Ti6Al4V) using 8-facet drill under no cooling condition," *The International Journal of Advanced Manufacturing Technology,* vol. 90, pp. 3249-3264, 2017.

[11] P. Zhang, N. Churi, Z. J. Pei, and C. Treadwell, "Mechanical drilling processes for titanium alloys: a literature review," *Machining Science and Technology,* vol. 12, pp. 417-444, 2008.

[12] D. Dornfeld, J. Kim, H. Dechow, J. Hewson, and L. Chen, "Drilling burr formation in titanium alloy, Ti-6AI-4V," *CIRP Annals-Manufacturing Technology,* vol. 48, pp. 73-76, 1999.

[13] J. Pujana, A. Rivero, A. Celaya, and L. L. de Lacalle, "Analysis of ultrasonic-assisted drilling of Ti6Al4V," *International Journal of Machine Tools and Manufacture,* vol. 49, pp. 500-508, 2009.

[14] H. Schulz and A. Emrich, "Limitations of Drilling in Difficult-to-Machine Materials such as Titanium TiA16V4, 1998," *Production Engineering,* vol. 5, p. 1, 1998.

[15] E. Brinksmeier and R. Janssen, "Drilling of multi-layer composite materials consisting of carbon fiber reinforced plastics (CFRP), titanium and aluminum alloys," *CIRP Annals-Manufacturing Technology,* vol. 51, pp. 87-90, 2002.

[16] D. Kim and M. Ramulu, "Study on the drilling of titanium/graphite hybrid composites," *Journal of Engineering Materials and Technology,* vol. 129, pp. 390-396, 2007.

[17] M. Ramulu, T. Branson, and D. Kim, "A study on the drilling of composite and titanium stacks," *Composite Structures,* vol. 54, pp. 67-77, 10// 2001.

[18] D. Kim and M. Ramulu, "Drilling process optimization for graphite/bismaleimide–titanium alloy stacks," *Composite Structures,* vol. 63, pp. 101-114, 2004/01/01/ 2004.

[19] V. Krishnaraj, R. Zitoune, and F. Collombet, "Comprehensive review on drilling of Multimaterial stacks," *Journal of Machining and Forming Technologies,* vol. 2, pp. 1-32, 2010.

[20] Z. Linbo, W. Lijiang, and W. Xin, "Study on vibration drilling of fiber reinforced plastics with hybrid variation parameters method," *Composites Part A: Applied Science and Manufacturing,* vol. 34, pp. 237-244, 2003.

[21] V. Tagliaferri, G. Caprino, and A. Diterlizzi, "Effect of drilling parameters on the finish and mechanical properties of GFRP composites," *International Journal of Machine Tools and Manufacture,* vol. 30, pp. 77-84, 1990.

[22] E. Persson, I. Eriksson, and L. Zackrisson, "Effects of hole machining defects on strength and fatigue life of composite laminates," *Composites Part A: Applied Science and Manufacturing,* vol. 28, pp. 141-151, 1997/01/01/ 1997.

[23] W.-C. Chen, "Some experimental investigations in the drilling of carbon fiber-reinforced plastic (CFRP) composite laminates," *International Journal of Machine Tools and Manufacture,* vol. 37, pp. 1097-1108, 1997.

[24] V. Gaitonde, S. Karnik, J. C. Rubio, A. E. Correia, A. Abrao, and J. P. Davim, "Analysis of parametric influence on delamination in high-speed drilling of carbon fiber reinforced plastic composites," *Journal of materials processing technology,* vol. 203, pp. 431-438, 2008.

[25] L. Romoli and G. Dini, "Experimental study on the influence of drill wear in CFRP drilling processes," in *ICME 08*, 2008.

[26] K. Debnath and I. Singh, "Low-frequency modulation-assisted drilling of carbon-epoxy composite laminates," *Journal of Manufacturing Processes,* vol. 25, pp. 262-273, 2017.

[27] C. C. Tsao, K. L. Kuo, and I. C. Hsu, "Evaluation of a novel approach to a delamination factor after drilling composite laminates using a core–saw drill," *The International Journal of Advanced Manufacturing Technology,* vol. 59, pp. 617-622, March 01 2012.

[28] D. N. R. d. Silva, "Image processing methodology for assessment of drilling induced damage in CFRP," Faculdade de Ciências e Tecnologia, 2013.

[29] D. Geng, Y. Liu, Z. Shao, Z. Lu, J. Cai, X. Li*, et al.*, "Delamination formation, evaluation and suppression during drilling of composite laminates: A review," *Composite Structures,* 2019.

[30] H. Ho-Cheng and C. Dharan, "Delamination during drilling in composite laminates," *Journal of engineering for industry,* vol. 112, pp. 236-239, 1990.

[31] D. Liu, Y. Tang, and W. Cong, "A review of mechanical drilling for composite laminates," *Composite Structures,* vol. 94, pp. 1265-1279, 2012.

[32] D. Che, I. Saxena, P. Han, P. Guo, and K. F. Ehmann, "Machining of carbon fiber reinforced plastics/polymers: a literature review," *Journal of Manufacturing Science and Engineering,* vol. 136, p. 034001, 2014.

[33] M. Durante, L. Boccarusso, D. De Fazio, and A. Langella, "Circular cutting strategy for drilling of carbon fiber-reinforced plastics (CFRPs)," *Materials and Manufacturing Processes,* pp. 1-13, 2019.

[34] R. Piquet, B. Ferret, F. Lachaud, and P. Swider, "Experimental analysis of drilling damage in thin carbon/epoxy plate using special drills," *Composites Part A: Applied Science and Manufacturing,* vol. 31, pp. 1107-1115, 2000.

[35] L. M. P. Durão, D. J. Gonçalves, J. M. R. Tavares, V. H. C. de Albuquerque, A. A. Vieira, and A. T. Marques, "Drilling tool geometry evaluation for reinforced composite laminates," *Composite structures,* vol. 92, pp. 1545-1550, 2010.

[36] C. Tsao and H. Hocheng, "Taguchi analysis of delamination associated with various drill bits in drilling of composite material," *International Journal of Machine Tools and Manufacture,* vol. 44, pp. 1085-1090, 2004.

[37] C. C. Tsao and H. Hocheng, "Computerized tomography and C-Scan for measuring delamination in the drilling of composite materials using various drills," *International Journal of Machine Tools and Manufacture,* vol. 45, pp. 1282-1287, 2005/09/01/ 2005.

[38] J. F. Chatelain, I. Zaghbani, G. Lebrun, and K. Hasni, "Effect of Support Distance on Damage of Drilled Thin CFRP Laminates," *International Journal of Mechanical, Aerospace, Industrial and Mechatronics Engineering,* vol. 7, 2013.

[39] C. C. Tsao and H. Hocheng, "Effects of exit back-up on delamination in drilling composite materials using a saw drill and a core drill," *International Journal of Machine Tools and Manufacture,* vol. 45, pp. 1261-1270, 2005/09/01/ 2005.

[40] A. Sadek, M. Meshreki, and M. Attia, "Effect of Tool Kinematics on the Drilling Forces and Temperature in Low Frequency High Amplitude Vibration Assisted Drilling," in *ASME 2014 International Mechanical Engineering Congress and Exposition*, 2014, pp. V02AT02A035-V02AT02A035.

[41] I. S. E. M. Shyha, "Drilling of carbon fibre reinforced plastic composites," University of Birmingham, 2010.

[42] J. P. Davim and P. Reis, "Drilling carbon fiber reinforced plastics manufactured by autoclave—experimental and statistical study," *Materials & design,* vol. 24, pp. 315-324, 2003.

[43] J. P. Davim and P. Reis, "Study of delamination in drilling carbon fiber reinforced plastics (CFRP) using design experiments," *Composite Structures,* vol. 59, pp. 481-487, 2003/03/01/ 2003.

[44] V. Krishnaraj, A. Prabukarthi, A. Ramanathan, N. Elanghovan, M. Senthil Kumar, R. Zitoune*, et al.*, "Optimization of machining parameters at high speed drilling of carbon fiber reinforced plastic (CFRP) laminates," *Composites Part B: Engineering,* vol. 43, pp. 1791-1799, 2012/06/01/ 2012.

[45] H. Hocheng and C. Tsao, "Effects of special drill bits on drilling-induced delamination of composite materials," *International Journal of Machine Tools and Manufacture,* vol. 46, pp. 1403-1416, 2006.

[46] C. Tsao, "Investigation into the effects of drilling parameters on delamination by various step-core drills," *Journal of materials processing technology,* vol. 206, pp. 405-411, 2008.

[47] C. Tsao, "Experimental study of drilling composite materials with step-core drill," *Materials & Design,* vol. 29, pp. 1740-1744, 2008.

[48] M. S. Won and C. Dharan, "Chisel edge and pilot hole effects in drilling composite laminates," *Journal of manufacturing science and engineering,* vol. 124, pp. 242-247, 2002.

[49] E. U. Enemuoh, A. S. El-Gizawy, and A. C. Okafor, "An approach for development of damage-free drilling of carbon fiber reinforced thermosets," *International Journal of Machine Tools and Manufacture,* vol. 41, pp. 1795-1814, 2001.

[50] X. Wang, L. Wang, and J. Tao, "Investigation on thrust in vibration drilling of fiber-reinforced plastics," *Journal of Materials Processing Technology,* vol. 148, pp. 239-244, 2004.

[51] C. Murphy, G. Byrne, and M. Gilchrist, "The performance of coated tungsten carbide drills when machining carbon fibre-reinforced epoxy composite materials," *Proceedings of the Institution of Mechanical Engineers, Part B: Journal of Engineering Manufacture,* vol. 216, pp. 143-152, 2002.

[52] C. Zhang and M. Lu, "A novel variable-dimensional vibration-assisted actuator for drilling CFRP," *The International Journal of Advanced Manufacturing Technology,* vol. 99, pp. 3049-3063, December 01 2018.

[53] V. A. Phadnis, F. Makhdum, A. Roy, and V. V. Silberschmidt, "Experimental and numerical investigations in conventional and ultrasonically assisted drilling of CFRP laminate," *Procedia CIRP,* vol. 1, pp. 455-459, 2012.

[54] F. Makhdum, L. T. Jennings, A. Roy, and V. V. Silberschmidt, "Cutting forces in ultrasonically assisted drilling of carbon fibre-reinforced plastics," in *Journal of Physics: Conference Series*, 2012, p. 012019.

[55] F. Makhdum, D. N. P. Norddin, A. Roy, and V. V. Silberschmidt, "Ultrasonically assisted drilling of carbon fibre reinforced plastics," in *Solid State Phenomena*, 2012, pp. 170-175.

[56] F. Makhdum, V. A. Phadnis, A. Roy, and V. V. Silberschmidt, "Effect of ultrasonically-assisted drilling on carbon-fibre-reinforced plastics," *Journal of Sound and Vibration,* vol. 333, pp. 5939-5952, 11/24/ 2014.

[57] A. Sanda, I. Arriola, V. G. Navas, I. Bengoetxea, and O. Gonzalo, "Ultrasonically assisted drilling of carbon fibre reinforced plastics and Ti6Al4V," *Journal of Manufacturing Processes,* vol. 22, pp. 169-176, 2016.

[58] K. Gupta and R. Laubscher, *Sustainable Machining of Titanium Alloys: A Critical Review* vol. 231, 2016.

[59] E. M. Trent and P. K. Wright, *Metal cutting*: Butterworth-Heinemann, 2000.

[60] M. C. Shaw and J. Cookson, *Metal cutting principles* vol. 2: Oxford university press New York, 2005.

[61] J. L. Cantero, M. M. Tardío, J. A. Canteli, M. Marcos, and M. H. Miguélez, "Dry drilling of alloy Ti–6Al–4V," *International Journal of Machine Tools and Manufacture,* vol. 45, pp. 1246-1255, 2005/09/01/ 2005.

[62] Z. Zhu, S. Sui, J. Sun, J. Li, and Y. Li, "Investigation on performance characteristics in drilling of Ti6Al4V alloy," *The International Journal of Advanced Manufacturing Technology,* pp. 1-10, 2017.

[63] E. Rahim, K. Kamdani, and S. Sharif, *Performance Evaluation of Uncoated Carbide Tool in High Speed Drilling of Ti6Al4V* vol. 2, 2008.

[64] R. Li, P. Hegde, and A. J. Shih, "High-throughput drilling of titanium alloys," *International Journal of Machine Tools and Manufacture,* vol. 47, pp. 63-74, 2007.

[65] R. Li and A. J. Shih, "Spiral point drill temperature and stress in high-throughput drilling of titanium," *International Journal of Machine Tools and Manufacture,* vol. 47, pp. 2005-2017, 2007/10/01/ 2007.

[66] R. P. Zeilmann and W. L. Weingaertner, "Analysis of temperature during drilling of Ti6Al4V with minimal quantity of lubricant," *Journal of Materials Processing Technology,* vol. 179, pp. 124-127, 2006/10/20/ 2006.

[67] L. S. Ahmed, N. Govindaraju, and M. Pradeep Kumar, "Experimental investigations on cryogenic cooling in the drilling of titanium alloy," *Materials and Manufacturing Processes,* vol. 31, pp. 603-607, 2016.

[68] L. S. Ahmed and M. P. Kumar, "Cryogenic drilling of Ti–6Al–4V alloy under liquid nitrogen cooling," *Materials and Manufacturing Processes,* vol. 31, pp. 951-959, 2016.

[69] E. Ezugwu and Z. Wang, "Titanium alloys and their machinability—a review," *Journal of materials processing technology,* vol. 68, pp. 262-274, 1997.

[70] M. J. Donachie, "Titanium: A technical guide ASM International," *New York: The Materials Information Society,* 2000.

[71] J. P. Davim, *Machining of titanium alloys*: Springer, 2014.

[72] W. A. Knight and G. Boothroyd, *Fundamentals of metal machining and machine tools* vol. 198: CRC Press, 2005.

[73] P. D. Hartung, B. Kramer, and B. Von Turkovich, "Tool wear in titanium machining," *CIRP Annals,* vol. 31, pp. 75-80, 1982.

[74] R. M'Saoubi, D. Axinte, S. L. Soo, C. Nobel, H. Attia, G. Kappmeyer*, et al.*, "High performance cutting of advanced aerospace alloys and composite materials," *CIRP Annals,* vol. 64, pp. 557-580, 2015.

[75] M. Armendia, A. Garay, L. M. Iriarte, and P. J. Arrazola, "Comparison of the machinabilities of Ti6Al4V and TIMETAL® 54M using uncoated WC–Co tools," *Journal of Materials Processing Technology,* vol. 210, pp. 197-203, 2010/01/19/ 2010.

[76] P. Dearnley and A. Grearson, "Evaluation of principal wear mechanisms of cemented carbides and ceramics used for machining titanium alloy IMI 318," *Materials Science and Technology,* vol. 2, pp. 47-58, 1986.

[77] W. Ni, "Orbital drilling of aerospace materials," SAE Technical Paper 0148-7191, 2007.

[78] H. Li, G. He, X. Qin, G. Wang, C. Lu, and L. Gui, "Tool wear and hole quality investigation in dry helical milling of Ti-6Al-4V alloy," *The International Journal of Advanced Manufacturing Technology,* vol. 71, pp. 1511-1523, 2014.

[79] V. I. Babitsky, A. N. Kalashnikov, and F. V. Molodtsov, "Autoresonant control of ultrasonically assisted cutting," *Mechatronics,* vol. 14, pp. 91-114, 2004/02/01/ 2004.

[80] H. Paris, D. Brissaud, A. Gouskov, N. Guibert, and J. Rech, "Influence of the ploughing effect on the dynamic behaviour of the self-vibratory drilling head," *CIRP Annals,* vol. 57, pp. 385-388, 2008/01/01/ 2008.

[81] Z. Deyuan and W. Lijiang, "Investigation of chip in vibration drilling," *International Journal of Machine Tools and Manufacture,* vol. 38, pp. 165-176, 1998.

[82] Y. Guo and J. B. Mann, "Experimental Evaluation of Cutting Kinematics and Chip Evacuation in Drilling With Low-Frequency Modulation-Assisted Machining," in *ASME 2017 12th International Manufacturing Science and Engineering Conference collocated with the JSME/ASME 2017 6th International Conference on Materials and Processing*, 2017, pp. V001T02A017-V001T02A017.

[83] S. S. F. Chang and G. M. Bone, "Thrust force model for vibration-assisted drilling of aluminum 6061-T6," *International Journal of Machine Tools and Manufacture,* vol. 49, pp. 1070-1076, 2009/11/01/ 2009.

[84] O. Pecat and I. Meyer, "Low frequency vibration assisted drilling of aluminium alloys," in *Advanced Materials Research*, 2013, pp. 131-138.

[85] O. Pecat and E. Brinksmeier, "Low damage drilling of CFRP/titanium compound materials for fastening," *Procedia CIRP,* vol. 13, pp. 1-7, 2014.

[86] J. Xu, A. Mkaddem, and M. El Mansori, "Recent advances in drilling hybrid FRP/Ti composite: a state-of-the-art review," *Composite Structures,* vol. 135, pp. 316-338, 2016.

[87] K.-H. Park, A. Beal, P. Kwon, and J. Lantrip, "A comparative study of carbide tools in drilling of CFRP and CFRP-Ti stacks," *Journal of Manufacturing Science and Engineering,* vol. 136, p. 014501, 2014.

[88] O. Isbilir and E. Ghassemieh, "Comparative study of tool life and hole quality in drilling of CFRP/titanium stack using coated carbide drill," *Machining Science and Technology,* vol. 17, pp. 380-409, 2013.

[89] E. Rahim and S. Sharif, "Tool failure modes and wear mechanism of coated carbide tools when drilling Ti-6Al-4V," *International Journal of Precision Technology,* vol. 1, pp. 30-39, 2007.

[90] E. Ghassemieh, "Performance and wear of coated carbide drill in machining of carbon fibre reinforced composite/titanium stack," *International Journal of Materials and Product Technology,* vol. 43, pp. 165-183, 2012.

[91] X. Wang, P. Y. Kwon, C. Sturtevant, and J. Lantrip, "Comparative tool wear study based on drilling experiments on CFRP/Ti stack and its individual layers," *Wear,* vol. 317, pp. 265-276, 2014.

[92] J. Xu, "Numerical and experimental study of machining titanium-composite stacks," Paris, ENSAM, 2016.

[93] J. Xu and M. El Mansori, "Experimental study on drilling mechanisms and strategies of hybrid CFRP/Ti stacks," *Composite Structures,* vol. 157, pp. 461-482, 12/1/ 2016.

[94] D. Kim, C. Sturtevant, and M. Ramulu, "Usage of PCD tool in drilling of titanium/graphite hybrid composite laminate," *International Journal of Machining and Machinability of Materials,* vol. 13, pp. 276-288, 2013.

[95] N. Guibert, "Etude et modélisation de l'influence des phénomènes de coupe sur les performances du forage vibratoire," Université Joseph-Fourier-Grenoble I, 2008.

[96] K.-H. Park, A. Beal, P. Kwon, and J. Lantrip, "Tool wear in drilling of composite/titanium stacks using carbide and polycrystalline diamond tools," *Wear,* vol. 271, pp. 2826-2835, 2011.

[97] A. Poutord, F. Rossi, G. Poulachon, R. M'Saoubi, and G. Abrivard, "Local approach of wear in drilling Ti6Al4V/CFRP for stack modelling," *Procedia CIRP,* vol. 8, pp. 316-321, 2013.

[98] S. Sharif and E. A. Rahim, "Performance of coated- and uncoated-carbide tools when drilling titanium alloy—Ti–6Al4V," *Journal of Materials Processing Technology,* vol. 185, pp. 72-76, 4/30/ 2007.

[99] I. Shyha, S. L. Soo, D. Aspinwall, S. Bradley, R. Perry, P. Harden*, et al.*, "Hole quality assessment following drilling of metallic-composite stacks," *International Journal of Machine Tools and Manufacture,* vol. 51, pp. 569-578, 2011.

[100] I. S. Shyha, D. K. Aspinwall, S. L. Soo, and S. Bradley, "Drill geometry and operating effects when cutting small diameter holes in CFRP," *International Journal of Machine Tools and Manufacture,* vol. 49, pp. 1008-1014, 10// 2009.

[101] U. Alonso, M. Calamaz, F. Girot, and E. Iriondo, "Influence of flute number and stepped bit geometry when drilling CFRP/Ti6Al4V stacks," *Journal of Manufacturing Processes,* vol. 39, pp. 356-370, 2019/03/01/ 2019.

[102] V. Krishnaraj, A. Prabukarthi, M. Santhosh, M. Senthilkumar, and R. Zitoune, "Optimization of machining parameters in CFRP/Ti stacks drilling," in *ASME 2012 International Manufacturing Science and Engineering Conference collocated with the 40th North American Manufacturing Research Conference and in participation with*

*the International Conference on Tribology Materials and Processing*, 2012, pp. 269-275.

[103] V. Krishnaraj, R. Zitoune, and F. Collombet, "Comprehensive review on drilling of multimaterials stacks," *Journal of Machining and Forming Technologies,* vol. 2, pp. 1-32, 2010.

[104] C. Li, J. Xu, M. Chen, Q. An, M. El Mansori, and F. Ren, "Tool wear processes in low frequency vibration assisted drilling of CFRP/Ti6Al4V stacks with forced air-cooling," *Wear,* vol. 426, pp. 1616-1623, 2019.

[105] O. Pecat and E. Brinksmeier, "Tool wear analyses in low frequency vibration assisted drilling of CFRP/Ti6Al4V stack material," *Procedia CIRP,* vol. 14, pp. 142-147, 2014.

[106] A. N. Dahnel, H. Ascroft, and S. Barnes, "The Effect of Varying Cutting Speeds on Tool Wear During Conventional and Ultrasonic Assisted Drilling (UAD) of Carbon Fibre Composite (CFC) and Titanium Alloy Stacks," *Procedia CIRP,* vol. 46, pp. 420-423, // 2016.

# Chapter 2

## Surface and Microstructure Characterization of Low-frequency Vibration Assisted Drilling of Ti6Al4V

**Complete Citation:**

Hussein, R., Sadek, A., Elbestawi, M.A., Attia, M.H. (2019). Surface and Microstructure Characterization of Low-frequency Vibration Assisted Drilling of Ti6Al4V. *The International Journal of Advanced Manufacturing Technology*. Doi: 10.1007/s00170-019-03608-2

**Copyright:**

**Relative Contributions:**

| | |
|---|---|
| R. Hussein: | Performed experiments, analysis, and data interpretation; wrote the first draft of the manuscript; helped with submitting the final manuscript to the journal (corresponding author). |
| A. Sadek: | Helped with the experiments and analysis; revised the manuscript. |
| M. A. Elbestawi: | Supervisor of R. Hussein. Revised and edited the manuscript and gave the final approval to be submitted. |
| M. H. Attia: | Revised the manuscript. |

**Abstract:**

A continuous curled chip formation with a high thermal load is a critical challenge during conventional drilling process of Ti6Al4V. In addition, adverse side effects will take place on the drilled hole quality, as well as the drill tool performance, which is not acceptable in the aerospace industry. Chip segmentation using low-frequency vibration assisted drilling (LF-VAD) is a promising technology aimed at reducing the difficulties associated with conventional drilling. Compressive residual stresses, lower cutting zone temperature, higher hole size accuracy, and smoother surface finish are of the main advantages that could be achieved with the interrupted cutting technique.

The primary objective of this paper is to investigate the effect of LF-VAD machining parameters on the Ti6Al4V residual stresses, microstructure, and surface integrity, for a wide range of modulation amplitude, feed, and cutting speed, for a new frequency range for the first time. The effect of LF-VAD on the chip morphology and subsurface examination of microstructure, surface, and depth profile of residual stress are examined.

The experimental results showed that LF-VAD has a significant influence on the induced residual stress. A 35.8% reduction in the cutting temperature has been observed at the exit surface. This method has improved the residual stress to compressive which has a significant impact on the part fatigue life.

**Keywords:**

Low-frequency vibration-assisted drilling; Ti6Al4V material; Advanced machining; Residual stresses; Chip morphology. Subsurface examination.

**Acronyms:**

| | |
|---|---|
| VAD | Vibration-assisted drilling |
| LF-VAD | Low frequency-vibration assisted drilling |
| HF-VAD | High frequency-vibration assisted drilling |
| CD | Conventional drilling |
| WC | Tungsten carbide |

**Notations:**

| | |
|---|---|
| $N$ | Cutting speed [m/min] |
| $f$ | Feed rate [mm/rev] |
| $A_m$ | Modulation amplitude [mm] |
| $F$ | Frequency [oscillation/rev] |
| $t_o$ | Uncut chip thickness [mm] |
| $\theta$ | Chip radian [°] |
| $\gamma$ | Tool rotational angle [°] |
| $t_D$ | Duty cycle (ms) |
| $t_C$ | Cooling cycle (ms) |
| $Z$ | Axial cutting edge position (mm) |
| $Z_k(\gamma)$ | Maximum height of the previous rotation |

**Acknowledgment:**

This study was performed using the facilities of the Canadian National Research Council (CNRC), Aerospace Manufacturing Group. The use of their facilities, equipment and the technical support is greatly appreciated.

The authors gratefully thank Mr. M.Balbaa, for his assistance during the SEM examination.

## 2.1 Introduction

Titanium alloys are widely used in the aerospace industry due to their mechanical properties. The high strength to weight ratio, corrosion resistance, excellent fatigue and creep resistance increased the use of Ti6Al4V in the aircraft load carrying structure [1]. Chip evacuation [2], high cutting temperatures [3], and burr formation [4, 5] are some of the main problems that arise during conventional drilling of Ti-based alloys. Low thermal conductivity combined with a high chemical affinity with the majority of the drill tool materials make Ti-based alloys difficult to machine, particularly during the drilling process [1, 6, 7]. As a consequence of poor chip evacuation mechanism, long and continuous curled chips has a damaging impact on the machined surface. Moreover, the high tool-chip friction mechanism has a negative effect on the machining quality and productivity[1, 8].

Several approaches have been investigated to optimize the Titanium alloys manufacturing process such as tool coating [2, 9], enhancing the cooling process[10, 11], and using a special tool design [1]. In general, innovative methods are still required to maintain higher machining efficiency and productivity.

Vibration-assisted drilling (VAD) results in chip segmentation through axial tool oscillation. The VAD techniques are typically classified as follows:

- Low-frequency, high amplitude, vibration assisted drilling (LF-VAD): where the generated frequency is lower than 1000 Hz combined with a relatively high amplitude (close to the feed rate) [12].
- High-frequency, low amplitude, vibration assisted drilling (HF-VAD): where the generated frequency is higher than 1000 Hz [13, 14].

Chip geometry and evacuation mechanism can be controlled using LF-VAD technique. A study of vibration-assisted drilling chip breaking phenomena was presented in [15], where the necessary conditions to achieve the chip breaking criteria were presented. The relationship between normalized frequency and amplitude showed a direct impact on the chip morphology and thrust force profile [16]. Consequently, the machining performance such as the cutting forces, generated temperature, burr formation, and tool wear could be enhanced [17]. Moreover, chip evacuation, cooling mechanism, and the internal surface integrity are controlled by the chip radian.

A kinematic model was proposed to study the effect of using 1.5 oscillation/rev frequency module on the chip radian, effective cutting time, and tool impact velocity in [18]. The effect of modulation amplitude showed a direct impact on the chip radian and the effective cutting time reduction, which enhances the chip evacuation mechanism and cutting temperature [19]. Moreover, studying the LF-VAD machining parameters showed an increase in the heat transfer coefficient by adding a convection cooling mechanism in the air gap created, which reduces the cutting zone temperature [20].

Previous investigations in LF-VAD have mainly focused on the effect of LF-VAD machining parameters on the cutting forces and temperatures. However, little information is known about the effect of LF-VAD machining parameters and the associated mechanical and thermal loads on surface integrity, microstructure, and residual stresses.

In this paper, a 2.5 oscillation/rev frequency is used to investigate the effect of a wide range of machining parameters, on the chip morphology and chip evacuation effectiveness during LF-VAD of Ti6Al4V. The chip evacuation effectiveness was investigated by relating the LF-VAD conditions to the achieved chip thickness and radian and the resulting thermal load and surface integrity in terms of microstructure and residual stresses.

## 2.2 Experimental setup

A full factorial design of experiment consisting of two levels of cutting speeds (37.68 and 56.52 m/min), three levels of feed rates (0.025,0.05, and 0.075 mm/rev), and five cutting amplitudes (0.07, 0.1, 0.16, 0.25, and 0.48 mm) under a fixed 2.5 oscillation/rev (83.5 and 125 Hz) has been used. The selection of these machining conditions (cutting speed, and feed) is based on the literature review [8, 9, 21], and the LF-VAD tool holder limitation ($N_{max} \leq 3500$ rpm). The 2.5 oscillation/rev was generated with a commercially available MITIS tool holder PG8045B3_HSK-A100_ER40[22], which has an adjustable amplitude of 0.01 - 0.48 mm and 3500 rpm speed limitation. All the cutting conditions were repeated three times to confirm the results achieved under dry condition. Conventional drilling tests were also performed at identical cutting conditions (two Cutting speed × three Feed rate) for comparison purposes.

The experiments were performed using a 5-axis Makino A88ε machining centre. A Kistler four-component dynamometer type 9272 was placed behind the drilled workpiece and a supporting Kistler Multichannel Charge Amplifier Type 5019B was attached for thrust force measurement. The cutting temperature was monitored using a thermo-vision infrared camera. A special support was used to create enough distance between the drilled material and the dynamometer to achieve a direct thermal vision of the tool once it fully penetrates the bottom surface, as shown in Figure 2-1.

For material surface topography analysis, the drilled holes were split using waterjet cutting to reduce any probability of heat generation that could affect the material characteristics. The chip morphology was observed using a Keyence Digital Microscope VHX-6000 Series and a TESCAN VP.SEM Scanning Electron Microscopy. Surface roughness values were evaluated using a Surftest SJ-410 stylus profilometry with 0.0001 μm resolution, and the Alicona instrument used to study the surface topography in the 3D. The average surface roughness of each hole was measured at three locations along the drilling direction. For each spot, four measurements were collected. For subsurface examination, the exit machined surface was grinded with 320 mesh SIC paper. The grinded surface was cleaned and polished with 9 µm and 3 µm diamond solvent. The polished specimens were etched with (0.5 ml HF, 3 ml HNO3, and 96.5 ml pure water). The curvature X-ray residual stress measurements, were performed using a copper target at a Bragg angle of 142° and 11 tilt angles (up to 40°), for both drilling techniques.

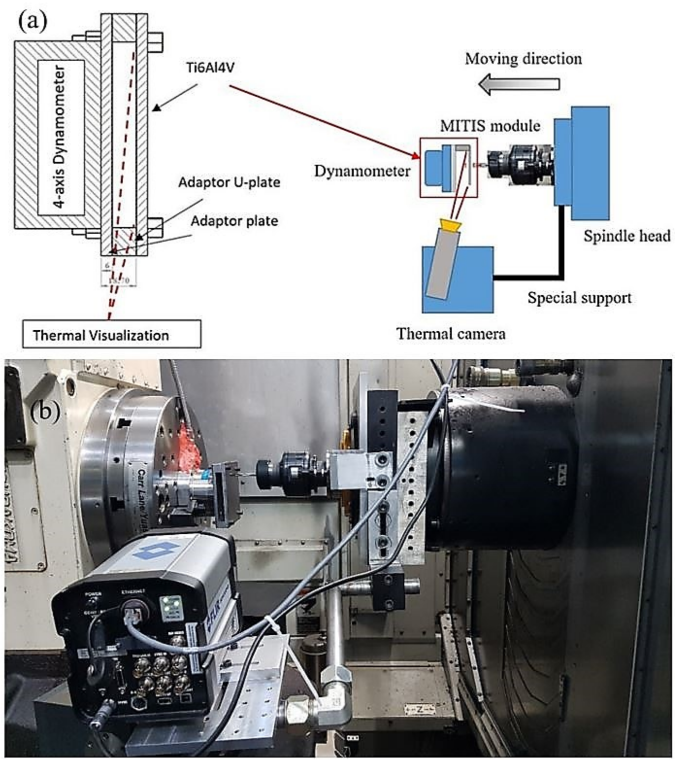


**Figure 2-1:** Cutting experimental setup (a) schematic diagram (b) clamping system for workpiece material and thermal camera.

An OSG 6 mm diameter WC twist drill with 118° point angle and 20° helix angle was used for the test matrix. The 6 mm drill diameter was selected since it is commonly used in the aerospace industry. A new drill bit was used for each three drilled hole to neutralize the tool wear effect. The Ti6Al4V titanium alloy plate thickness is 6.75 mm and the chemical composition of the plate is the same as the wrought Ti6Al4V. The Ti6Al4V plate was produced according to grade 5 standard procedure.

## 2.3 Effect of VAD kinematics on chip formation

A kinematic model based on equations (2.1-3), was developed to determine the effect of the LF-VAD parameters on the time-varying chip size, namely, the chip radian and the uncut chip thickness. The direct relationship between the chip size and the cutting energy (forces and temperature) was used to relate the process kinematics to the obtained microstructure, surface microcracks formation and residual stresses. In the developed kinematic model, the following equations represent the instantaneous cutting edges positions in VAD [18, 20]:

$$Z_1 = \frac{\gamma}{360^\circ} * f + A * \sin(\gamma * F) \tag{2.1}$$

$$\mathrm{Z}_2 = \frac{(\gamma - 180^\circ)}{360^\circ} * \mathrm{f} + \mathrm{A} * \sin[\,(\gamma - 180) * \mathrm{F}] \tag{2.2}$$

The dynamic uncut chip thickness could be expressed as:

$$t_o = \begin{cases} Z(\gamma) - \max\big(Z_k(\gamma)\big) & , \; Z(\gamma) > \max\big(Z_k(\gamma)\big) \\ 0 & , \; otherwise \end{cases} \tag{2.3}$$

Where max ($Z_k(\gamma)$) represents the maximum height of the preceding rotation.

Based on equation (2.3), for the investigated parameter ranges ($f$=0.025-to-0.075mm/rev and $A_m$ =0.07-to–0.48 mm), the dynamic uncut chip thickness showed a linearly increasing behavior with the modulation amplitude until $A_m$= 1.12$f$, where it plateaued to a constant value. Such trends were found to be consistent with other investigations on LF-VAD of Al and Ti materials [18, 23]. Figure 2-2, illustrates the effect of the modulation amplitude on the actual feed, that represents the maximum per tooth for *f*=0.075 mm/rev. The actual feed is The profiles were calculated assuming steady state cutting, which takes place starting from the fourth tool rotation. For low modulation amplitude, the actual uncut chip thickness showed a gradual increase till a certain point (uncut chip thickness < double the programmed feed) after which it declined gradually. For high $A_m$, the actual uncut chip thickness experienced a sudden increase to the maximum value ($t_o=2f$) for a relatively wide interval followed by a sudden reduction. This behaviour has a significant impact on the chip morphology as will be presented in section 2.4.1. Moreover, increasing $A_m$ shifted the cutting start point, which reduced the chip radian and consequently, the chip evacuation effectiveness enhances.

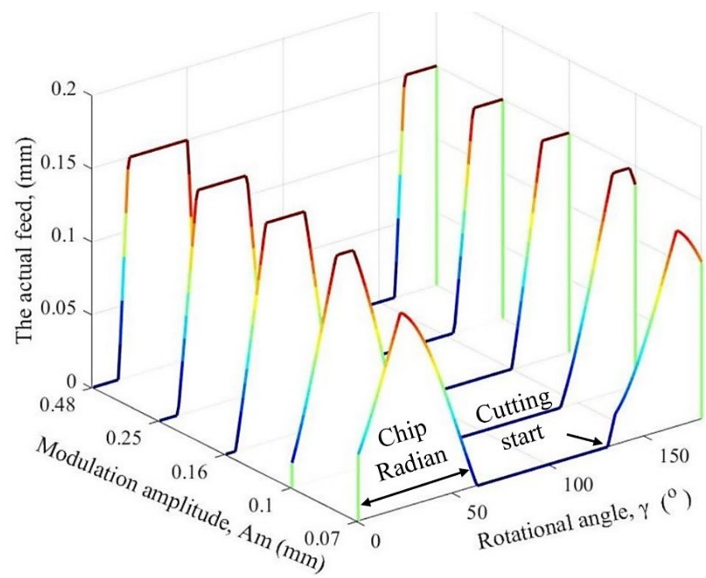


**Figure 2-2:** The effect of LF-VAD modulation amplitude and rotational angle on the actual feed profile.

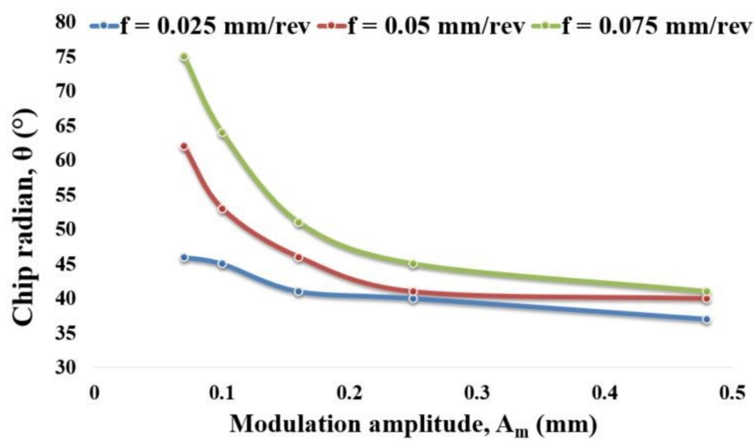


**Figure 2-3:** The effect of LF-VAD amplitude on the chip radian.

The results shown in Figure 2-3, demonstrate a significant reduction in the chip radian at $A_m < 0.2$ mm, while such reduction rate declined at higher $A_m$. The chip radian reduction changed from 22.9% to be 45.33% under 0.025 and 0.075 mm/rev feed rate, respectively. Consequently, the use of LF-VAD is more effective during the higher feed. Lower chip radian leads to effective chip evacuation, as mention in [18]. However, LF-VAD with $A_m \leq 0.25$ mm, is a recommended range to achieve the chip radian reduction and reduce the negative effect of the dynamic component, as will be described in section 2.3.1.

### 2.3.1 Material and machine Effect of VAD kinematics on the mechanical load

Figure 2-4 shows the effect of LF-VAD modulation amplitude on the duty cycle based on the instantaneous tool displacement and velocity. The figure shows that the maximum tool displacement took place at zero tool velocity, while increasing the amplitude shifted the cutting starting point. This shift can show a significant effect on the duty and cooling cycles, as will be presented in section 2.3.2. Figure 2-4 shows that increasing the modulation amplitude produced the following effects:

- Reducing the duty cycle duration ($t_D$).
- Increasing the tool velocity variation range by 560% (from a range between -2,925 3,080 mm/min to a range between -17,469 and 16,150 mm/min at $A_m$ = 0.07 mm and 0.48 mm, respectively). This significant increase in the tool velocity is adding a dynamic component to the thrust force, as will be described in section 2.4.2.

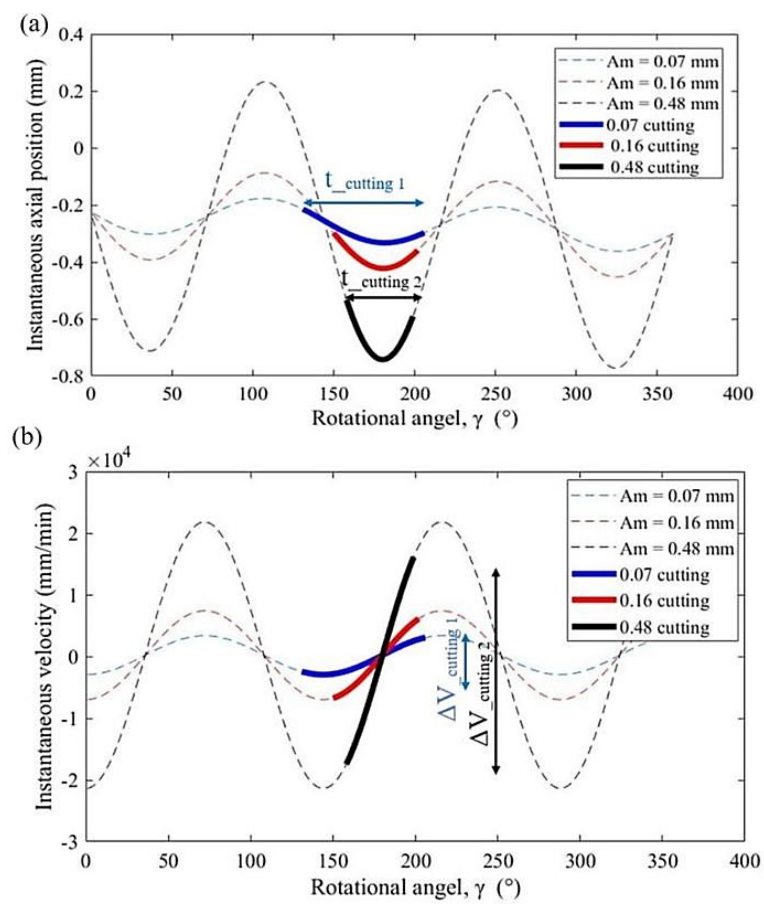


**Figure 2-4:** Effect of LF-VAD modulation amplitude on (a) the cutting duration and (b) the cutting edge velocity.

Based on the theoretical study of the actual feed and the dynamic component, VAD can show a higher mechanical load compared to conventional drill, as will be described in section 2.4.2.

## 2.3.2 Effect of VAD kinematics on the thermal load

### *2.3.2.1 Heat generation and dissipation cycles.*

Based on the cutting profile analysis, Figure 2-5 shows the effect of $A_m$ on the generated heat flux and the duration of the heat generation and dissipation cycles associated with the superimposed harmonic motion in LF-VAD. Based on the presented intervals and the cutting speed, the effect of modulation amplitude on the duty (heating interval) and cooling cycles can be calculated. Figure 2-6, shows the effect of modulation amplitude on both duty and cooling cycles at different feed. Increasing the modulation amplitude resulted in reducing $t_D$ by 45% from 4.2 ms to 2.3 ms at $A_m$=0.07mm, and 0.48 mm, respectively. This reduction has a direct impact on reducing the total amount of heat flux during the duty cycle. A thermal load investigation during the milling process [24], showed that decreasing the duty cycle ($t_D$) has a higher impact on the total cutting zone temperature compared to the cooling cycle. On the other hand, the cooling cycle was also increased by 47% from 3.8 ms to 5.7 ms at $A_m$ = 0.07 mm and 0.48 mm $A_m$, respectively, which also results in increasing the total amount of heat dissipated during the cooling regime. The benefit of LFVAD on the duty and cooling cycle is more significant at the higher feed. Further increase of the modulation amplitude ($A_m \geq 0.25$ mm) resulted in negligible effects on both intervals, which attributed to the limited effect on the chip radian, as showed in Figure 2-3.

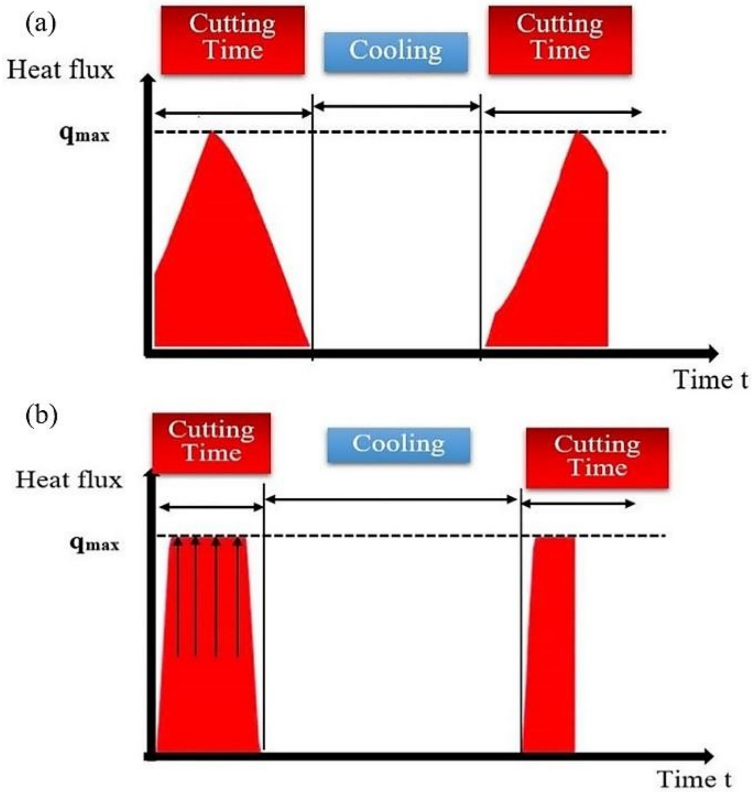


**Figure 2-5:** Effect of LF-VAD modulation amplitude on the heating cycle using 0.075 mm/rev feed rate, for (a) $A_m$ = 0.07 mm (b) $A_m$ = 0.48mm.

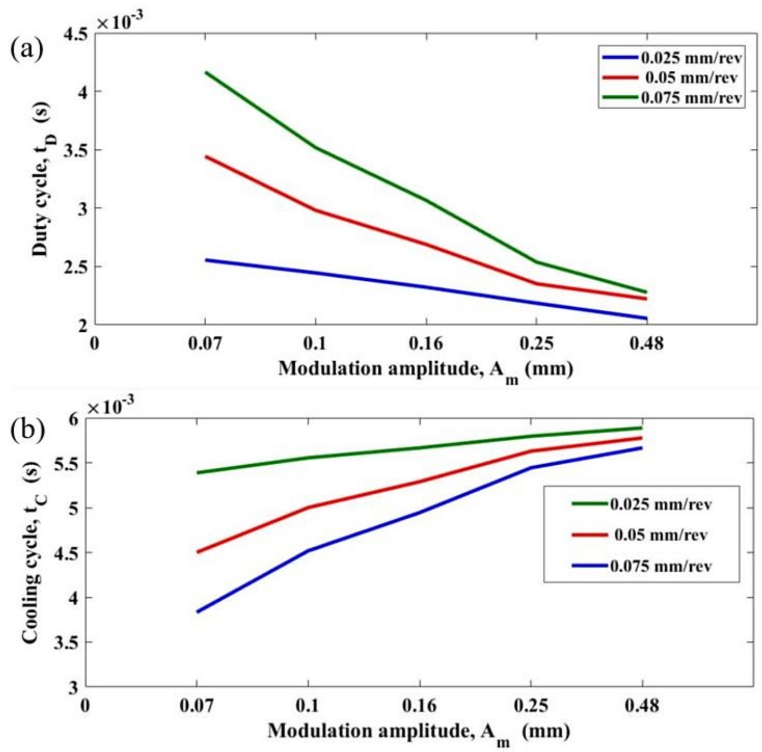


**Figure 2-6:** Effect of the LF-VAD modulation amplitude on the (a) Duty cycle and (b) cooling cycle durations.

Based on the theoretical study of VAD on the duty and separation time (cutting and cooling interval), VAD can show a lower thermal load compared to the conventional drill, as will be described in section 2.4.3.

## 2.4 Results and discussion

### 2.4.1. Chip morphology

Based on the theoretical chip geometry Figure 2-3, the chip radian was reduced by 22.9% with increasing the modulation amplitude. Microscopic examination of the chips collected after machining, illustrated the chip radian reduction, as shown in Figure 2-7. The chip width decreased from 1200 μm to 880 μm at $A_m$ = 0.07 mm and 0.48 mm, respectively. The measured chip radian showed a 26.6% reduction with increasing the modulation amplitude.

Figure 2-8 confirms the effect of modulation amplitude on the uncut chip thickness profile (in Figure 2-2). The cases of lower and higher amplitude ($A_m$ = 0.07 and 0.48 mm) shown in Figure 2-8 (a and b) reflect the same geometry shown in the Scanning electron microscopic (SEM) images of the chips, in Figure 2-8 (c and d). At LF-VAD with $A_m$=0.48mm showed a significant change of the uncut chip thickness which takes place in the middle of the cutting process, followed by a sudden decrease. Chips formed using $A_m$= 0.07 mm showed a smoother change of chip profile. This change in the chip morphology confirms the higher mechanical load during VAD, and consequently, higher cutting forces compared to conventional drill, which agrees with the theoretical study described in section 2.3.1.

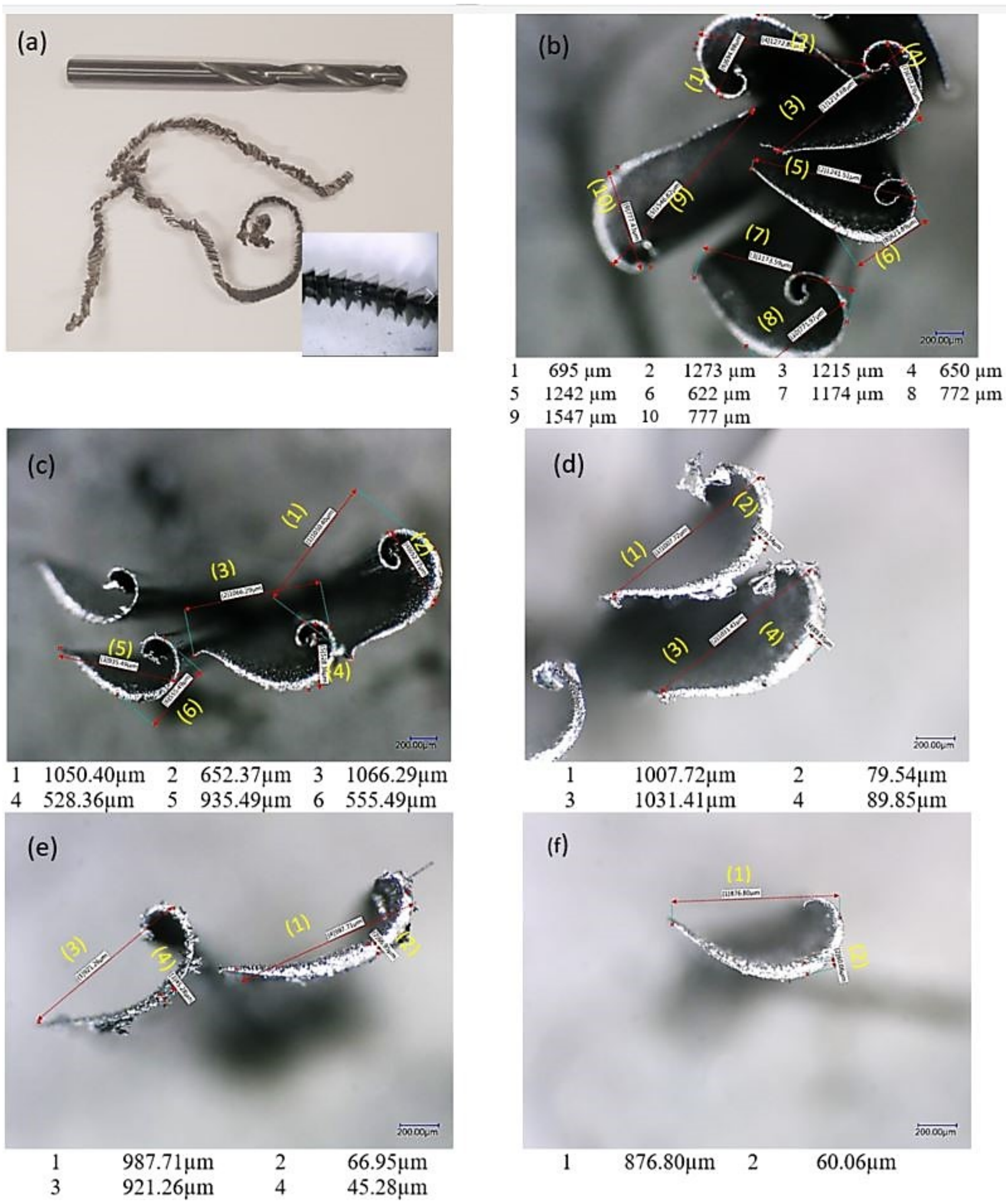


**Figure 2-7:** Effect of LF-VAD module amplitude on the Ti6Al4V chip morphology (a) Conventional, (b) $A_m$ = 0.07 mm, (c) $A_m$ = 0.1 mm, (d) $A_m$ = 0.16 mm, (e) $A_m$ = 0.25 mm, and (f) $A_m$ = 0.48 mm.

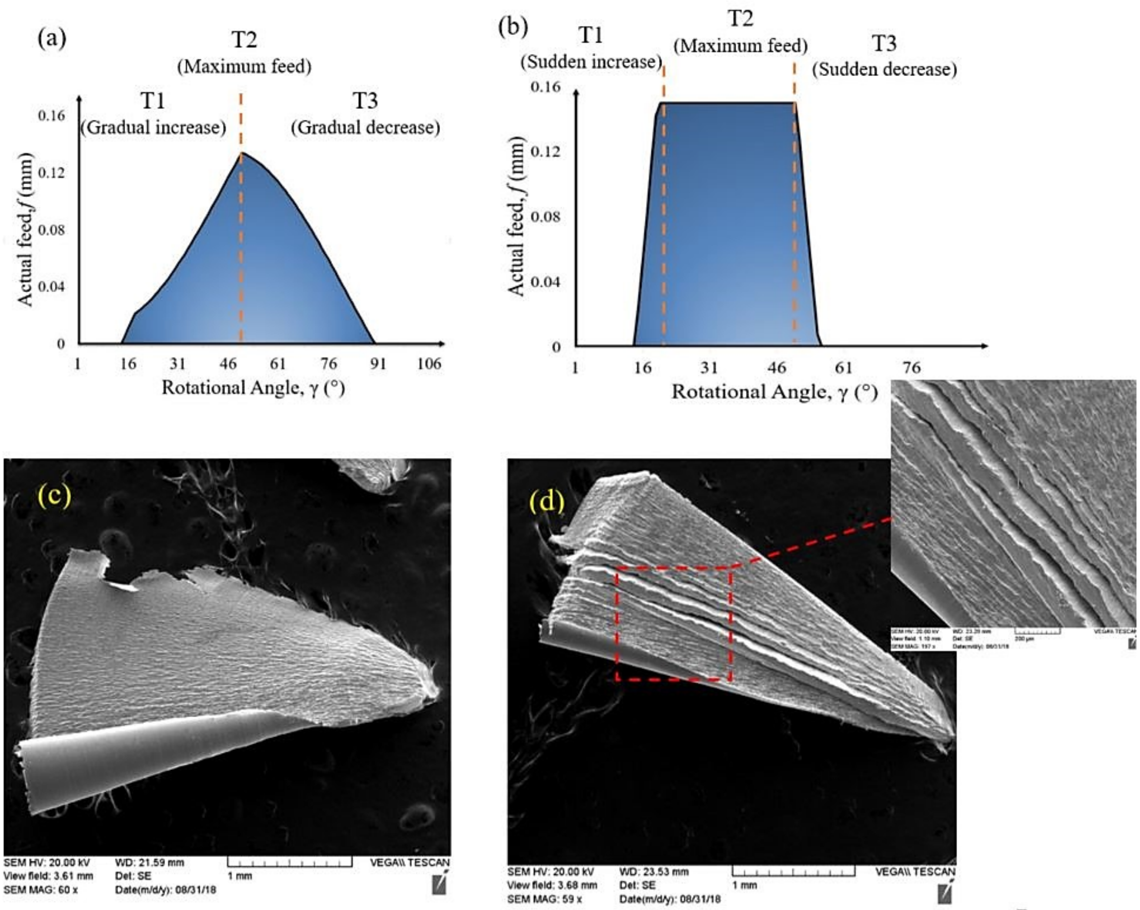


**Figure 2-8:** Effect of LF-VAD modulation amplitude on the chip microstructure for (a) $A_m = 0.07mm$ and (b) $A_m = 0.48mm$.

Figure 2-9, presents the influence of lower cutting temperature and the resulting improved chip evacuation effectiveness of LF-VAD on the chip back surface, compared to the conventional drill. SEM chip back surface examination of LF-VAD showed a smooth surface without any observation of scratch marks or adhesion defect, as shown in Figure 2-9 (b). On the other hand, higher cutting temperature with poor chip evacuation in conventional drilling showed significant scratch marks, and severe material adhesion, as shown in Figure 2-9 (a). The marks observed indicate an adverse effect on tool life as well.

High cutting temperature, and chips jamming result in chip-tool welding, as observed during the conventional drilling (Figure 2-10).

The SEM examination of chip back surface and the observation of tool-chip welding criteria confirm the effect of VAD on the thermal load reduction shown in section 2.3.2.

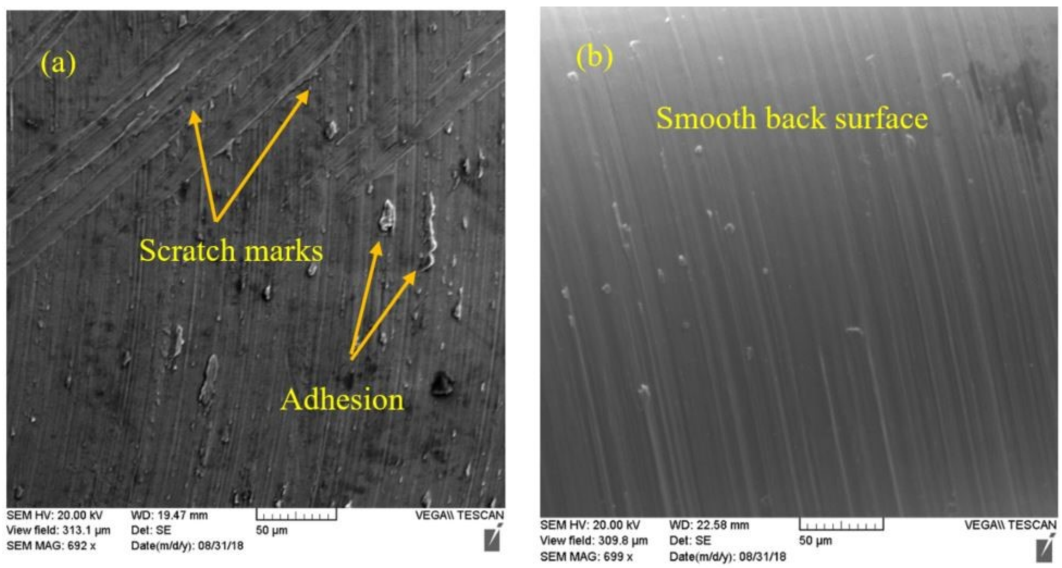


**Figure 2-9:** The effect of LF-VAD on the chip back surface for (a) Conventional (b) LF-VAD $A_m$ = 0.07mm.

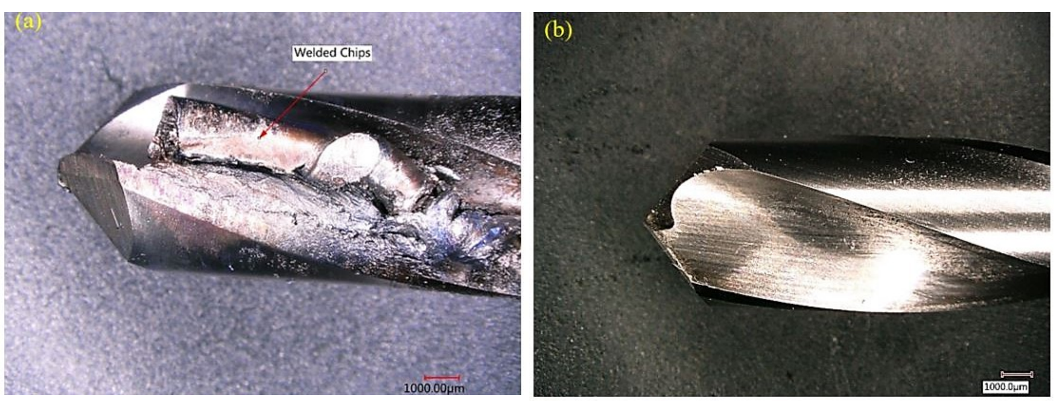


**Figure 2-10:** Effect of cutting technique on the cutting tool during Ti6Al4V drilling for (a) Conventional (b) LF-VAD.

### 2.4.2. The effect of LF-VAD on thrust force.

The thrust forces generated during Ti6Al4V drilling operation were recorded for both LF-VAD and CD for different machining parameters. The force signal recorded was used on a developed MATLAB for conversion to the frequency domain. The frequency content of the measured force signals was verified via the FFT of such signals. The measured frequency was found to be identical to the applied frequency for both cutting speeds (83.33 Hz for 37.68 m/min and 125 Hz for 56.52 m/min) with an accuracy of 98 %.

Figure 2-11 shows the effect of modulation amplitude on the measured thrust force. For all machining conditions, LF-VAD has shown a higher thrust force (mechanical load), compared to the CD under the same feed and rotational speed, which agrees with section 2.3.1. This increase can be attributed to the following:

- The increased actual uncut chip thickness by 100% in LF-VAD, agree with Figure 2-2.
- The dynamic force component associated with the tool impact, agree with Figure 2-4 (b).

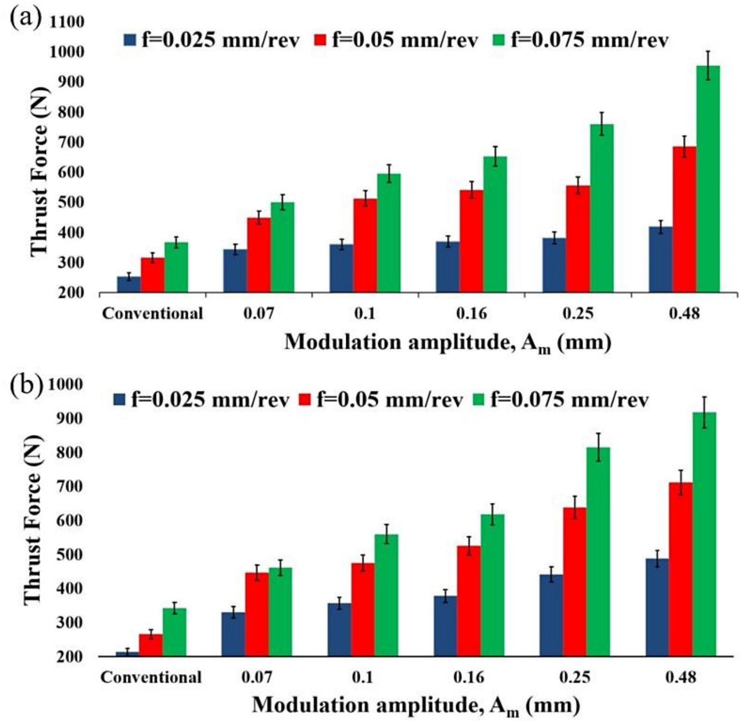


**Figure 2-11:** Effect of LF-VAD modulation amplitude and feed rate on the thrust force for (a) *N*= 37.68 m/min (b) *N*= 56.52 m/min.

### 2.4.3. Effect of LF-VAD on tool temperature.

Figure 2-12 shows the drilling tool tip temperature at the hole exit surface. LF-VAD resulted in an apparent thermal load reduction under all investigated machining parameters, agree with the theoretical study as shown in section 2.3.2. The tool-tip temperature behavior could be described as follows:

- Chip segmentation combined with axial tool oscillation, enhances the chip evacuation efficiency, which reduces the temperature [25].
- Increasing the modulation amplitude has a positive effect through reduces the duty cycle and increases the cooling cycle.

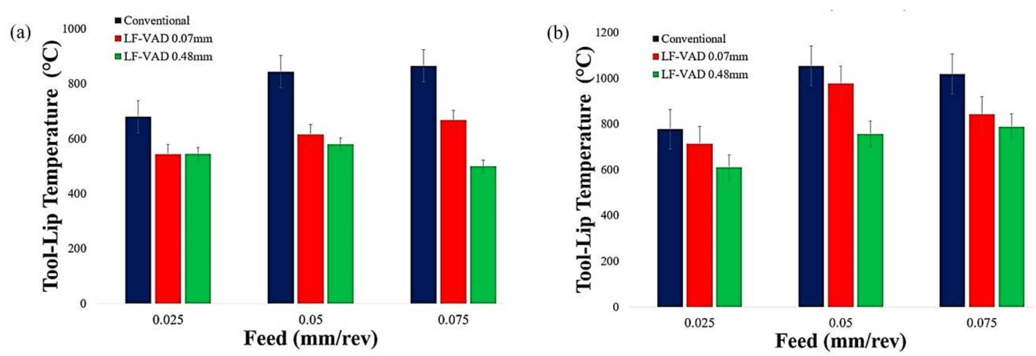


**Figure 2-12:** Effect of Cutting Technique and Am on the Ti6Al4V Cutting tool temperature.

### 2.4.4. Hole quality and surface integrity

*2.4.4.1. Hole size error*

The measured hole size accuracy for both conventional and LF-VAD at different machining conditions was assessed according to the standard tolerance grades ISO 286 [26]. Proper chip evacuation mechanism and low cutting temperature are of the main LF-VAD advantages, that reduced the hole tolerance grade from IT10 grade (48 µm - 75µm) for conventional, to IT9 grade (30 µm – 48 µm) for LF-VAD.

*2.4.4.2. Surface roughness*

The surface roughness ($R_a$) was measured for both conventional and LF-VAD at different machining conditions. Higher cutting speed (*N*=3000 rpm) showed a higher Ra for both techniques. However, LF-VAD showed a lower Ra for all machining parameters. The CD and LF-VAD resulted in Ra > 2 µm and Ra≤ 1.5 µm, respectively. This enhancement can be attributed to the improved chip evacuation, which reduces the machined surface scratching.

*2.4.4.3. Surface and subsurface examination*

Surface textures formation and subsurface microstructure defects such as severe plastic deformation (SPD) layer and microcracks observation, are of the main challenge during the hard to cut material machining process [27]. The generated heat during cutting combined with a low thermal conductivity of Ti6Al4V concentrates the temperature increase on and near the machined surface, which can lead to phase transformation in this zone in the case of high cooling rates. The high magnification (x1500) optical macroscopic examination of the machined subsurface structure showed two different layers (A and B) that were formed near the machined surface, as shown in Figure 2-13.

- Layer A: Thin white layer mainly attributed to Severe plastic deformation (SPD) and extreme heating and cooling rates. Based on the phase transformation diagram of the $\alpha + \beta$ phase distribution of Ti6Al4V, the formation of white layer martensitic microstructure takes place due to a temperature rise up to $900° C$ followed by a rapid cooling [28]. High tensile residual stresses and the higher tendency of microcrack formation are among the most adverse white layer effects. Consequently, the white layer is more susceptible to fatigue failure [29, 30].
- Layer B: Plastic deformation layer: Formed due to the high plastic deformation, that rotates the orientation of the microstructure grain boundaries and elongates the grains into a specific crystallographic direction aligned with the machining stress direction, causing anisotropic behavior. A portion of the machining stress is stored in the material structure in the form of residual stress. Based on that, if the mechanical stress was dominant then the residual stresses

is compressive, while if the dominant stress is thermal the residual stress is tensile [31]. However, the deformed grain is adding some limitation for microcrack initiation or growing in the normal direction to the machined surface.

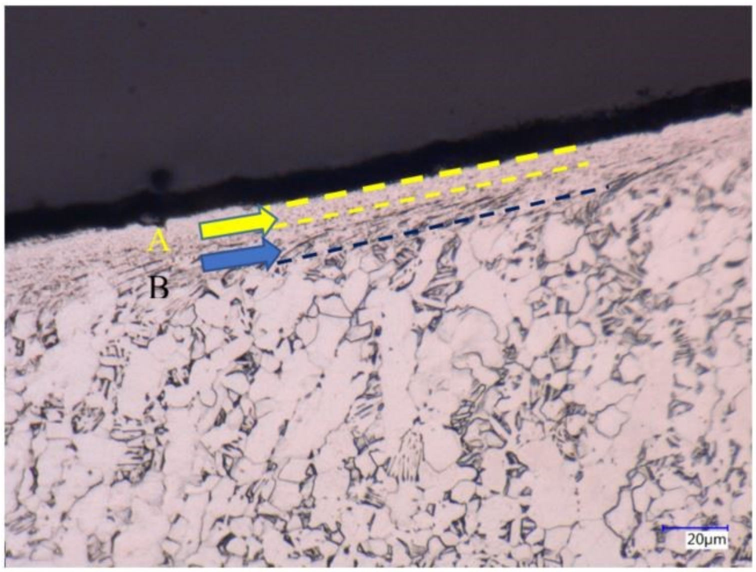


**Figure 2-13:** Microscopic examination of a subsurface machined surface.

Figure 2-14 shows the microstructure examination of the conventional drilled process for a different machining parameter. The white layer observation demonstrates the dominant effect of an extreme thermal load. Figure 2-14 (a) shows that the total affected layer thickness at feed=0.025 mm/rev and $N$ = 37.68 m/min was 21 μm (thicknesses of layers 'A' and 'B' were 5 μm and 16 μm, respectively). For the same feed at a higher speed ($N$ = 56.52 m/min), the total affected layer thickness was 20 μm (thicknesses of layers 'A' and 'B' were 7 μm and 13 μm, respectively) as shown in Figure 2-14 (c). The increase in the thickness of layer 'A' can be attributed to the higher cutting temperature induced by higher cutting speed (see Figure 2-12). Figure 2-14 (b) shows the total affected layer thickness at feed = 0.075 mm/rev and $N$ = 37.68 m/min was 18 μm (Layer 'A' = 6 μm and 12 μm Layer 'B'). For the same feed at a higher speed (*N* = 56.52 m/min), the total affected layer thickness was 29 μm (Layer 'A' = 10 μm and 19 μm Layer 'B'), as shown in Figure 2-14 (d). Figure 2-15 shows that the conventionally drilled material experienced surface notches due to higher cutting temperature and poor chip evacuation mechanism, as well as the tensile residual stress, which will be shown in the next section.

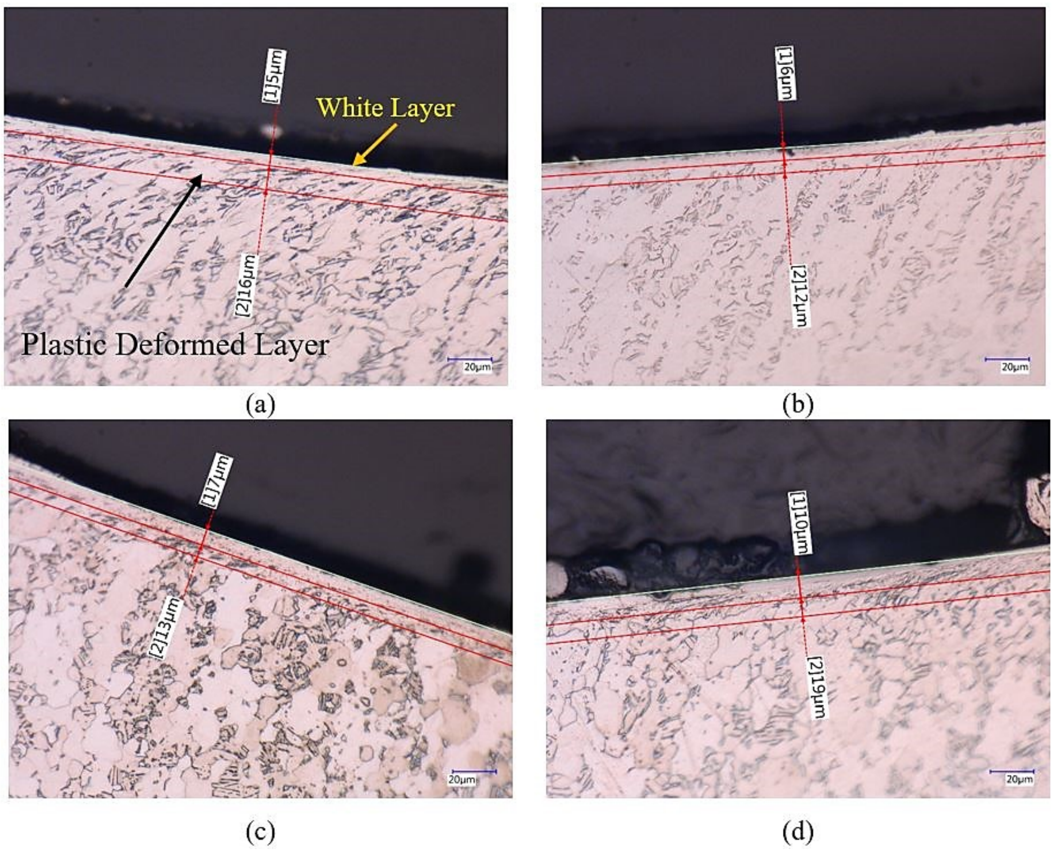


**Figure 2-14:** Subsurface examination of conventional drill process for a different feed (a,c) 0.025 mm/rev and (b,d) 0.075 mm/rev with different cutting speed (a,b) 37.68 m/min and (c,d) 56.52 m/min.

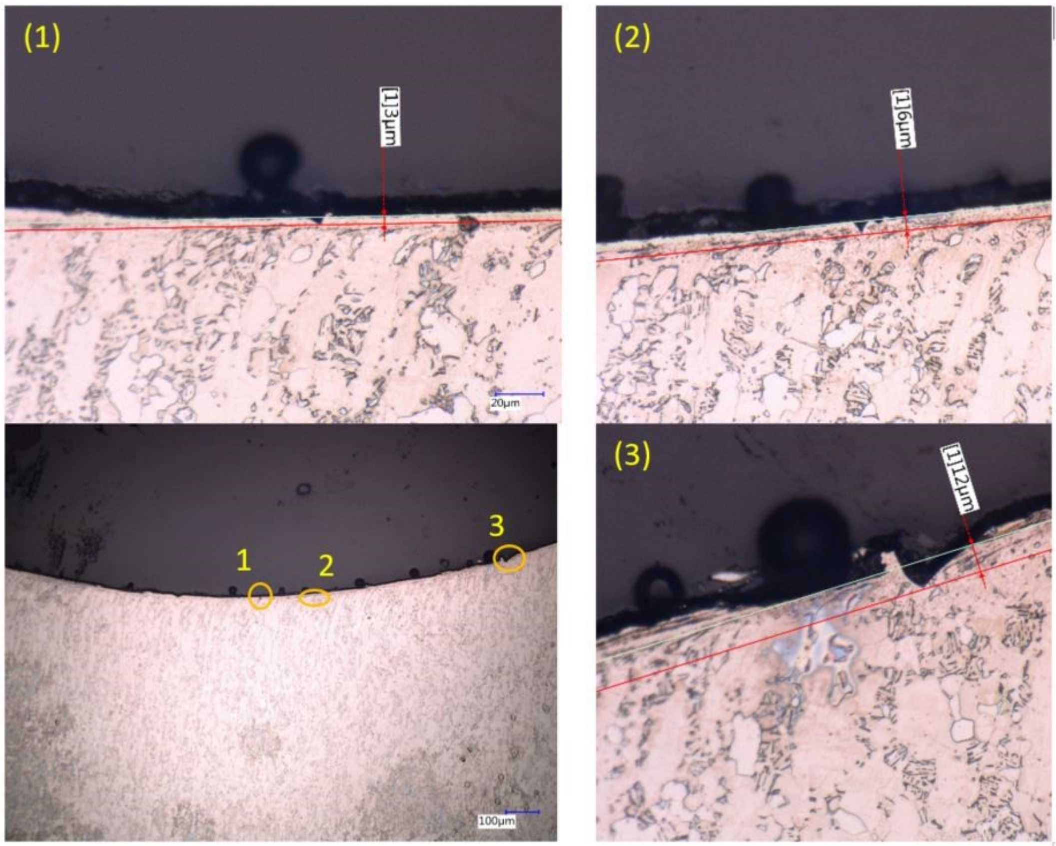


**Figure 2-15:** Surface defects in CD at $f$=0.025 mm/rev and $N$ = 56.52 m/min.

All the tested LF-VAD machining conditions have shown a significant enhancement in the subsurface quality compared to CD. This is mainly due to the thermal load reduction, lower tool-workpiece contact time, chip segmentation, and effective chip evacuation, agree with section 2.3.2, 2.4.1, and 2.4.3.

Figure 4-16 shows such enhancement in the subsurface quality in LF-VAD at the higher feed, for different amplitudes and cutting speed. Figure 4-16 (a) shows non-defect subsurface for LF-VAD with low modulation amplitude ($A_m$ = 0.07) at $f$ = 0.075 mm/rev and $N$ = 37.68 m/min. For the higher cutting speed ($N$ = 56.52 m/min) and the total affected layer thickness was 18 µm (thickness of layer 'A' and 'B' were 0 µm and 18 µm, respectively), as shown in Figure 4-16. Figure 4-16 (b) shows the affected layer thickness of LF-VAD with high modulation amplitude ($A_m$ = 0.48) was 18 µm (thickness of layer 'A' and 'B' were 8 µm and 10 µm, respectively). For higher cutting speed ($N$ = 56.52 m/min) the total affected layer was 28 µm (thickness of layer 'A' and 'B' were 8 µm and 20 µm, respectively) for $N$ = 37.68 m/min, and $N$ = 56.52 m/min, respectively, as shown in Figure 4-16 (d). The observation of layer 'A' and 'B' subsurface defect at higher amplitude attributed to the higher tool axial speed that lead to an increase in the Tool-workpiece friction.

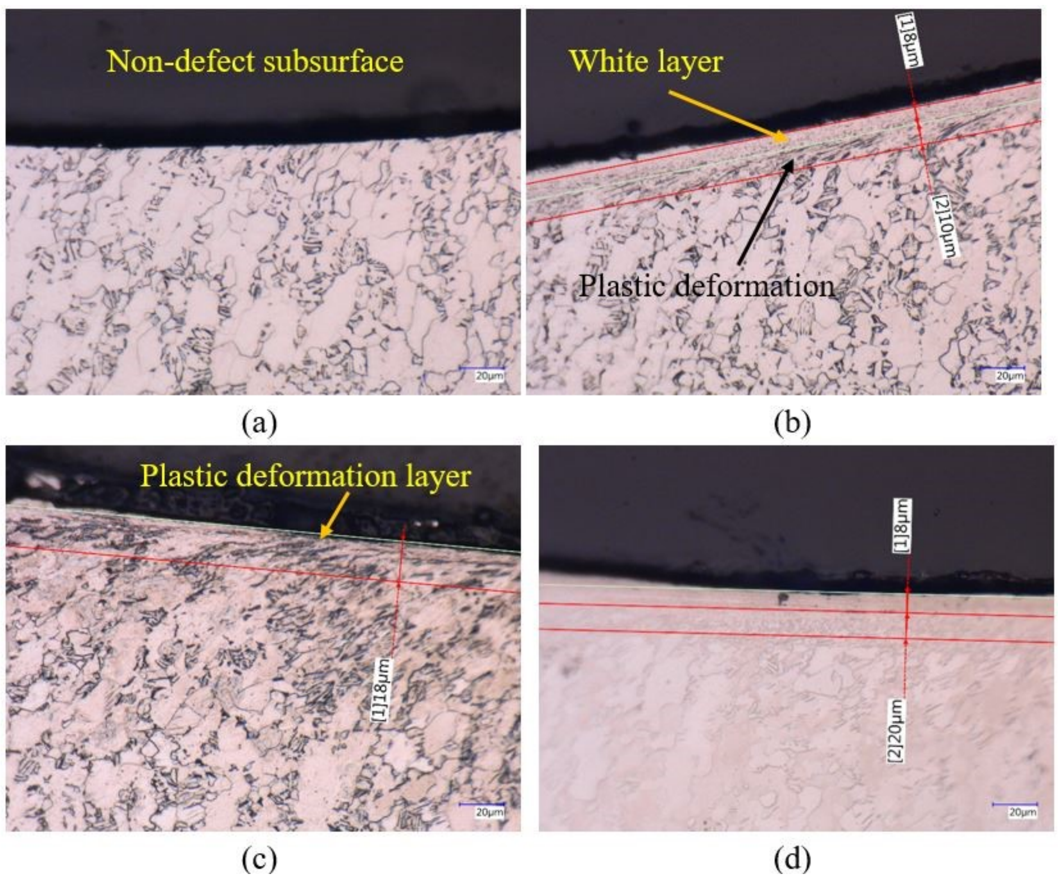


**Figure 2-16:** Subsurface examination of LF-VAD drill process at $f$= 0.075 mm/rev under (a,c) $A_m$ = 0.07 mm and (b,d) $A_m$ = 0.48 mm with different cutting speed (a,b) $N$ = 37.68 m/min and (c,d) $N$ = 56.52 m/min.

### 2.4.5. Residual stresses

Figure 2-17 compares the residual stresses (RS) measured on the wall surfaces of holes produced using CD and LF-VAD at *f* = 0.025 mm/rev and 0.075 mm/rev, $A_m$ = 0.07 mm and 0.48 mm and (a) *N*=37.68 m/min and (b) *N*=56.52 m/min. All the RS were measured at a normal distance of 400 µm from the hole exit surface. All CD and LF-VAD conditions in Figure 2-17 (a) experienced positive (tensile) RS except for the LF-VAD at $A_m$ = 0.48 mm where a negative (compressive) RS was generated. This negative value confirms the significant effect of LF-VAD on reducing the thermal load during the drilling process. Therefore, the dominant effect of mechanical load resulted in compressive residual stress (negative).

The figure also shows that LF-VAD resulted in lower RS compared to CD. This could be related to the LF-VAD enhanced cooling, and chip evacuation effectiveness, which was found to further improve at higher $A_m$, as was shown in sections 2.3.2 and 2.4.1. Higher cutting feed increased the residual stress for CD and LF-VAD. Figure 2-17 (a) and (b) shows higher tensile surface RS with *N* = 56.52 m/min compared to *N* = 37.68 m/min, which could also be attributed to the higher temperature associated with higher rotational speed as shown in section 2.4.3.

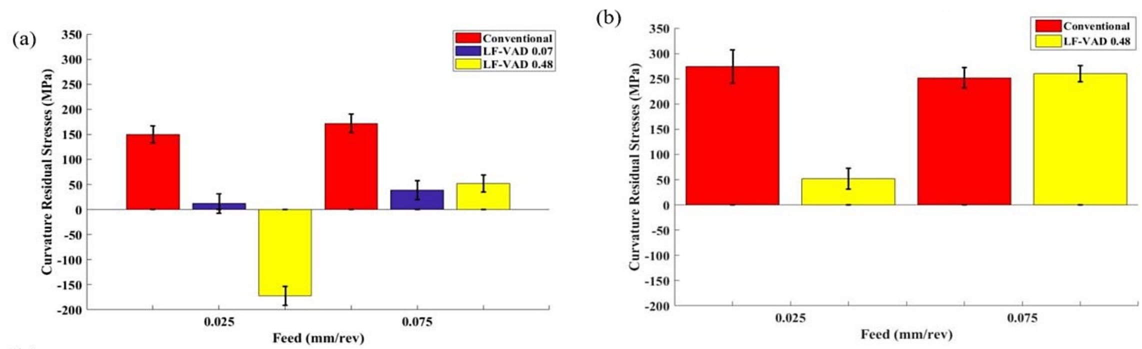


**Figure 2-17:** Surface residual stresses in CD and LF-VAD at (a) $N$=37.68 m/min (b) $N$=56.52 m/min.

Due to the observed RS sign inflection in the case of LF-VAD with $A_m$ = 0.48 mm, further investigation of this case was conducted on the RS distribution below the surface until a depth of 0.45 mm. Based on the subsurface examination, Table 2-1 shows the affected layer thickness at high feed (0.075 mm/rev) and low cutting speed conditions for CD, LF-VAD with $A_m$ = 0.07 mm, and 0.48 mm. The white layer observation at CD and LF-VAD with $A_m$ = 0.48 mm is an evidence of a higher thermal load. However, the surface residual stresses measurement on white layer cannot indicate the real residual stress of the material [32].

**Table 2-1:** Effect of modulation amplitude on the surface defect.

| | layer 'A' | layer 'B' |
|---|---|---|
| Conventional | 6 µm | 12 µm |
| LF-VAD $A_m$ = 0.07mm | ---- | ---- |
| LF-VAD $A_m$ = 0.48mm | 8 µm | 10 µm |

Figure 2-18 compares the subsurface residual stresses measurement of LF-VAD at $A_m$ = 0.07 mm and 0.48 mm and CD at $N$ = 37.68 m/min and feed = 0.075 mm/rev. The figure shows that the LF-VAD at $A_m$ = 0.48 mm and the CD showed a residual stress change at a depth of 20 µm, while LF-VAD at $A_m$ = 0.07 mm did not experience any change. This observation is matching with the white layer observation, as shown in Figure 2-16 (a, b). Moreover, LF-VAD leads to a significant increase in the compressive residual stresses to reach -242 MPa at a depth of 93 µm, which enhances the bearing fatigue life of the machined part [32]. The significant effect of LF-VAD on residual stresses measurement agrees with the results reported in [33].

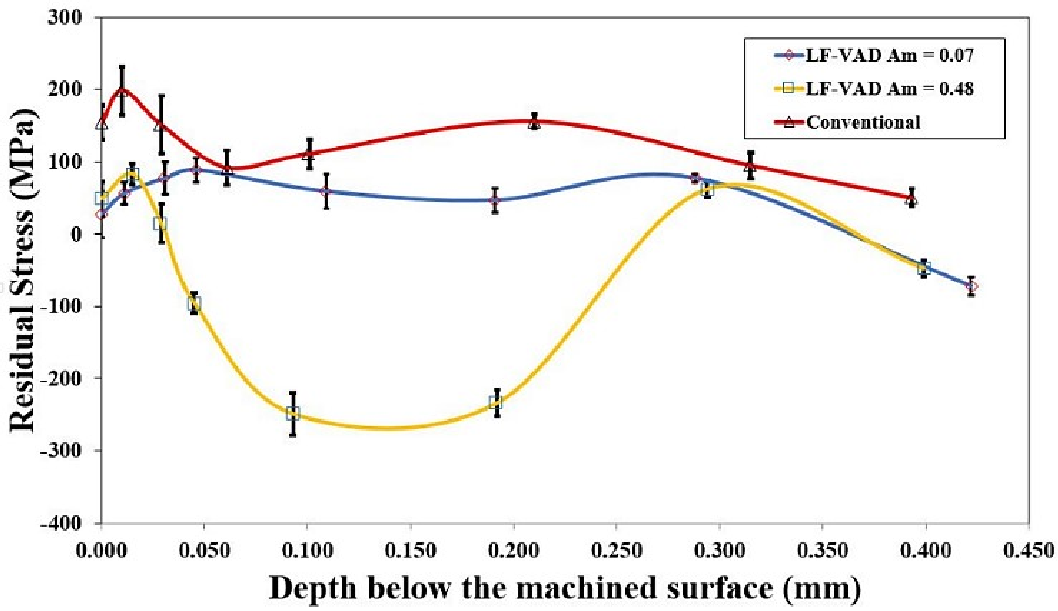


**Figure 2-18:** The subsurface residual stresses measurement of LF-VAD with $A_m$ = 0.07 and 0.48mm compared to CD at *f*=0.075 mm/rev and *N*=37.68 m/min.

## Conclusions

Kinematics of chip formation were used to study the effect of LF-VAD machining parameters on the chip geometry (uncut chip thickness and the chip radian). Higher modulation amplitude increased the uncut chip thickness to be twice the programmed feed rate, which affects the cutting energy ( cutting forces and temperature). A fully factorial design of experiments was implemented to investigate the performance of LF-VAD. The main experimental observation are:

- Higher modulation amplitude showed a direct impact on the amount of applied force to the cutting system as an effect of the higher periodical tool impact energy.
- LF-VAD showed a significant reduction in the cutting process temperature by switching from continuous to interrupting cutting.
- Higher modulation amplitude showed a positive effect on both duty and cooling cycles.
- A significant reduction of up to 35.8% in the tool-tip temperature has been observed by using the LF-VAD technique.
- The resulting chip evacuation mechanism enhanced the drilled hole size error, reaching IT9 on the standard tolerance grades combined with more than 50% reduction in the hole surface roughness (at 0.16mm modulation amplitude).
- LF-VAD with lower modulation amplitude led to elimination or a significant reduction on the surface and subsurface defects (SPD and deformed layer thickness), for all test conditions. Consequently, a higher fatigue life could be achieved.
- LF-VAD induced compressive residual stress when a higher modulation amplitude applied.
- The compressive residual stresses reached 242 MPa at a depth of 93 μm (at 0.48mm amplitude).

## References

[1] Z. Li, D. Zhang, X. Jiang, W. Qin, and D. Geng, "Study on rotary ultrasonic-assisted drilling of titanium alloys (Ti6Al4V) using 8-facet drill under no cooling condition," *The International Journal of Advanced Manufacturing Technology,* vol. 90, pp. 3249-3264, 2017.

[2] K.-H. Park, A. Beal, P. Kwon, and J. Lantrip, "Tool wear in drilling of composite/titanium stacks using carbide and polycrystalline diamond tools," *Wear,* vol. 271, pp. 2826-2835, 2011.

[3] W.-C. Chen, "Some experimental investigations in the drilling of carbon fiber-reinforced plastic (CFRP) composite laminates," *International Journal of Machine Tools and Manufacture,* vol. 37, pp. 1097-1108, 1997.

[4] D. Dornfeld, J. Kim, H. Dechow, J. Hewson, and L. Chen, "Drilling burr formation in titanium alloy, Ti-6AI-4V," *CIRP Annals-Manufacturing Technology,* vol. 48, pp. 73-76, 1999.

[5] I. S. Shyha, S. L. Soo, D. K. Aspinwall, S. Bradley, R. Perry, P. Harden*, et al.*, "Hole quality assessment following drilling of metallic-composite stacks," *International Journal of Machine Tools and Manufacture,* vol. 51, pp. 569-578, 7// 2011.

[6] P. Zhang, N. Churi, Z. J. Pei, and C. Treadwell, "Mechanical drilling processes for titanium alloys: a literature review," *Machining Science and Technology,* vol. 12, pp. 417-444, 2008.

[7] J. Pujana, A. Rivero, A. Celaya, and L. L. de Lacalle, "Analysis of ultrasonic-assisted drilling of Ti6Al4V," *International Journal of Machine Tools and Manufacture,* vol. 49, pp. 500-508, 2009.

[8] J. L. Cantero, M. M. Tardío, J. A. Canteli, M. Marcos, and M. H. Miguélez, "Dry drilling of alloy Ti–6Al–4V," *International Journal of Machine Tools and Manufacture,* vol. 45, pp. 1246-1255, 2005/09/01/ 2005.

[9] S. Sharif and E. A. Rahim, "Performance of coated- and uncoated-carbide tools when drilling titanium alloy—Ti–6Al4V," *Journal of Materials Processing Technology,* vol. 185, pp. 72-76, 4/30/ 2007.

[10] S. Y. Hong, Y. Ding, and W.-c. Jeong, "Friction and cutting forces in cryogenic machining of Ti–6Al–4V," *International Journal of Machine Tools and Manufacture,* vol. 41, pp. 2271-2285, 2001.

[11] M. I. Sadik and G. Grenmyr, "Application of different cooling strategies in drilling of metal matrix composite (MMC)," in *Materials Science Forum*, 2016, pp. 3-12.

[12] A. Sadek, "Vibration Assisted Drilling of Multidirectional Fiber Reinforced Polymer Laminates," Ph.D. Thesis, McGill University Libraries, 2014.

[13] V. I. Babitsky, A. N. Kalashnikov, and F. V. Molodtsov, "Autoresonant control of ultrasonically assisted cutting," *Mechatronics,* vol. 14, pp. 91-114, 2004/02/01/ 2004.

[14] H. Paris, D. Brissaud, A. Gouskov, N. Guibert, and J. Rech, "Influence of the ploughing effect on the dynamic behaviour of the self-vibratory drilling head," *CIRP Annals,* vol. 57, pp. 385-388, 2008/01/01/ 2008.

[15] Z. Deyuan and W. Lijiang, "Investigation of chip in vibration drilling," *International Journal of Machine Tools and Manufacture,* vol. 38, pp. 165-176, 1998.

[16] Y. Guo and J. B. Mann, "Experimental Evaluation of Cutting Kinematics and Chip Evacuation in Drilling With Low-Frequency Modulation-Assisted Machining," in *ASME 2017 12th International Manufacturing Science and Engineering Conference collocated with the JSME/ASME 2017 6th International Conference on Materials and Processing*, 2017, pp. V001T02A017-V001T02A017.

[17] S. S. F. Chang and G. M. Bone, "Thrust force model for vibration-assisted drilling of aluminum 6061-T6," *International Journal of Machine Tools and Manufacture,* vol. 49, pp. 1070-1076, 2009/11/01/ 2009.

[18] O. Pecat and I. Meyer, "Low frequency vibration assisted drilling of aluminium alloys," in *Advanced Materials Research*, 2013, pp. 131-138.

[19] O. Pecat and E. Brinksmeier, "Low damage drilling of CFRP/titanium compound materials for fastening," *Procedia CIRP,* vol. 13, pp. 1-7, 2014.

[20] A. Sadek, M. Meshreki, and M. Attia, "Effect of Tool Kinematics on the Drilling Forces and Temperature in Low Frequency High Amplitude Vibration Assisted Drilling," in *ASME 2014 International Mechanical Engineering Congress and Exposition*, 2014, pp. V02AT02A035-V02AT02A035.

[21] V. Krishnaraj, R. Zitoune, and F. Collombet, "Comprehensive review on drilling of Multimaterial stacks," *Journal of Machining and Forming Technologies,* vol. 2, pp. 1-32, 2010.

[22] MITIS Engineer. *MITIS Tool Holder*. Available: https://www.mitis.fr/

[23] E. Brinksmeier, O. Pecat, and R. Rentsch, "Quantitative analysis of chip extraction in drilling of Ti 6 Al 4 V," *CIRP Annals-Manufacturing Technology,* vol. 64, pp. 93-96, 2015.

[24] D. Stephenson and A. Ali, "Tool temperatures in interrupted metal cutting," *Journal of Engineering for Industry,* vol. 114, pp. 127-136, 1992.

[25] M. C. Shaw and J. Cookson, *Metal cutting principles* vol. 2: Oxford university press New York, 2005.

[26] E. DIN, "286-2, 2010,"Geometrical product specification (GPS)-ISO system of limits and fits-Part 1: Basis of tolerances, deviations and fits"," ed: Beuth Press.

[27] E. A. H. Kishawy, "Chip formation and surface integrity in high speed machining of hardened steel," 1998.

[28] T. Ahmed and H. Rack, "Phase transformations during cooling in α+ β titanium alloys," *Materials Science and Engineering: A,* vol. 243, pp. 206-211, 1998.

[29] A. Puri and B. Bhattacharyya, "Modeling and analysis of white layer depth in a wire-cut EDM process through response surface methodology," *The International Journal of Advanced Manufacturing Technology,* vol. 25, pp. 301-307, 2005.

[30] A. Hasçalık and U. Çaydaş, "Electrical discharge machining of titanium alloy (Ti–6Al–4V)," *Applied Surface Science,* vol. 253, pp. 9007-9016, 2007/09/15/ 2007.

[31] D. R. Askeland and W. J. Wright, *Science and engineering of materials*: Nelson Education, 2015.

[32] Y. Guo, A. Warren, and F. Hashimoto, "The basic relationships between residual stress, white layer, and fatigue life of hard turned and ground surfaces in rolling contact," *CIRP Journal of manufacturing Science and Technology,* vol. 2, pp. 129-134, 2010.

[33] R. Hussein, A. Sadek, M. A. Elbestawi, and M. H. Attia, "Low-frequency vibration-assisted drilling of hybrid CFRP/Ti6Al4V stacked material," *The International Journal of Advanced Manufacturing Technology,* vol. 98, pp. 2801-2817, October 01 2018.

# Chapter 3

## Chip Morphology and Metallurgical Analysis for Vibration Assisted Drilling of Ti6Al4V

**Complete Citation:**

Hussein, R., Sadek, A., Elbestawi, M.A., Attia, M.H. (2019). Chip Morphology and Metallurgical Analysis for Vibration Assisted Drilling of Ti6Al4V. Submitted to *The International Journal of Advanced Manufacturing Technology*.

**Relative Contributions:**

| | |
|---|---|
| R. Hussein: | Performed experiments, analysis, and data interpretation; wrote the first draft of the manuscript; helped with submitting the final manuscript to the journal (corresponding author). |
| A. Sadek: | Helped with the experiments and analysis; revised the manuscript. |
| M. A. Elbestawi: | Supervisor of R. Hussein. Revised and edited the manuscript and gave the final approval to be submitted. |
| M. H. Attia: | Revised the manuscript. |

**Abstract:**

Vibration-assisted drilling (VAD) of Ti6Al4V is typically used in the aerospace industry to enhance the performance of the machining process. Saw-tooth chip formation is associated with VAD of Ti6Al4V. A comprehensive experimental study is developed to identify and examine the dominant chip formation mechanisms. The results indicate a significant change of the chips free surface produced by VAD. In agreement with the theory of saw-tooth formation due to cyclic crack formation, the scanning electron microscopy (SEM) examination showed a gross crack (GC) and micro crack (MC) along the shear plane. The GC increased from 20 μm for conventional drilling to 224 μm for VAD at the highest amplitude. Moreover, the study presents the influence of VAD on the tool wear mechanisms through the composition analysis of the chips machined surface using Energy Dispersion X-ray Spectroscopy (EDS).

**Keywords:**

Low-frequency vibration-assisted drilling; Ti6Al4V material; Advanced machining; Crack; Chip formation; Chip morphology.

**Abbreviations:**

| | |
|---|---|
| VAD | Vibration assisted drilling |
| LF-VAD | Low frequency-vibration assisted drilling |
| CD | Conventional drilling |
| ASB | Adiabatic Shear Band |
| SB | Shear Band |
| WC | Tungsten carbide |
| SD | Segment degree |
| GC | Gross Crack |
| MC | Micro crack |

**Notations:**

| | |
|---|---|
| $N$ | Cutting speed [rpm] |
| $f$ | Feed rate [mm/rev] |
| $A_m$ | Modulation amplitude [mm] |
| $F$ | Frequency [Hz] |
| $W_f$ | Modulation frequency [oscillation/rev] |
| $h_{max}$ | Maximum saw-tooth height [µm] |
| $h_{min}$ | Minimum saw-tooth height [µm] |
| Lc | Deformed chip length [µm] |
| $S_d$ | Sliding distance [µm] |

## 3.1 Introduction

The critical mechanical characteristics for a load- carrying structure, such as high strength to weight ratio and excellent fatigue life, increased the use of Ti6Al4V to more than 16% of the total weight of an aircraft. Conventional drilling of Ti6Al4V prior to the assembly process poses several challenges such as chip evacuation [1], high cutting temperature, burr formation [2], and high chemical affinity resulting in poor machining quality and productivity [3, 4]. Consequently, several approaches have been devised to enhance Ti6Al4V drilling as it represents an important machining process in the aerospace industry. These approaches were focused on chip evacuation enhancement, which was achieved by using interrupted cutting technology through helical milling [5, 6], and vibration assisted drilling (VAD) [7, 8].

The study of chip formation is essential for better identification of the thermal and mechanical loads during the machining process. Machining of high hardness, low thermal conductivity materials such as titanium alloys [9-12], nickel alloys [13], and hardened steels [14-16] are typically associated with segmented chips. Segmented chips are classified into four types [17], the most important of which for the current study is saw-tooth chip. The study of saw-tooth chips is essential for understanding surface integrity, tool wear, cutting forces and temperature, and residual stresses prediction [18, 19].

The root mechanism of saw-tooth formation was found to be a problematic issue during the machining process of titanium alloys. Thermo-plastic instability was identified as the main causes of the saw-tooth chips. This theory was based on two features as reported in [9, 12]. Firstly, the generation of a chip segment ahead of tool-tip resulting in a higher shear stress along line 5, see Figure 3-1(a). This shear stress keeps increasing until a critical shear strain is reached, where the rate of thermal softening is higher than the rate of strain hardening, in what is known as the thermo-plastic instability phenomenon [20]. As a consequence, surface 2 and 3 will be separated (see Figure 3-1(a)). Secondly, the material phase transformation from the β phase that has a hexagonal close-packed structure (limited number of slip systems) to the α phase having a body-centered cubic structure (more slip systems) as reported in [9]. This phase transformation occurred due to the thermal energy from the plastic deformation and resulted in extended shear strain. Additional experimental studies confirmed thermo-plastic instability as a root cause of saw-tooth chip formation, based on the severe microstructure elongation observed along the shear plane and known as an adiabatic shear band (ASB), as reported in [21-23].

Cyclic crack is the second theory of saw-tooth formation [17, 19], illustrated in Figure 3-1(b). The generation of the chip segment resulted in the movement of point C located on the material free surface towards point D (deck of cards analogy). The proposed movement direction is parallel to the resultant force (R) located at the tool rake face. As a result, a shear crack propagates from point D towards point O at the tool-tip causing the outward sliding movement of the aforementioned segment. At first, the shear crack will be continuous, where the maximum shear stress is combined with a zero normal stress (see the principle stresses diagram Figure 3-1(b)), known as gross crack (GC). As the crack approaches the tool-tip, the normal stress will increase resulting in a discontinuous crack known as micro crack (MC). Following the cyclic crack theory and based on the machined surface irregularities (surface cracks, voids, microscopic ridges, etc.), further studies [15, 24] presented the influence of surface layer energy on the surface crack initiation and propagation direction. Therefore, the main reasons that promote cyclic crack theory are based on the observation of a sharp segment edge and the elongated micro cracks along the shear plane, as reported in [11, 15, 19].

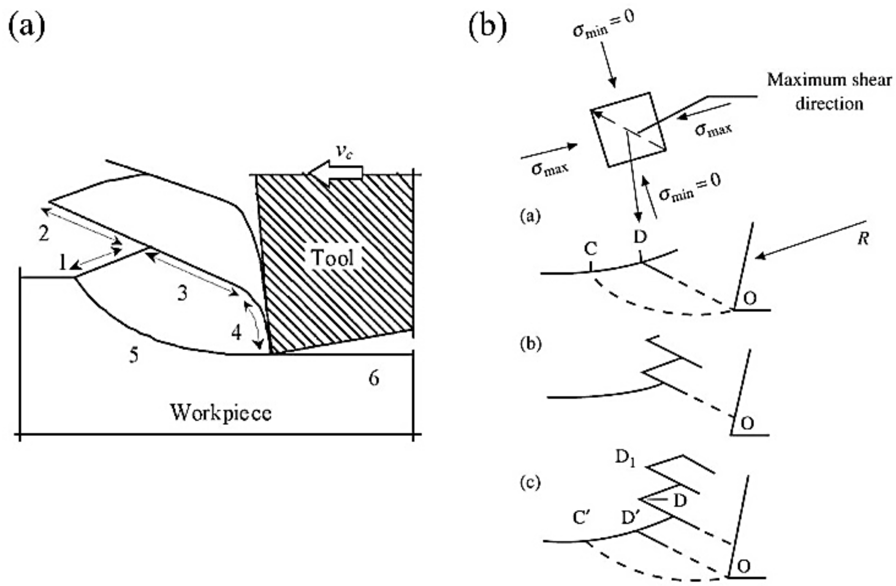


**Figure 3-1:** Theory of Saw-tooth chip formation mechanism (a) Adiabatic shear band [9, 12] and (b) Cyclic crack [17, 19].

All of the previous studies focused on conventional machining processes where the undeformed chip thickness is constant. In Vibration Assisted Drilling (VAD) the uncut chip thickness is dynamically changing due to the superimposed vibratory motion, which was shown to be the main reason for the significant improvements in the cutting temperatures, chip evacuation effectiveness, machined surface integrity, and the machining-induced residual stresses, as reported in [25]. Therefore this research is aiming at understanding the effect of the VAD process parameters on the chip formation mechanisms through investigating the formed chip morphology, which has not been studied before. In addition, the study presents a further understand the experimental results previously reported in [25], by taking into consideration the evidence observed for the chips generated and the subsequent reduction of the tool wear with VAD.

## 3.2. Experimental setup

The drilling process of a 6.75 mm thick Ti6Al4V plate was conducted using a 5-axis Makino A88ε machining centre. A 6 mm tungsten carbide twist (WC) drill with a 118° point angle and a 20° helix angle was used. In order to eliminate the effect of tool wear, the drill bit was used for a maximum of three drill experiments under dry cooling conditions. A full factorial design of experiments consisting of two cutting speeds, three feed rates, two vibration frequencies, and five vibration amplitudes was set up as shown in Table 3-1. The experimental setup was fully described in the authors' previous publication [25].

**Table 3-1:** Experimental conditions for conventional and VAD machining technology.

| | **Unit** | **Conditions** |
|---|---|---|
| Cutting Speed, *N* | rpm | 2,000 and 3,000 |
| Feed rate, *f* | mm/rev | 0.025, 0.05, and 0.075 |
| Vibration amplitude, $A_m$ | μm | 70, 100, 160, 250, 480 |
| Vibration frequency, F | Hz | 83.5 and 125 |

The chips collected after the drilling process were mounted for metallographic examination, ground and polished with 320 mesh SiC paper, 9 μm and 3 μm diamond solvent, respectively. For the microstructural examination (Ti6Al4V phase identification), the polished samples were etched with a solution consisting of 0.5 ml HF and 3 ml $HNO_3$ in 100 ml $H_2O$. The etched chips were examined under an optical microscope, while

Scanning Electron Microscopy (SEM) was used for phase examination and the adhered particles composition was identified by the Energy Dispersion X-ray Spectroscopy (EDS).

## 3.3. Results and discussion

### 3.3.1. Effect of machining parameter on the chip free surface

The effect of VAD modulation amplitude on the chip free surface topography was examined using the scanning electron microscopy (SEM). Strong evidence of saw-tooth morphology for all machining conditions can be observed, as shown in Figure 3-2. Increasing the vibration amplitude resulted in a significant change in the segments geometry and frequency. Compared to conventional drilling (Figure 3-2 (a)), increasing VAD amplitude to 480 μm resulted in a significant increase of the undeformed surface (A) produced by chip-workpiece separation at the previous cutting tool rotation, and slipping surface (B) produced by chip segment sliding during the current cutting operation as marked by A and B in Figure 3-2 (d). This increase in surfaces A and B suggests a lower shear band (SB) frequency, as will be described in more details in section 3.3.2.

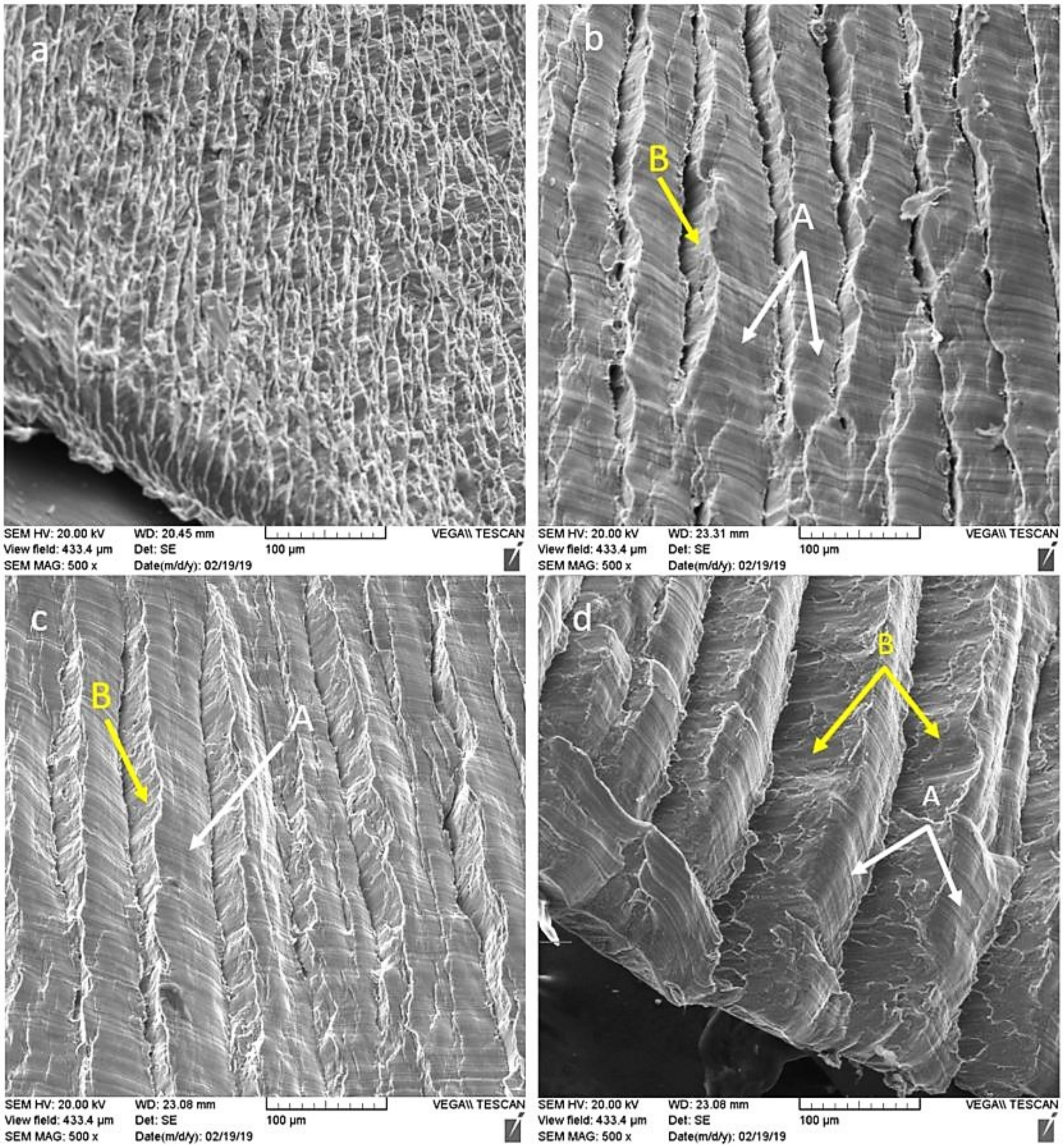


**Figure 3-2:** The effect of vibration amplitude on the chips free surface topography for (a) $A_m$ =0 mm, (b) $A_m$= 0.07 mm, (c) $A_m$= 0.25 mm, and (d) $A_m$= 0.48 mm at $N$= 3,000 rpm and $f$= 0.075 mm/rev.

### 3.3.2. Geometrical characterization of the chip cross-section

Figure 3-3 shows the influence of vibration amplitude ($A_m$) on the chip length at *N*= 3,000 rpm and *f*= 0.025 mm/rev. The microscopic examination of the chips collected after machining process illustrates the significant change from a continuous chip during CD (see Figure 3-3 (a)) to a discontinuous chip type (segmented chips) during VAD (see Figure 3-3 (b,c)). This change has a positive effect on the cutting temperature, chip evacuation effectiveness, and the machining-induced residual stresses as reported in [25].


**Figure 3-3:** The effect of vibration amplitude on the chip length at *N*= 3,000 rpm, *f*= 0.025 mm/rev, and F=125Hz for (a) $A_m$= 0 µm (b) $A_m$= 70 µm(c) $A_m$=480 µm.

The chip length (Lc) was measured for different VAD machining conditions, as shown in Figure 3-4 (a). For the investigated machining range, increasing the vibration amplitude resulted in a 63% reduction of the Lc, see Figure 3-5. This reduction may provide a positive impact on chip evacuation effectiveness. In addition, the chip length provides a direct indication of the tool-chip contact area. This area is a critical parameter that controls the frictional interface, and consequently the thermal load generated in the secondary deformation zone [26, 27]. Therefore, the Lc reduction significantly reduces the cutting temperature, tool wear, and the machining-induced residual stress.

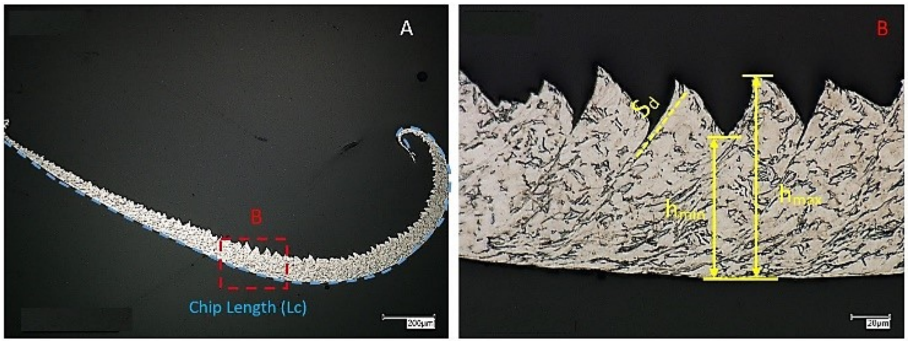


**Figure 3-4:** The investigated geometrical features of the Ti6Al4V Saw-tooth chips.

Based on the circumferential length of chip machined surface (chip radian) - amplitude relationship reported in [25], a regression model was developed to calculate the chip radian (Θ), as described in equation (3.1) with a correlation coefficient ($R^2$) of 91%. As a consequence, the undeformed chip length (L) is represented by the arc length for the corresponding chip radian (Θ) as described in equation (3.2). Hence, the influence of $A_m$ on the undeformed chip length (L), and the chip length (Lc) is used to map out the chip thickness ratio. Chip thickness ratio (r) is a direct indication of the machining mechanical load and can be calculated as described in equation (3.3) [19].

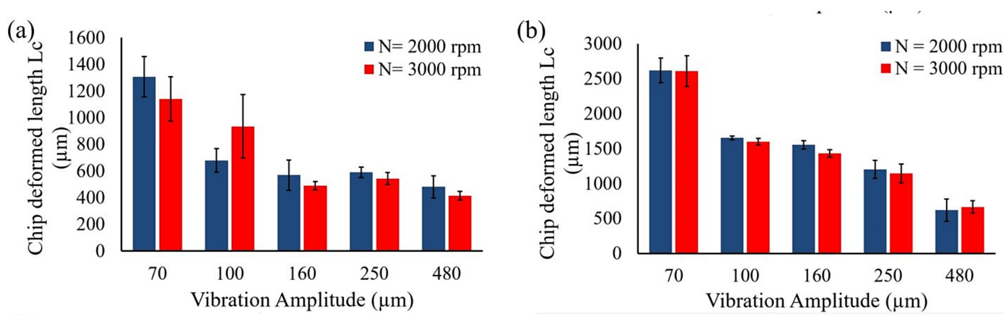


**Figure 3-5:** The effect of VAD amplitude on the chip length at (a) *f*=0.025 mm/rev (b) *f*= 0.075 mm/rev.

$$\Theta = 63.2 - 425\ A_m + 460.1\ f + 1696\ A_m^2 - 944\ A_m * f - 1900\ A_m^3 \quad (3.1)$$

$$L = \Theta * (\text{tool diameter }/2) \tag{3.2}$$

$$Chip\ thickness\ ratio\ (r) = \frac{L_c}{L} \tag{3.3}$$

Figure 3-6 presents the calculated chip thickness ratio (r) at different VAD machining conditions. Increasing the vibration amplitude from 70 μm to 480 μm resulted in a reduction of 50 % to the chip thickness ratio (r). In addition, increasing the vibration amplitude will result in a higher mechanical load for all machining feeds. This increase could alter the material structure along the shear plane, as will be discussed further.

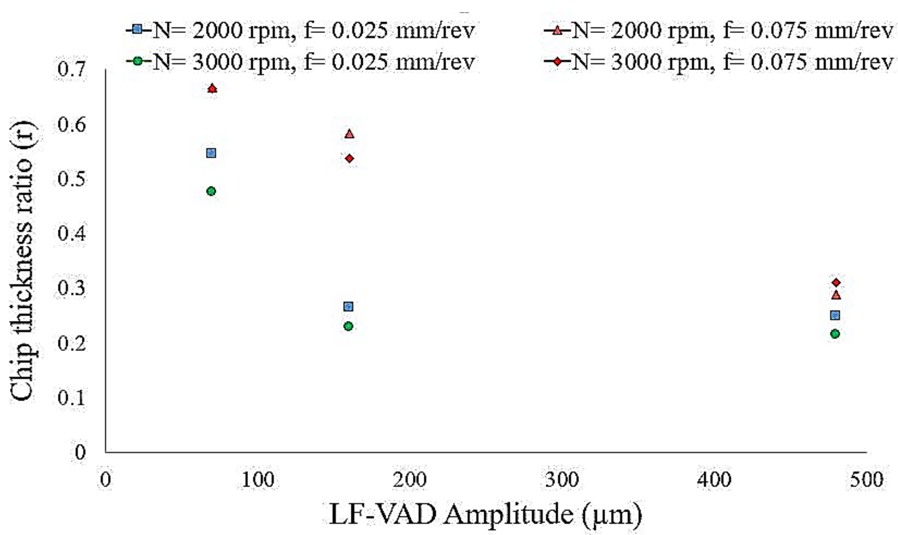


**Figure 3-6:** The effect of VAD machining condition on the chip thickness ratio (r).

Figure 3-7 shows the optical micrographs of chip cross-sections generated at different VAD machining conditions. The increase of $A_m$ resulted in a prominent change of the chip cross-section geometry particularly at the mid-section where the maximum dynamic feed and load occur, as reported in [25]. The geometrical characterization of the chips cross-section is presented by the maximum chip thickness ($h_{max}$), minimum chip thickness ($h_{min}$), sliding distance ($S_d$), and segmentation degree (SD) calculated as described by equation (3.4)[23].

$$\text{Segmentation Degree (SD)} = \frac{h_{max} - h_{min}}{h_{max}} \tag{3.4}$$

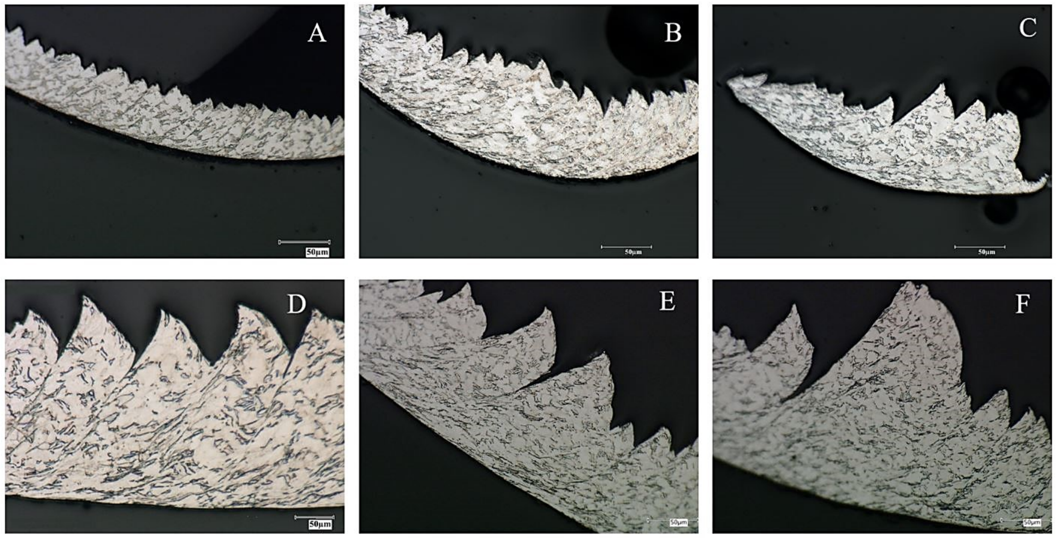


**Figure 3-7:** Optical micrographs for VAD chips cross section at *N*= 2,000 rpm for (a) $A_m$= 70 µm & *f*= 0.025 mm/rev, (B) $A_m$= 250 µm & *f*= 0.025 mm/rev, (C) $A_m$= 480 µm & *f*= 0.025 mm/rev, (D) $A_m$= 70 µm & *f*= 0.075 mm/rev, (E) $A_m$= 250 µm & *f*= 0.075 mm/rev, and (F) $A_m$= 480 & *f*= 0.075 mm/rev.& *f*= 0.075 mm/rev.

The variation of chip geometric features was used to map out the influence of VAD machining conditions, as presented in Figure 3-8 and Figure 3-9. Increasing the vibration amplitude has a dominant effect on the segment sliding distance ($S_d$), see Figure 3-8. For cutting speed *N* = 2,000 rpm, the $S_d$ increased from 16.9 µm at $A_m$ = 70 µm to 68.5 µm at $A_m$ = 480 µm for *f* = 0.025 mm/rev, while the $S_d$ increased from 57 µm at $A_m$ = 70 µm to 176 µm at $A_m$ = 480 µm for *f* = 0.075 mm/rev. Increasing the cutting speed to *N* = 3,000 rpm resulted in an increase of $S_d$ specifically at $A_m$ = 480 µm and *f* = 0.075 mm/rev where the $S_d$ increased to 224 µm.

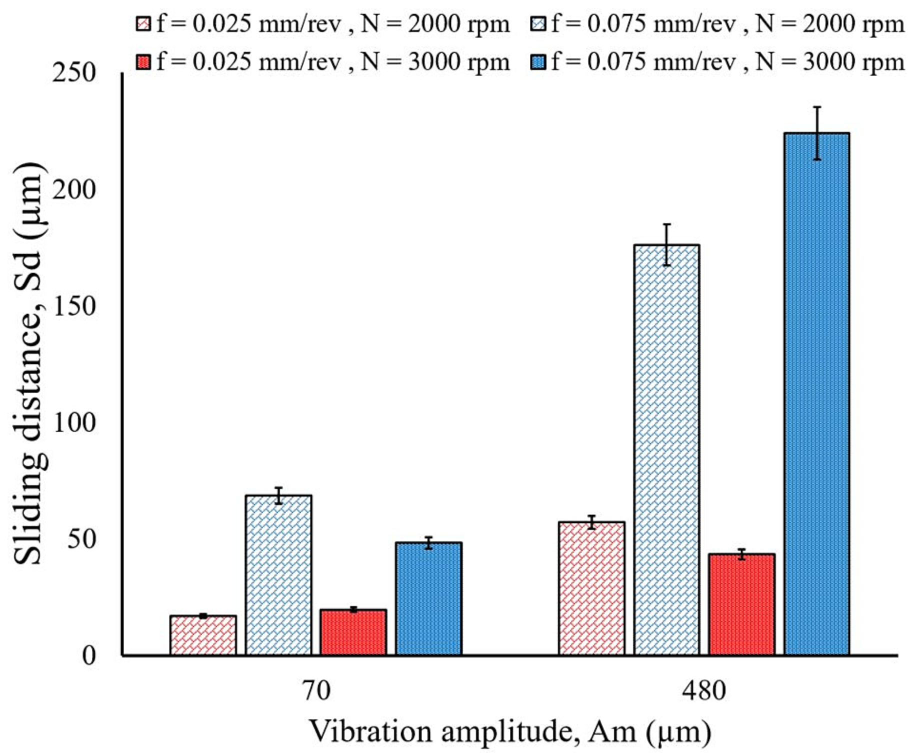


**Figure 3-8:** The effect of VAD amplitude on the maximum segment sliding distance.

With $S_d$ increasing, the vibration amplitude resulted in a clear difference between the $h_{max}$ and $h_{min}$ for all machining conditions, see Figure 3-9 (a & b). The material showed a higher tendency for $S_d$ formation when the $A_m$ becomes more than 160 μm. This observation is in agreement with the significant increase in the machining force as reported in [25]. Figure 3-9 (c & d) presents the effect of VAD machining conditions on the segmentation degree (SD), as calculated using equation (4). The SD values proportionally increased with the VAD $A_m$. For VAD at $N$ = 2,000 rpm, the SD increased from 0.15 to 0.3 for $f$ = 0.025 mm/rev, and from 0.27 to 0.67 for $f$ = 0.075 mm/rev. Increasing the VAD cutting speed to $N$ = 3,000 rpm, resulted in an increase of SD from 0.2 to 0.3 for $f$ = 0.025 mm/rev, and from 0.3 to 0.77 for $f$ = 0.075 mm/rev. This observation is due to the effect of higher chip thickness ($h_{max}$) at high $A_m$. Alternatively, SD did not change with the cutting speed. The observation of constant SD at different cutting speeds supports the observation that cyclic crack theory is the dominant mechanism for saw-tooth formation. This conclusion is in a good agreement with [28]. In addition, increasing the SD results in a lower tool wear.

Based on the influence of cryogenic coolant on Ti6Al4V chip formation [29], reducing the jet temperature from 20°C to -196°C resulted in a significant increase of SD from 0.3 to 0.55. Therefore, VAD could be a possible alternative to cryogenic cooling.

Table 3-2, shows the list of regression equations with a high coefficient of determination ($R^2$) that could be used to calculate the influence of VAD machining conditions on the chip cross-section geometric features.

**Table 3-2:** Empirical "regression" equations presenting the influence of VAD machining conditions on the chip geometric cross-section characterization.

| | Regression equations | $R^2$ |
|---|---|---|
| Lc | $= 2315 + 26193 f - 31.49\ A_m + 0.1299\ A_m^2 - 48.6 f \times A_m - 0.000151\ A_m^3$ | 95.27% |
| $h_{max}$ | $= 14.0 + 0.01185 N + 149 f + 0.289\ A_m - 0.000647\ A_m^2 + 6.159 f \times A_m$ | 95.48% |
| r | $= 0.8820 - 0.000028\ N - 0.73 f - 0.006125\ A_m + 0.000010\ A_m^2 + 0.0633 f \times A_m - 0.000123 f \times A_m^2$ | 99.24% |
| SD | $= 0.488 + 0.000079\ N - 1.41 f - 0.00902\ A_m + 0.000041\ A_m^2 + 0.01937 f \times A_m$ | 90.86% |
| $h_{min}$ | $= -47.5 + 0.0191\ N + 1143 f + 0.896\ A_m - 0.00426\ A_m^2 - 0.512\ N \times f + 8.20 f \times A_m + 0.000006\ A_m^3 - 0.01746 f \times A_m^2$ | 88.70% |

The presented regression analysis is used to summarize the influence of VAD $A_m$ on the chip geometric features at different machining conditions, as shown in Figure 3-10. Based on the presented chip geometric behavior, increasing the $A_m$ will result in a higher mechanical load due to low chip thickness ratio, and high segmentation degree. Alternatively, the thermal load will be reduced due to the lower chip length that has a positive impact on the chip evacuation effectiveness, which is in agreement with references [8, 25, 30].

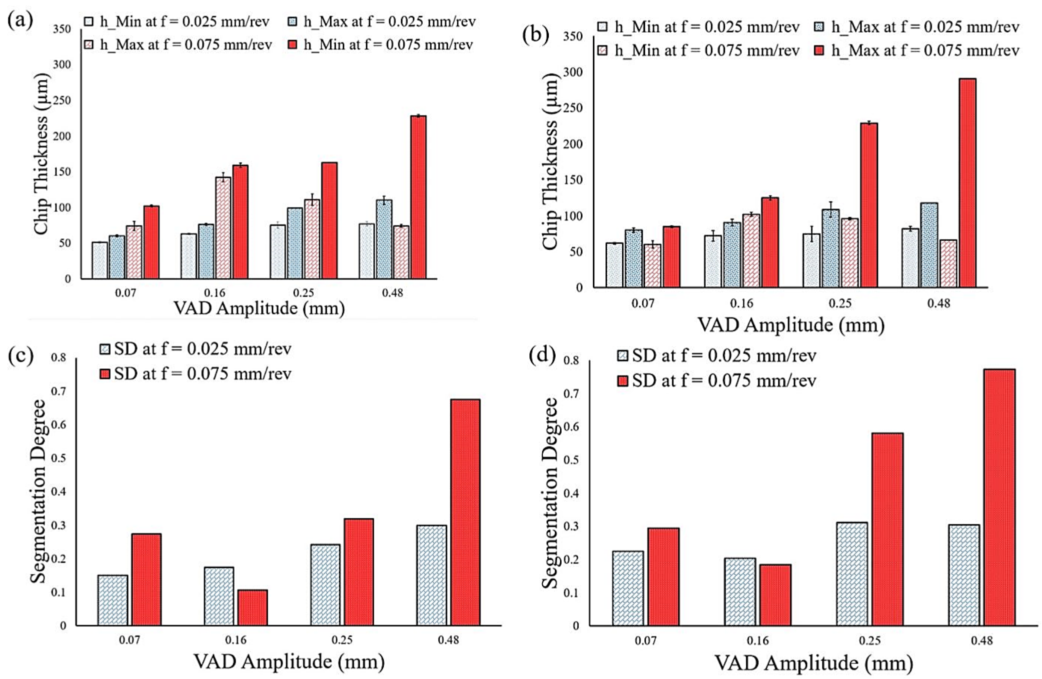


**Figure 3-9:** Geometric characterization for VAD chips cross section for (a) $h_{max}$, $h_{min}$ for *N*=2,000 rpm (b) $h_{max}$, $h_{min}$ for *N*=3,000 rpm, (c) SD for *N*=2,000 rpm, and (d) SD for *N*=3,000 rpm.

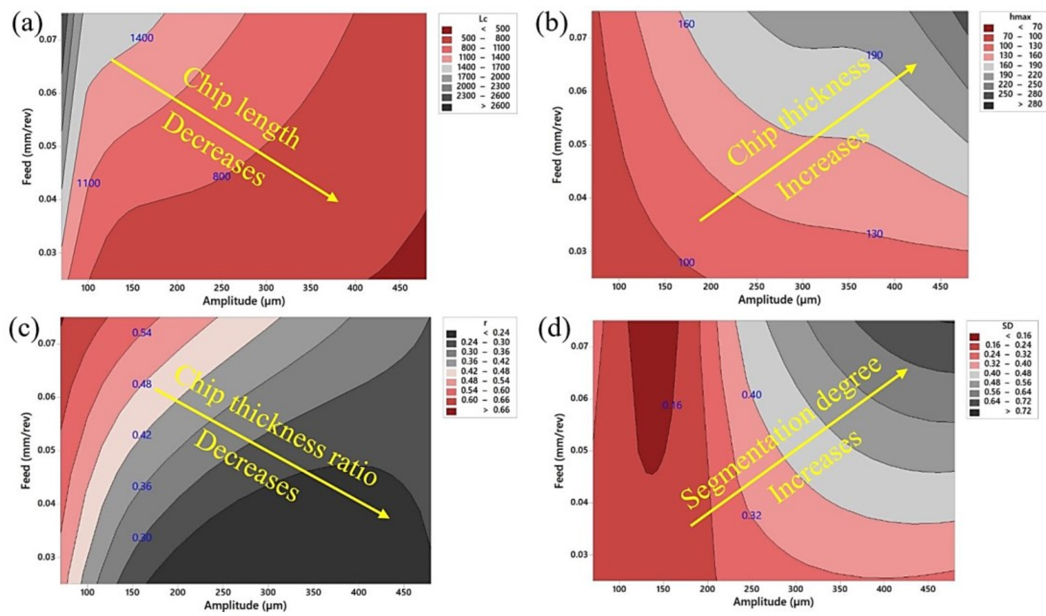


**Figure 3-10:** Contour plots for the influence of VAD machining conditions on (a) Chip length (Lc), (b) Chip thickness height ($h_{max}$), (c) Chip thickness ratio (r), and (d) Segmentation degree (SD).

### 3.3.3. Surface microstructure Effect of VAD on the cutting mechanism.

Figure 3-11 shows the chips microstructure at different feed rates during conventional drilling (CD). The CD resulted in aperiodic saw-tooth chips with a segment sliding distance ($S_d$) less than 20 μm. The $S_d$ is independent of the investigated machining conditions (cutting speed and feed rate). The scanning electron microscopy (SEM) examination showed micro cracks or adiabatic shear band (ASB) along the shear plane. Therefore, there is no strong evidence that could be used to identify the main root mechanism of the saw-tooth chip formation. The Shear Band (SB) was localized in two regions, see Figure 3-11 (b). The first region located between chip segments representing the primary shear plane, while the second region was recognized under the chips machined surface where the secondary shear band took place. The variation of segments spacing could be attributed to machined surface topography (during the previous tool rotation), as reported in [15].

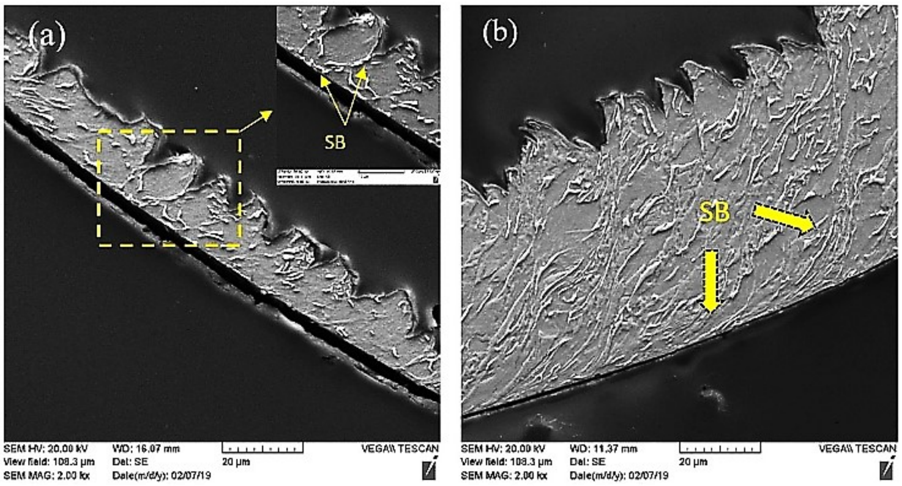


**Figure 3-11:** Effect of conventional drill (CD) on the chip microstructure for (a) *f*= 0.025 mm/rev and (b) *f*= 0.075mm/rev.

Figure 3-12 presents the influence of the VAD $A_m$ on the shear band structure at *f* = 0.025 mm/rev. For a low vibration amplitude ($A_m$= 70 µm), the shear band structure did not display a clear change compared to the CD. However, increasing the vibration amplitude to 160 µm resulted in severe structure elongation with an SB thickness of 5 µm, as seen in Figure 3-12 (E). Further increase of the vibrational amplitude to 480 µm, resulted in a different SB structure exhibiting a clear formation of Gross Crack (GC) and Micro crack (MC), as seen in Figure 3-12 (F). The formation of GC and MC resulted in a significant increase of $S_d$ length to four times the CD (70 µm), and clear observation of a non-continuous micro crack with a 5 µm length, respectively. This could be attributed to the increase of the tool axial velocity [25], that resulted in higher shear stress, and shear crack initiation (GC) along the shear plane (DO) (Figure 3-1 (b) [19]). The GC will advance until the equilibrium between the normal and shear stresses is met, then a non-continuous crack (MC) formation will be dominant.

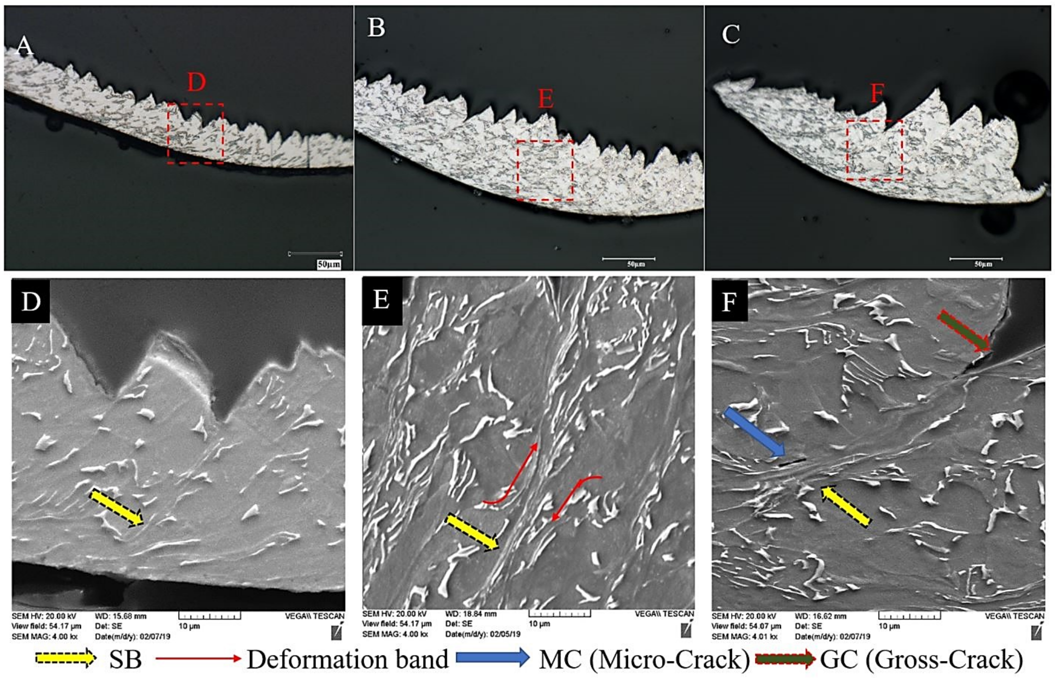


**Figure 3-12:** Effect of VAD amplitude on the shear band structure at *f* = 0.025 mm/rev for (a) $A_m$= 70 µm, (b) $A_m$= 160 µm, and (c) $A_m$= 480 µm.

Figure 3-13 shows the effect of vibration amplitude on the shear band structure at *f* = 0.075 mm/rev. Unlike the shear band for low feed rate condition (*f*= 0.025 mm/rev), the GC and MC formation were clearly observed for all VAD amplitudes. For $A_m$= 70 µm, the GC periodically extended between the chip-segments from the free surface towards the tooltip, as seen in Figure 3-13 (C and D). In addition, the MC was located along the shear plane with up to 20 µm length, as represented by the dashed line in Figure 3-1 (b) and reported in [17, 19]. Based on the SEM examination, neither the adiabatic shear band nor severe plastic deformation was observed. Furthermore, by increasing the $A_m$ to 480 µm the material structure at the shear band was the same as the undeformed structure, as seen in

Figure 3-13 (E). Accordingly, the cyclic crack theory best explains the root cause of sawtooth chips formation. Hence, the $S_d$ values could be used to represent the GC length, which has a significant impact on the saw-tooth specific energy, as reported in [19].

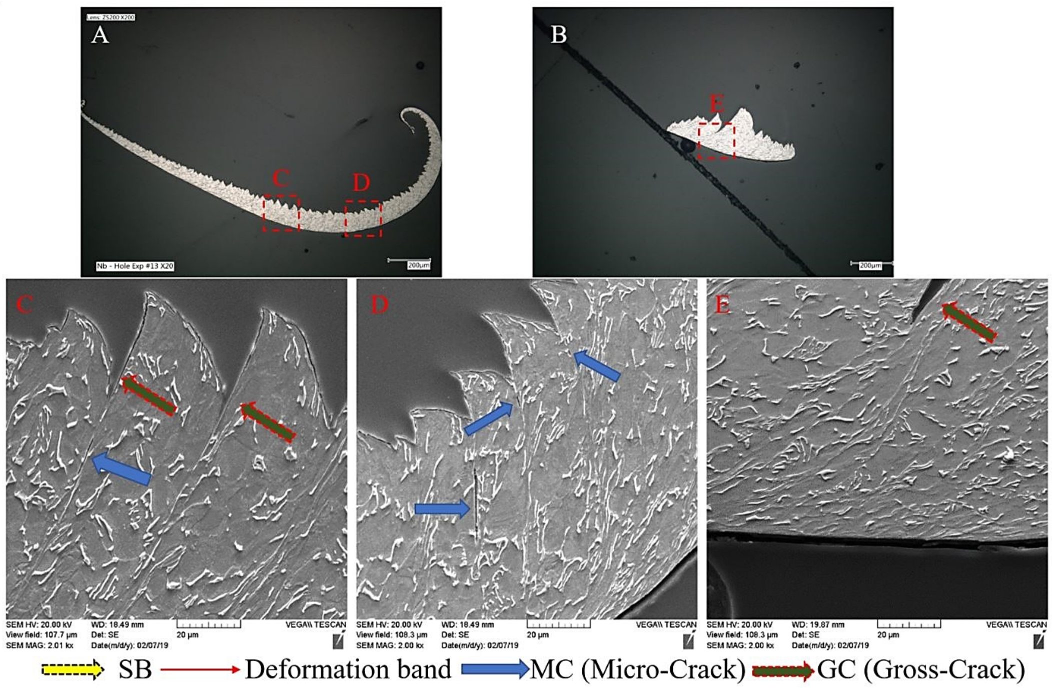


**Figure 3-13:** Effect of VAD amplitude on the shear band structure at $f$ = 0.075 mm/rev for (a) $A_m$= 70 µm, (b) $A_m$= 480 µm.

### 3.3.4. Effect of VAD on the chip back surface

Figure 3-14 shows the influence of machining feed rates and VAD amplitude on the chip back surface (tool contact surface). For $f$ = 0.025 mm/rev, the SEM surface examination of the conventionally machined chips ($A_m$= 0 µm) showed a considerable amount of adhered particles, as shown in Figure 3-14 (A). This observation indicates a severe chip-tool rake face interaction that resulted in a high machining temperature. Further investigation of the adhered particles was conducted using the Energy Dispersion X-ray Spectroscopy (EDS) to identify the particles element. Figure 3-15 (A) shows the spectra analysis for the selected particle. The spectra analysis presents a high carbon peak (**c**) at and a relatively small peak of tungsten (**W**). The composition analysis confirms 48.77% and 0.42% for C, and W, respectively, as shown in Table 3-3. Both elements are believed to be lost from the cutting tool rake face (WC) to form titanium carbide (TiC) due to the diffusion mechanism, which is in an agreement with [23, 31, 32]. The amount of adhered particles was greatly reduced by increasing the machining feed rate to $f$ = 0.075 mm/rev, as seen in Figure 3-14 (D). However, the adhered particles appearance becomes darker compared to the low feed rate condition (Figure 3-14 (A)). The EDS spectra present a high tungsten peak (**W**) followed by carbon peak (**C**), as seen in Figure 3-15 (B). The composition analysis confirms 34.57% and 9.7% for **W**, and **C**, respectively, as presented by spectrum 4 in Table 3-3. Adhesion or welding process of the tool surface particles that pulled out on the chip machined surface was identified as adhesive or attritional wear [33]. This type of tool wear contributed to the severe reduction of tool material hardness by a phenomenon known as thermal softening. The experimental results showed an increase of the drill bit temperature from 790°C at $f$ = 0.025 mm/rev to 1050°C at $f$ = 0.075 mm/rev, as reported in [25]. Based on the hardness-temperature relations [33, 34], this increase resulted in a drop of the WC-Co alloy (tool material) hardness to less than 500 HV. As a result adhesion wear mechanism was initiated [35].

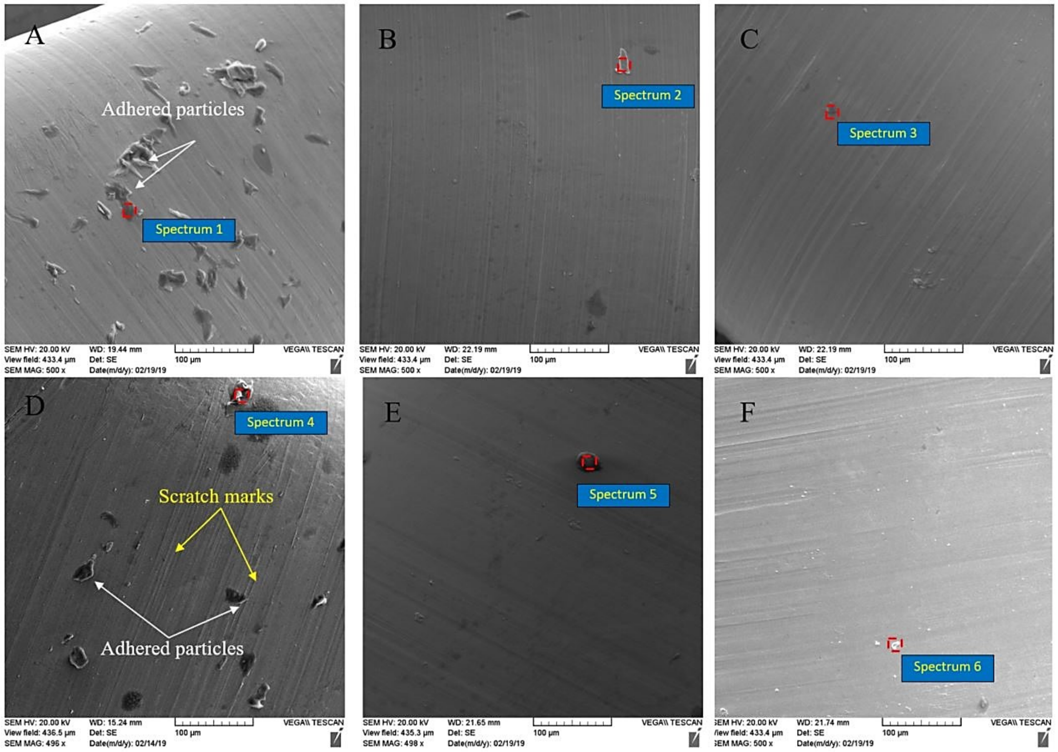


**Figure 3-14:** Chips machined surface SEM examination at $N$= 3,000 rpm for (A) $A_m$= 0 mm & $f$= 0.025 mm/rev, (B) $A_m$= 70 µm & $f$= 0.025 mm/rev, (C) $A_m$= 480 µm & $f$= 0.025 mm/rev, (D) $A_m$= 0 mm & $f$= 0.075 mm/rev, (E) $A_m$= 70 µm & $f$= 0.075 mm/rev, and (F) $A_m$= 480 µm & $f$= 0.075 mm/rev.

Compared to the CD, the SEM examination showed an enhancement of the chips machined with VAD technique for all machining conditions, (see Figure 3-14 (B)(C) and (E)(F)). The VAD chip machined surface appeared to be scratch free and had almost no adhered particles. This enhancement was confirmed by the EDS composition analysis, as shown in Table 3-3. The observed enhancement is an indication of the positive influence of VAD amplitude on the tool life. Moreover, the cutting tool temperature reduction has a significant impact on the workpiece surface residual stress and the subsurface thermally affected zone. This zone can be identified by the depth where the residual stress changed from tensile to compressive stress, as reported in [25].

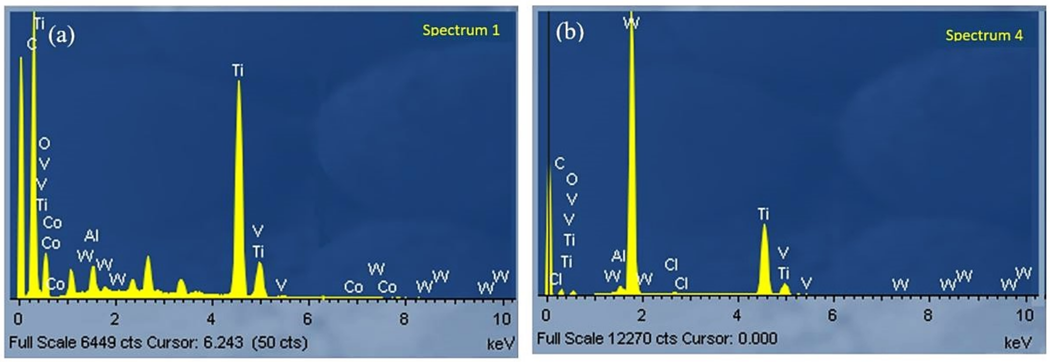


**Figure 3-15:** The EDS spectra for the selected particle in Figure 14 (A) and (D).

**Table 3-3:** EDS Element composition analysis for the selected points in Figure 14.

| Elements by weight % | | | | | | | |
|---|---|---|---|---|---|---|---|
| | C | O | Al | Ti | V | W | Total |
| Spectrum 1 | 48.77 | 24.08 | 1.15 | 24.44 | 1.14 | 0.42 | 100.0 |
| Spectrum 2 | 11.34 | 0.00 | 6.93 | 78.42 | 3.30 | 0.00 | 100.0 |
| Spectrum 3 | 37.41 | 15.65 | 3.14 | 42.25 | 1.55 | 0.00 | 100.0 |
| Spectrum 4 | 9.71 | 10.76 | 2.26 | 41.28 | 1.42 | 34.57 | 100.0 |
| Spectrum 5 | 54.49 | 40.51 | 0.48 | 4.27 | 0.25 | 0.00 | 100.0 |
| Spectrum 6 | 12.22 | 0.00 | 5.19 | 79.08 | 3.52 | 0.00 | 100.0 |

## Conclusions

The results of an experimental study dealing with the metallurgy and morphology of saw-tooth chip formation during vibration assisted drilling of Ti6Al4V is presented in this investigation. Cyclic cracks, where gross and micro cracks are located along the shear band, are identified as the prevailing mechanism for saw-tooth chips. The formation of these cracks showed a significant dependency on the vibrational amplitude. Chip morphology, specifically chip length, chip dimensions, and segmentation degree are examined. The results showed a reduction in the chip thickness ratio and an increase in the segmentation degree when increasing the vibration amplitude. The experimental observations reported in this work contribute to the understanding of the mechanics of chip formation in vibration-assisted drilling of Ti6Al4V. The results are of significance to the aerospace and automotive industries that are frequent users of drilling technologies for Ti6Al4V material.

## References

[1] K.-H. Park, A. Beal, P. Kwon, and J. Lantrip, "Tool wear in drilling of composite/titanium stacks using carbide and polycrystalline diamond tools," *Wear,* vol. 271, pp. 2826-2835, 2011.

[2] D. Dornfeld, J. Kim, H. Dechow, J. Hewson, and L. Chen, "Drilling burr formation in titanium alloy, Ti-6AI-4V," *CIRP Annals-Manufacturing Technology,* vol. 48, pp. 73-76, 1999.

[3] Z. Li, D. Zhang, X. Jiang, W. Qin, and D. Geng, "Study on rotary ultrasonic-assisted drilling of titanium alloys (Ti6Al4V) using 8-facet drill under no cooling condition," *The International Journal of Advanced Manufacturing Technology,* vol. 90, pp. 3249-3264, 2017.

[4] J. L. Cantero, M. M. Tardío, J. A. Canteli, M. Marcos, and M. H. Miguélez, "Dry drilling of alloy Ti–6Al–4V," *International Journal of Machine Tools and Manufacture,* vol. 45, pp. 1246-1255, 2005/09/01/ 2005.

[5] R. B. D. Pereira, L. C. Brandão, A. P. de Paiva, J. R. Ferreira, and J. P. Davim, "A review of helical milling process," *International Journal of Machine Tools and Manufacture,* vol. 120, pp. 27-48, 2017/09/01/ 2017.

[6] R. M'Saoubi, D. Axinte, S. L. Soo, C. Nobel, H. Attia, G. Kappmeyer*, et al.*, "High performance cutting of advanced aerospace alloys and composite materials," *CIRP Annals,* vol. 64, pp. 557-580, 2015.

[7] O. Pecat and I. Meyer, "Low frequency vibration assisted drilling of aluminium alloys," in *Advanced Materials Research*, 2013, pp. 131-138.

[8] R. Hussein, A. Sadek, M. A. Elbestawi, and M. Attia, "Low-frequency vibration-assisted drilling of hybrid CFRP/Ti6Al4V stacked material," *International Journal of Advanced Manufacturing Technology,* vol. 98, pp. 2801-2817, Oct 2018.

[9] R. Komanduri, "Some clarifications on the mechanics of chip formation when machining titanium alloys," *Wear,* vol. 76, pp. 15-34, 1982.

[10] R. Komanduri and B. Von Turkovich, "New observations on the mechanism of chip formation when machining titanium alloys," *Wear,* vol. 69, pp. 179-188, 1981.

[11] A. Vyas and M. Shaw, "Mechanics of saw-tooth chip formation in metal cutting," *Journal of Manufacturing Science and Engineering,* vol. 121, pp. 163-172, 1999.

[12] J. Barry, G. Byrne, and D. Lennon, "Observations on chip formation and acoustic emission in machining Ti–6Al–4V alloy," *International Journal of Machine Tools and Manufacture,* vol. 41, pp. 1055-1070, 2001.

[13] I. Choudhury and M. El-Baradie, "Machinability of nickel-base super alloys: a general review," *Journal of Materials Processing Technology,* vol. 77, pp. 278-284, 1998.

[14] J. Barry and G. Byrne, "Study on acoustic emission in machining hardened steels Part 1: Acoustic emission during saw-tooth chip formation," *Proceedings of the Institution of Mechanical Engineers, Part B: Journal of Engineering Manufacture,* vol. 215, pp. 1549-1559, 2001.

[15] M. Elbestawi, A. Srivastava, and T. El-Wardany, "A model for chip formation during machining of hardened steel," *CIRP annals,* vol. 45, pp. 71-76, 1996.

[16] T. El-Wardany, H. Kishawy, and M. Elbestawi, "Surface integrity of die material in high speed hard machining, Part 1: Micrographical analysis," *Journal of manufacturing science and engineering,* vol. 122, pp. 620-631, 2000.

[17] K. Nakayama, "On the formation of" saw-toothed chip" in metal cutting," *J Japan Soc Prec Eng,* vol. 43, pp. 117-122, 1977.

[18] E. A. H. Kishawy, "Chip formation and surface integrity in high speed machining of hardened steel," 1998.

[19] M. C. Shaw and J. Cookson, *Metal cutting principles* vol. 2: Oxford university press New York, 2005.

[20] R. Recht, "Catastrophic thermoplastic shear," *Journal of Applied Mechanics,* vol. 31, pp. 189-193, 1964.

[21] R. Li, L. Riester, T. R. Watkins, P. J. Blau, and A. J. Shih, "Metallurgical analysis and nanoindentation characterization of Ti–6Al–4V workpiece and chips in high-throughput drilling," *Materials Science and Engineering: A,* vol. 472, pp. 115-124, 2008.

[22] Z. Wan, Y. Zhu, H. Liu, and Y. Tang, "Microstructure evolution of adiabatic shear bands and mechanisms of saw-tooth chip formation in machining Ti6Al4V," *Materials Science and Engineering: A,* vol. 531, pp. 155-163, 2012.

[23] S. Sun, M. Brandt, and M. S. Dargusch, "Effect of tool wear on chip formation during dry machining of Ti-6Al-4V alloy, part 1: effect of gradual tool wear evolution," *Proceedings of the Institution of Mechanical Engineers, Part B: Journal of Engineering Manufacture,* vol. 231, pp. 1559-1574, 2017.

[24] G. Sih, "Surface layer energy and strain energy density for a blunted crack or notch, Prospect of Fracture Mechanics, edited by GC Sih, HC van Elst and D Broek," ed: Noordhoff International Publishing, Leyden, 1974.

[25] R. Hussein, A. Sadek, M. A. Elbestawi, and M. H. Attia, "Surface and microstructure characterization of low-frequency vibration-assisted drilling of Ti6Al4V," *The International Journal of Advanced Manufacturing Technology,* vol. 103, pp. 1443-1457, April 05 2019.

[26] S. Iqbal, P. Mativenga, and M. Sheikh, "A comparative study of the tool–chip contact length in turning of two engineering alloys for a wide range of cutting speeds," *The International Journal of Advanced Manufacturing Technology,* vol. 42, p. 30, 2009.

[27] M. Bermingham, J. Kirsch, S. Sun, S. Palanisamy, and M. Dargusch, "New observations on tool life, cutting forces and chip morphology in cryogenic machining Ti-6Al-4V," *International Journal of Machine Tools and Manufacture,* vol. 51, pp. 500-511, 2011.

[28] Y. Sánchez, F. Trujillo, C. Bermudo Gamboa, and L. Sevilla, *Experimental Parametric Relationships for Chip Geometry in Dry Machining of the Ti6Al4V Alloy* vol. 11, 2018.

[29] W. Zhao, L. Gong, F. Ren, L. Li, Q. Xu, and A. M. Khan, "Experimental study on chip deformation of Ti-6Al-4V titanium alloy in cryogenic cutting," *The International Journal of Advanced Manufacturing Technology,* vol. 96, pp. 4021-4027, 2018.

[30] E. Brinksmeier, O. Pecat, and R. Rentsch, "Quantitative analysis of chip extraction in drilling of Ti 6 Al 4 V," *CIRP Annals-Manufacturing Technology,* vol. 64, pp. 93-96, 2015.

[31] P. Dearnley and A. Grearson, "Evaluation of principal wear mechanisms of cemented carbides and ceramics used for machining titanium alloy IMI 318," *Materials Science and Technology,* vol. 2, pp. 47-58, 1986.

[32] P. D. Hartung, B. Kramer, and B. Von Turkovich, "Tool wear in titanium machining," *CIRP Annals,* vol. 31, pp. 75-80, 1982.

[33] D. A. Stephenson and J. S. Agapiou, *Metal cutting theory and practice*: CRC press, 2016.

[34] A. Santhanam, P. Tierney, and J. Hunt, "Cemented carbides," *ASM International, Metals Handbook, Tenth Edition,* vol. 2, pp. 950-977, 1990.

[35] S. Sun, M. Brandt, and M. S. Dargusch, "Effect of tool wear on chip formation during dry machining of Ti-6Al-4V alloy, part 2: Effect of tool failure modes," *Proceedings of the Institution of Mechanical Engineers, Part B: Journal of Engineering Manufacture,* vol. 231, pp. 1575-1586, 2017.

# Chapter 4

## Chip Morphology and Delamination Characterization for Vibration Assisted Drilling of Carbon Fiber Reinforced Polymer Complete

**Citation:**

Hussein, R., Sadek, A., Elbestawi, M.A., Attia, M.H. (2019). Chip Morphology and Delamination Characterization for Vibration Assisted Drilling of Carbon Fiber Reinforced Polymer. *Journal of Manufacturing and Materials Processing*, Volume 3, Issue 1.
Doi: 10.3390/jmmp3010023

**Relative Contributions:**

| | |
|---|---|
| R. Hussein: | Performed experiments, analysis, and data interpretation; wrote the first draft of the manuscript; helped with submitting the final manuscript to the journal (corresponding author). |
| A. Sadek: | Helped with the experiments and analysis; revised the manuscript. |
| M. A. Elbestawi: | Supervisor of R. Hussein. Revised and edited the manuscript and gave the final approval to be submitted. |
| M. H. Attia: | Revised the manuscript. |

**Abstract:**

Carbon fiber-reinforced polymers (CFRP) are widely used in the aerospace industry. A new generation of aircraft is being built using CFRP for up to 50% of their total weight, to achieve higher performance. Exit delamination and surface integrity are significant challenges reported during conventional drilling. Exit delamination influences the mechanical properties of machined parts and, consequently, reduces fatigue life. Vibration-assisted drilling (VAD) has much potential to overcome these challenges. This study is aimed at investigating exit delamination and geometrical accuracy during VAD at both low- and high-frequency ranges. The kinematics of VAD are used to investigate the relationship between the input parameters (cutting speed, feed, vibration frequency, and amplitude) and the uncut chip thickness. Exit delamination and geometrical accuracy are then evaluated in terms of mechanical and thermal load. The results show a 31% reduction in cutting temperature, as well as a significant enhancement in exit delamination, by using the VAD technology.

**Keywords:**

Low-frequency vibration-assisted drilling; High-frequency vibration-assisted drilling; Multi-directional carbon fiber reinforced polymer laminates; Advanced machining. Delamination free.

**Acknowledgment:**

The experimental work in this study was performed using the laboratories of the Canadian National Research Council (CNRC), Aerospace and Manufacturing Group, Montreal, Canada. The technical support is greatly appreciated.

## 4.1 Introduction

Lightweight materials such as carbon fiber-reinforced polymers (CFRP), titanium, and aluminum alloys are widely used in the aerospace industry, typically representing, collectively, more than 75% of the total weight of new-generation aircraft [1-3]. High strength-to-weight ratio, high stiffness, superior corrosion resistance, and near net shape capabilities are significant advantages of using CFRP [4, 5]. These capabilities result in significant enhancement of performance, operation and maintenance costs, and environmental impact.

CFRP is considered a “difficult-to-cut material” due to its high sensitivity to cutting energy [5-7]. Entry and exit delamination is a typical surface integrity defect resulting from conventional drilling [8-11]. Delamination damage deteriorates the mechanical properties of the machined part and reduces in-service life due to fatigue [12, 13]. Research efforts have focussed on the selection of machining parameters aimed at overcoming the delamination issue [5, 6, 14-16]. Delamination defects have been attributed mainly to higher thrust forces [13]. Accordingly, higher cutting speeds with lower feed were recommended to reduce the mechanical and thermal damage [17, 18].

Vibration assisted drilling (VAD) has been used to overcome these machining challenges[19]. Cutting geometry, chip evacuation, and lower tool-workpiece contact time are the main advantages of VAD. As a consequence, lower mechanical and thermal loads are generated [20, 21]. VAD of CFRPs can be classified as:

- Low-frequency vibration-assisted drilling (LF-VAD); vibration frequency lower than 1 KHz [4, 20, 21].

- High-frequency vibration-assisted drilling (HF-VAD); frequency is in the range of 1 KHz to 18 KHz.
- Ultrasonically assisted drilling (UAD); frequency is higher than 18 KHz [22-26].

Several studies have focused on the optimization of LF-VAD machining parameters. LF-VAD with a frequency of 100 – 300 Hz and 22,000 rpm cutting speed showed a 30% reduction on the thrust force [21]. This reduction was attributed to the low uncut chip thickness. However, the effect of LF-VAD on cutting temperature must also be evaluated, since high temperatures may cause thermal deterioration.

Investigation of LF-VAD with a modulation frequency of 5.5 cycle/rev showed up to 15% increase in the thrust force combined with a 15% reduction in the delamination factor [4]. The study used a fixed feed-to-amplitude ratio and focused on the effect of tool geometry. Another LF-VAD study showed a significant reduction of 50% for the cutting temperature, and 40% for the thrust force [20]. The frequency range examined was 30-60 Hz with 800 μm amplitude. A delamination-free process was achieved at 0.025 mm/rev feed.

In contrast to LF-VAD, the UAD of CFRP resulted in a significant reduction in the thrust force [22, 23, 25-27]. This reduction was attributed to a lower coefficient of friction. Moreover, UAD showed some improvements in the exit delamination and geometrical accuracy (circularity, centricity, and diameter accuracy)[23, 25, 27]. However, the results reported in the literature regarding the influence of UAD on cutting temperature are sometimes contradictory. Compared to the conventional drilling (CD), a significantly higher temperature was reported in [23], which was attributes to the tool impact mechanism. On the other hand, a lower cutting temperature compared to CD was reported in [27], which was attributed to the intermittent cutting mechanism.

Most of the aforementioned VAD studies examined LF-VAD at a specific amplitude [4]. Other studies examined the effect of drill bit material [21], and the workpiece oscillation method [20]. On the other hand, the UAD research focused mainly on the thrust force study at frequency ranges typically outside the dynamometer capability, which increased the uncertainty of the measurements. In addition, additional research is needed to investigate the effect of VAD on the uncut chip thickness and its relation to the cutting forces, temperature, and delamination. Furthermore, the effect of HF-VAD on the CFRP needs to be evaluated as well. This study aims to investigate the effects of LF-VAD and HF-VAD, for a wide range of machining parameters, on the thrust force, cutting temperature, and delamination factor. Kinematics modeling is used to evaluate the effect of VAD on the cutting energy, delamination, and the uncut chip thickness.

## 4.2 Experimental setup

Figure 4-1 presents the experimental setup, which includes a five-axis Makino A88" machining center. The axial tool oscillations for LF-VAD were generated using the MITIS tool holder PG8045B3_HSK-A100_ER40[28], as shown in Figure 4-1 (a). The tool holder has a 2.5 cycle/rev fixed frequency ratio (F) with an adjustable amplitude (Am) range between 0.01 and 0.48 mm. Figure 1b shows the HF-VAD tool holder (designed by the National Research Center of Montreal)[29]. The experimental setup ensures continuous recording of the cutting forces and the cutting tool temperature at the exit surface. A U-shaped plate was used to create enough space behind the CFRP plate for direct thermal vision. A FLIR SC8000 infrared camera was used for the cutting tool tip thermal measurement. The thrust forces were monitored using a 9272 Kistler-type dynamometer and a Kistler multichannel charge amplifier (Type 5019B). Scanning electron microscopy type TESCAN VP.SEM was used for examining chip morphology, and for exit wall examination. The delamination analysis was performed with a Keyence optical microscope. Surface roughness values (Ra and Rz) were evaluated using a Surftest SJ-410 stylus profilometry, which has 0.0001 µm resolution.

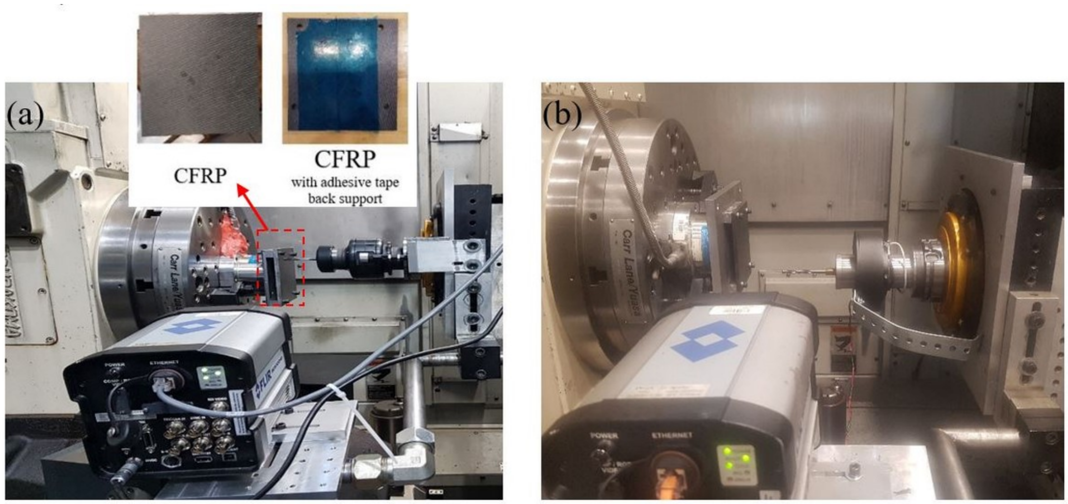


**Figure 4-1:** The developed experimental setup for (a) low-frequency vibration-assisted drilling (LF-VAD) (b) high-frequency vibration-assisted drilling (HF-VAD).

Table 4-1 presents the experimental VAD machining parameters, cutting tool, and the CFRP material specification. Conventional cutting tests with identical machining conditions were performed for comparison purposes.

**Table 4-1:** Applied cutting conditions, cutting tool, and workpiece material

| Machining Parameters | | |
|---|---|---|
| Cutting speeds $N$ (rpm) | 2000 and 3000 | |
| Feed $f$ (mm/rev) | 0.025, 0.05, and 0.075 | |
| Cooling medium | Dry | |
| | LF-VAD | HF-VAD |
| Amplitude $A_m$ (μm) | 70, 100, 160, 250, and 480 | 3 |
| Frequency F (Hz) | 83.33, 125 | 1500, and 2150 |
| **Cutting Tool** | | |
| Material | Tungsten Carbide | |
| Diameter | 6 mm | |
| Point angle | 118° | |
| Helix angle | 20° | |
| Number of flutes | 2 | |
| **Workpiece material specification** | | |
| CFRP | 5.8 ± 0.02 mm of 42 × L-930(GT700) woven plies with the configuration [[0,90]21]s, and flame retardant modified epoxy prepreg. | |
| Flash breaker | AIRTECH flashbreaker® 1 with a thickness of 64 μm [30] | |

## 4.3 Kinematics of VAD

Figure 4-2, presents the effect of VAD on the actual uncut chip thickness at $N$= 2,000 rpm for different machining conditions. Based on the instantaneous cutting edge position described in [31, 32], the uncut chip thickness was calculated for VAD at the selected machining conditions. The $A_m$ range (0.07 mm – 0.48mm) at LF-VAD (F=83.33 Hz) resulted in chip segmentation as described in [3, 33]. Consequently, periodic cooling cycles were generated, as shown in Figure 4-2 (a). In contrast, HF-VAD at $A_m$ = 3 μm did not display tool-workpiece separation. Consequently, a continuous cutting process is shown in Figure 4-2. HF-VAD showed a positive influence by reducing the uncut chip thickness up to 50% compared to CD. Moreover, increasing the cutting speed to $N$ = 3,000 rpm at HF-

VAD with F= 1500 Hz, resulted in an even modulation frequency with a continuous cutting profile, as shown in Figure 4-3.

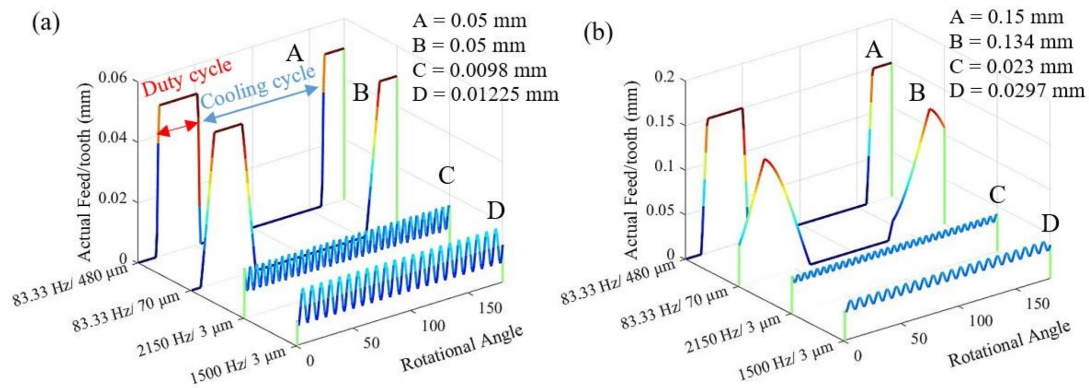


**Figure 4-2:** Effect of Vibration assisted drilling (VAD) frequency and amplitude on the uncut chip thickness at (a) feed ($f$) = 0.025 mm/rev and (b) $f$ = 0.075 mm/rev.

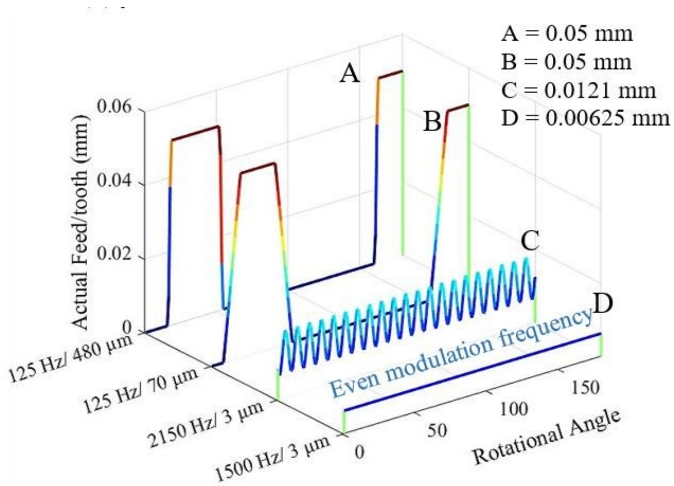


**Figure 4-3:** Effect of Vibration-assisted drilling frequency and amplitude on the uncut chip thickness at $f$ = 0.025 mm/rev and $N$ = 3,000 rpm.

Based on the kinematics study of VAD at the selected machining conditions, the VAD influences are summarized as follows:

- HF-VAD has the lowest mechanical load compared to LF-VAD and CD.

- LF-VAD has a higher mechanical load compared to CD. Moreover, increasing the amplitude resulted in higher impact energy during the periodic tool engagement mechanism.
- Based on the uncut chip thickness analysis, VAD has a lower thermal load compared to CD.
- A reduction in the cutting temperature was achieved during LF-VAD cooling cycle.
- Lower thrust force and thermal load are the main reasons to achieve a delamination-free process for utilization of VAD technology.

## 4.4 Results and discussion

### 4.4.1 Effect of VAD on the thrust force

Figure 4-4 shows the effect of VAD on the thrust force measured at different machining conditions. For all machining conditions, the LF-VAD showed a higher thrust force compared to the CD. The measured thrust forces were 64 N to 143 N for LF-VAD and 41 N to 65 N for CD, respectively. These forces showed an increase of 30 % to 120 % compared to the CD. This increase could be attributed to the followings:

- High uncut chip thickness, as described in section 4.3. This agrees with references [3, 31, 34].
- Periodical tool impact caused a dynamic force component. This force adds to the total thrust force, as described in section 4.3. These results agree with [3, 4].

On the other hand, HF-VAD showed up to 16% reduction in the thrust force compared to the CD, at $N$= 2,000 rpm. This reduction could be attributed to the followings:

- Lower uncut chip thickness compared to CD, as described in section 4.3.
- The ability of the axial tool oscillation to discard the non-cutting process under the chisel edge.

However, there is no apparent influence of HF-VAD at $N$ = 3,000 rpm on the thrust force. This could be attributed to the higher cutting temperature induced during the CD at $N$ = 3000 rpm. Increasing the cutting temperature leads to material softening, and consequently the thrust force decreases. The HF-VAD at F=2150 Hz resulted in a higher friction force that leads to an increase in the thrust force.

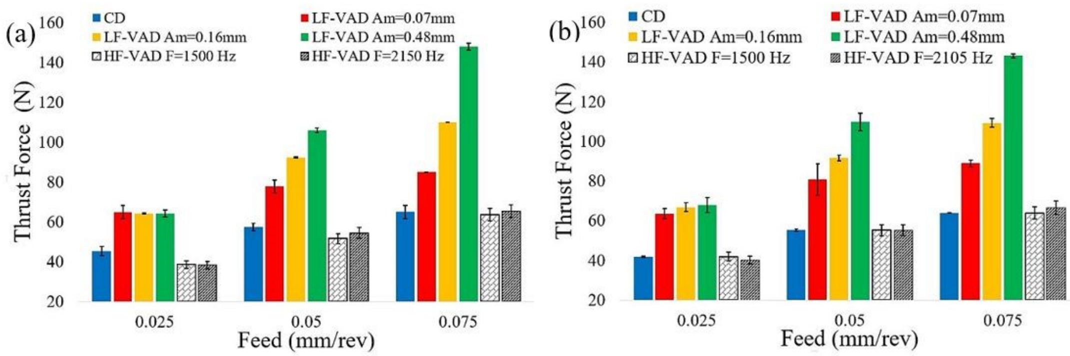


**Figure 4-4:** Effect of VAD on the thrust force at (a) $N$=2,000 rpm (b) $N$=3,000 rpm.

Figure 4-5 shows the effect of $A_m$ on the thrust force profile. For the CD, the steady cutting interval (T) showed low force fluctuation (35 N to 65 N) (see Figure 4-5 (a)). This fluctuation could be attributed to the dynamic change of the rake face- fiber attack angle during tool rotation, as reported in [4]. In contrast, LF-VAD thrust force profile showed major and minor fluctuation ranges. The minor fluctuation represents the dynamic change of the rake face- fiber attack angle, while the major fluctuation attributed to the tool duty and separation mechanism. The major fluctuation ranges were 0 N to 80 N for $A_m$ = 0.07 mm and 0 N to 148 N for $A_m$ = 0.48 mm respectively (see Figure 4-5(b,c)).

The HF-VAD did not show significant variation in the thrust force profile compared to CD, which is attributed to the lower amplitude of vibration.

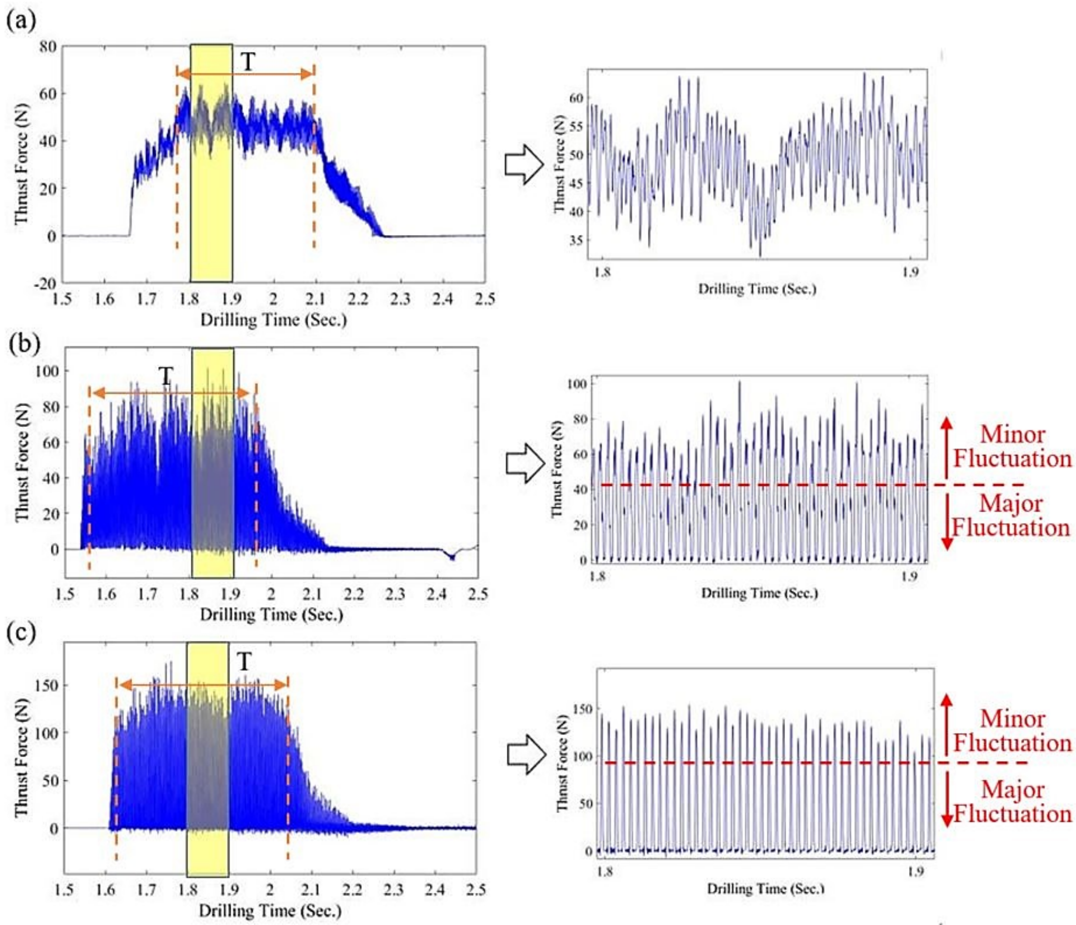


**Figure 4-5:** Effect of the LF-VAD on the thrust force profile at $f$ = 0.075 mm/rev and $N$ =3,000 rpm for (a) CD (b) $A_m$ = 0.07 mm (c) $A_m$ = 0.48 mm.

### 4.4.2 Effect of VAD on the tool temperature

Figure 4-6 shows the effect of the VAD on the cutting tool temperature at the exit surface. For all machining conditions, the VAD showed a lower cutting temperature compared to the CD. Tool temperatures measured during CD were 169°C to 185°C at $N$ = 2,000 rpm and 195°C to 202°C at $N$ = 3,000 rpm, respectively. The tool temperature showed a gradual reduction as cutting feed increases. This reduction is attributed to a lower duty time [20]. The exit tool temperatures for LF-VAD were 130°C to 159°C at $N$ = 2,000 rpm and 138°C to 160°C at $N$ = 3,000 rpm.

Increasing the LF-VAD amplitude from $A_m$= 0.07 mm to $A_m$= 0.48 led to a reduction in the cutting temperature, as seen in Figure 4-6 (b).

In contrast, at a lower thermal load ($N$ = 2,000 rpm), increasing the LF-VAD amplitude resulted in a higher impact velocity and larger uncut chip thickness (see section 4.3.).

Compared to the LF-VAD, the HF-VAD showed a limited reduction in the cutting temperature. The cutting temperature reduction was 13 % for HF-VAD and 31% for LF-VAD. The higher reduction of LF-VAD could be attributed to the interrupted cutting process. This process reduces the cyclic tool duty time, as described in section 4.3.

For all machining conditions, The HF-VAD at F=2150 Hz showed a lower cutting temperature compared to HF-VAD at F=1500 Hz and CD. This reduction is attributed to the lower uncut chip thickness at $N$ = 2,000 rpm, as described in Figure 4-2. For higher cutting speed $N$ = 3,000 rpm, an even $W_f$ leads to a constant tool-workpiece contact area, and accordingly higher heat concentration. The HF-VAD at F= 1500 Hz showed lower uncut chip thickness, however the negative influence of constant tool-workpiece contact area is more dominant.

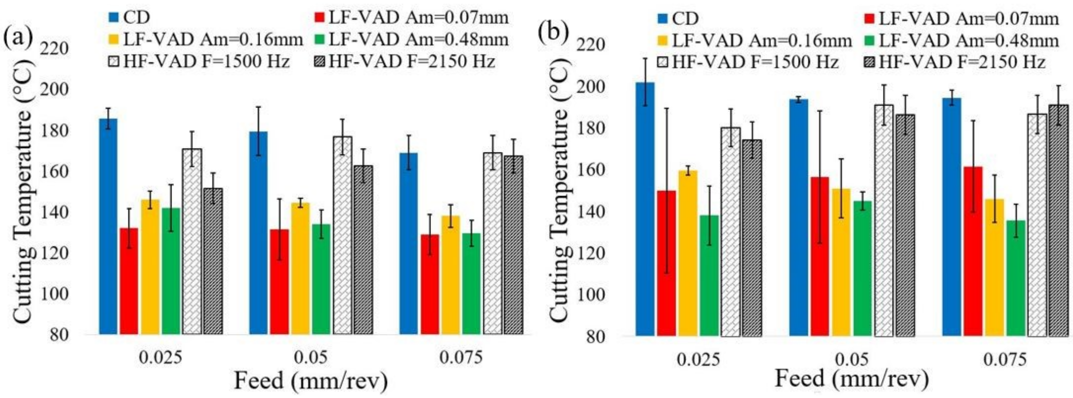


**Figure 4-6:** Effect of VAD on the cutting temperature at (a) *N*=2,000 rpm (b) *N*=3,000 rpm.

### 4.4.3 Chip morphology

The non-cutting process under the chisel edge is a major factor resulting in fiber extrusion, and delamination damage. Superimposing a harmonic motion over the conventional axial feed results in a periodic chisel edge movement. This impact loading reduces the energy absorbed by the material for the following reasons [35, 36] :

- There is a localized material response over a small region [36, 37].
- The non-cutting process under the chisel edge is discarded through the axial oscillation mechanism.
- A conically-shaped shear zone creation at the impact point (the chisel edge) [36].

Figure 4-7, presents a schematic diagram to describe the fiber behavior at steady-state tool movement (CD) and the periodical chisel edge impact mechanism. Further analysis was performed on the chips collected using scanning electron microscopic (SEM) examination, to investigate the VAD influence on the fiber-cutting process. The chips collected during LF-VAD appears sharper and more organized, (see Figure 4-8). On the other hand, Figure 4-9 shows a blunt fiber during CD. This observation could be attributed to the following:

- Changing the cutting mechanism under the chisel edge to periodic impact.
- Lower cutting temperature at LF-VAD resulting in maintaining the material stiffness, and consequently resisting the fiber-matrix debonding mechanism.

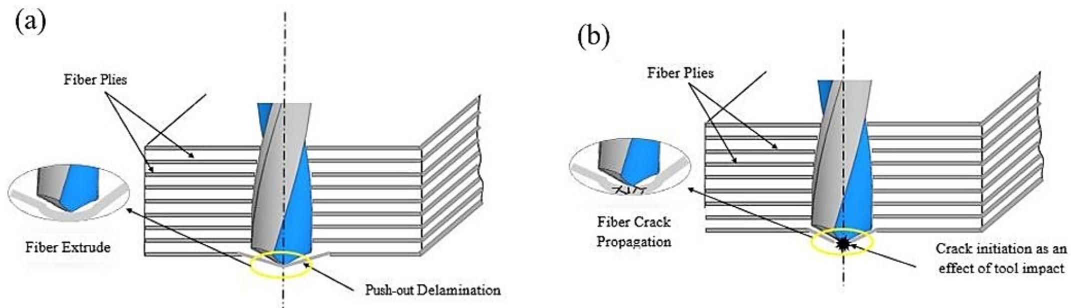


**Figure 4-7:** Effect of drilling technique on the carbon fiber-reinforced polymers (CFRP) fibers (a) CD (b) VAD.

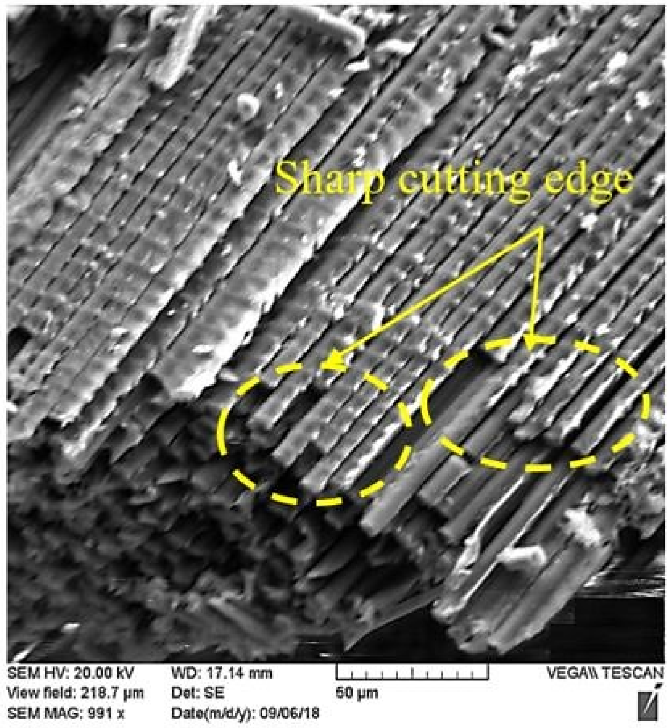


**Figure 4-8:** Effect of LF-VAD on the CFRP chips at $f$=0.075 mm/rev, $N$=3,000 rpm, and $A_m$=0.48 mm.

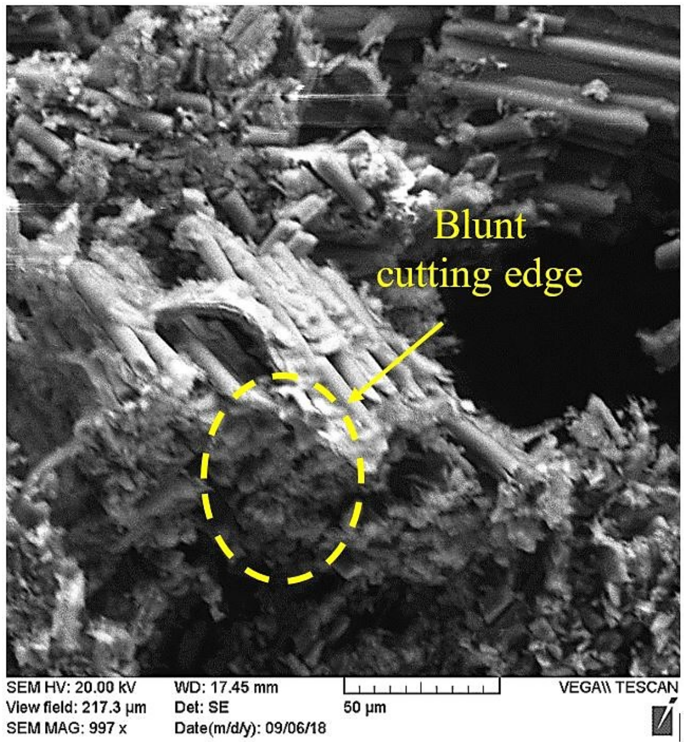


**Figure 4-9:** Effect of CD on the CFRP chips at $f$ = 0.075 mm/rev and $N$ = 3,000 rpm.

Figure 4-10 shows the effect of LF-VAD amplitude on the machined fiber length at $f$ = 0.075 mm/rev and $N$ = 3,000 rpm. Increase the LF-VAD amplitude led to increased machined fiber length by 50%. The machined fiber length was 200 µm at $A_m$= 0.07 mm and 300 µm at $A_m$= 0.48 mm. On the other hand, the maximum fiber length during CD was 80 µm. This increase is attributed to the influence of cyclic cooling, as presented in section 4.3. Such trends are comparable to the UAD investigation presented in [24].

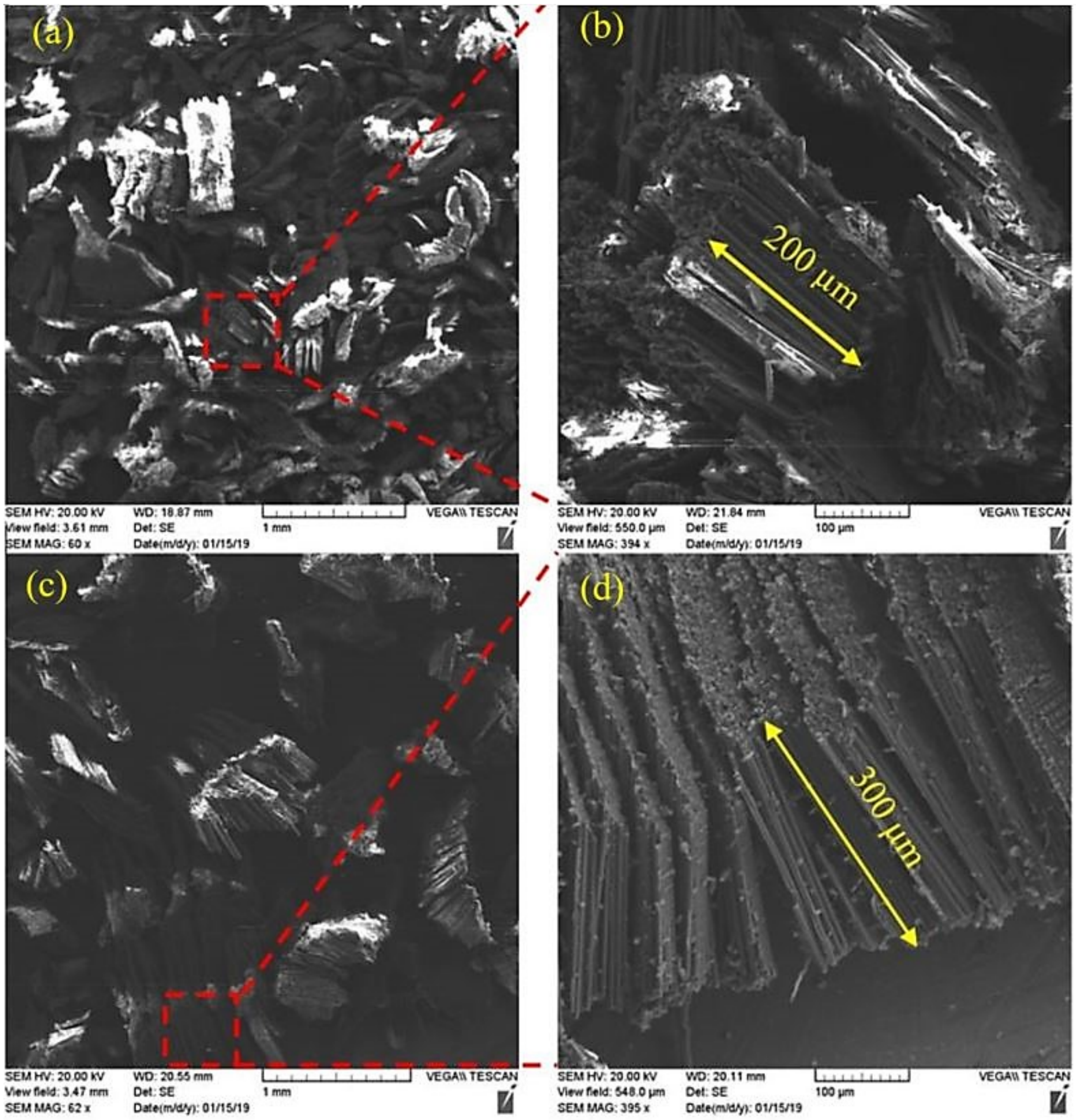


**Figure 4-10:** Effect of LF-VAD amplitude on the fiber length (a,b) $A_m$= 0.07 mm and (c,d) $A_m$= 0.48mm.

### 4.4.4 Geometric and surface integrity

#### *4.4.4.1 Delamination*

Figure 4-11 compares the effect of LF-VAD and CD on the exit delamination in the case of free and adhesive tape back support. For all machining parameters, LF-VAD showed a significant enhancement at exit delamination (including the free support case). The delamination factor '$\varphi_d$' was evaluated using equation (4.1), as described in [3].

$$\varphi_d = \frac{D_{actual} - D_{nominal}}{D_{nominal}} \tag{4.1}$$

Where $D_{actual}$ is the diameter of a circle including the circumscribing delamination, while $D_{nominal}$ representing the nominal hole diameter.

The delamination factor for CD was ≤ 0.5 at $N$= 2,000 rpm and ≥ 0.5 at $N$= 3,000 rpm, at free support. On the other hand, the $\varphi_d$ for LF-VAD was ≤ 0.2, for all machining conditions. This enhancement is attributed to lower cutting temperature and the proper fiber-cutting process under the chisel edge.

For adhesive back support, the delamination factor was ≤ 0.5 for CD and ≤ 0.2 for LF-VAD, at all machining conditions. The adhesive tape increased the matrix stiffness and reduces the thrust force negative effect, and consequently, the fiber-cutting process is enhanced.

The delamination factor achieved is lower than the one reported in [20] for LF-VAD, due to the higher frequency range which reduces the cyclic tool duty interval. Moreover, using a higher modulation amplitude showed a smaller delamination factor reduction compared to the LF-VAD study reported in [4], for the same reason.

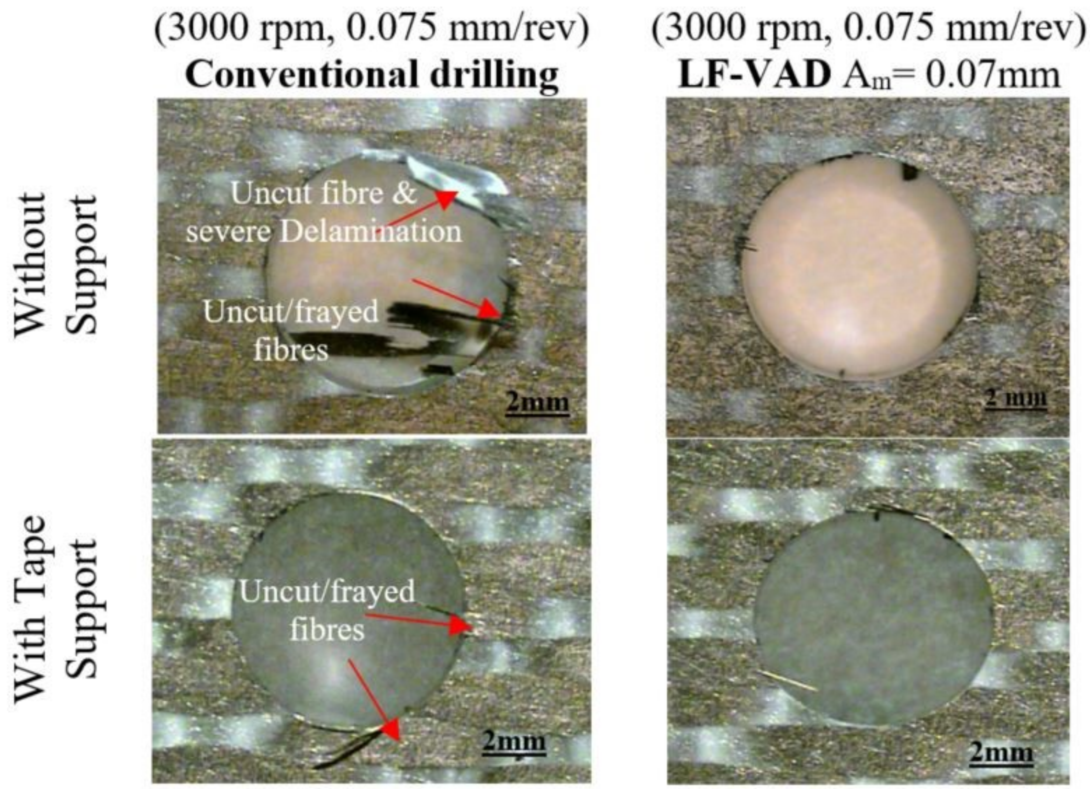


**Figure 4-11:** Effect of cutting technique, adhesive back support, and machining parameters on the exit delamination.

The HF-VAD showed a lower delamination factor compared to the CD, for all machining conditions. The maximum delamination factor measured during HF-VAD was 0.2. The free delamination process was achieved at the maximum machining load $f = 0.075$ mm/rev and $N = 3{,}000$ rpm, as shown in Figure 4-12. This enhancement is attributed to lower uncut chip thickness, cutting temperature, and thrust force (see sections 4.3., 4.4.1, and 4.4.2).

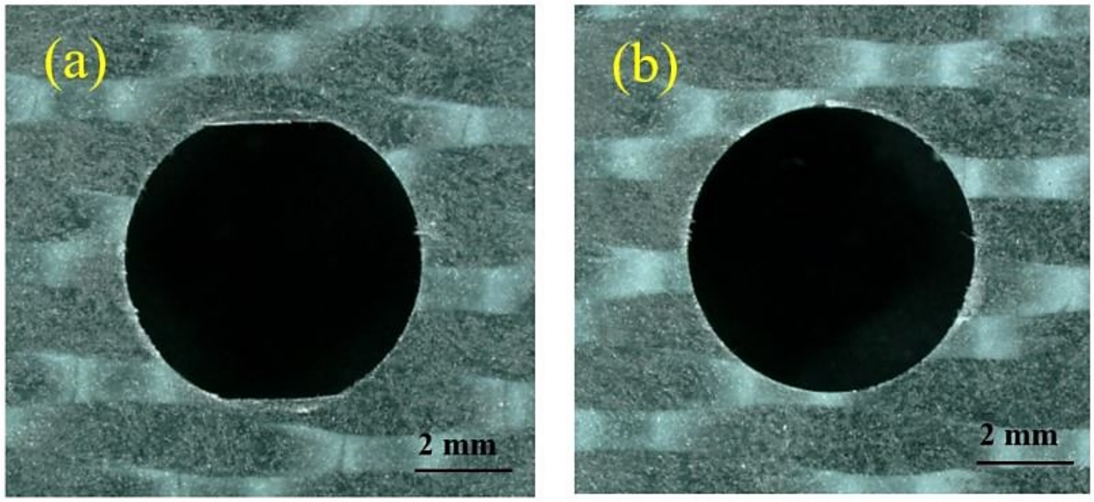


**Figure 4-12:** Effect of HF-VAD on the exit delamination at $f$ = 0.075 mm/rev and $N$ = 3,000 rpm for (a) F= 1500 Hz and (b) F = 2150 Hz.

*4.4.4.2 Exit hole wall quality*

Matrix debonding, fiber pull-out, and uneven surface are typical defects during CD [7]. Figure 4-13, presents the effect of CD on the exit hole wall. The high cutting temperature leads to matrix melting and, consequently, severe debonding damage is initiated. This observation agrees with the temperature analysis in section 4.4.2. Debonding damage reduces the matrix resistance, and consequently the fiber pull-out damage. The damaged area observed extended to 300 µm from the exit surface. LF-VAD showed a significant enhancement to the machining surface. The damaged area was reduced by more than 50 % with a smooth machined surface, as shown in Figure 4-14 This enhancement is attributed to the following:

- Lower cutting temperature (section 4.4.2).
- Lower duty time (section 4.3.).
- Proper fiber-cutting process under the chisel edge (section 4.4.3).

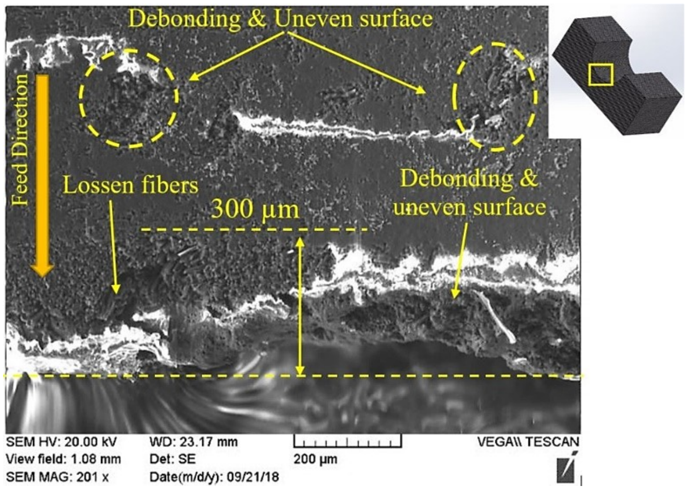


**Figure 4-13:** The SEM examination of CD machined hole at *f* = 0.075 mm /rev and *N* =3,000 rpm.

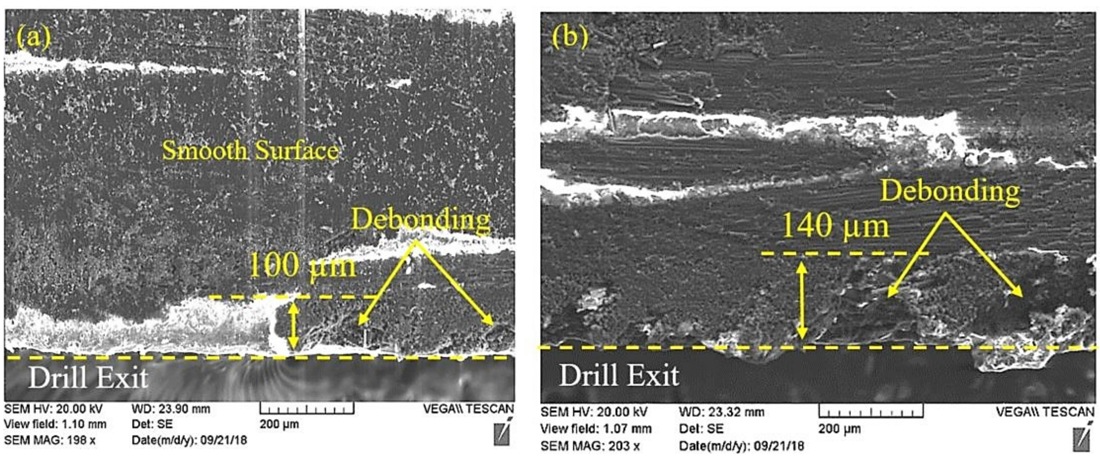


**Figure 4-14:** The scanning electron microscopic (SEM) examination of LF-VAD machined hole at *f* = 0.075 mm /rev and *N* =3,000 rpm on the exit surface for (a) $A_m$= 0.07 mm and (b) $A_m$=0.48mm.

Figure 4-15, presents the effect of HF-VAD on the exit wall quality. Lower uncut chip thickness led to cutting energy reduction. As a consequence, the total damage reduced to 80 µm at F= 1500 Hz and to 120 µm at F= 2150 Hz. The higher damaged area at F= 2150 Hz could be attributed to the higher tool-wall friction forces.

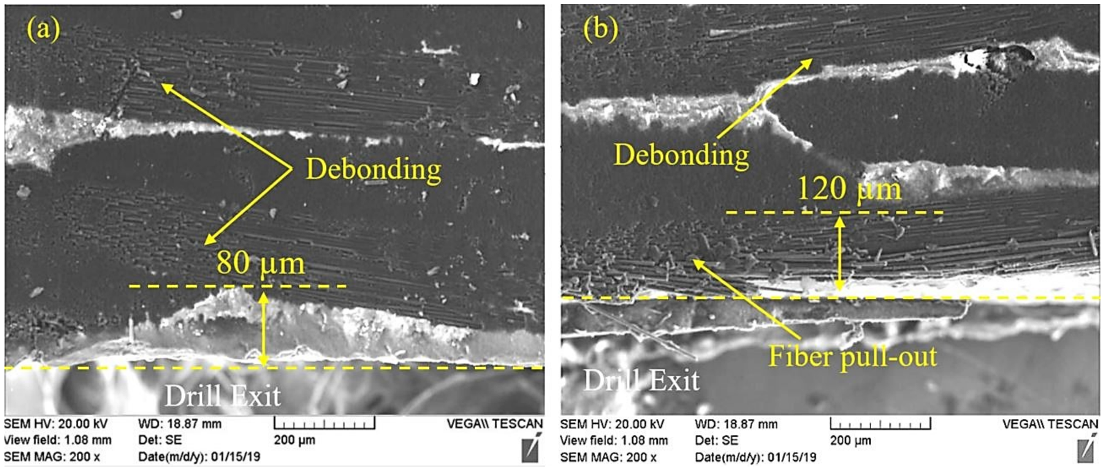


**Figure 4-15:** The SEM examination of HF-VAD machined hole at $f$ = 0.075 mm /rev and $N$ =3,000 rpm on the exit surface for (a) F= 1500 Hz and (b) F= 2150 Hz.

*4.4.4.3 Surface roughness*

Analysis of the surface roughness (Ra, Rz) at N = 2,000 rpm, indicated no significant difference between VAD and CD. For all machining conditions, the maximum Ra and Rz were 1.5 µm and 10 µm, respectively for both machining techniques. However, increasing the cutting speed to $N$ = 3,000 rpm resulted in a higher Ra and Rz for CD (3 µm and 17 µm), while the maximum Ra and Rz for VAD were 1.5 µm and 10 µm, respectively. This reduction is attributed to the lower cutting temperature which enhances the matrix stiffness.

Figure 4-16 shows the surface texture analysis for VAD and CD machined surfaces. The minimum depth for VAD was 6 µm and 14.5 µm for CD. This observation confirms the benefits of VAD regarding cutting temperature, as described in section 4.4.2.

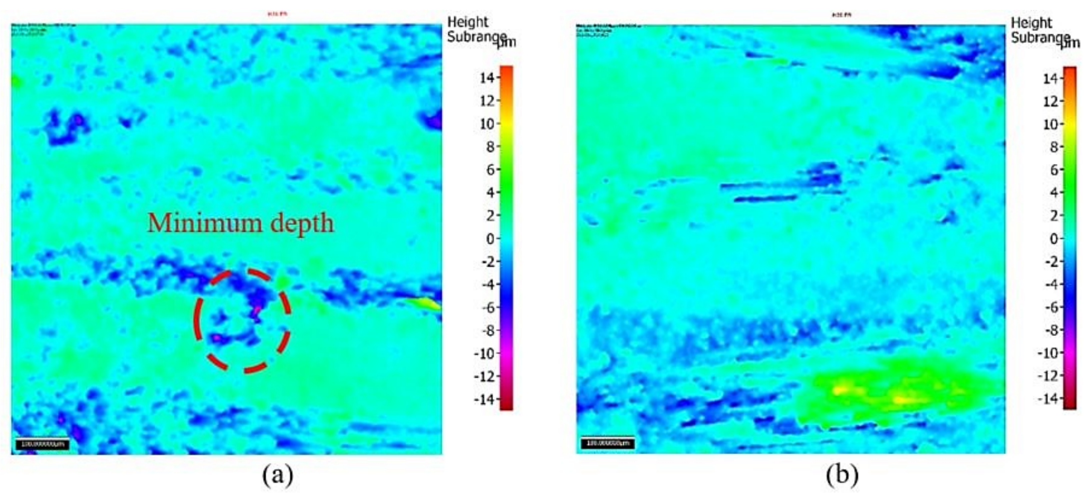


**Figure 4-16:** Effect of machining technique on the CFRP surface texture measurement. (a) CD (b) LF-VAD at $A_m$=0.48 mm.

## Conclusions

This experimental study evaluated the machining response during vibration assisted drilling (VAD) of CFRP material. The LF-VAD study results are obtained at $W_f$ = 2.5 cycles/rev (F= 83.3 Hz and 125 Hz) for different cutting speeds, feeds, and amplitudes. On the other hand, the HF-VAD study results are obtained at F= 1500 Hz and 2150 Hz and $A_m$ = 3 µm for different machining conditions. The kinematics of the instantaneous cutting tool position were used to study the effect of VAD machining parameters on the mechanical and thermal load compared to conventional drilling. Furthermore, the study compared the effect of LF-VAD on exit delamination, to the CD with and without flash breaker back support. The following are of the main experimental observations:

1. For all machined parameters, LF-VAD showed higher thrust forces as compared to the CD. This increase is due to higher uncut chip thickness and tool impact.
2. HF-VAD showed up to 16% reduction in the thrust force compared to CD.

3. VAD showed a significant reduction in cutting temperature compared to CD. The cutting temperature reduction for LF-VAD was 31% and 13% for HF-VAD.
4. Free delamination drilling was successfully achieved by using VAD due to lower thermal load. The delamination factor for CD was ≤ 0.5 at $N$= 2,000 rpm and ≥ 0.5 at $N$= 3,000 rpm respectively. On the other hand, the VAD resulted in delamination factor ≤ 0.2 for all machining conditions.
5. The adhesive tape back support reduced the delamination factor for CD to ≤ 0.5 for all machining conditions.
6. LF-VAD resulted in a longer machined fiber compared to CD. The fiber length increased from 80 µm at CD to 300 µm at LF-VAD with $A_m$ = 0.48mm.
7. Based on the SEM examination of the machined wall surface, VAD resulted in a significant enhancement to the machined surface quality compared to the CD

## References

[1] S. L. Soo, A. M. Abdelhafeez, M. Li, R. Hood, and C. M. Lim, "The drilling of carbon fibre composite–aluminium stacks and its effect on hole quality and integrity," *Proceedings of the Institution of Mechanical Engineers, Part B: Journal of Engineering Manufacture,* p. 0954405417728312, 2017.

[2] E. Brinksmeier and R. Janssen, "Drilling of multi-layer composite materials consisting of carbon fiber reinforced plastics (CFRP), titanium and aluminum alloys," *CIRP Annals-Manufacturing Technology,* vol. 51, pp. 87-90, 2002.

[3] R. Hussein, A. Sadek, M. A. Elbestawi, and M. Attia, "Low-frequency vibration-assisted drilling of hybrid CFRP/Ti6Al4V stacked material," *International Journal of Advanced Manufacturing Technology,* vol. 98, pp. 2801-2817, Oct 2018.

[4] K. Debnath and I. Singh, "Low-frequency modulation-assisted drilling of carbon-epoxy composite laminates," *Journal of Manufacturing Processes,* vol. 25, pp. 262-273, 2017.

[5] D. Che, I. Saxena, P. Han, P. Guo, and K. F. Ehmann, "Machining of carbon fiber reinforced plastics/polymers: a literature review," *Journal of Manufacturing Science and Engineering,* vol. 136, p. 034001, 2014.

[6] D. Liu, Y. Tang, and W. Cong, "A review of mechanical drilling for composite laminates," *Composite Structures,* vol. 94, pp. 1265-1279, 2012.

[7] R. Fu, Z. Jia, F. Wang, Y. Jin, D. Sun, L. Yang*, et al.*, "Drill-exit temperature characteristics in drilling of UD and MD CFRP composites based on infrared thermography," *International Journal of Machine Tools and Manufacture,* vol. 135, pp. 24-37, 2018.

[8] E. Persson, I. Eriksson, and L. Zackrisson, "Effects of hole machining defects on strength and fatigue life of composite laminates," *Composites Part A: Applied Science and Manufacturing,* vol. 28, pp. 141-151, 1997/01/01/ 1997.

[9] W.-C. Chen, "Some experimental investigations in the drilling of carbon fiber-reinforced plastic (CFRP) composite laminates," *International Journal of Machine Tools and Manufacture,* vol. 37, pp. 1097-1108, 1997.

[10] V. Gaitonde, S. Karnik, J. C. Rubio, A. E. Correia, A. Abrao, and J. P. Davim, "Analysis of parametric influence on delamination in high-speed drilling of carbon fiber reinforced plastic composites," *Journal of materials processing technology,* vol. 203, pp. 431-438, 2008.

[11] L. Romoli and G. Dini, "Experimental study on the influence of drill wear in CFRP drilling processes," in *ICME 08*, 2008.

[12] Z. Linbo, W. Lijiang, and W. Xin, "Study on vibration drilling of fiber reinforced plastics with hybrid variation parameters method," *Composites Part A: Applied Science and Manufacturing,* vol. 34, pp. 237-244, 2003.

[13] V. Tagliaferri, G. Caprino, and A. Diterlizzi, "Effect of drilling parameters on the finish and mechanical properties of GFRP composites," *International Journal of Machine Tools and Manufacture,* vol. 30, pp. 77-84, 1990.

[14] H. Ho-Cheng and C. Dharan, "Delamination during drilling in composite laminates," *Journal of engineering for industry,* vol. 112, pp. 236-239, 1990.

[15] J. Xu, C. Li, S. Mi, Q. An, and M. Chen, "Study of drilling-induced defects for CFRP composites using new criteria," *Composite Structures,* vol. 201, pp. 1076-1087, 2018/10/01/ 2018.

[16] M. Durante, L. Boccarusso, D. De Fazio, and A. Langella, "Circular cutting strategy for drilling of carbon fiber-reinforced plastics (CFRPs)," *Materials and Manufacturing Processes,* pp. 1-13, 2019.

[17] I. Shyha, S. L. Soo, D. Aspinwall, S. Bradley, R. Perry, P. Harden*, et al.*, "Hole quality assessment following drilling of metallic-composite stacks," *International Journal of Machine Tools and Manufacture,* vol. 51, pp. 569-578, 2011.

[18] I. S. Shyha, D. K. Aspinwall, S. L. Soo, and S. Bradley, "Drill geometry and operating effects when cutting small diameter holes in CFRP," *International Journal of Machine Tools and Manufacture,* vol. 49, pp. 1008-1014, 10// 2009.

[19] C. Zhang and M. Lu, "A novel variable-dimensional vibration-assisted actuator for drilling CFRP," *The International Journal of Advanced Manufacturing Technology,* vol. 99, pp. 3049-3063, December 01 2018.

[20] A. Sadek, M. Attia, M. Meshreki, and B. Shi, "Characterization and optimization of vibration-assisted drilling of fibre reinforced epoxy laminates," *CIRP Annals-Manufacturing Technology,* vol. 62, pp. 91-94, 2013.

[21] X. Wang, L. Wang, and J. Tao, "Investigation on thrust in vibration drilling of fiber-reinforced plastics," *Journal of Materials Processing Technology,* vol. 148, pp. 239-244, 2004.

[22] F. Makhdum, D. N. P. Norddin, A. Roy, and V. V. Silberschmidt, "Ultrasonically assisted drilling of carbon fibre reinforced plastics," in *Solid State Phenomena*, 2012, pp. 170-175.

[23] F. Makhdum, V. A. Phadnis, A. Roy, and V. V. Silberschmidt, "Effect of ultrasonically-assisted drilling on carbon-fibre-reinforced plastics," *Journal of Sound and Vibration,* vol. 333, pp. 5939-5952, 11/24/ 2014.

[24] A. Gupta, S. Barnes, I. McEwen, N. Kourra, and M. A. Williams, "Study of cutting speed variation in the ultrasonic assisted drilling of carbon fibre composites," in *ASME*

*2014 International Mechanical Engineering Congress and Exposition*, 2014, pp. V02BT02A038-V02BT02A038.

[25] F. Makhdum, L. T. Jennings, A. Roy, and V. V. Silberschmidt, "Cutting forces in ultrasonically assisted drilling of carbon fibre-reinforced plastics," in *Journal of Physics: Conference Series*, 2012, p. 012019.

[26] V. A. Phadnis, F. Makhdum, A. Roy, and V. V. Silberschmidt, "Experimental and numerical investigations in conventional and ultrasonically assisted drilling of CFRP laminate," *Procedia CIRP,* vol. 1, pp. 455-459, 2012.

[27] A. Sanda, I. Arriola, V. G. Navas, I. Bengoetxea, and O. Gonzalo, "Ultrasonically assisted drilling of carbon fibre reinforced plastics and Ti6Al4V," *Journal of Manufacturing Processes,* vol. 22, pp. 169-176, 2016.

[28] MITIS Engineer. *MITIS Tool Holder*. Available: https://www.mitis.fr/

[29] J. Panju, M. Meshreki, and M. Attia, "Design of a Retrofittable Spindle Attachment for High Frequency Vibration-Assisted Drilling," in *ASME 2014 International Mechanical Engineering Congress and Exposition*, 2014, pp. V02AT02A034-V02AT02A034.

[30] A. company. *Flash breaker data sheet*. Available: https://www.freemansupply.com/datasheets/Airtech/flashbreaker125.pdf

[31] O. Pecat and I. Meyer, "Low frequency vibration assisted drilling of aluminium alloys," in *Advanced Materials Research*, 2013, pp. 131-138.

[32] A. Sadek, M. Meshreki, and M. Attia, "Effect of Tool Kinematics on the Drilling Forces and Temperature in Low Frequency High Amplitude Vibration Assisted Drilling," in *ASME 2014 International Mechanical Engineering Congress and Exposition*, 2014, pp. V02AT02A035-V02AT02A035.

[33] Z. Deyuan and W. Lijiang, "Investigation of chip in vibration drilling," *International Journal of Machine Tools and Manufacture,* vol. 38, pp. 165-176, 1998.

[34] A. Sadek, "Vibration Assisted Drilling of Multidirectional Fiber Reinforced Polymer Laminates," Ph.D., McGill University Libraries, 2014.

[35] Q. Chen, Z. Guan, Z. Li, Z. Ji, and Y. Zhuo, "Experimental investigation on impact performances of GLARE laminates," *Chinese Journal of Aeronautics,* vol. 28, pp. 1784-1792, 2015.

[36] W. Cantwell and J. Morton, "Comparison of the low and high velocity impact response of CFRP," *Composites,* vol. 20, pp. 545-551, 1989.

[37] W. Cantwell, "The influence of target geometry on the high velocity impact response of CFRP," *Composite Structures,* vol. 10, pp. 247-265, 1988.

# Chapter 5

## Low-Frequency Vibration Assisted Drilling of Hybrid CFRP/Ti6Al4V stacked material

**Complete Citation:**

Hussein, R., Sadek, A., Elbestawi, M.A., Attia, M.H. (2018). Low-Frequency Vibration Assisted Drilling of Hybrid CFRP/Ti6Al4V stacked material. *The International Journal of Advanced Manufacturing Technology*, Volume 98, Issue 9-12, pp 2801-2817. DOI: 10.1007/s00170-018-2410-2

**Copyright:**

**Relative Contributions:**

| | |
|---|---|
| R. Husseint: | Performed experiments, analysis, and data interpretation. Wrote the first draft of the manuscript. Helped with submitting the final manuscript to the journal (corresponding author). |
| A. Sadek: | Helped with the experiments. Revised the manuscript |
| M. A. Elbestawi: | Supervisor of R. Hussein. Revised the manuscript. Was responsible of submitting the final manuscript to the journal (corresponding author). |
| M. H. Attia: | Revised the manuscript. |

**Abstract:**

The drilling of Carbon fibre reinforced polymers (CFRP) and Ti6Al4V alloy stacked materials play a significant role in the aerospace industry's ability to achieve improved machinability and assembly. Conventional drilling has resulted in various challenges such as CFRP delamination, unacceptable hole accuracy, and high tool wear. In addition, high cutting temperatures and poor chip evacuation mechanisms were also identified as important difficulties necessitating the drilling of each material separately. Low-frequency vibration-assisted drilling (LF-VAD) promises a high potential for overcoming these challenges.

The primary objective of this study was to investigate the effect of machining parameters (Cutting speed, feed rate, Modulation amplitude, and Modulation frequency) on the LF-VAD stacked drilling of CFRP/Ti6Al4V. The effect of applying a 2.5 cycles/rev frequency modulation to a wide range of machining parameters is reported, and the results are discussed. The variables considered included: cutting speed, feed rate, and modulation amplitude. The results show up to a 56% reduction in cutting temperature, as well as a change in chip morphology. The effects on hole quality and surface roughness are also presented.

**Keywords:**

Vibration Assisted Drilling; Low-Frequency Vibration Assisted Drilling; CFRP/Ti6Al4V; stacked material; Advanced machining.

**Acronyms:**

| | |
|---|---|
| CFRP | Carbon fibre reinforced polymers |
| VAD | Vibration assisted drilling |
| LF-VAD | Low frequency-vibration assisted drilling |
| SPD | Severe plastic deformation |
| MQL | Minimum quantity lubrication |
| ANOVA | Analysis of variance |

**Notations:**

| | |
|---|---|
| $N$ | Cutting speed (rpm) |
| $f$ | Feed rate (mm/rev) |
| $A_m$ | Modulation amplitude (mm) |
| $F$ | Frequency (µm) |
| $Ø_d$ | Delamination factor |

**Acknowledgment:**

This study was performed using the facilities at the Canadian National Research Council (CNRC), Aerospace Manufacturing Group. The use of their facilities, equipment and the technical support is greatly appreciated.

The authors gratefully thank Mrs. Victoria Jarvis, XRD2/XRD3 specialist at McMaster University, for her assistance during the XRD measurements and analysis.

## 5.1 Introduction

Composites such as CFRP carbon fibre reinforced polymers (CFRP), titanium, and aluminum alloys are widely used in the aircraft industry, with more than 75% of the new generation of aircraft being built using these composite materials [1, 2]. This can be attributed to their high strength to weight ratio, which results in improved fuel economy and lower environmental impact.

Mechanical fastening is typically used for assembling load-carrying members of different materials in the aircraft structure. The practice of drilling each material separately could result in as much as 60% of composite material parts being rejected due to unacceptable hole quality leading to potential delamination issues [2, 3]. Also, several other machining difficulties have been reported, such as matrix thermal damage during the drilling of CFRP [4], chip evacuation of aluminum alloys and low thermal conductivity combined with a high chemical affinity of titanium alloys [5, 6]. These machinability problems result in higher tool wear, and failure to meet the high precision requirements of the aircraft industry.

Single process drilling of the composite materials in-situ, known as stacked drilling, is generating considerable interest in dealing with these challenges. Stacked drilling can lead to a significant reduction in machining time and cost. The first approach taken to manufacture CFRPs and titanium alloys was developed using conventional drilling techniques while attempting to optimize machining parameters. The effect of machining parameters (speed and feed) and cutting tool material has been investigated during drilling of CFRP/Ti6Al4V stack [7]. The dependence of the thrust force on the feed rate was evaluated in [8]. It is generally accepted that titanium alloys are difficult to machine due to their low thermal conductivity, high chemical affinity, and their production of continuous chips during cutting [9, 10]. During single process drilling, which has limited evacuation space, the extended titanium chips accumulate inside the drill flutes, resulting in increasing the cutting zone temperature. Thermal damage of the CFRP material and tool-chip welding occur, particularly under dry-cutting conditions.

Increasing the cutting speed to avoid chip accumulation inside the drill flutes, is not effective since it results in increased cutting zone temperature leading to material softening [11, 12]. This practice can also cause thermal damage and increased tool wear leading to poor surface finish [3, 13].

Chip evacuation to maintain lower cutting temperature is necessary for optimizing the performance of the CFRP machining process. Several methods have been reported in the literature which attempts to achieve this goal [14]. One method suggested, is to use a two-step drilling technique to reduce the amount of material passing through the tool flutes [2]. A second approach suggested reducing the tool-chip friction by using tool coatings and advanced lubrication strategies [15]. The third approach suggested the use of techniques such as orbital or vibration assisted drilling (VAD) in order to prevent the formation of continuous chips[16]. This method is of particular interest since chip size can be controlled, which facilitates chip evacuation and reduces the cutting temperature during the drilling process [17].

In LF-VAD superimposing a harmonic motion in the axial direction, over the conventional tool feed movement, are used to control the tool engaging and retracting mechanism about the mean path motion. The instantaneous cutting edge position defines the chip geometry in terms of the maximum uncut chip thickness and the cutting duration which represent the chip width. Controlling the chip geometry has a direct impact on the cutting energy, represented by the cutting forces and temperature. Studying the vibration assisted drilling harmonic motion (frequency and amplitude) aims to improve the material removal process in terms of cutting forces, temperature, surface integrity, and tool life. On the other hand, the continuous cutting process through the conventional drilling showed a higher chip-rake face frictional forces, higher cutting temperature, poor and destructive chip evacuation mechanism.

The influence of VAD on-chip morphology is discussed in [18]. In general, chip morphology can be classified into three different regimes; ribbon chip (non-breaking), sawtooth-like chip (partial breaking), and segmented chip (complete breaking). Each regime has been associated with different chip extraction efficiencies. The modulation amplitude ($A_m$) and feed rate (f) were found to be the critical parameters in determining chip morphology and extraction efficiency in several experimental and theoretical studies [17-20]. The effect of the normalized frequency (oscillation/rev per cutting edge), and the normalized amplitude (amplitude to feed rate per cutting edge), on-chip evacuation during drilling of copper and Ti6Al4V, is discussed in [21].

The research reported in [22], investigated the effect of applying low frequency-vibration assisted drilling (LF-VAD) on Ti6Al4V and CFRP/Ti6Al4V stacked material. In this study, a 1.5 cycle/rev Modulation frequency ratio (F) was used with Minimum Quantity Lubrication (MQL). A 43% reduction in temperature was achieved during the Ti6Al4V drilling process. This was attributed to better chip evacuation and cooling mechanisms. Furthermore, the stacked drilling process resulted in improved surface integrity due to the lower cutting temperature. Analysis of tool wear for the same cutting parameters with different tool coatings was also reported in [23]. Generally, there is limited research that investigates the resulting cutting performance obtained by applying VAD with low frequency (less than 1KHz) on the stacked drilling of CFRP/Ti6Al4V. The influence of parameters such as Cutting speed (N), feed rate (f), Modulation amplitude ($A_m$), and Modulation frequency (F) on the cutting performance during stacked drilling of CFRP/Ti6Al4V is of particular relevance and interest.

## 5.2 Experimental procedures

The drilling tests were performed using a 5-axis Makino A88 machining centre with a maximum spindle speed (N) of 18,000 rpm. Axial oscillations were generated using a commercially available MITIS tool holder PG8045B3_HSK-A100_ER40, which has a 2.5 cycles/rev fixed frequency ratio (F) with an adjustable amplitude ($A_m$) range between 0.01-0.48 mm. A 6 mm drill diameter WC tool was chosen, since it is commonly used in the aerospace industry [24-26]. The setup shown in Figure 5-1 b) was used to monitor the tool-tip temperature during drilling. A stack of one CFRP and one Ti6Al4V plate was fixed on a U-Shaped Aluminum frame mounted on the front plate of the dynamometer. The U-shape allowed for the imaging of the tool-tip at the hole exit to be captured using an IR camera. The maximum tool-tip temperature at the hole exit was measured using FLIR SC8000 HD Series Infrared Camera. By tilting the camera's position towards the cutting direction, direct vision was achieved at all drilling processes, as shown in Figure 5-1. The cutting forces were monitored using a 4-component dynamometer (Kistler type 9272) and a Kistler multichannel charge amplifier (Type 5019B).

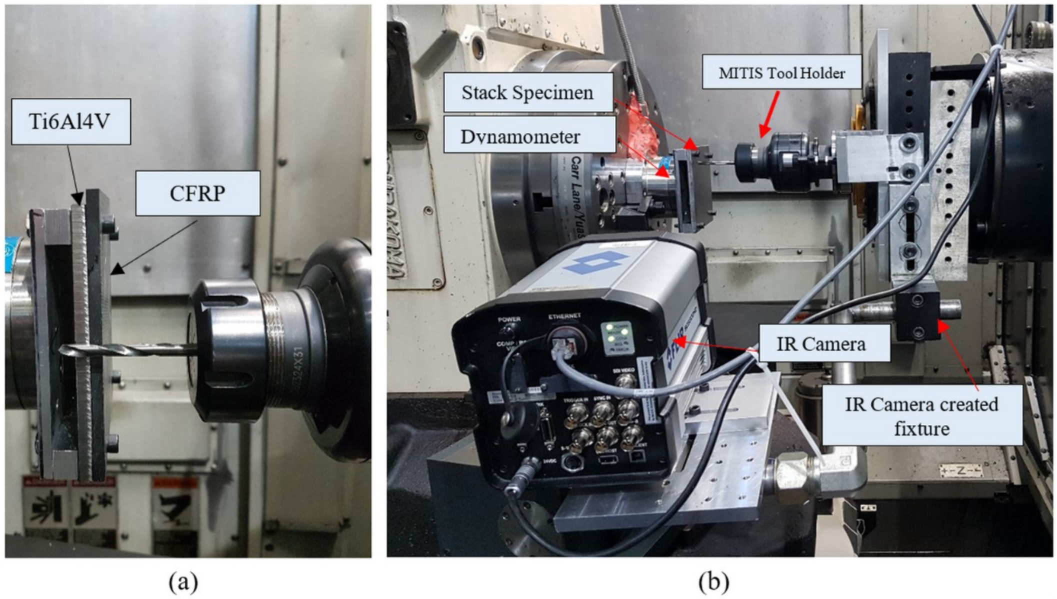


**Figure 5-1:** a) Workpiece materials stacking Sequence, b) Experimental Setup for the tool holder, Workpiece, and infrared camera.

A full factorial experimental study of LF-VAD (two levels of cutting speeds, three levels of feed rates, and five levels of cutting amplitude), with at least two repeat measurements for each condition, was carried out. Conventional cutting tests were also performed for comparison purposes. The cutting conditions and tool specifications are presented in Table 5-1. The average hole diameter and circularity were measured at the top and bottom surfaces for the CFRP and Ti6Al4V by taking an average of ten points on each circle using a Mitutoyo Coordinate Measuring Machine. The entry and exit delamination were measured using an Olympus Model GZX 12 optical microscope. Carbon fibre surface integrity and Ti6Al4V chip morphology were characterized using a Keyence Digital Microscope VHX-6000 Series. The Alicona surface roughness measurement instrument was used for the drilled hole surface roughness analysis of both materials. For microstructural examination, specimens were mounted and polished using a 3μm fine resin bonded diamond and etched with the following solution (1% HF, 2% HNO3, balance distilled H2O) for 15 seconds.

**Table 5-1:** Applied cutting conditions, cutting tool, and workpiece material.

| | |
|---|---|
| **Cutting conditions** | |
| Cutting speed *N* (rpm) | 2000, 3000 |
| Feed rate *f* (mm/rev) | 0.025, 0.05, and 0.075 |
| Amplitude $A_m$ (mm) | 0.07, 0.1, 0.16, 0.25, and 0.48 |
| Frequency F | 2.5 cycles/rev (83.33Hz at 2000 rpm and 125Hz at 3000 rpm) |
| Cooling | Dry |
| **Cutting Tool** | |
| Material | Tungsten Carbide |
| Diameter | 6 mm |
| Point angle | 118° |
| Helix angle | 20° |
| Tool Manufacturer | Fullerton |
| Model | 15107 |
| **Workpiece material specification** | |
| CFRP | - 42 × L-930(GT700) woven plies with the configuration $[[0,90]_{21}]s$, and flame retardant modified epoxy prepreg<br>- Decomposition temperature is 320°C. |
| Titanium alloy | Ti6Al4V |
| Stacking Sequence | CFRP: 5.8 ± 0.02 mm/Ti6Al4V: 6.75± 0.02 mm |

## 5.3 Results and Discussion

### 5.3.1 Thrust force

Figure 5-2, compares the average thrust forces measured in conventional drilling with LF-VAD of stacked CFRP and Ti6Al4V at different cutting conditions. Compared to conventional drilling, the LF-VAD technique resulted in a higher thrust force at all $A_m$ for both materials.

The thrust force for CFRP ranged between 45 N and 175 N, while for the Ti6Al4V it ranged from 240N and 944 N depending on $A_m$ and feed f. The thrust force gradually increased for two main reasons. The first is the higher impact force generated between the drilling tool and the part material. This is due to the increased in axial speed as a result of using 2.5 cycles/rev with a higher modulation amplitude. This higher impact force was also observed for 1.5 oscillation/rev [17]. This increase depends mainly on the applied $A_m$ and feed f. The second reason is using a higher $A_m$ which will increase the actual uncut chip thickness. This results in a higher thrust force for CFRP and Ti6Al4V, found to be 152% and 149%, respectively, achieved under f = 0.075 mm/rev, $A_m$ = 0.48 mm and $N$ =3,000 rpm.

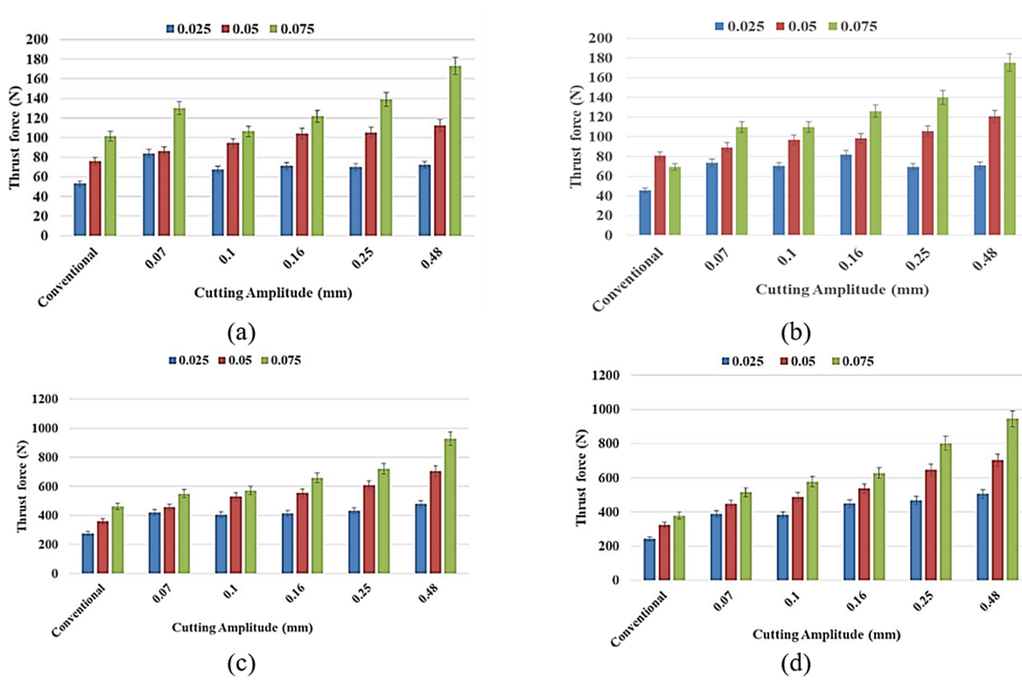


**Figure 5-2:** The effect of LF-VAD with different Am on the measured thrust force of CFRP and Ti6Al4V during stack drilling a,b) CFRP c,d)Ti6Al4V for $N$= 2000 and 3000 rpm respectively.

The determination of the uncut chip dimensions is important to the understanding of the performance of each drilling technique, and subsequently its effect on the observed thrust force. The instantaneous uncut chip thickness at each $A_m$ was calculated using the general formula introduced in [19].

$$d_{\mathrm{i}}(t_{\mathrm{i}}) = -f_r.\,\omega_T.\,t_{\mathrm{i}} + A_{\mathrm{m}}.\sin(2\pi\omega_{\mathrm{m}}t_{\mathrm{i}}) \tag{5.1}$$

The above formula determines the uncut chip thickness based on the difference between the axial positions of the two cutting edges at different angular positions. Figure 5-3, shows the calculated instantaneous uncut chip thickness at different $A_m$. The amount of uncut chip thickness in LF-VAD was found to be six times the uncut chip thickness in conventional drilling in the case of 0.48 mm modulation amplitude. The linear relation between $A_m$ and uncut chip thickness creates the gradual increase of thrust force with LF-VAD cutting amplitude.

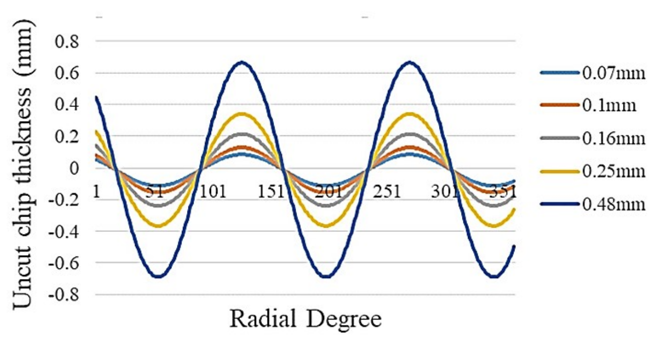


**Figure 5-3:** The effect of LF-VAD cutting amplitude on the instantaneous depth of the cut with a different feed rate.

#### *5.3.1.1 Statistical and Regression Analysis*

ANOVA statistical analysis was used to determine the machining parameters which impact the measured thrust force during Ti6Al4V plate drilling. The results obtained confirmed that feed rate has the highest impact with followed by modulation amplitude. The cutting speed had a negligible effect, as shown in Figure 5-4.

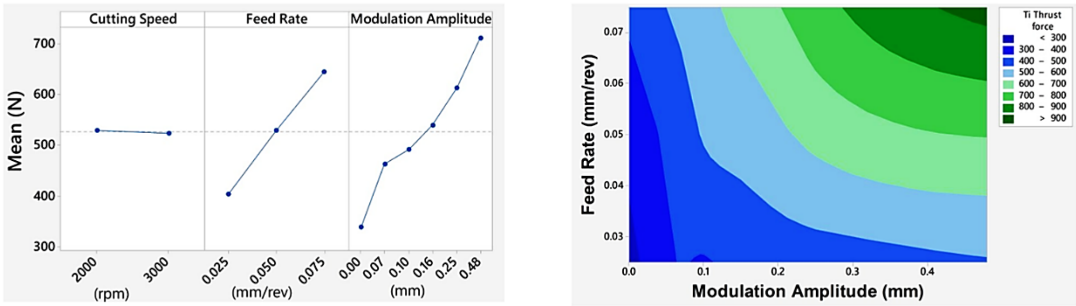


(a) (b)

**Figure 5-4:** a) The main effect of LF-VAD machining parameters plot for Ti6Al4V Thrust force, b) Thrust force as a function of feed rate and modulation amplitude.

A regression analysis was performed to identify the relationship between the thrust force (response), and the various cutting variables (predictors). It was also used to determine the influence of each variable on the thrust force. The results obtained are given in equations (5.2) and (5.3) below.

$$\text{Ti6Al4V Thrust force} = 291.7 - 0.0056\,N + 2437\,f + 48\,A_m + 13359\,f{*}A_m \quad (5.2)$$

$$\text{CFRP Thrust force} = 56.7 - 0.00192\,N + 595\,f - 60.2A_m + 2978\,f{*}A_m \quad (5.3)$$

where: N is the rotation speed in (rpm), f is the feed rate in (mm/rev), and $A_m$ is the modulation amplitude in (mm). The correlation coefficients (R2) of equations (5.2,3) are 93.34% and 91.41% respectively.

### 5.3.2 Cutting temperature

The results shown in Figure 5-5, demonstrate a significant reduction in cutting temperature when using LF-VAD as compared to conventional drilling, for all modulation amplitudes and feed rates. The following observations are made:

1. Switching from continuous to interrupted cutting reduces the duty cycle time. Consequently, more thermal energy dissipates through the cut chips rather than being transferred to the cutting tool.
2. The heat dissipation mechanism during disengagement cycles enhances the cutting tool cooling efficiency.
3. Interrupted cutting changes the chip morphology from extended helical to segmented.

This change enhances chip evacuation, thereby reducing the heat sources in the cutting region. The axial tool velocity increases linearly with increasing $A_m$ as the result of the fixed F ratio at 2.5 cycles/rev. This increase creates higher impact energy at the tool-workpiece interface, which adds more thermal energy to the cutting system. Consequently, the highest heat reduction (55.9%) was obtained at a lower feed rate combined with $A_m$ = 0.25 mm, while for the same feed rate with $A_m$ = 0.48 mm, the amount of heat reduction has been reduced as an effect of higher impact.

The cutting temperature was found to increase with increasing the feed rate. Within the tested range of machining parameters, the “optimum” LF-VAD conditions were obtained at a range of 0.1mm to 0.25 mm Am with a lower feed rate (0.025 mm/rev).

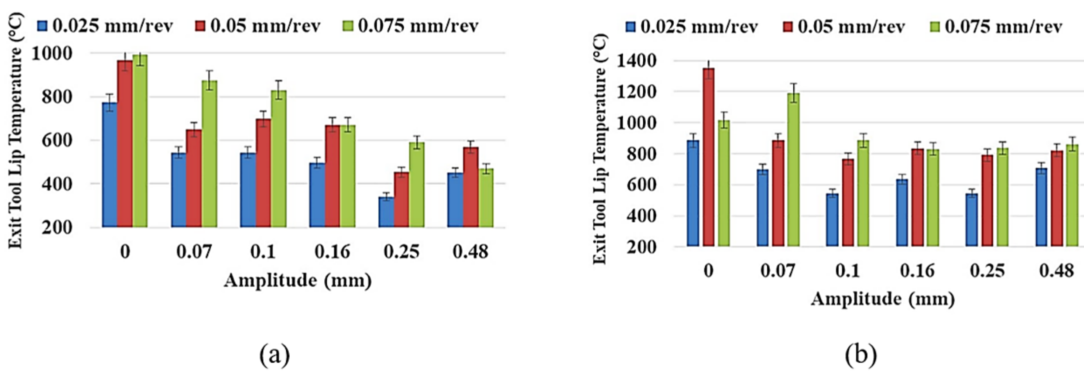


**Figure 5-5:** The effect of LF-VAD feed rate and cutting amplitude on the exit Tool-lip temperature for a) $N = 2000$ rpm, b) $N = 3000$ rpm.

### 5.3.3 Chip morphology

As shown in Figure 5-6, LF-VAD produced broken titanium chips (Figure 5-6 (b) and (c)), when compared to the long helical chips observed in conventional drilling (Figure 5-6 (a)). Fully segmented titanium chips were obtained during LF-VAD with an $A_m$ greater than or equal to 0.1 mm. Figure 5-6 (b) shows partially segmented chips (welded at the tips) produced at a modulation amplitude of 0.07 mm. This outcome could be due to one of the following reasons:

1. An incomplete chip breaking mechanism.
2. Chip welding due to higher cutting temperature.

The relation between the normalized amplitude and normalized frequency can be used to calculate the required modulation amplitude to verify the intermittent cutting condition as following [18, 21]:

$$\frac{4A}{f} \geq \frac{1}{\left| \sin\left(\frac{W_f \pi}{2}\right) \right|} \tag{5.4}$$

Accordingly, the modulation amplitude necessary to satisfy the chip breaking condition was determined to be lower than 0.07 mm.

The coefficient of heat transfer in the air gap between the cutting tool and the workpiece was evaluated for various modulation amplitude. The lowest value was found at a gap of 0.07 mm [27]. At this gap, the high temperature may result in chip welding Figure 5-6 (b)). This may adversely affect the hole quality in the CFRP during chip evacuation.

(a) (b) (c)

**Figure 5-6:** The effect of machining technique and cutting amplitude on-chip morphology a) Conventional drilling, b) LF-VAD $A_m$= 0.07mm, and c) LF-VAD $A_m$ =0.1mm.

*5.3.3.1 Effect of Chip Morphology on the cutting tool life*

Changing titanium chip morphology showed a significant effect on the cutting temperature, as illustrated in the temperature section. Moreover, segmented chips present a significant enhancement of the chip evacuation mechanism. This improvement gets rid of the tool-chip welding problem, as shown in Figure 5-7. Both tools are non-coated tungsten carbide, which used for the presented experimental work (conventional and VAD). In the current study, the chip-welding process has been observed under conventional drilling at N= 3000 rpm and f= 0.05, 0.075 mm/rev. On the other side, applying LF-VAD under all cutting conditions did not reveal any tool problems. Reducing chip-welding probability has a significant effect on increasing tool life even at higher cutting speed and feed rate, which has a high impact in reducing machining time and cost.

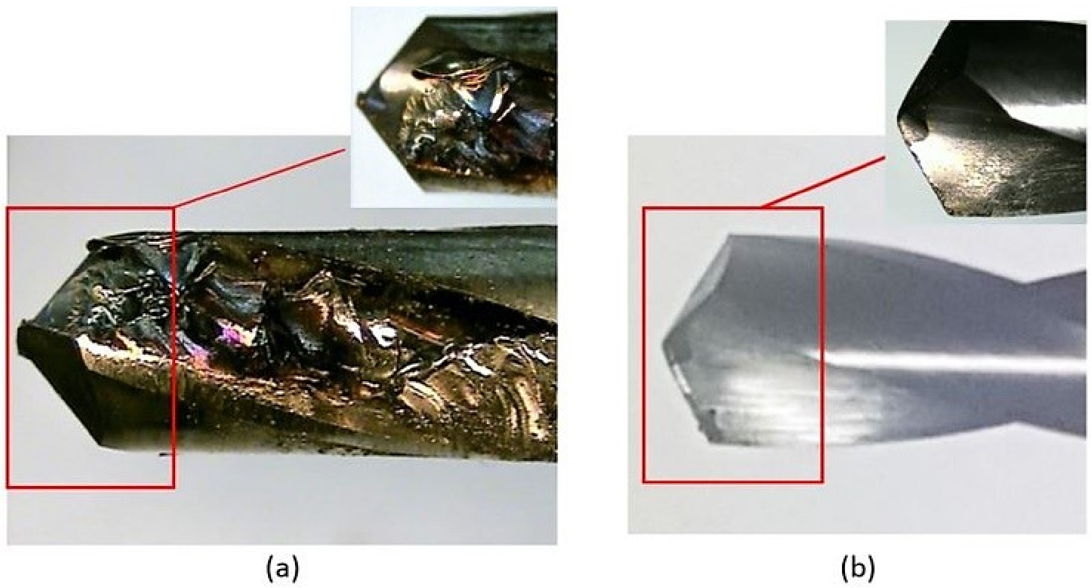


**Figure 5-7:** The effect of cutting technique on cutting tool during CFRP/Ti6Al4V stack material. a) Conventional drilling b) LF-VAD with $A_m$= 0.1 mm.

*5.3.3.2 Effect of Chip Morphology on the CFRP drilled hole surface*

Examination of the CFRP drilled hole surface showed considerable surface damage occurring during the chip evacuation mechanism under conventional drilling. Figure 5-8 demonstrates the improvement in surface quality obtained as result of the segmented chips produced during LF-VAD. However, during LF-VAD with $A_m$ = 0.07mm, fibre pull-out and fibre breakage can still be observed during the surface examination, as shown in Figure 5-8 (b). Under LF-VAD with $A_m$ = 0.1 mm, titanium chips in the range of 38-136 μm (maximum length) have been observed.

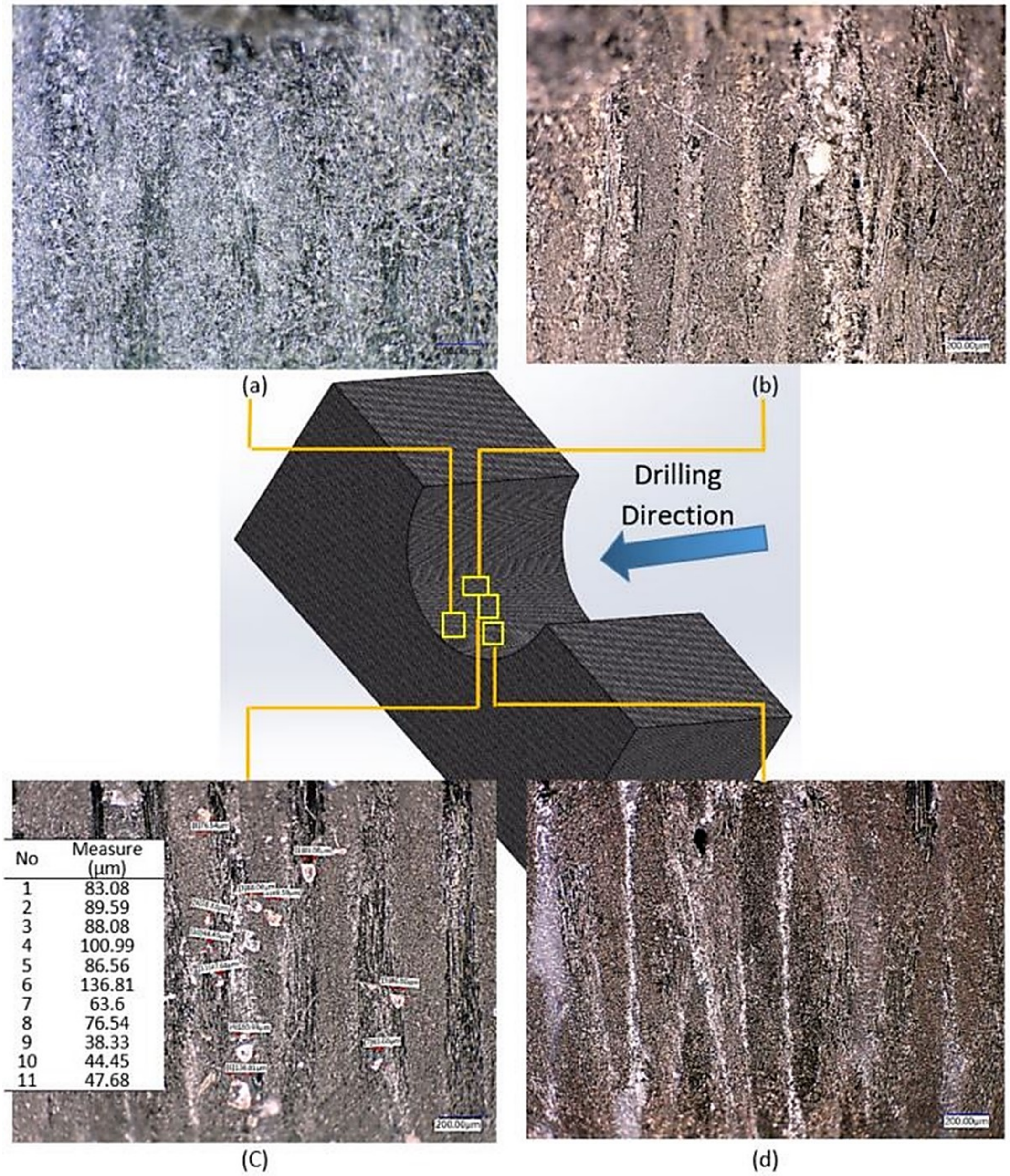


**Figure 5-8:** The effect of conventional and LF-VAD cutting amplitude on the CFRP drilled hole surface a) Conventional drilling, b) $A_m$ = 0.07 mm, c) $A_m$ = 0.1 mm, d) $A_m$ = 0.16 mm.

### 5.3.4 Hole quality

#### *5.3.4.1 Delamination*

The results of all conventional drilling tests completed in this research exceeded the acceptable entry and exit delamination limit as defined by aerospace manufactures ($Ø_d \leq 0.5$)[27]. However, the same cutting conditions with LF-VAD produced holes within acceptable delamination levels, as shown in Figure 5-9. The delamination factor "$Ø_d$" was evaluated using equation (5.5).

$$Ød = \frac{D\ actual - D\ nominal}{D\ nominal} \tag{5.5}$$

where ($D_{actual}$) represents the diameter of a circle that is concentric to the hole and circumscribing the delamination extents, while ($D_{nominal}$) is the nominal hole diameter.

Figure 5-9, Represents the measured entry and exit delamination factor for conventional drilling and LF-VAD at different cutting conditions. The figure shows that LF-VAD at an $A_m$ greater than or equal to 0.1 mm, produced delamination free holes and holes within acceptable delamination limits. Higher entry and exit delamination took place in conventional drilling and LF-VAD at $A_m$ = 0.07 mm only due to high temperature.

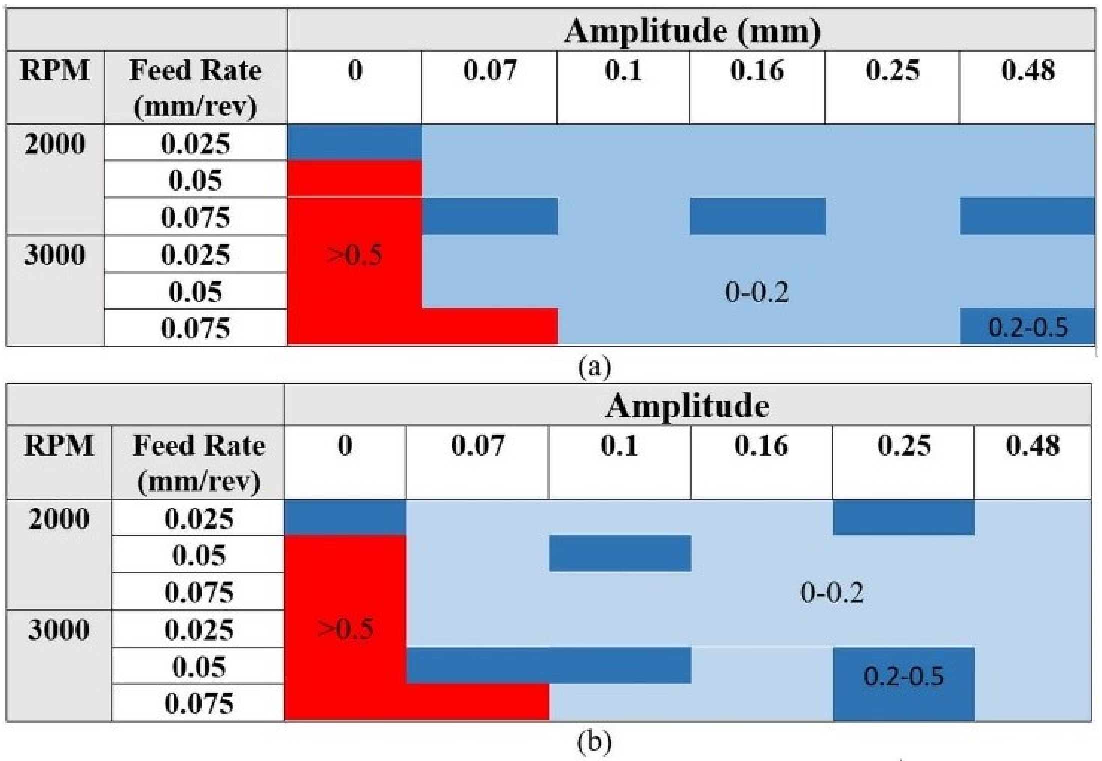


**Figure 5-9:** The effect of LF-VAD machining parameters on delamination during CFRP drilling a) Entry delamination, and b) Exit delamination.

As shown in Figure 5-10, the higher interface temperature during titanium layer drilling can lead to a burn out of the polymer matrix, which took place during conventional and LF-VAD drilling under low $A_m$ (0.07 mm). These results agree with those reported in section 5.3.2 on tool temperature.

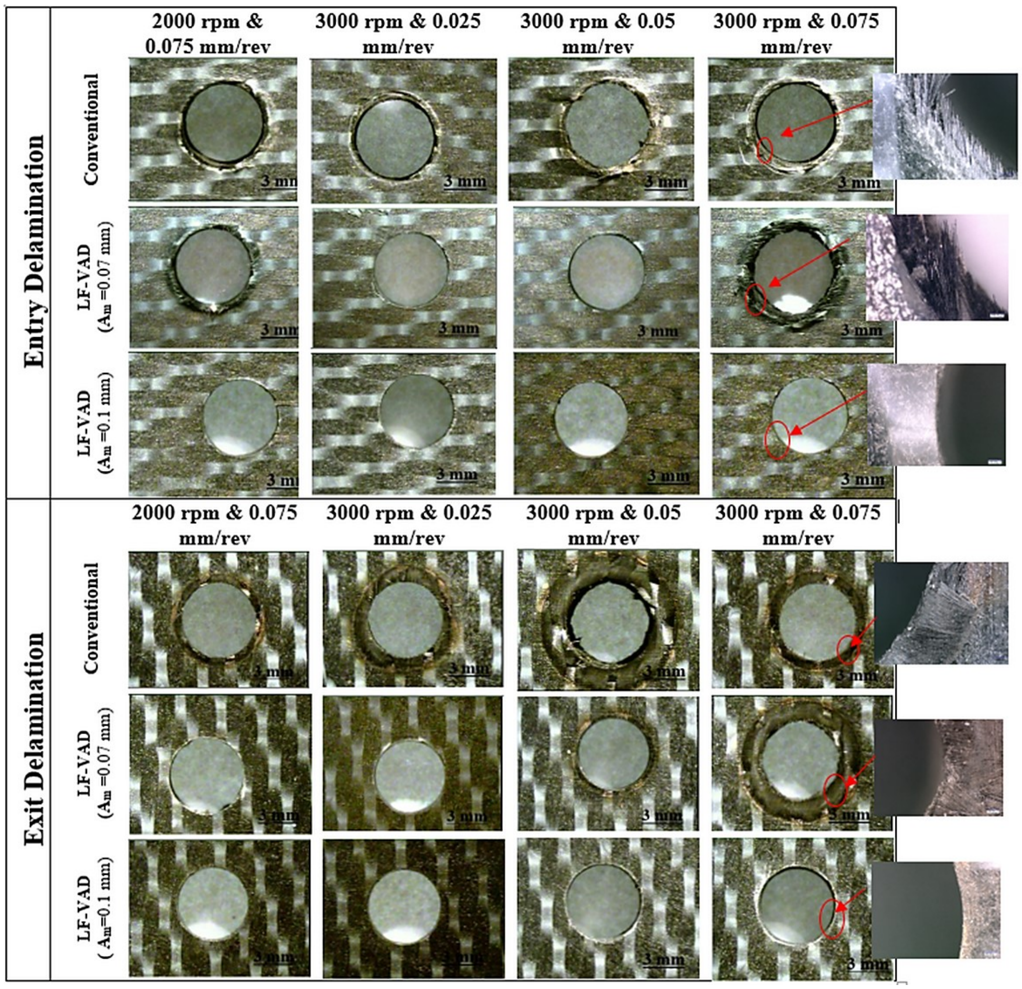


**Figure 5-10:** The effect of machining technique under different parameters on CFRP Entry and Exit delamination during stacked drilling.

### *5.3.4.2 Geometric Accuracy*

a. Hole Size Error

Acceptable hole size error in the aerospace industry range between -0.7% and 0.4% from the design drill diameter [27]. Conventional drilling and LF-VAD at $A_m$ = 0.07 mm and high feed rate, produced hole sizes in the CFRP layer which do not meet industry standards. However, the drilled holes in titanium were all within acceptable industry tolerance levels. Reducing the cutting temperature, as well as segmenting chip formation during LF-VAD at an $A_m$ greater than or equal to 0.07mm resulted in a lower error range, as shown in Figure 5-11.

| | | Amplitude (mm) | | | | | |
|---|---|---|---|---|---|---|---|
| RPM | Feed Rate (mm/rev) | 0 | 0.07 | 0.1 | 0.16 | 0.25 | 0.48 |
| 2000 | 0.025 | ± 0.4% | | | | | |
| | 0.05 | | | | | | |
| | 0.075 | | | | ± 0.1% | | |
| 3000 | 0.025 | | | | | | |
| | 0.05 | >0.4% | | | | | |
| | 0.075 | | | | | | |

(a)

| | | Amplitude (mm) | | | | | |
|---|---|---|---|---|---|---|---|
| RPM | Feed Rate (mm/rev) | 0 | 0.07 | 0.1 | 0.16 | 0.25 | 0.48 |
| 2000 | 0.025 | | | | | | |
| | 0.05 | | | | | | |
| | 0.075 | | | | | | |
| 3000 | 0.025 | | | | ± 0.1% | | |
| | 0.05 | | | | | | |
| | 0.075 | | ± 0.4% | | | | |

(b)

**Figure 5-11:** The effect of cutting parameters of both cutting techniques on the drilled hole size error for a) CFRP and b) Ti6Al4V.

**b.** Circularity

The measured hole circularity for all tests demonstrates the same behaviour observed for the hole dimension error, as shown in Figure 5-12.

The results indicate a strong interrelationship between cutting temperature, chip morphology, delamination, hole size, and circularity. Changing from high-temperature continuous chips to segments with a lower temperature, reduces thermal and mechanical damage. The elimination of both types of damage clearly contributes to enhancing the drilled hole quality (delamination, size, circularity, and surface roughness). Conventional and LF-VAD with $A_m$= 0.07 mm under a high feed rate showed an unacceptable hole circularity lower than 0.02 which is in agreement with the results presented in [27].

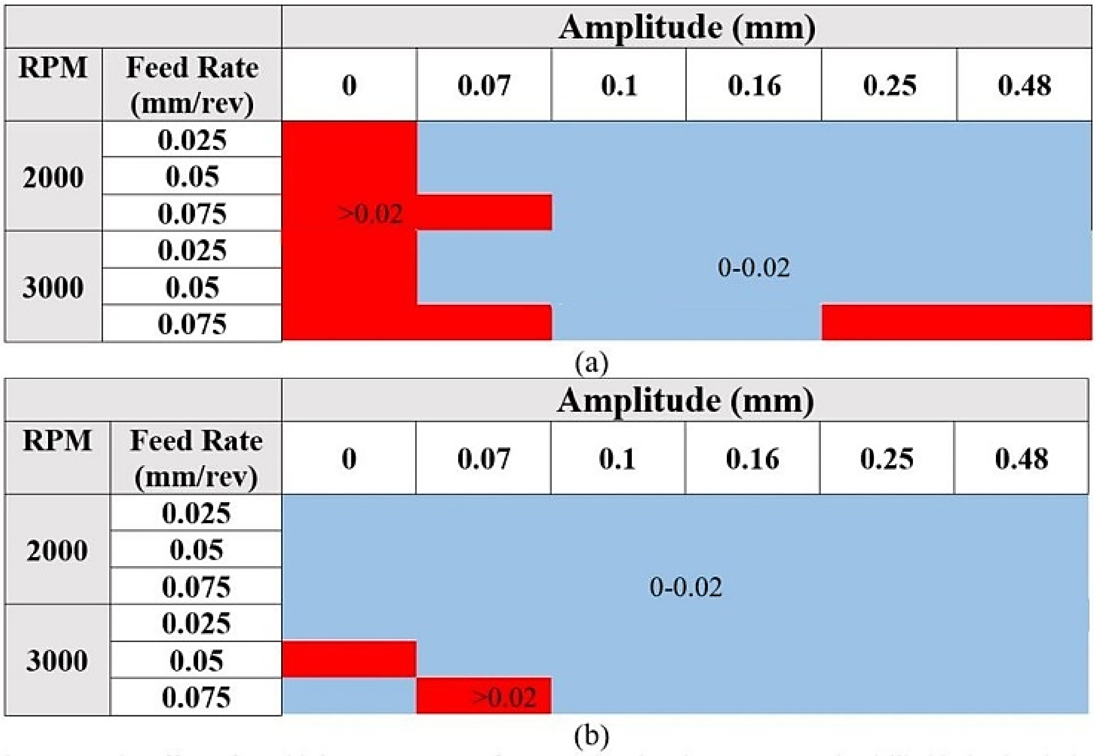


**Figure 5-12:** The effect of machining parameters of Conventional and LF-VAD on the drilled hole circularity of a) CFRP and b) Ti6Al4V.

### *5.3.4.3 Surface Roughness*

Figure 5-13, Compares the effect of conventional drilling and LF-VAD under different machining parameters on CFRP surface roughness (Ra). Each surface roughness measured value is the average of six measurements on different surface locations along the drilling direction. The CFRP surface roughness increased with increasing the cutting speed and the feed rate. LF-VAD significantly reduced the surface roughness at all machining parameters as compared to conventional drilling. This reduction is attributed to enhancing the Titanium chip evacuation, as well as reducing the cutting temperature. The evacuation of smaller chip sizes reduces the potential of CFRP surface scratching or damage, while reducing the cutting temperature eliminates the CFRP matrix melting. The CFRP surface roughness ranges for conventional drilling and LF-VAD were (1.19 µm and 5.86 µm ) and (6.72 µm to 45 µm), respectively.

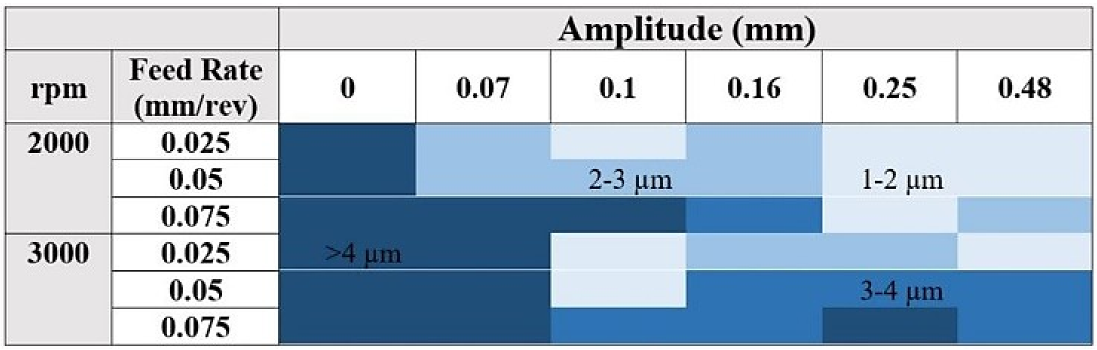


**Figure 5-13:** The effect of machining technique under different parameters on CFRP Surface Roughness.

Three-dimensional surface topographies are presented in Figure 5-14, outlining the effect of LF-VAD on the CFRP surface roughness. The negative effect of long continuous titanium chip evacuation as well as the welded segments during the drilling process, can be observed during conventional, and LF-VAD under $A_m$ = 0.07 mm (Figure 5-14 (a,b)). Increasing the cutting speed while keeping the same feed rate, showed a noticeable effect under both conventional and LF-VAD, with a 0.07 mm cutting amplitude. Moreover, a negligible effect was observed with LF-VAD at $A_m$ = 0.25 mm Figure 5-14 (c).

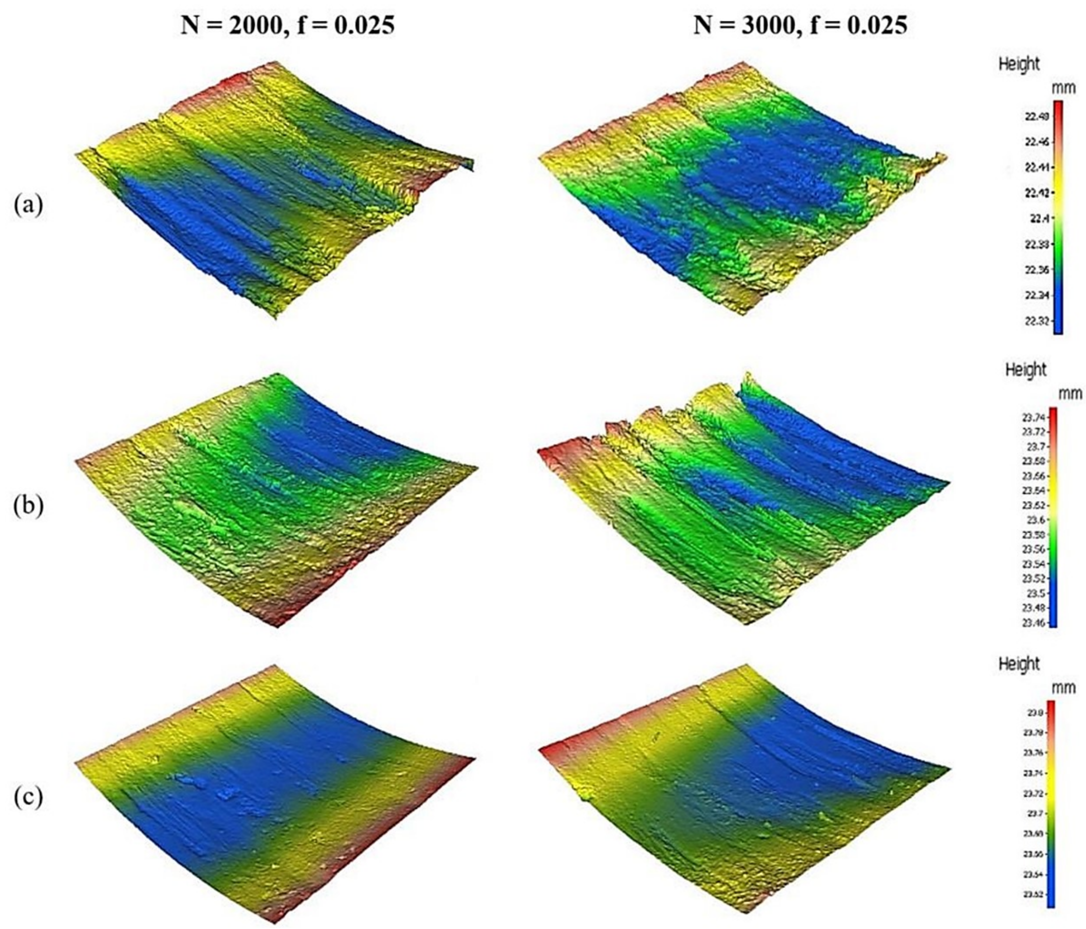


**Figure 5-14:** Effect of machining technique under different parameters on the CFRP surface roughness topography a) Conventional, b) LF-VAD $A_m$= 0.07 mm, and c) LF-VAD $A_m$= 0.25 mm.

The measured surface roughness in Ti6Al4V was lower than that of CFRP. At the lower speeds N, no significant difference between conventional drilling and LF-VAD was observed, and the Ti6Al4V surface roughness ranged from (1.54 µm to 1.94 µm) for conventional drilling, and (0.054 µm to 1.62 µm) for LF-VAD respectively. At higher rotational speed ($N$ = 3,000 rpm), the surface roughness ranged from (3.7 µm to 8.98 µm) for conventional drilling, and (0.069 µm to 1.89 µm) for LF-VAD at $A_m \geq 0.1$ mm, as shown in Figure 5-15.

| | | Amplitude | | | | | |
|---|---|---|---|---|---|---|---|
| **rpm** | **Feed Rate** | **0** | **0.07** | **0.1** | **0.16** | **0.25** | **0.48** |
| **2000** | **0.025** | | | | | | |
| | **0.05** | 1-2 µm | | | | | |
| | **0.075** | | | | | 0.5-1 µm | |
| **3000** | **0.025** | | | | | | |
| | **0.05** | >4 µm | 2-4 µm | | | | |
| | **0.075** | | | | | | 1-2 µm |

**Figure 5-15:** The effect of machining technique under different parameters on Ti6Al4V Surface Roughness.

The three-dimensional topography of the Ti6Al4V, shown in Figure 5-16, demonstrates the significant effect of the LF-VAD technique on enhancing the machined surface topography. Again, this is attributed to better chip evacuation, and reduction in the cutting temperature, which limits the adhesive process at the Tool-Chip interface.

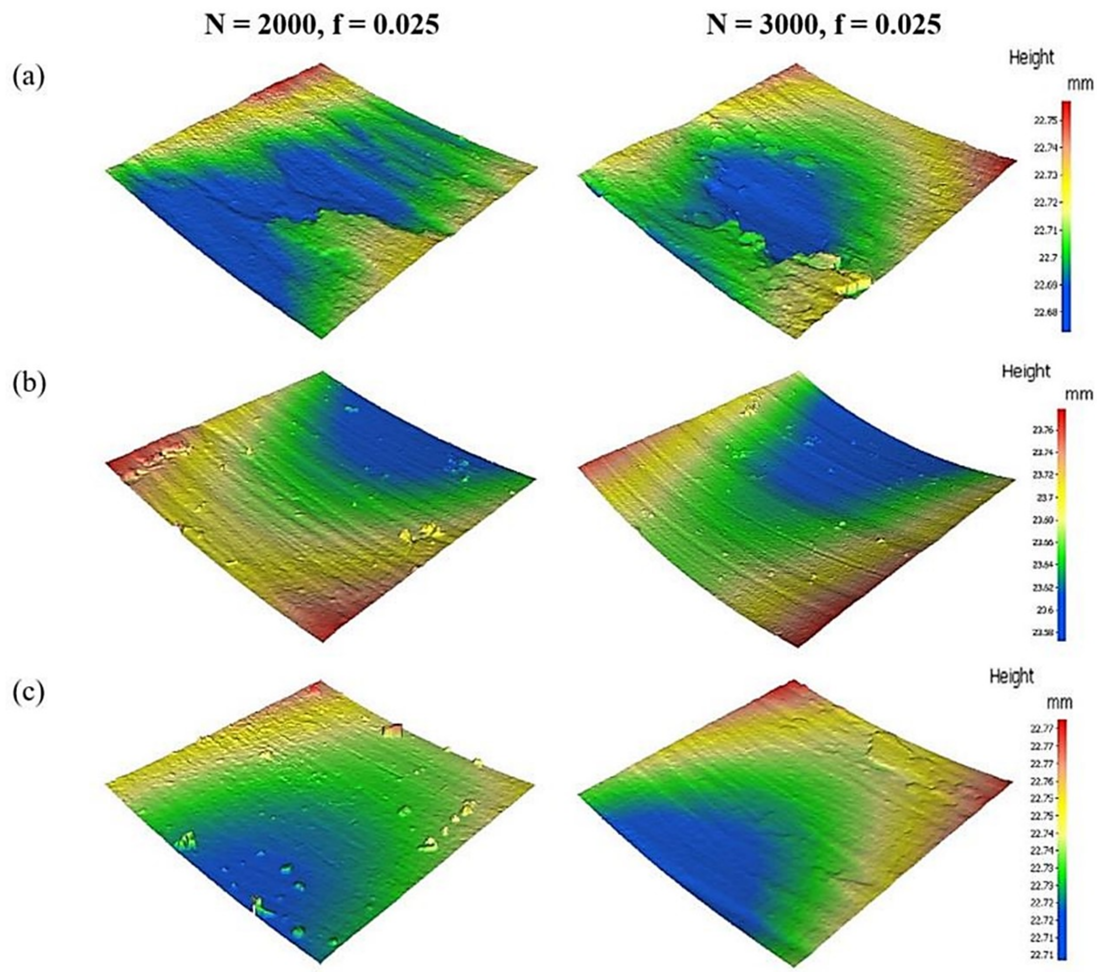


**Figure 5-16:** The effect of the machining technique under different parameters on the Ti6Al4V three-dimensional topography (a) Conventional, (b) LF-VAD $A_m$= 0.07 mm, and (c) LF-VAD $A_m$= 0.25 mm.

### 5.3.5 Microstructure and Residual Stresses.

This section examines the main aspects of the microstructure and residual stresses produced during LF-VAD of the stacked material. Figure 5-17 (a), shows the location near the exit surface used to examine the resulting microstructure and residual stresses. Figure 5-17 (b) shows the X-ray diffraction profile of the Titanium plate before drilling. The formation of new peaks, changes in peak intensity, or changes in the total number of lattice planes on the same preferred orientation, will indicate material phase transformation[28, 29], plastic deformation, and material anisotropy [30].

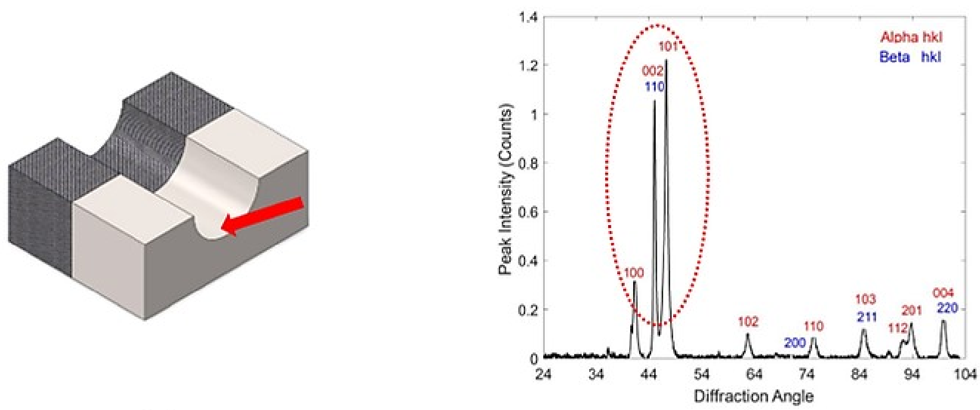


(a) (b)

**Figure 5-17:** The position of the X-ray Diffraction profile and the Ti6Al4V phase profile before machining process.

Figure 5-18, shows the variation in Ti6Al4V texture under different machining processes at a 2000 rpm cutting speed. A significant change in peak intensity is observed under the different cutting conditions. To determine the cause of the change in peak intensity, the microstructure of the exit surface was examined for VAD with $A_m$=0.25mm at a 0.025 feed rate. The microstructure examination shown in Figure 5-19 illustrates a non-homogenous localized layer with an 18 μm maximum thickness of deformed grains. Material drag or plastic deformation was observed along the perforation direction during elevated machining temperature, especially with materials having low thermal conductivity. Such an effect was also observed by other investigations [31].

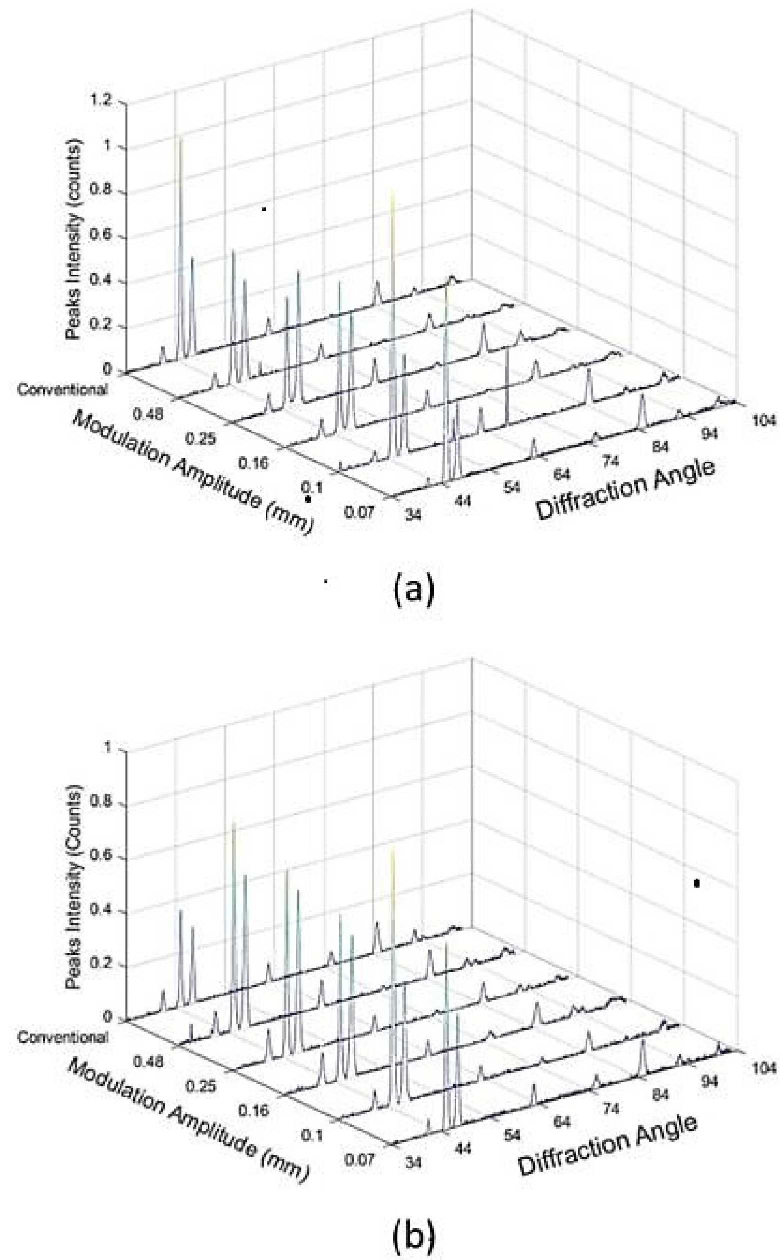


**Figure 5-18:** The effect of the machining processes on Ti6Al4V under 2000 rpm: (a) 0.025 and (b) 0.075 mm/rev feed rate.

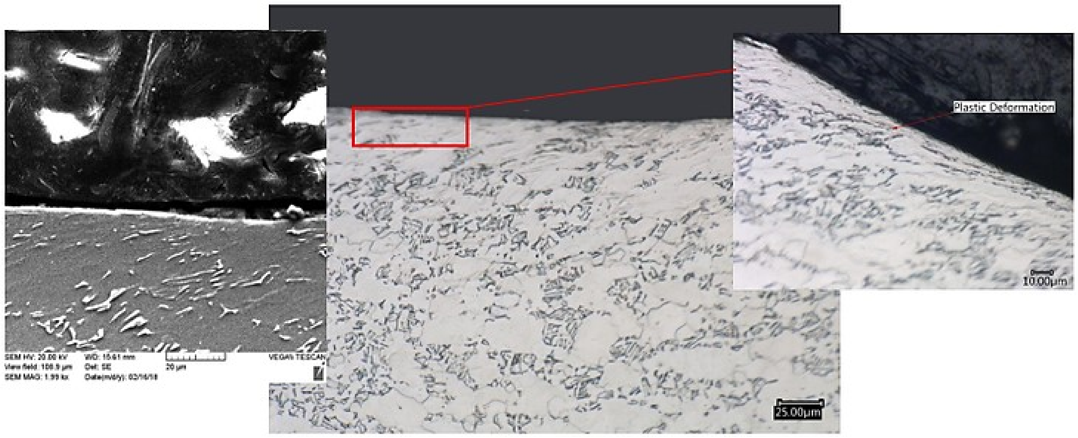


**Figure 5-19:** Microstructural examination of VAD under $A_m$=0.25 mm, $f$=0.025 mm/rev, and $N$=2000 rpm.

Increasing the thermo-mechanical fields under higher feed rates or cutting speeds will gradually increase material microstructure defects. Severe plastic deformation (SPD), known as the white layer, can take place in the absence of appropriate cooling which could lead to crack initiation due to high tensile residual stress. SPD can be formed during the machining process through three mechanisms:

1. Plastic flow.
2. Rapid heating and cooling rates.
3. Surface reaction [32-35].

Figure 5-20, shows the SPD, as well as the plastic deformation layer thickness, beneath the machined surface. The total defected thickness under $A_m$=0.25 mm was found to be approximately 14 µm (SPD = 6 µm and 8 µm plastic deformation), compared to approximately 19 µm (SPD = 7.5 µm and 11.5 µm plastic deformation). This suggests a reduction of more than 25% in the thickness of the plastic deformation layer when using VAD.

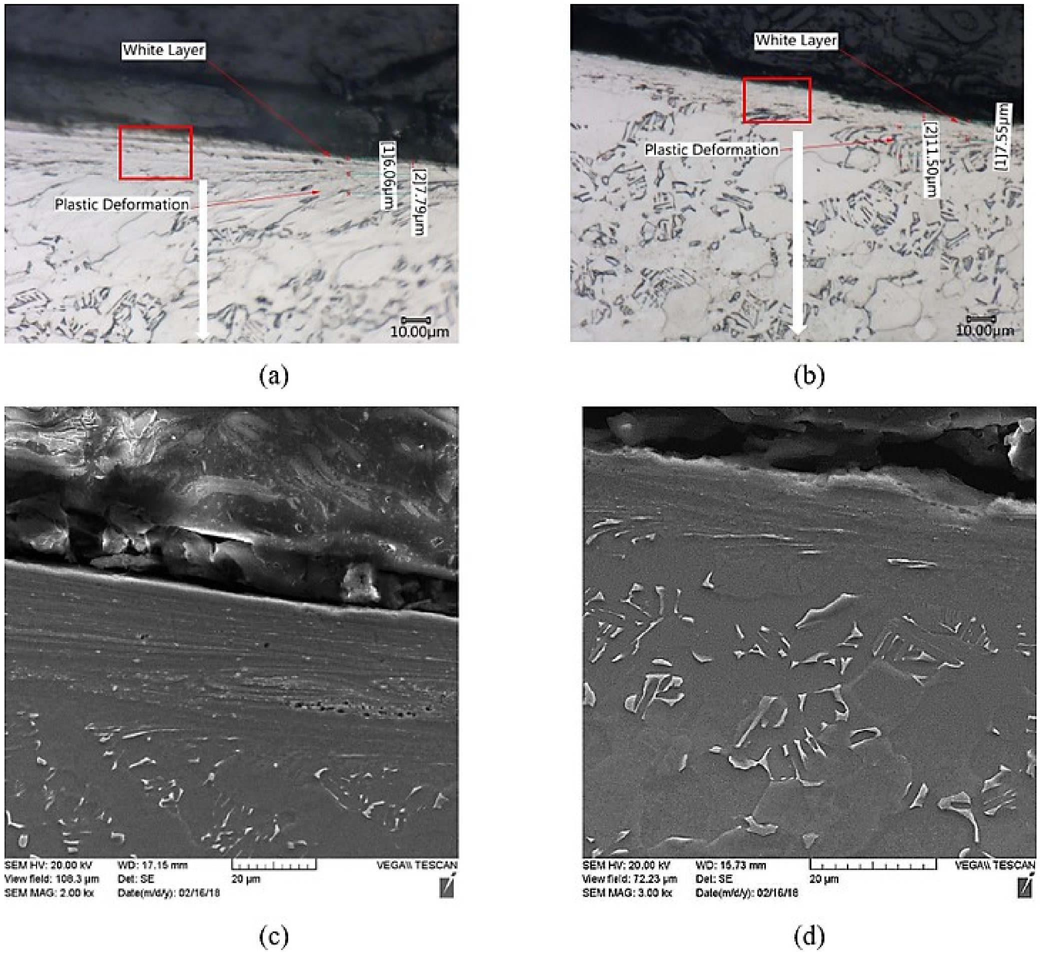


**Figure 5-20:** A microstructural examination of VAD with $A_m$=0.25 mm and Conventional under 0.075 feed rate.

Figure 5-21, presents the residual stresses at the selected point (shown in Figure 5-17) , which is 400 µm from the Ti6Al4V exit surface. The curvature X-Ray residual stress measurement at a Bragg angle of 140° and 11-tilt angles (up to 40°), for both conventional and LF-VAD with $A_m$=0.25 mm. It can be seen that compressive residual stresses are generated under VAD potentially due to:

1. Improved chip evacuation mechanisms.
2. Improved cooling mechanism.

Continuous chip formation will likely occur during conventional drilling leading to high tool temperature. On the other hand, VAD typically leads to segmented chip formation resulting in lower tool temperature [22]. The conventional drilling process showed tensile residual stresses under the same machining conditions, mainly due to high cutting temperature.

To study the effect of higher cutting speed, Figure 5-22 compares the effect of both techniques under lower and higher feed rate. For the lower feed rate (0.025 mm/rev), the tensile residual stress has been reduced from (274 ±22 MPa) for conventional drilling, (45 ±30 MPa) for LF-VAD with $A_m$=0.25 mm (Figure 5-22 a). While for the higher feed rate (0.075 mm/rev), tensile residual stress was reduced from (225 ±27) for conventional drilling to (174 ±32) for LF-VAD with $A_m$=0.25 mm (Figure 5-22 a). While for the higher feed rate (0.075 mm/rev), tensile residual stress was reduced from (225 ±27) for conventional drilling to (174 ±32) for LF-VAD with $A_m$=0.25 mm (Figure 5-22 b).

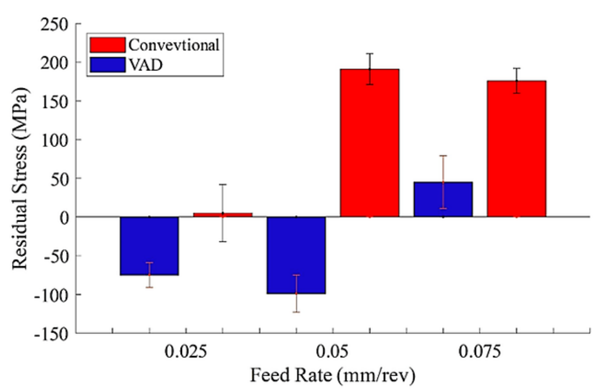


**Figure 5-21:** The Residual Stress measurements of VAD with a 0.25mm Modulation amplitude and Conventional drilling under 2000 rpm and different feed rates.

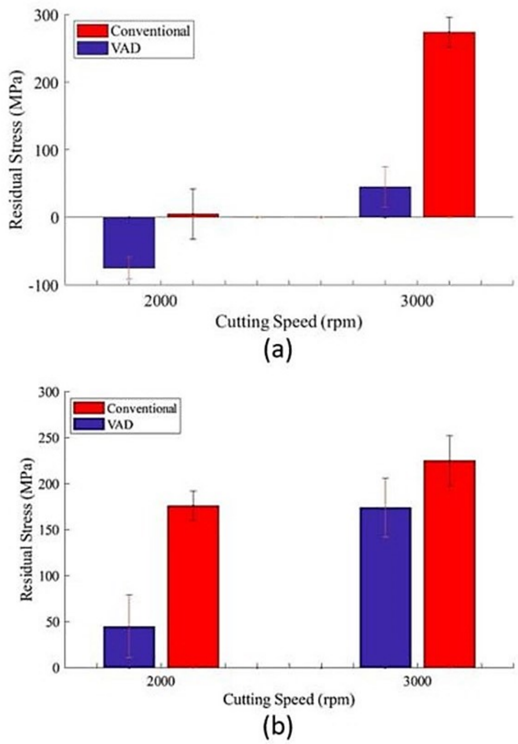


**Figure 5-22:** The effect of Cutting Speed under conventional drilling and VAD with 0.25mm modulation amplitude and different feed rates: (a) 0.025 and (b) 0.075 mm/rev.

Figure 5-23, shows the variation of residual stresses under the machined surface for both machining techniques under a 2000 rpm cutting speed. The reduction in residual stresses under VAD conditions is clearly observed which may suggest an improved fatigue life.

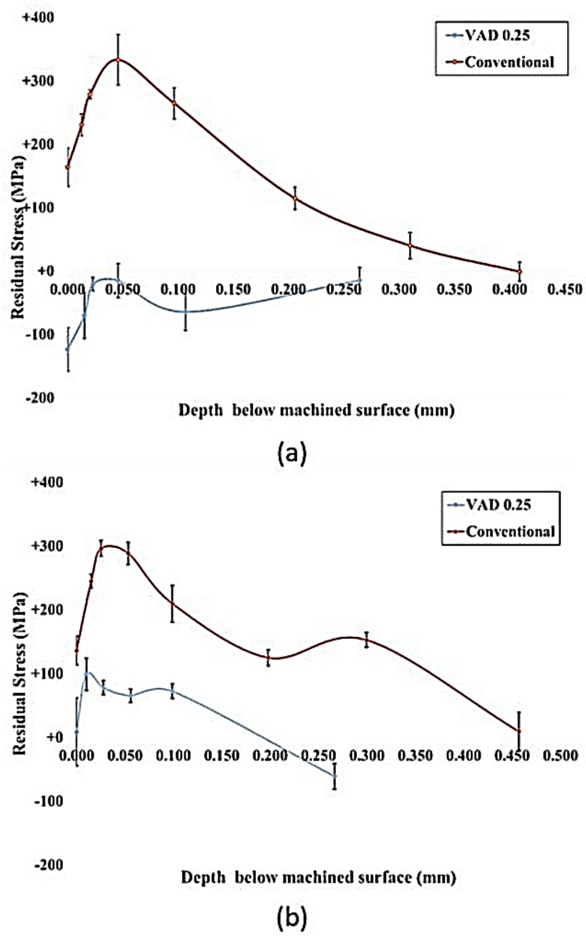


**Figure 5-23:** The effect of VAD and Conventional drilling under 2000 rpm on the subsurface residual stress (a) $f$=0.05 (b) $f$=0.075 mm/rev.

## Conclusions

This experimental study examines the cutting performance of low-frequency vibration assisted drilling process (LF-VAD) of CFRP/Ti6Al4V stacked material. The study included an examination of the influence of the cutting amplitude of oscillation $A_m$, feed rate, and cutting speed on several variables such as thrust force, cutting temperature, hole geometry (delamination, hole size, circularity, and surface roughness), and chip morphology, as well as the microstructure and residual stresses. A full factorial experimental design was implemented at two levels of cutting speeds, three levels of feed rates and five levels of cutting amplitude. The following observations are made for the range of cutting conditions considered in this study:

1. LF-VAD showed a higher thrust force as compared to conventional drilling. This increase depends mainly on the cutting amplitude, and the feed rate. The effect of the cutting speed was found to be negligible.
2. A significant reduction of cutting tool temperature was observed during LF-VAD. This reduction is influenced mainly by the cutting amplitude.
3. In terms of hole quality and cutting temperature, the recommended cutting parameters for the Ti6Al4V layer were found to be within a 0.1-0.24 mm cutting amplitude, with a lower feed rate of 0.025 mm/rev.
4. The use of LF-VAD resulted in changing the titanium chip morphology, which impacted the CFRP hole quality.
5. Entry and exit delamination defects were largely eliminated using LF-VAD. This is mainly due to a reduction in the cutting temperature and an enhancement in the chip evacuation mechanism. In addition, an enhancement of LF-VAD hole geometry error, circularity, and surface roughness was observed.
6. Compressive residual stress or lower tensile stresses (compared to conventional drilling), were observed within a range of cutting conditions under LF-VAD. The results obtained during conventional technique showed higher tensile stresses under all machining conditions.

# References

[1] S. L. Soo, A. M. Abdelhafeez, M. Li, R. Hood, and C. M. Lim, "The drilling of carbon fibre composite–aluminium stacks and its effect on hole quality and integrity," *Proceedings of the Institution of Mechanical Engineers, Part B: Journal of Engineering Manufacture,* p. 0954405417728312, 2017.

[2] E. Brinksmeier and R. Janssen, "Drilling of multi-layer composite materials consisting of carbon fiber reinforced plastics (CFRP), titanium and aluminum alloys," *CIRP Annals-Manufacturing Technology,* vol. 51, pp. 87-90, 2002.

[3] M. Ramulu, T. Branson, and D. Kim, "A study on the drilling of composite and titanium stacks," *Composite Structures,* vol. 54, pp. 67-77, 10// 2001.

[4] I. Shyha, S. L. Soo, D. Aspinwall, S. Bradley, R. Perry, P. Harden*, et al.*, "Hole quality assessment following drilling of metallic-composite stacks," *International Journal of Machine Tools and Manufacture,* vol. 51, pp. 569-578, 2011.

[5] K.-H. Park, A. Beal, P. Kwon, and J. Lantrip, "Tool wear in drilling of composite/titanium stacks using carbide and polycrystalline diamond tools," *Wear,* vol. 271, pp. 2826-2835, 2011.

[6] T. Tashiro, J. Fujiwara, and K. Inada, "Drilling of CFRP/Ti-6Al-4V stacks," in *Advanced Materials Research*, 2011, pp. 369-374.

[7] J. Xu and M. El Mansori, "Experimental study on drilling mechanisms and strategies of hybrid CFRP/Ti stacks," *Composite Structures,* vol. 157, pp. 461-482, 12/1/ 2016.

[8] Z. Zhu, S. Sui, J. Sun, J. Li, and Y. Li, "Investigation on performance characteristics in drilling of Ti6Al4V alloy," *The International Journal of Advanced Manufacturing Technology,* pp. 1-10, 2017.

[9] J. Prasanna, L. Karunamoorthy, M. V. Raman, S. Prashanth, and D. R. Chordia, "Optimization of process parameters of small hole dry drilling in Ti–6Al–4V using Taguchi and grey relational analysis," *Measurement,* vol. 48, pp. 346-354, 2014.

[10] S. Ramesh, L. Karunamoorthy, and K. Palanikumar, "Surface roughness analysis in machining of titanium alloy," *Materials and Manufacturing Processes,* vol. 23, pp. 174-181, 2008.

[11] D. Kim and M. Ramulu, "Study on the drilling of titanium/graphite hybrid composites," *Journal of Engineering Materials and Technology,* vol. 129, pp. 390-396, 2007.

[12] D. Kim, C. Sturtevant, and M. Ramulu, "Usage of PCD tool in drilling of titanium/graphite hybrid composite laminate," *International Journal of Machining and Machinability of Materials,* vol. 13, pp. 276-288, 2013.

[13] O. Isbilir and E. Ghassemieh, "Comparative study of tool life and hole quality in drilling of CFRP/titanium stack using coated carbide drill," *Machining Science and Technology,* vol. 17, pp. 380-409, 2013.

[14] J. Jallageas, J.-Y. K'nevez, M. Chérif, and O. Cahuc, "Modeling and optimization of vibration-assisted drilling on positive feed drilling unit," *The International Journal of Advanced Manufacturing Technology,* pp. 1-12, 2013.

[15] N. Guibert, "Etude et modélisation de l'influence des phénomènes de coupe sur les performances du forage vibratoire," Université Joseph-Fourier-Grenoble I, 2008.

[16] B. Denkena, D. Boehnke, and J. Dege, "Helical milling of CFRP–titanium layer compounds," *CIRP Journal of manufacturing Science and Technology,* vol. 1, pp. 64-69, 2008.

[17] O. Pecat and I. Meyer, "Low frequency vibration assisted drilling of aluminium alloys," in *Advanced Materials Research*, 2013, pp. 131-138.

[18] Z. Deyuan and W. Lijiang, "Investigation of chip in vibration drilling," *International Journal of Machine Tools and Manufacture,* vol. 38, pp. 165-176, 1998.

[19] A. Sadek, M. Meshreki, and M. Attia, "Effect of Tool Kinematics on the Drilling Forces and Temperature in Low Frequency High Amplitude Vibration Assisted Drilling," in *ASME 2014 International Mechanical Engineering Congress and Exposition*, 2014, pp. V02AT02A035-V02AT02A035.

[20] K. Okamura, H. Sasahara, T. Segawa, and M. Tsutsumi, "Low-frequency vibration drilling of titanium alloy," *JSME International Journal Series C Mechanical Systems, Machine Elements and Manufacturing,* vol. 49, pp. 76-82, 2006.

[21] Y. Guo and J. B. Mann, "Experimental Evaluation of Cutting Kinematics and Chip Evacuation in Drilling With Low-Frequency Modulation-Assisted Machining," in *ASME 2017 12th International Manufacturing Science and Engineering Conference collocated with the JSME/ASME 2017 6th International Conference on Materials and Processing*, 2017, pp. V001T02A017-V001T02A017.

[22] O. Pecat and E. Brinksmeier, "Low damage drilling of CFRP/titanium compound materials for fastening," *Procedia CIRP,* vol. 13, pp. 1-7, 2014.

[23] O. Pecat and E. Brinksmeier, "Tool wear analyses in low frequency vibration assisted drilling of CFRP/Ti6Al4V stack material," *Procedia CIRP,* vol. 14, pp. 142-147, 2014.

[24] A. Sadek, M. Attia, M. Meshreki, and B. Shi, "Characterization and optimization of vibration-assisted drilling of fibre reinforced epoxy laminates," *CIRP Annals-Manufacturing Technology,* vol. 62, pp. 91-94, 2013.

[25] B. Luo, K. Zhang, Y. Li, H. Cheng, and S. Liu, "Modelling of thrust force for worn drill bits characterised by cutting edge radius in drilling carbon fibre–reinforced

plastic/Ti-6Al-4V alloy stacks," *Proceedings of the Institution of Mechanical Engineers, Part B: Journal of Engineering Manufacture,* p. 0954405416682791, 2017.

[26] K. Okamura and H. Sasahara, "Prediction of drilling temperature during low-frequency vibration drilling of titanium alloy," *Journal of Advanced Mechanical Design, Systems, and Manufacturing,* vol. 11, pp. JAMDSM0036-JAMDSM0036, 2017.

[27] A. Sadek, "Vibration Assisted Drilling of Multidirectional Fiber Reinforced Polymer Laminates," Ph.D. Thesis, McGill University Libraries, 2014.

[28] G. Rotella, O. Dillon, D. Umbrello, L. Settineri, and I. Jawahir, "The effects of cooling conditions on surface integrity in machining of Ti6Al4V alloy," *The International Journal of Advanced Manufacturing Technology,* vol. 71, pp. 47-55, 2014.

[29] R. Li, L. Riester, T. R. Watkins, P. J. Blau, and A. J. Shih, "Metallurgical analysis and nanoindentation characterization of Ti–6Al–4V workpiece and chips in high-throughput drilling," *Materials Science and Engineering: A,* vol. 472, pp. 115-124, 2008.

[30] J. Connolly, "Diffraction Basics–Part 2," ed: Introduction to X-Ray Powder Diffraction, 2012.

[31] R. M'Saoubi, D. Axinte, S. L. Soo, C. Nobel, H. Attia, G. Kappmeyer*, et al.*, "High performance cutting of advanced aerospace alloys and composite materials," *CIRP Annals,* vol. 64, pp. 557-580, 2015.

[32] A. Thakur, S. Gangopadhyay, and K. Maity, "Effect of cutting speed and tool coating on machined surface integrity of Ni-based super alloy," *Procedia CIRP,* vol. 14, pp. 541-545, 2014.

[33] D. Jin and Z. Liu, "Effect of cutting speed on surface integrity and chip morphology in high-speed machining of PM nickel-based superalloy FGH95," *The International Journal of Advanced Manufacturing Technology,* vol. 60, pp. 893-899, 2012.

[34] D. Ulutan and T. Ozel, "Machining induced surface integrity in titanium and nickel alloys: A review," *International Journal of Machine Tools and Manufacture,* vol. 51, pp. 250-280, 2011.

[35] C. Che-Haron and A. Jawaid, "The effect of machining on surface integrity of titanium alloy Ti–6% Al–4% V," *Journal of Materials Processing Technology,* vol. 166, pp. 188-192, 2005.

# Chapter 6

## Elimination of Delamination and Burr Formation Using High-Frequency Vibration-Assisted Drilling of Hybrid CFRP/Ti6Al4V Stacked Material

**Complete Citation:**

Hussein, R., Sadek, A., Elbestawi, M.A., Attia, M.H. (2019). Elimination of Delamination and Burr Formation Using High-Frequency Vibration-Assisted Drilling of Hybrid CFRP/Ti6Al4V Stacked Material. Has been accepted for publication at *The International Journal of Advanced Manufacturing Technology*, 2019.

**Relative Contributions:**

| | |
|---|---|
| R. Hussein: | Performed experiments, analysis, and data interpretation; wrote the first draft of the manuscript; helped with submitting the final manuscript to the journal (corresponding author). |
| A. Sadek: | Helped with the experiments and analysis; revised the manuscript. |
| M. A. Elbestawi: | Supervisor of R. Hussein. Revised and edited the manuscript and gave the final approval to be submitted. |
| M. H. Attia: | Revised the manuscript. |

## Abstract:

The superior physical and mechanical characteristics of CFRP/Ti6Al4V stacked structures explain their widespread use in the aerospace industry. However, the unacceptable machining-induced tensile residual stresses and reduced surface integrity are the main challenges that are faced in the conventional drilling process. These types of damage are attributed to the relatively high thermal load and poor chips evacuation mechanism. Vibration assisted drilling is a promising technique to control the uncut chip thickness, and consequently, reducing the cutting energy. Moreover, the axial tool oscillation provides a mechanism for effective chip evacuation. This study presents an experimental investigation relating the high frequency vibration assisted drilling (HF-VAD) machining parameters to the Ti6Al4V burr formation and induced residual stresses, as well as CFRP delamination during the drilling of CFRP/Ti6Al4V staked material. Additionally, this study presents an assessment and comparison between HF-VAD and LF-VAD of CFRP/Ti6Al4V hybrid structure. The results showed up to approximately 26 %, 37 %, and 86 % reduction in the thrust force, cutting temperature, and the exit burr height, respectively. The effect of HF-VAD on surface integrity and Ti6Al4V residual stresses are also presented. The drilling process of HF-VAD resulted in free exit delamination of CFRP with compressive residual stress on the Ti6Al4V machined surface.



## Keywords:

High-frequency vibration-assisted drill. Machining. CFRP. Ti6Al4V. Stacked material. Surface integrity. Residual stresses. Delamination free. burr formation.

**Acknowledgments:**

The experimental investigation was performed using the National Research Council Canada, Aerospace Manufacturing Technologies Centre (AMTC) facilities. The assistance of AMTC Advanced Material removal Technology Group is greatly appreciated.

**Acronyms:**

| | |
|---|---|
| VAD | Vibration assisted drilling |
| LF-VAD | Low frequency-vibration assisted drilling |
| CD | Conventional drilling |
| HF-VAD | High frequency-vibration assisted drilling |
| CFRP | Carbon fiber reinforced polymers |
| RS | Residual Stress |

**Notations:**

| | |
|---|---|
| $N$ | Rotation speed [rpm] |
| $f$ | Feed rate [mm/rev] |
| $A_m$ | Modulation amplitude [µm] |
| $F$ | Frequency [Hz] |
| $W_f$ | Modulation frequency [Cycle/rev] |
| $Ø_d$ | Delamination factor [%] |
| $E$ | Axial cutting edge position [mm] |

## 6.1 Introduction

The use of carbon fiber reinforced polymers (CFRP) in the aerospace industry has been steadily growing because of their high strength-to-weight ratio, high specific stiffness, corrosion resistance, low coefficient of thermal expansion, and fatigue resistance. In the new generation of aircrafts, hybrid CFRP-titanium-aluminum structures presents more than 75% of their total weight [1-3]. Drilling of these hybrid structural components is required during the assembly operations. Despite the advantages of the CFRPs, it is classified as hard-to-cut material [4-6] due to the their anisotropy of mechanical properties, the abrasive and powdery-like nature of carbon chips, and their sensitivity to cutting temperatures. Consequently, machining-induced mechanical and thermal damages, such as delamination, and fiber breakout may result in as much as 60% of the total parts rejection [7].

The high strength to weight ratio, high fatigue and creep resistance, and excellent corrosion resistance promotes the use of Ti6Al4V alloy for the aircraft load carrying structure [8, 9]. However, the low thermal conductivity, poor chip evacuation, and the tendency of burr formation pose a major challenge to the machining of Ti-based alloys [9-11]. In addition, the flute chips accumulation at elevated cutting temperature increases the probability of adhesive tool wear, due to the high chemical affinity of titanium alloy. Consequently, this adds more limitation for aerospace applications [12].

Mechanical fastening is commonly used for the assembly of aerospace components made of different materials. Therefore, drilling operations are essential in this industry. The drilling process and strategy of individual materials can readily be optimized. However, the difficulty arises when drilling stacked materials, as these optimal strategies are conflicting and may cause undesirable effects. In drilling Ti/CFRP stacks, for example, the extended titanium chips in a limited evacuation space increase the chips accumulation probability and may result in CFRP thermal damage, and tool-chip adhesion. This explains why failure to meet the required aerospace precision level, along with unsatisfactory machining time and cost, are commonly reported.

Stack drilling of dissimilar materials in a single process has generated a considerable interest to overcome these challenges. Optimizing the machining parameters [13-15], using a two-step drilling technique [1], and reducing tool-chip friction through advanced lubrication and tool coatings strategies [16], are various approaches taken to drill CFRP/Ti6Al4V stacks. Advanced machining techniques, such as orbital drilling and vibration-assisted drilling (VAD), where a harmonic motion in the axial direction is superimposed over the normal tool feed motion [3, 17], showed promising results, as they are capable of preventing the formation of continuous chips and facilitating chip evacuation [3, 18]. The optimization of VAD machining parameters has a direct impact on the chip geometry, and consequently, the cutting energy. Based on the frequency range of study, VAD is classified as: Low-frequency vibration assisted drilling (LF-VAD), where the frequency is ≤ 1000 Hz [17], and High frequency vibration assisted drilling (HF-VAD), where the frequency is > 1000 Hz [19].

The effect of the machining parameters of LF-VAD of CFRP/Ti6Al4V stacked material (at up to 125 Hz, and 70 μm to 480 μm amplitude) on the cutting temperature, chip morphology, hole quality and surface roughness was reported in [3]. A segmented chip morphology with a 56% reduction in the cutting temperature was achieved. Compared to conventional drilling (CD), LF-VAD resulted in a significant enhancement of the surface integrity, generation of compressive residual stresses in the Ti6Al4V machining surface, as well as reduction of the CFRP entry and exit delamination factor, and the tool-chip adhesion, as shown in Figure 6-1.

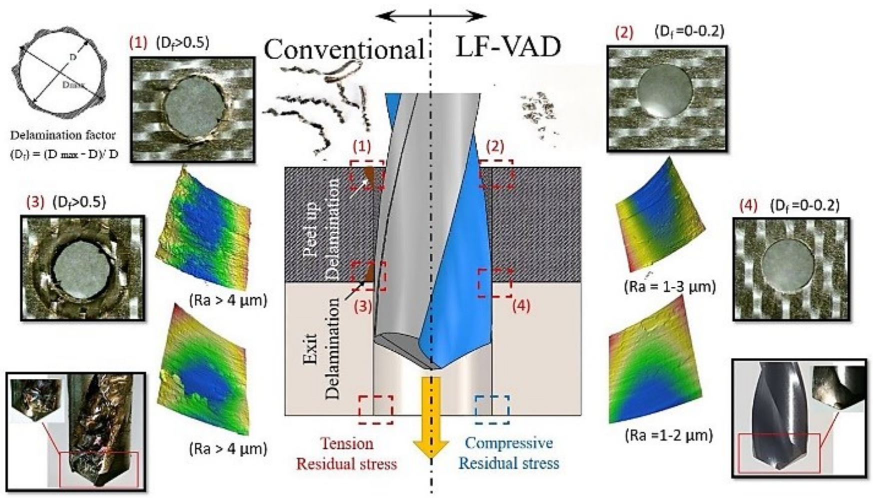


**Figure 6-1:** Effect of LF-VAD on the CFRP/Ti6Al4V stack material [3].

The previous studies in VAD have mainly focused on the low frequency range. However, at LF-VAD high uncut chip thickness and thrust forces occur [20, 21]. In this paper, the effect of HF-VAD is presented, using a specially-designed piezoelectric actuator system to generate high frequency (up to 2,500 Hz) and low amplitude (up to 5 μm) vibrational motion to the tool, excluding resonance condition. The effect of HF-VAD on the cutting energy, residual stresses, delamination, burr formation, and surface integrity were investigated by relating the HF-VAD conditions to actual uncut chip thickness. Moreover, the feeds and rotational speeds used in this study are similar to those reported in [3], to establish the effects and the characteristics of low- and high- frequency VAD.

## 6.2 Experimental work

Figure 6-2, shows the 3D model of the HF-VAD spindle head designed by the National Research Council Canada (NRC), Aerospace Manufacturing Technology Centre

[22]. The system consists of HSK 100A tool holder that was machined to accommodate a piezoelectric actuator and a ball spline axial transmission device. The actuator has a blocking force of 10,000 N, a resonant frequency of 68 kHz and is able to provides a displacement amplitude of up to 20 μm. To minimize the actuator axial load, a shrink fit tool adaptor with a U7/h6 shaft basis tolerance was used to clamp the drill bit, as shown in Figure 6-3 (b). A high-speed slip ring (6,000 rpm) was used to ensure the transfer of sufficient power to the actuator, as shown in Figure 6-3 (a).

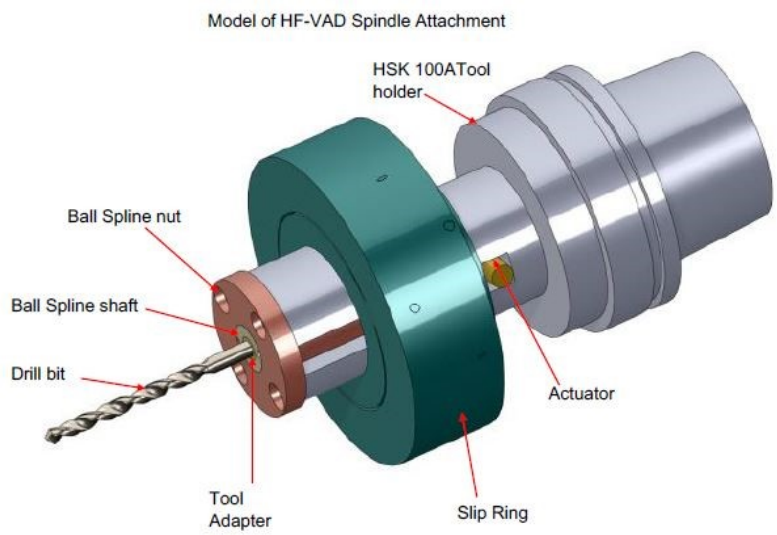


**Figure 6-2:** 3D model of the designed HF-VAD spindle head [20].

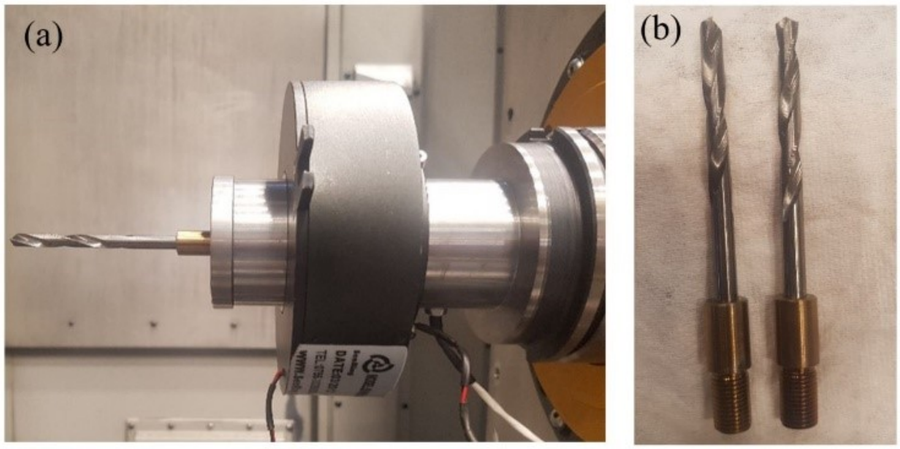


**Figure 6-3:** The final HF-VAD designed mechanism and the shrink fit tool clamp.

Figure 6-4 presents a schematic block diagram of the calibration set up used to measure the system frequency response under load, and at no load conditions. The Brüel & Kjaer (B&K) precision sweep function generator, model 4040A, was used to generate the signal frequency and amplitude. The generated signal was delivered to the piezoelectric actuator through the KC-N15-1 amplifier. The actual system oscillation was recorded using the spline shaft movement through the B&K 35335 and PCB 352A21 accelerometers. To calibrate the recorded signals, the accelerometers' signals were amplified and double integrated using charge amplifiers and MATLAB integration function.

Based on the conventional drilling (CD) thrust forces, an axial load was generated at the same feeds ($f$ = 0.025 mm/rev - 0.075 mm/rev) through a high stiffness spring, to calibrate the high frequency actuator system under load condition, as shown in Figure 6-4 (b). The first two resonance frequency were measured at F = 1,500 Hz and F = 2,150 Hz, with a controllable amplitude in the range of 3 μm and 5.5 μm (6 to 11 μm peak-to-peak displacement).

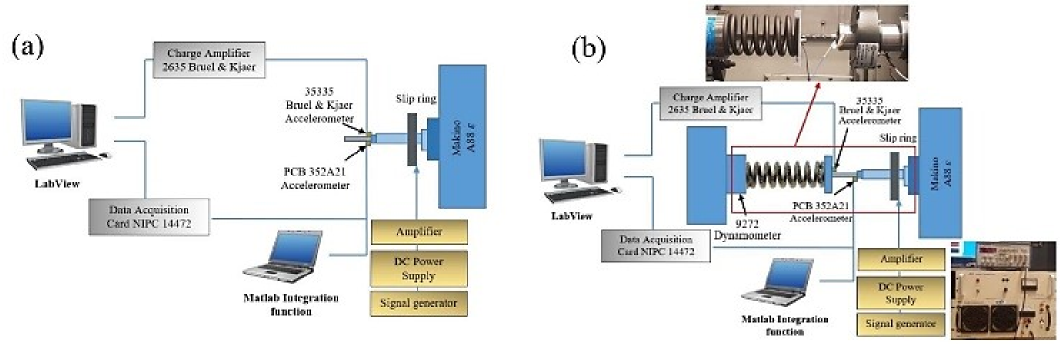


**Figure 6-4:** A schematic diagram of the calibration set up to study the HF-VAD response at (a) no load (b) expected load condition.

A full factorial experimental study of HF-VAD (two levels of rotational speeds and frequency, three levels of feeds, and amplitudes), with two repetition measurements for each condition, was carried out. Table 6-1 presents the applied machining parameters, cutting tool, and CFRP/Ti6Al4V stacked material used for test conditions.

The experimental study was performed using a 5-axis Makino A88ε machining center. A Kistler force measurement system, which consists of a dynamometer type 9272 and a multichannel charge amplifier Type 5019B, was used for the cutting force measurements. This system was used to ensure accurate measurement of forces for both frequency ranges (≤ 6 KHz). For the tool temperature measurement, a thermo-vision infrared camera (FLIR SC8000 HD series with 0.4 emissivity) was tilted to achieve a direct vision of the drill bit at the Ti6Al4V exit surface. For the examination of surface integrity, the waterjet cutting method was used to split the drilled holes. A Keyence Digital Microscope, VHX-6000 Series, was used for CFRP entry and exit delamination measurements. With 0.0001 μm resolution, a Surftest SJ-410 stylus profilometry was used for surface roughness evaluation. The X-Ray residual stresses measurement method was used at a normal distance of 400 μm from the exit surface, using a copper target instrument. A 142° Bragg angle was used with 11 tilt angles (up to 40°), for the CD and HF-VAD tests.

**Table 6-1:** Applied cutting conditions, cutting tool, and cutting materials.

| | | |
|---|---|---|
| **Machining Parameters** | | |
| Rotational Speed, *N* | rpm | 2,000 and 3,000 |
| Feed rate, *f* | mm/rev | 0.025, 0.05, and 0.075 |
| Amplitude, $A_m$ | μm | 3, 4.5, and 5.5 |
| Frequency, F | Hz | 1,500 and 2,150 |
| **Cooling medium** | Dry | |
| **Cutting Tool** | | |
| **Material** | Tungsten Carbide | |
| **Diameter** | 6 mm | |
| **Point angle** | 118° | |
| **Helix angle** | 20° | |
| **Manufacturer** | OSG | |
| **Model** | 220-2362 | |
| **Workpiece material specification** | | |
| **CFRP** | - 5.8 ± 0.02 mm of 42 × L-930(GT700) woven plies with the configuration [[0,90]$_{21}$]s, and flame retardant modified epoxy prepreg.<br>- Decomposition temperature is 320°C. | |
| **Titanium alloy** | Ti6Al4V, grade 5 (396 Hv) | |
| **Stacking sequence** | CFRP 5.8 ± 0.02 mm/Ti6Al4V 6.75 ± 0.02 mm | |

## 6.3 Effect of HF-VAD Kinematics on chip formation

A kinematic model was developed to study the effect of the HF-VAD inputs parameters on the actual uncut chip thickness and chip morphology. Consequently, these parameters can be related to the thrust force, thermal load, residual stresses, delamination, and burr formation, as will be described in section 6.4. The model was developed based on the instantaneous cutting edge position and the actual feed per tooth equations, as described in [20, 23];

$$E_1 = \frac{\gamma}{360°} * f + A * \sin(\gamma * F) \tag{6.1}$$

$$E_2 = \frac{(\gamma - 180°)}{360°} * f + A * \sin[(\gamma - 180) * F] \tag{6.2}$$

The dynamic uncut chip thickness could be expressed as:

$$t_o = \begin{cases} Z(\gamma) - \max\big(Z_k(\gamma)\big) \ , & Z(\gamma) > \max\big(Z_k(\gamma)\big) \\ 0 \ , & otherwise \end{cases} \quad (6.3)$$

Based on the selected rotational speeds and frequencies, Table 6-2 shows the related modulation frequency ($W_f$) for each case. Table 6-3 shows the calculated actual uncut chip thickness for the investigated HF-VAD machining conditions. The actual uncut chip thickness showed a different behavior based on the $W_f$ as follows:

- Odd modulation frequency $W_f$ presents the optimum phase difference to verify the chip segmentation condition at minimum $A_m$ as described in [24]. Figure 6-5 shows the effect of odd $W_f$ at different modulation amplitudes $A_m$ on the instantaneous cutting edge position after fourth tool rotation (steady cutting). Higher $A_m$ resulted in the intersection of the current cutting edge profile with the previous profile, known as chip segmentation, as shown in Figure 6-5 (b). Consequently, by increasing the $A_m$, the actual feed per tooth increases until it reaches the programmed feed, while the minimum feed per tooth decreases until it becomes zero (chip segmentation phenomenon), as shown in Table 6-3 (F= 1,500 Hz at $N$ = 2,000 rpm and F = 2,150 Hz at $N$ = 3,000 rpm).
- Figure 6-6 shows the effect of $A_m$ at even modulation frequency $W_f$ (30 cycles/rev), on the instantaneous cutting edge position. High frequency VAD at even $W_f$ reduces the actual feed/tooth by 50 % compared to conventional drilling (CD), for all conditions. However, the cutting profiles are synchronized with an identical axial offset (constant uncut chip thickness). This behavior is attributed to the non-phase shift between the instantaneous cutting edge profile and the previously machined surface. Consequently, $A_m$ has no effect on the actual feed, as shown in

Table 6-3 (F = 1500 Hz at $N$ = 3,000 rpm). This is in agreement with zero phases difference axial vibration drilling (ZVD) described in [24].

- Fraction modulation frequency $W_f$ showed a low uncut chip thickness compared to the odd $W_f$. However, the critical amplitude required for chip segmentation is higher compared to the odd $W_f$. This explains why the minimum values of the uncut chip thickness are higher for the same $f$ and $A_m$, as shown in Table 6-3 ( F= 2150 Hz with $N$ = 2,000 rpm).

For better clarification, Figure 6-7 presents the dynamic change of the actual uncut chip thickness at F= 1500 Hz for $N$ = 2,000 rpm (odd $W_f$) and $N$ = 3,000 rpm (even $W_f$). The flat peak presents the chip segmentation phenomenon, as described at odd $W_f$. On the other hand, Figure 6-7 (b) show the continuous cutting profile with non-$A_m$ effect, as described for even $W_f$.

**Table 6-2:** Effect of rotational speed and frequency on the tool cycles/rev.

| ***Rotational Speed (rpm)*** | ***2,000*** | ***3,000*** |
|---|---|---|
| ***Frequency (Hz)*** | ***Modulation frequency $W_f$ (cycles/rev)*** | |
| ***1,500*** | 45 | 30 |
| ***2,150*** | 64.5 | 43 |

**Table 6-3:** Effect of HF-VAD machining parameters on the actual feed/tooth.

| *Cutting Speed (rpm)* | | | *2,000* | | *3,000* | |
|---|---|---|---|---|---|---|
| | | | *Actual Feed (mm)* | | *Actual Feed (mm)* | |
| *Frequency (Hz)* | *Feed (mm/rev)* | *Amplitude (μm)* | *Maximum* | *Minimum* | *Maximum* | *Minimum* |
| ***1500*** | ***0.025*** | ***3*** | 0.01225 | 0.00025 | 0.00625 | 0.00625 |
| | | ***4.5*** | 0.0125 | 0 | 0.00625 | 0.00625 |
| | | ***5.5*** | 0.0125 | 0 | 0.00625 | 0.00625 |
| | ***0.05*** | ***3*** | 0.0185 | 0.0065 | 0.0125 | 0.0125 |
| | | ***4.5*** | 0.0216 | 0.0035 | 0.0125 | 0.0125 |
| | | ***5.5*** | 0.024 | 0.0015 | 0.0125 | 0.0125 |
| | ***0.075*** | ***3*** | 0.0248 | 0.0128 | 0.0187 | 0.01875 |
| | | ***4.5*** | 0.0278 | 0.0098 | 0.0187 | 0.01875 |
| | | ***5.5*** | 0.0297 | 0.0077 | 0.0187 | 0.01875 |
| ***2150*** | ***0.025*** | ***3*** | 0.0098 | 0.0034 | 0.0121 | 0.0006 |
| | | ***4.5*** | 0.0108 | 0 | 0.0125 | 0 |
| | | ***5.5*** | 0.0118 | 0 | 0.0125 | 0 |
| | ***0.05*** | ***3*** | 0.0167 | 0.008 | 0.01837 | 0.0069 |
| | | ***4.5*** | 0.0189 | 0.006 | 0.0213 | 0.0036 |
| | | ***5.5*** | 0.0203 | 0.0048 | 0.0233 | 0.0016 |
| | ***0.075*** | ***3*** | 0.023 | 0.0146 | 0.0246 | 0.0128 |
| | | ***4.5*** | 0.0251 | 0.0125 | 0.0274 | 0.0098 |
| | | ***5.5*** | 0.0265 | 0.011 | 0.0295 | 0.0078 |

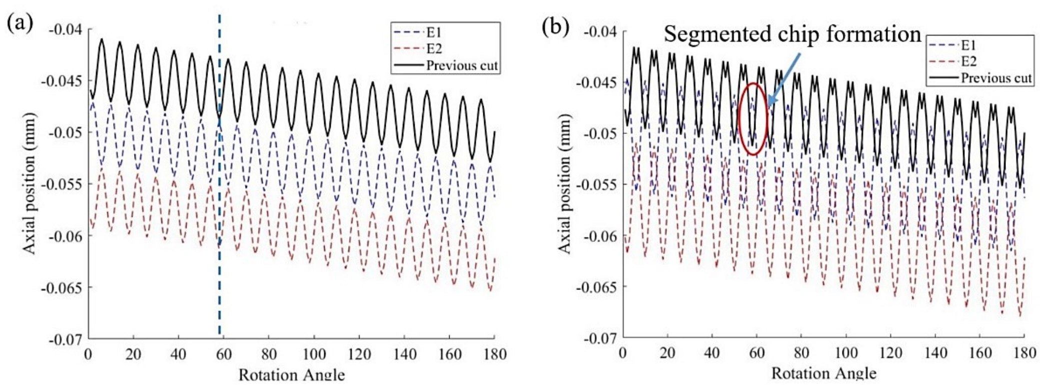


**Figure 6-5:** Effect of $A_m$ (a) 3 μm, (b) 5.5 μm on the uncut chip thickness at odd $W_f$.

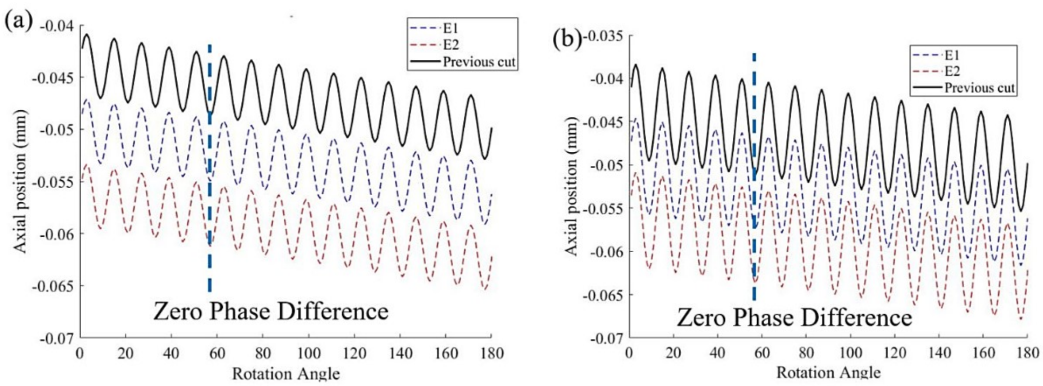


**Figure 6-6:** Effect of $A_m$ (a) 3 µm, (b) 5.5 µm on the uncut chip thickness at even $W_f$.

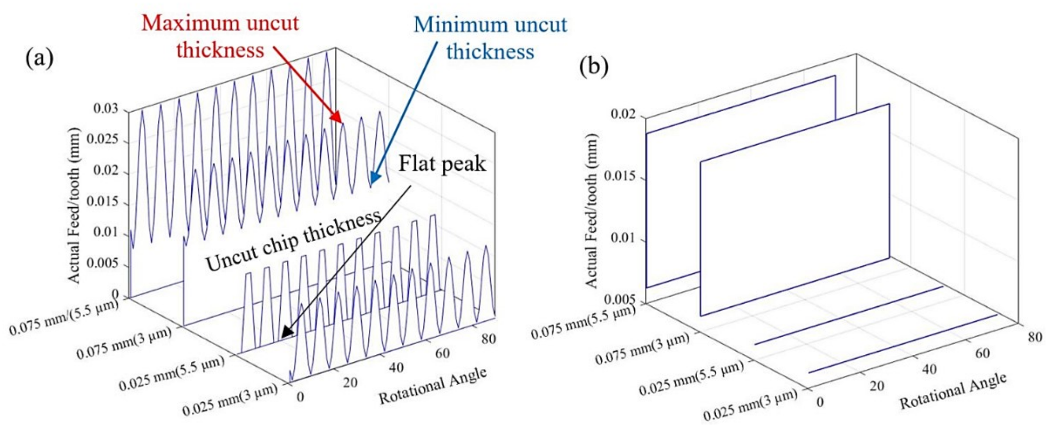


**Figure 6-7:** The effect of HF-VAD at F=1,500 Hz on the uncut chip thickness at (a) $N$ = 2,000 rpm, and (b) $N$ = 3,000 rpm.

Based on the HF-VAD kinematics study for the selected frequencies and amplitudes, the following behaviour can be expected:

- Based on the actual uncut chip thickness analysis, HF-VAD has a lower mechanical and thermal load compared to CD.
- For all feeds, the increase in $A_m$ has a negative effect on the mechanical and thermal load, due to the higher uncut chip thickness.

- HF-VAD with F = 1500 Hz is more recommended to achieve low mechanical and thermal load at *N* = 3,000. As a result of the non-$A_m$ effect, $A_m$ = 3 µm is recommended to reduce the friction force. This is due to the lower axial tool movement.
- In the case of chip segmentation (minimum actual feed = 0), a force-dynamic component can increase the mechanical and thermal load, due to the repetitive tool impact action.

## 6.4 Results and discussion

### 6.4.1 Cutting forces

Figure 6-8 , shows the effect of modulation amplitude and frequency on the measured thrust force for CFRP and Ti6Al4V layers at *N* = 2,000 rpm. For all feeds, HF-VAD showed a reduction in the thrust force compared to CD. Based on F, $A_m$, and *f*, the thrust force ranged from (40 N to 75 N) for CFRP layer, and (215 N to 450 N) for Ti6Al4V respectively. On the other hand, the measured thrust force for CD ranged from (55 N to 105 N) for CFRP layer, and (275 N to 470 N) for Ti6Al4V, respectively. This reduction can be attributed to the following factors:

- Machining load: The low uncut chip thickness, as described in section 6.3.
- Chisel edge cutting mechanism: Discard the non-cutting process under the chisel edge through the axial oscillation.
- Evacuation mechanism: The axial oscillation has a positive effect on the chips morphology and evacuation effectiveness. However, increasing the modulation amplitude will add more resistance to chips evacuation effectiveness [25].

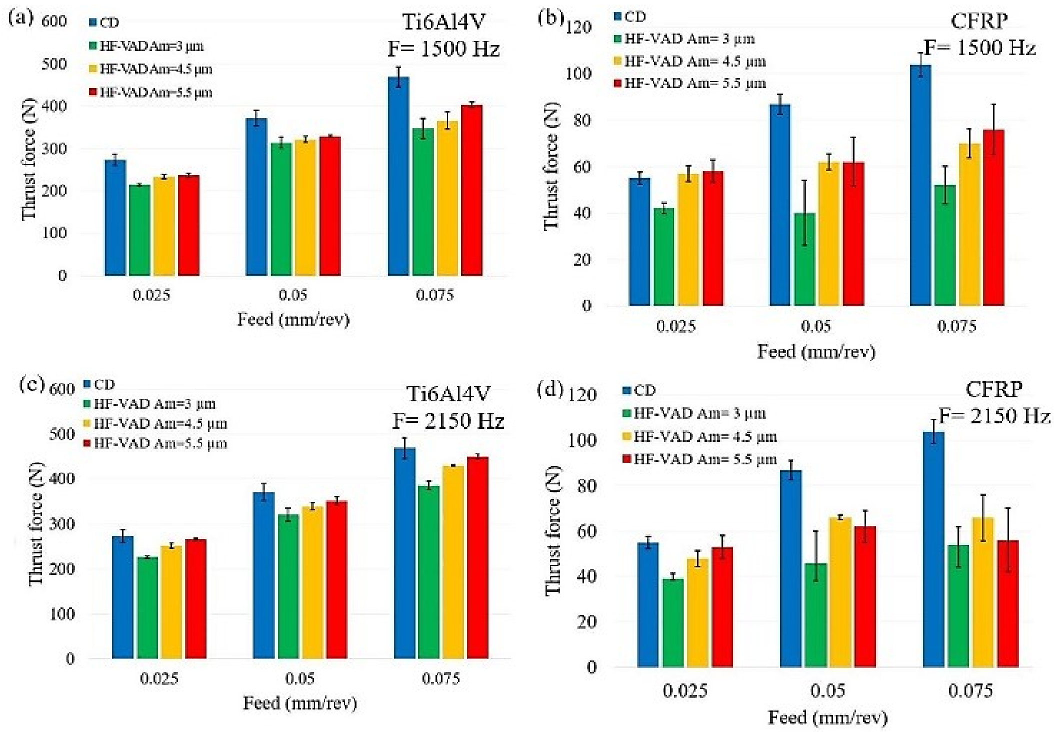


**Figure 6-8:** Effect of modulation amplitude and frequency (a,b) F =1,500 Hz (c,d) F = 2,150 Hz on the measured thrust force of (b,d) CFRP and (a,c) Ti6Al4V at $N$ = 2,000 rpm.

Figure 6-9 shows the effect of modulation frequency on the measured thrust force at $N$ = 3,000 rpm and $A_m$ = 3 µm. Compared to the CD, HF-VAD may cause a limited reduction in the thrust force with a maximum of 7% for Ti6Al4V, and 15% for CFRP, respectively. It should be noted that as rotational speed is changed from 2,000 rpm to 3,000 rpm, the thrust force of CD is reduced. For feeds in the range of 0.025 to 0.075 mm/rev, the CD thrust force of the Ti6Al4V is reduced from (273N to 470 N) at $N$ = 2,000 rpm to (241 N to 381 N) at $N$ = 3,000 rpm respectively. For the CFRP, however, the CD thrust force is reduced from (55 N to 104 N) at $N$ = 2,000 rpm to (47 N to 81 N) at $N$ = 3,000 rpm, respectively. This reduction is attributed to the higher cutting temperature that softening the material and consequently the cutting forces reduced, as will be described in section 6.4.2.

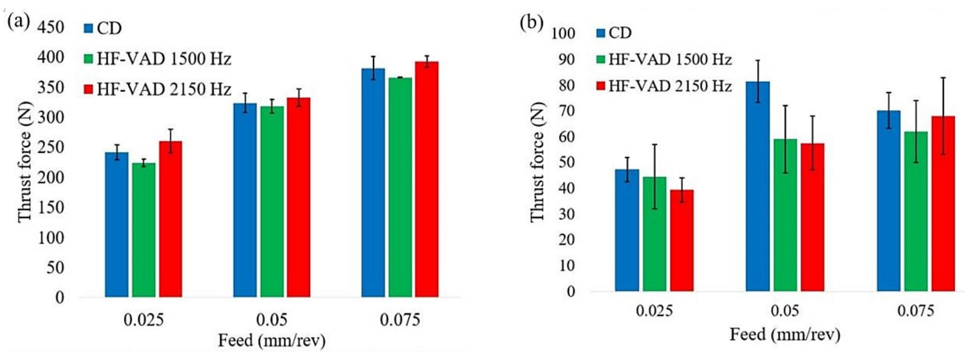


**Figure 6-9:** Effect of modulation frequency on the measured thrust force of (a) Ti6Al4V and (b) CFRP at $A_m$ = 3 µm and $N$ = 3,000 rpm.

Figure 6-10, shows the effect of Vibration-assisted drilling frequency (F = 83.3 and 1,500 Hz ) on the measured thrust force during CFRP/Ti6Al4V stack drilling at different conditions. Increasing the amplitude $A_m$ leads to an increase in the thrust force for both frequency range. This behavior can be attributed to the frictional force component, which is linearly related to the axial tool displacement ($A_m$). Moreover, for the same machining condition, HF-VAD showed a lower thrust force compared to LF-VAD and CD [3]. LF-VAD (F=83.3 Hz) showed an increase in the thrust force as $A_m$ increases from 70 µm to 480 µm, reaching 152% and 149% for CFRP and Ti6Al4V, respectively. On the other hand, HF-VAD showed up to 54% and 26% thrust force reduction for CFRP and Ti6Al4V, respectively. The lower thrust force at HF-VAD can be attributed to the lower uncut chip thickness, and the absence of periodical chisel impact mechanism.

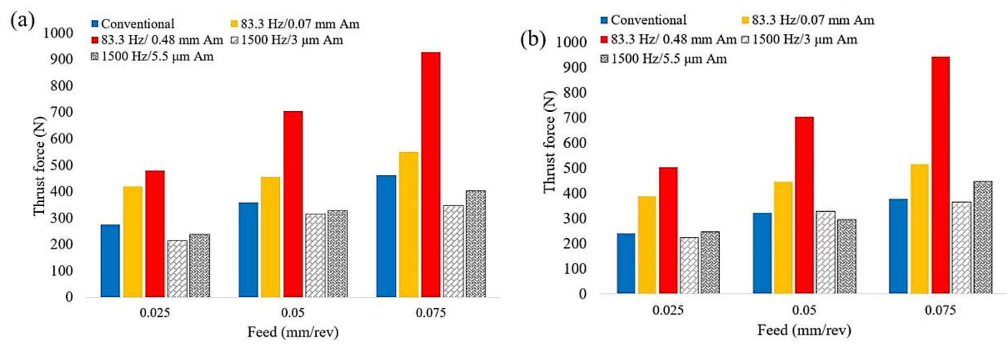


**Figure 6-10:** The effect of machining frequency and feed on the Ti6Al4V thrust force for (a) $N = 2{,}000$ rpm (b) $N = 3{,}000$ rpm.

### 6.4.2 Cutting temperature

Figure 6-11 shows the effect of the vibration amplitude $A_m$ and frequency F on the drilling tool tip temperature at the exit surface, since it indicates the maximum tool temperature during cutting. For the majority of tested machining conditions, the HF-VAD resulted in a lower thermal load compared to the CD, which is in agreement with the theoretical considerations presented in section 6.3 This reduction can be attributed to the following two factors: (a) lower cutting energy as a result of smaller actual uncut chip thickness, as shown in section 6.3, and (b) an improved chip evacuation efficiency, due to the axial tool oscillation.

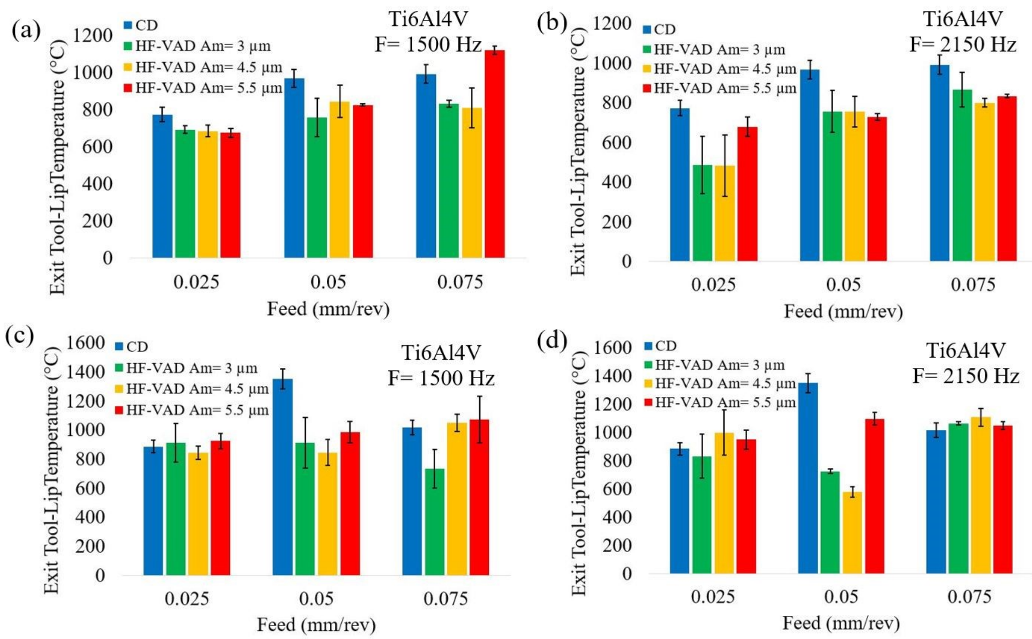


**Figure 6-11:** Effect of modulation amplitude and frequency (a, c) 1,500 Hz, and (b, d) 2,150 Hz on the exit Tool-lip temperature for different feeds at (a, b) $N$ = 2,000 rpm, and (c, d) $N$ =3,000 rpm.

When compared to conventional drilling (CD), the analysis of the results showed that the cutting tool temperature under LF-VAD and HF-VAD is reduced by up to 55.9 % for LF-VAD [3], and 37 % for HF-VAD, respectively, as shown in Figure 6-12. However, the modulation amplitude $A_m$ showed an adverse effect for both cutting frequency regimes. For LF-VAD, an increase the $A_m$ resulted in a lower cutting temperature. This reduction attributed to higher cooling cycle, lower duty cycle, and chip evacuation effectiveness. On the other hand, for HF-VAD, higher $A_m$ resulted in the higher cutting tool temperature. This could be due to the higher friction forces, the absence of chip segmentation, and higher uncut chip thickness (compared to the low amplitude).

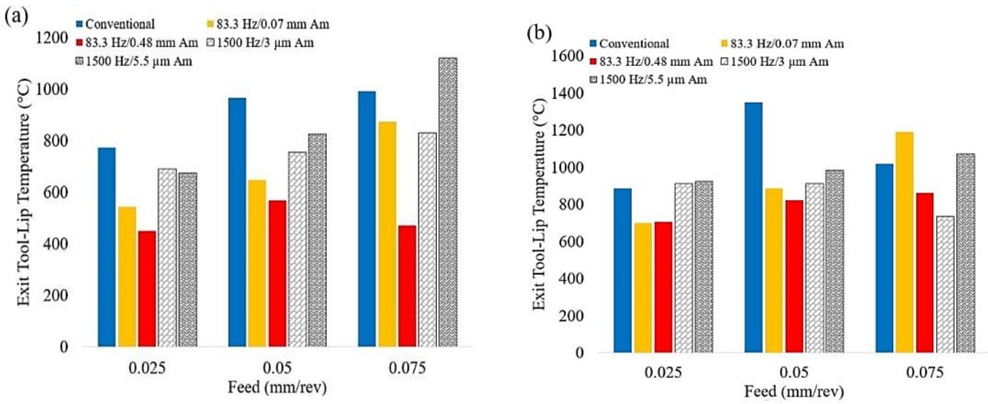


**Figure 6-12:** The effect of machining frequencies and feeds on the Ti6Al4V exit tool temperature for (a) $N = 2{,}000$ rpm (b) $N = 3{,}000$ rpm.

### 6.4.3 Residual stresses

*6.4.3.1 Effect of the modulation frequency*

Figure 6-13, compares the measured Ti6Al4V wall surface residual stresses (RS) of the holes drilled by CD and HF-VAD for different feeds, when $A_m = 3$ μm and $N = 2{,}000$ rpm. For all machining condition, HF-VAD resulted in a lower RS compared to CD. All CD feed conditions produced a positive (tensile) RS, while HF-VAD, at a frequency F = 1,500 Hz, produced a desirable negative (compressive) RS, except at $f = 0.05$ mm/rev, where a relatively small positive (tensile) RS was generated. The reduction in residual stresses under HF-VAD can be attributed to: (a) a low uncut chip thickness (compared to CD), as predicted by the kinematics model described in section 6.3, and (b) Proper chip evacuation mechanism. Based on the zero stress line, increasing the axial modulation frequency to F = 2,150 Hz resulted in a higher RS, when compared to the F = 1,500 Hz. This behavior could be attributed to higher tool axial amplitude that leads to increasing the friction force component. As a consequence of the RS sign inflection of HF-VAD with F=1500 Hz in the case of $f = 0.05$ mm/rev, further investigation of $f = 0.05$ mm/rev and $f = 0.075$ mm/rev were conducted on RS depth profile.

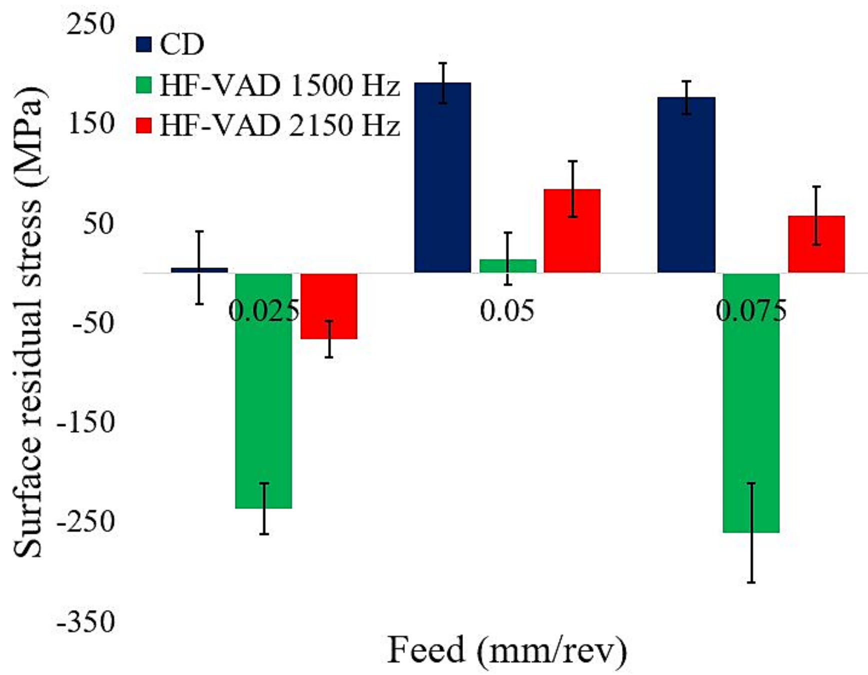


**Figure 6-13:** Effect of modulation frequency on the residual stress at the low amplitude 3 µm and low rotational speed $N = 2{,}000$ rpm.

*6.4.3.2 Effect of the modulation frequency on the residual stress depth profile*

Figure 6-14 compares the subsurface residual stresses of HF-VAD at $A_m = 3$ µm with that of CD at $N = 2{,}000$ rpm and $f = 0.05$ mm/rev, as well as $N = 2{,}000$ rpm and $f = 0.075$ mm/rev. In HF-VAD case, reduction in residual stresses was observed. HF-VAD at F= 1500 Hz showed the lowest residual stresses for both machining conditions. Figure 6-14 (a) shows that HF-VAD at F= 1500 Hz resulted in a compressive RS at a depth of 90 µm. The compressive RS increased to reach -123 MPa at a depth of 200 µm. Figure 6-14 (b) shows that HF-VAD at F= 1500 Hz resulted in -347 MPa RS with compressive stress until a depth of 120 µm. The CD showed tensile RS until 400 µm in depth with maximum magnitude of 333 MPa at f = 0.05 mm/rev and 269 MPa at f = 0.05 mm/rev, respectively.

This enhancement on the subsurface RS has a positive impact on the bearing fatigue life of the machined part. This conclusion agrees with the results reported in references [3, 26].

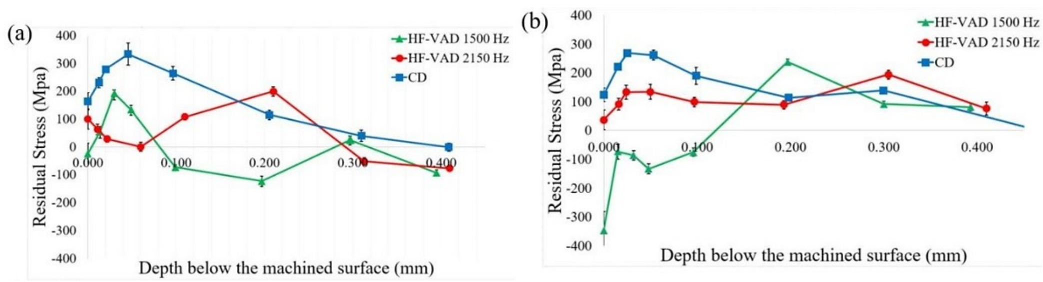


**Figure 6-14:** The subsurface residual stresses measurement of HF-VAD at $A_m$ = 3 µm and *N*=2,000 rpm compared to CD for (a) *f*=0.05 mm/rev and (b) *f*=0.075 mm/rev.

*6.4.3.3 Effect of the modulation amplitude*

Figure 6-15 , shows the effect of $A_m$ = 3 µm and 5.5 µm on the surface residual stresses RS at *f* = 0.025 mm/rev for different rotational speeds. At *N* = 2000 rpm, the increase in $A_m$ resulted in inducing tensile stresses for both modulation frequencies (Figure 6-15 (a)). This adverse effect could be attributed to the increase in the higher uncut chip thickness and the formation of segmented chips, as described in section 6.3 and confirmed in section 6.4.1. The higher uncut chip thickness resulted in a higher thermal load, while the segmented chips could be affected by evacuation resistance due to the high tool vibration frequency compared to the chips velocity [25]. At *N* = 3000 rpm, however, the increase in $A_m$ produced compressive RS for both frequencies, as shown in Figure 6-15 (b). This favorable effect could be attributed to the effectiveness of chip evacuation at higher axial tool velocity, where the gap between tool vibration frequency and chip velocity was reduced [25].

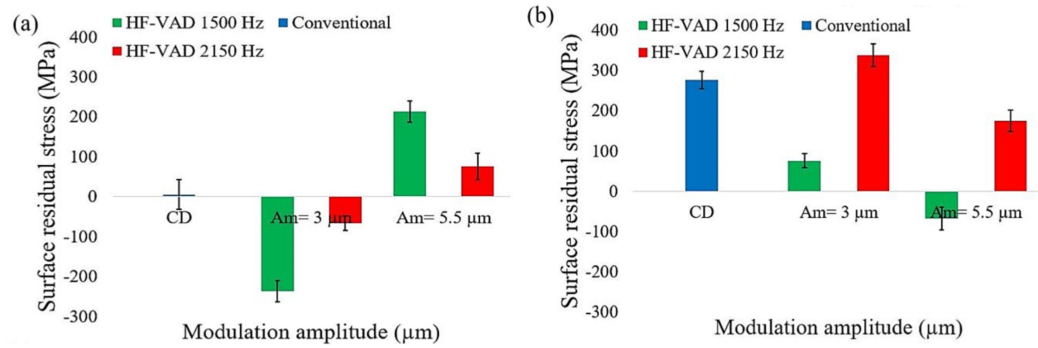


**Figure 6-15:** Effect of modulation amplitude and frequency on the residual stress at low feed condition $f = 0.025$ mm/rev for different rotational speeds (a) $N = 2{,}000$ rpm (b) $N = 3{,}000$ rpm.

Figure 6-16, shows the effect of $A_m$ at F = 1500 Hz and $f = 0.075$ mm/rev for different rotational speeds. Low uncut chip thickness and friction load are of the main reason to achieve low RS at $A_m = 3$ µm and $N = 2{,}000$ rpm. This behavior is consistent with the RS measurement at $f = 0.025$ mm/rev, as shown in Figure 6-15 (b) and the kinematic study section 6.3. At $N = 3{,}000$ rpm, however, low RS was produced at $A_m = 5.5$ µm, which is attributed to higher chip evacuation efficiency, as observed for $f = 0.025$ (Figure 6-15 (b)). Moreover, at a modulation frequency F = 1,500 Hz, the increase in $A_m$ has no effect on the uncut chip thickness (even $W_f$), as described in section 6.3. Consequently, the chip evacuation efficiency has the dominant effect on the surface RS, as demonstrated in Figure 6-15 (b).

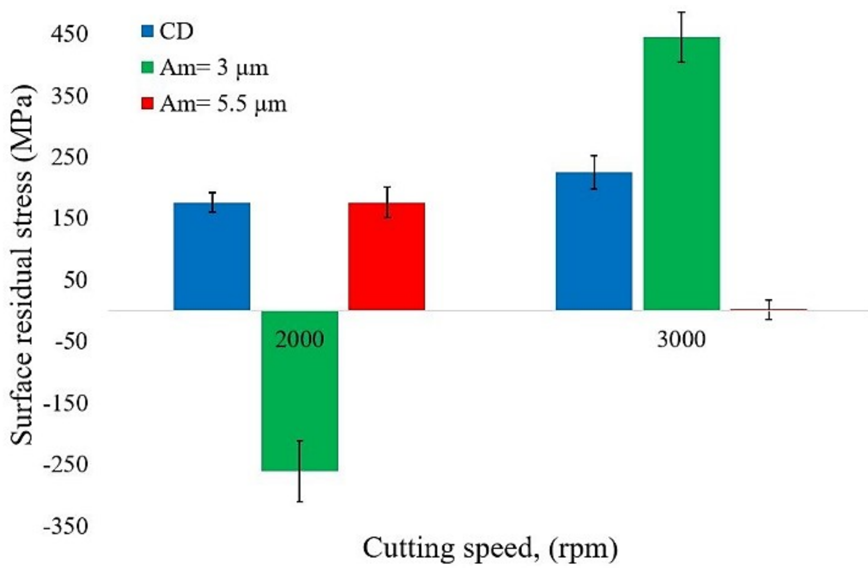


**Figure 6-16:** Effect of $A_m$ at F = 1,500 Hz and $f$ = 0.075 mm/rev for different rotation speeds.

### 6.4.4 Delamination

Based on the definition of the delamination factor ($\varphi_d$) [3, 27]:

$$\varphi_d = \frac{D_{actual} - D_{nominal}}{D_{nominal}} \tag{6.4}$$

where $D_{actual}$ is the diameter of a circle including the circumscribing delamination, while $D_{nominal}$ represents the nominal hole diameter.

The delamination factor in conventional drilling (CD) exceeds the acceptable entry and exit limit ($\varphi_d \leq 0.5$), as defined by aerospace manufactures [3, 17]. Low thermal load and proper chips evacuation efficiency (compared to CD), are of the main reasons for the HF-VAD benefits, that reduced the Entry $\varphi_d$ from (0.32 – 0.86) for CD, $\varphi_d \leq 0.4$ for HF-VAD. Moreover, the Exit $\varphi_d$, which is the main CFRP/Ti6Al4V drilling challenge, was reduced from (0.13 – 1.2) for CD, to less than 0.2 at $N$ = 2,000 rpm, and less than 0.5 at $N$

= 3,000 rpm, as summarized in Figure 6-17. Figure 6-18, shows the optical examination of the entry and exit delamination at different conditions for CD and HF-VAD.

| | **Cutting speed** (rpm) | **2000** | | | | **3000** | | | |
|---|---|---|---|---|---|---|---|---|---|
| | | **Amplitude** (μm) | | | | **Amplitude** (μm) | | | |
| **Feed** | **Frequency** Hz | **CD** | **3** | **4.5** | **5.5** | **CD** | **3** | **4.5** | **5.5** |
| **0.025** (mm/rev) | **1500** | 0.32 | | | | 0.52 | 0-0.2 | | |
| | **2150** | | | | | | | | |
| **005** (mm/rev) | **1500** | 0.55 | | | | 0.86 | | | |
| | **2150** | | 0-0.2 | | | | 0-0.2 | | |
| **0.075** (mm/rev) | **1500** | 0.6 | | | 0.2-0.4 | 0.8 | 0.2-0.4 | | |
| | **2150** | | | | | | 0-0.2 | | |

(a)

| | **Cutting speed** (rpm) | **2000** | | | | **3000** | | | |
|---|---|---|---|---|---|---|---|---|---|
| | | **Amplitude** (μm) | | | | **Amplitude** (μm) | | | |
| **Feed** | **Frequency** Hz | **CD** | **3** | **4.5** | **5.5** | **CD** | **3** | **4.5** | **5.5** |
| **0.025** (mm/rev) | **1500** | 0.13 | | | | 0.9 | 0-0.2 | | |
| | **2150** | | | | | | 0.2-0.4 | | |
| **005** (mm/rev) | **1500** | 0.58 | 0-0.2 | | | 1.2 | | | |
| | **2150** | | | | | | 0-0.2 | | |
| **0.075** (mm/rev) | **1500** | 0.6 | | | | 0.9 | | 0.4-0.5 | ≥ 0.5 |
| | **2150** | | | | | | | | |

(b)

**Figure 6-17:** The effect of HF-VAD machining parameters on CFRP delamination (a) Entry delamination, and (b) Exit delamination.

Based on the $\varphi_d$ analysis, HF-VAD showed promising results to overcome the delamination challenge. However, LF-VAD resulted in a lower $\varphi_d$ [3], which contributed to the significant benefits of the (a) lower cutting tool temperature that prevents CFRP matrix form burnout. (b) Segmented chip morphology which efficiently evacuates the main thermal source during the drilling process.

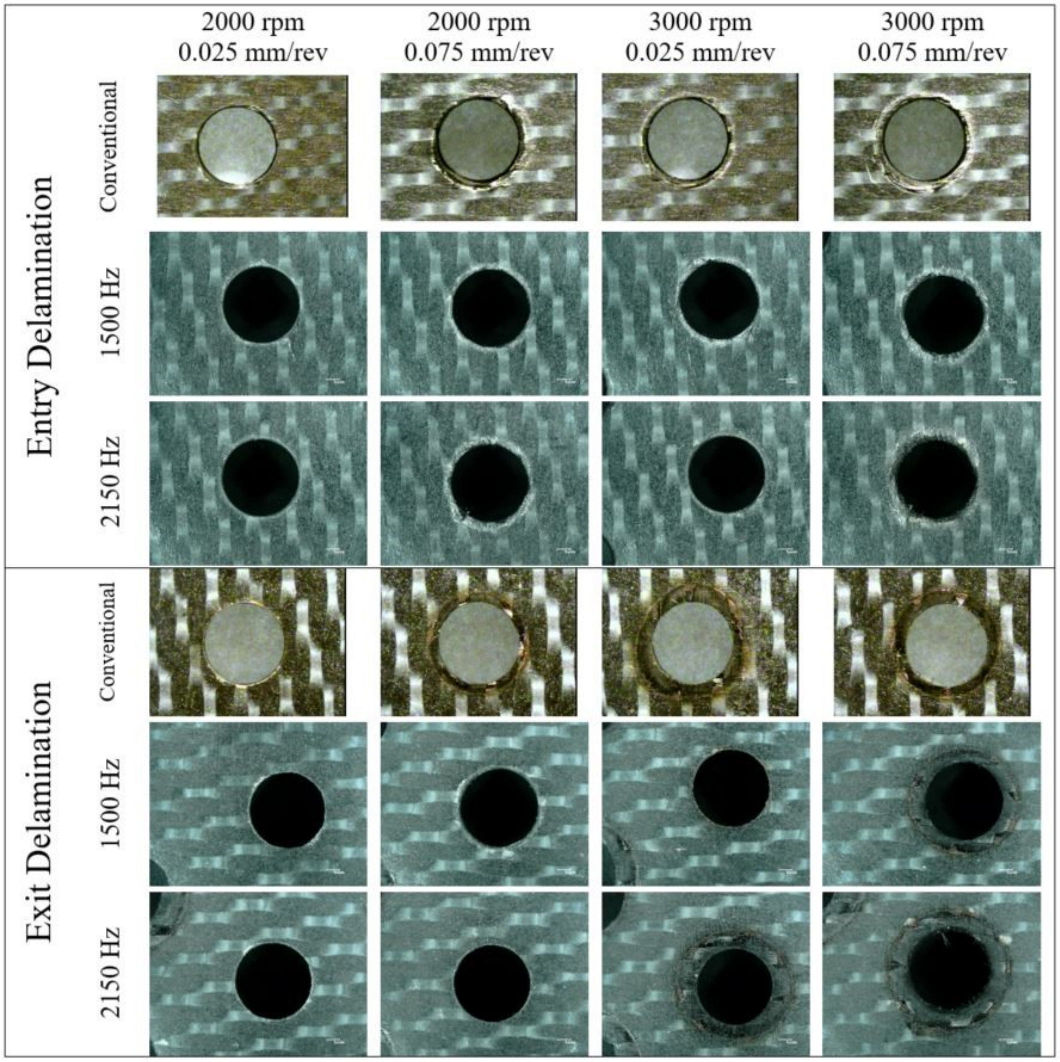


**Figure 6-18:** Effect of machining technique on the CFRP entry and Exit delamination under different machining conditions, at $A_m$ = 3 μm.

### 6.4.5 Surface roughness

Figure 6-19 compares the effect of modulation frequency on the measured surface roughness (Ra) for CFRP at $A_m$ = 3 μm and different cutting feeds and speeds. The percentage changes in Ra, are relative to the reference case of conventional drilling. The surface roughness showed a gradual increase with the cutting feed and speed. For all machining condition, HF-VAD showed up to 54 % reduction in the Ra value, except for 3000 rpm and $f$= 0.05 and 0.075 mm/rev. This reduction can be attributed to: (a) The lower thermal load which is a critical issue during the drilling process of CFRP [28-30]. Uneven surface [31], severe material softening, fiber pull-out, and bonding strength reduction [30], are of the main surface defects that are related to the excessive thermal load. (b) For the CFRP/Ti6Al4V stack drilling, the titanium machined chips evacuate 80% of the generated thermal energy [32]. In addition, the metallic sharp edges may cause severe surface scratches on the machined CFRP surface, in particular during the VAD process where the machined chips contain three sharp edges. Consequently, the proper chip evacuation effectiveness of VAD has significant benefits on the CFRP surface roughness.

Moreover, at $N$ = 3,000 rpm, HF-VAD at F =1500 Hz showed lower surface roughness compared to that at a higher frequency. This reduction is attributed to the lower uncut chip thickness, which ensures a lower mechanical and thermal load (see section 6.3). For all machining conditions, increasing the modulation amplitude ($A_m$) resulted in poor machined surface with high surface roughness. This observation could be attributed to the higher uncut chip thickness which increased the machining thermal load.

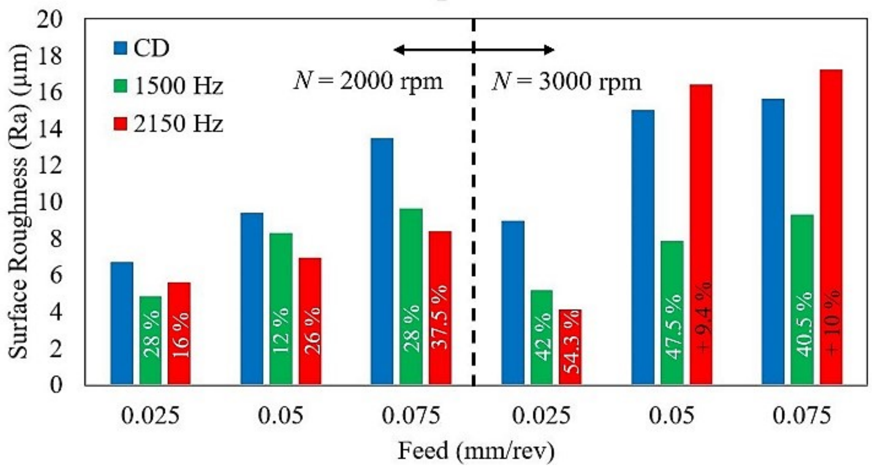


**Figure 6-19:** Effect of machining technique at $A_m$ = 3 μm on the CFRP surface roughness for different machining parameters.

Figure 6-20 shows the effect of different machining parameters on the measured surface roughness (Ra) for Ti6Al4V at $A_m$ = 3 μm. For all conditions, HF-VAD showed a lower Ra compared to CD. Lower uncut chip thickness (50% compared to CD), and proper chip evacuation mechanism are the main reasons to reduce the Ra by 66% at $N$ = 3,000 rpm.

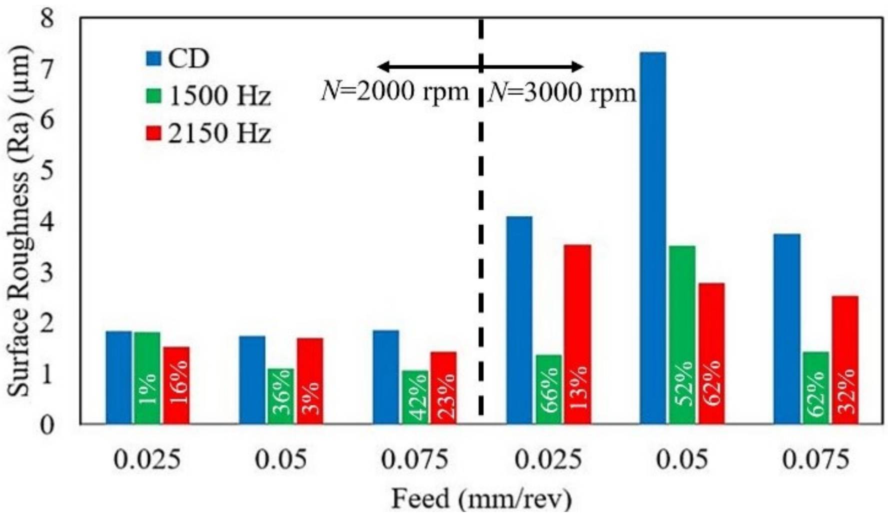


**Figure 6-20:** Effect of machining technique at $A_m$ = 3 µm on the Ti6Al4V surface roughness for different machining parameters.

### 6.4.6 Burr height

Figure 6-21 compares the effect of HF-VAD on the Ti6Al4V exit burr height. For all machining conditions, HF-VAD showed a lower burr height compared to the reference case of conventional drilling (CD). The higher thermal load at CD leads to reduce the material strength and consequently the material easily deform under the applied thrust force, as shown separately in Figure 6-21. On the other hand, lower cutting temperature and thrust force during HF-VAD resulted in up to 86.2 % burr reduction. For both rotation speeds, the percentage reduction increased with the feed rate. This enhancement could be attributed to the lower machining time contact which prevents the titanium material form the thermal softening defects. The significant enhancement at $N$= 2000 rpm and $f$= 0.05 mm/rev, could be attributed to improved machining conditions for chip evacuation effectiveness during the HF-VAD machining process.

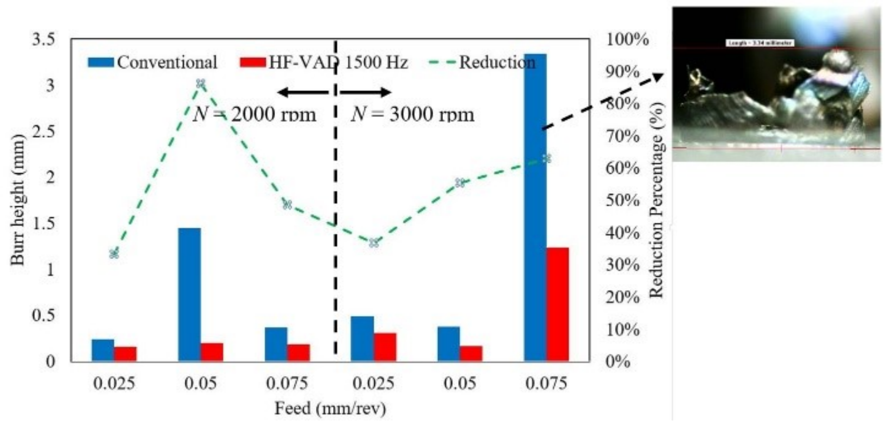


**Figure 6-21:** Effect of HF-VAD on the exit burr height compared to CD.

## Conclusions

Modulation frequency, amplitude, and feed are shown to be the main factors that control the uncut chip thickness during the Vibration assisted drilling. The kinematics of chip formation was used to study the independent effects of HF-VAD machining parameters. The relationship between rotation speed and frequency leads to the generation of an odd, even or fraction $W_f$, and consequently, a significant impact on the uncut chip profile was induced. A fully factorial design of experiments was implemented to investigate the performance of HF-VAD. The machining parameters were carefully selected to generate the three types of the modulation frequency. Moreover, for the purpose of comparison with LF-VAD [3], the same rotation speed and feed ranges were used. The main experimental observations are:

- A significant reduction of up to 26% in the thrust force, has been observed in HF-VAD.
- Compared to CD, HF-VAD showed an efficient evacuation mechanism with lower cutting energy that reduced the cutting temperature by up to 37%.

- HF-VAD can increase the machined part fatigue life by inducing a compressive residual stress on the Ti6Al4V machined surface.
- Entry and exit delamination defects were significantly enhanced using HF-VAD. This is mainly attributed to the observed cutting temperature reduction combined with proper chip evacuation mechanism.
- Titanium exit burr showed a significant reduction by up to 56 %. Reducing the cutting temperature and thrust force are of the main observation of HF-VAD machining process.

## References

[1] E. Brinksmeier and R. Janssen, "Drilling of multi-layer composite materials consisting of carbon fiber reinforced plastics (CFRP), titanium and aluminum alloys," *CIRP Annals-Manufacturing Technology,* vol. 51, pp. 87-90, 2002.

[2] S. L. Soo, A. M. Abdelhafeez, M. Li, R. Hood, and C. M. Lim, "The drilling of carbon fibre composite–aluminium stacks and its effect on hole quality and integrity," *Proceedings of the Institution of Mechanical Engineers, Part B: Journal of Engineering Manufacture,* p. 0954405417728312, 2017.

[3] R. Hussein, A. Sadek, M. A. Elbestawi, and M. H. Attia, "Low-frequency vibration-assisted drilling of hybrid CFRP/Ti6Al4V stacked material," *The International Journal of Advanced Manufacturing Technology,* vol. 98, pp. 2801-2817, October 01 2018.

[4] S. Malhotra, "Some studies on drilling of fibrous composites," *Journal of Materials Processing Technology,* vol. 24, pp. 291-300, 1990.

[5] S. Lin and I. Chen, "Drilling carbon fiber-reinforced composite material at high speed," *Wear,* vol. 194, pp. 156-162, 1996.

[6] A. Sadek, M. Attia, M. Meshreki, and B. Shi, "Characterization and optimization of vibration-assisted drilling of fibre reinforced epoxy laminates," *CIRP Annals-Manufacturing Technology,* vol. 62, pp. 91-94, 2013.

[7] R. Stone and K. Krishnamurthy, "A neural network thrust force controller to minimize delamination during drilling of graphite-epoxy laminates," *International Journal of Machine Tools and Manufacture,* vol. 36, pp. 985-1003, 1996.

[8] Z. Li, D. Zhang, X. Jiang, W. Qin, and D. Geng, "Study on rotary ultrasonic-assisted drilling of titanium alloys (Ti6Al4V) using 8-facet drill under no cooling condition," *The International Journal of Advanced Manufacturing Technology,* vol. 90, pp. 3249-3264, 2017.

[9] P. Zhang, N. Churi, Z. J. Pei, and C. Treadwell, "Mechanical drilling processes for titanium alloys: a literature review," *Machining Science and Technology,* vol. 12, pp. 417-444, 2008.

[10] D. Dornfeld, J. Kim, H. Dechow, J. Hewson, and L. Chen, "Drilling burr formation in titanium alloy, Ti-6AI-4V," *CIRP Annals-Manufacturing Technology,* vol. 48, pp. 73-76, 1999.

[11] J. Pujana, A. Rivero, A. Celaya, and L. L. de Lacalle, "Analysis of ultrasonic-assisted drilling of Ti6Al4V," *International Journal of Machine Tools and Manufacture,* vol. 49, pp. 500-508, 2009.

[12] H. Schulz and A. Emrich, "Limitations of Drilling in Difficult-to-Machine Materials such as Titanium TiA16V4, 1998," *Production Engineering,* vol. 5, p. 1, 1998.

[13] J. Xu and M. El Mansori, "Experimental study on drilling mechanisms and strategies of hybrid CFRP/Ti stacks," *Composite Structures,* vol. 157, pp. 461-482, 12/1/ 2016.

[14] D. Kim and M. Ramulu, "Study on the drilling of titanium/graphite hybrid composites," *Journal of Engineering Materials and Technology,* vol. 129, pp. 390-396, 2007.

[15] D. Kim, C. Sturtevant, and M. Ramulu, "Usage of PCD tool in drilling of titanium/graphite hybrid composite laminate," *International Journal of Machining and Machinability of Materials,* vol. 13, pp. 276-288, 2013.

[16] N. Guibert, "Etude et modélisation de l'influence des phénomènes de coupe sur les performances du forage vibratoire," Université Joseph-Fourier-Grenoble I, 2008.

[17] A. Sadek, "Vibration Assisted Drilling of Multidirectional Fiber Reinforced Polymer Laminates," Ph.D. Thesis, McGill University Libraries, 2014.

[18] B. Denkena, D. Boehnke, and J. Dege, "Helical milling of CFRP–titanium layer compounds," *CIRP Journal of manufacturing Science and Technology,* vol. 1, pp. 64-69, 2008.

[19] S. S. F. Chang and G. M. Bone, "Thrust force model for vibration-assisted drilling of aluminum 6061-T6," *International Journal of Machine Tools and Manufacture,* vol. 49, pp. 1070-1076, 2009/11/01/ 2009.

[20] O. Pecat and I. Meyer, "Low frequency vibration assisted drilling of aluminium alloys," in *Advanced Materials Research*, 2013, pp. 131-138.

[21] R. Hussein, A. Sadek, M. A. Elbestawi, and M. H. Attia, "Surface and microstructure characterization of low-frequency vibration-assisted drilling of Ti6Al4V," *The International Journal of Advanced Manufacturing Technology,* vol. 103, pp. 1443-1457, April 05 2019.

[22] J. Panju, M. Meshreki, and M. Attia, "Design of a Retrofittable Spindle Attachment for High Frequency Vibration-Assisted Drilling," in *ASME 2014 International Mechanical Engineering Congress and Exposition*, 2014, pp. V02AT02A034-V02AT02A034.

[23] A. Sadek, M. Meshreki, and M. Attia, "Effect of Tool Kinematics on the Drilling Forces and Temperature in Low Frequency High Amplitude Vibration Assisted Drilling," in *ASME 2014 International Mechanical Engineering Congress and Exposition*, 2014, pp. V02AT02A035-V02AT02A035.

[24] Z. Deyuan and W. Lijiang, "Investigation of chip in vibration drilling," *International Journal of Machine Tools and Manufacture,* vol. 38, pp. 165-176, 1998.

[25] Y. Liao, Y. Chen, and H. Lin, "Feasibility study of the ultrasonic vibration assisted drilling of Inconel superalloy," *International Journal of Machine Tools and Manufacture,* vol. 47, pp. 1988-1996, 2007.

[26] Y. Guo, A. Warren, and F. Hashimoto, "The basic relationships between residual stress, white layer, and fatigue life of hard turned and ground surfaces in rolling contact," *CIRP Journal of manufacturing Science and Technology,* vol. 2, pp. 129-134, 2010.

[27] R. Hussein, A. Sadek, M. A. Elbestawi, and M. H. Attia, "Chip Morphology and Delamination Characterization for Vibration-Assisted Drilling of Carbon Fiber-Reinforced Polymer," *Journal of Manufacturing and Materials Processing,* vol. 3, p. 23, 2019.

[28] D. Che, I. Saxena, P. Han, P. Guo, and K. F. Ehmann, "Machining of carbon fiber reinforced plastics/polymers: a literature review," *Journal of Manufacturing Science and Engineering,* vol. 136, p. 034001, 2014.

[29] D. Liu, Y. Tang, and W. Cong, "A review of mechanical drilling for composite laminates," *Composite Structures,* vol. 94, pp. 1265-1279, 2012.

[30] R. Fu, Z. Jia, F. Wang, Y. Jin, D. Sun, L. Yang*, et al.*, "Drill-exit temperature characteristics in drilling of UD and MD CFRP composites based on infrared thermography," *International Journal of Machine Tools and Manufacture,* vol. 135, pp. 24-37, 2018.

[31] X. M. Wang and L. Zhang, "An experimental investigation into the orthogonal cutting of unidirectional fibre reinforced plastics," *International journal of machine tools and manufacture,* vol. 43, pp. 1015-1022, 2003.

[32] M. C. Shaw and J. Cookson, *Metal cutting principles* vol. 2: Oxford university press New York, 2005.

# Chapter 7

## An investigation into tool wear and hole quality during Low-Frequency Vibration Assisted Drilling of CFRP/Ti6Al4V stack

**Complete Citation:**

Hussein, R., Sadek, A., Elbestawi, M.A., Attia, M.H. (2019). 7 An investigation into tool wear and hole quality during Low-Frequency Vibration Assisted Drilling of CFRP/Ti6Al4V. *Journal of Manufacturing and Materials Processing*, 2019. Volume 3, Issue 3. Doi. https://doi.org/10.3390/jmmp3030063.

**Copyright:**

**Relative Contributions:**

| | |
|---|---|
| R. Hussein: | Performed experiments, analysis, and data interpretation; wrote the first draft of the manuscript; helped with submitting the final manuscript to the journal (corresponding author). |
| A. Sadek: | Helped with the experiments and analysis; revised the manuscript. |
| M. A. Elbestawi: | Supervisor of R. Hussein. Revised and edited the manuscript and gave the final approval to be submitted. |
| M. H. Attia: | Revised the manuscript. |

**Abstract:**

The use of lightweight material such as CFRP/Ti6Al4V stacked structures in the aerospace industry is attributed to improved physical and mechanical characteristics. The drilling process of non-uniform structures plays a significant role prior to the assembly operation. However, this drilling process was typically associated with unacceptable CFRP delamination, hole accuracy, and high tool wear. These machining difficulties are attributed to high thermal load and poor chip evacuation mechanism. Low-frequency vibration assisted drilling (LF-VAD) is an advanced manufacturing technique where the dynamic change of the uncut chip thickness is used to manipulate the cutting energy. An efficient chip evacuation mechanism was achieved through axial tool oscillation. This study investigates the effect of vibration-assisted drilling machining parameters on tool wear mechanisms. The paper presents also the effect of tool wear progression on the drilled hole quality. This hole quality is described by CFRP entry and exit delamination, and hole accuracy. The results showed a significant reduction in the thrust force, cutting torque, cutting temperature, and flank wear land.



**Keywords:**

Vibration-assisted drilling. Low-frequency vibration-assisted drill. CFRP/ Ti6Al4V. Stacked material. Tool wear. Surface integrity. Delamination.


**Acronyms:**

| | |
|---|---|
| VAD | Vibration-assisted drilling |
| LF-VAD | Low frequency-vibration assisted drilling |
| CD | Conventional drilling |

| | |
|---|---|
| HSS | High-speed steel |
| BUE | Built-up edge |
| A | Initial wear region |
| B | Steady wear region |
| C | Severe wear region |
| CER | Cutting edge radius |
| VB | Average flank wear land |

**Notations:**

| | |
|---|---|
| $N$ | Cutting speed (m/min) |
| $f$ | Feed rate (mm/rev) |
| $A_m$ | Modulation amplitude (mm) |
| $F$ | Frequency (µm) |
| $Ø_d$ | Delamination factor |

## 7.1 Introduction

Superior physical and mechanical characteristics such as high strength to weight ratio, low coefficient of thermal expansion, fatigue resistance and corrosion/erosion resistance [1-3], explain the growing usage of carbon fiber reinforced polymers (CFRP) and Ti6Al4V in the aerospace industry. The hybrid structure of CFRP/ Ti coupling (CFRP/Ti, CFRP/Ti/CFRP, and Ti/CFRP/Ti) has been identified as the common selection in the new generation of aircraft [4, 5]. Good reliability, convenient inspection, and easy detachability are of the main advantages of mechanical fastening that are typically used in the assembly process of different materials in the load carrying members. Consequently, making the drilling process of CFRP and Ti6Al4V a necessity prior to the assembly process.

The conventional drilling process of CFRP is commonly associated with surface integrity defects such as entry and exit delamination and matrix thermal damage [6-9]. These machining difficulties are attributed to the high sensitivity to cutting energy and anisotropic mechanical properties [10, 11]. To achieve a long tool life with proper machining performance, excessive experimental investigation using different tool material were conducted to understand the main wear mechanism. Carbide drills showed a preferable drilling performance over the high-speed steel (HSS) for higher hot hardness, while polycrystalline diamond (PCD) cost adds more limitation for mass manufacturing. Abrasive wear has been identified as the dominant wear mechanism during the drilling process of CFRP [12-14]. This wear mechanism was attributed to hard and soft abrasion modes [14]. Hard mode located at WC grains due to the generated dynamic stresses from the broken fiber, material reinforcement, and powder like chips [15]. Consequently, the WC grains suffer crack initiation and propagation fracture [16]. On the other hand, the relatively low hardness Co binder is easier to be damaged by carbon fibers (CF) in a process known as soft abrasion mode [14, 17, 18]. Hence, the WC grain spalling is more rapid under the cyclic machining load.

High cutting temperature, poor chip evacuation mechanism, and burr formation are of the common issue during the drilling process of Ti6Al4V [19-21]. These problems resulted in a higher probability of flue-chips accumulation, progressive tool wear, and poor surface integrity [19, 20, 22]. Low thermal conductivity and high chemical affinity to the majority of tool materials are of the adverse titanium characteristics that resulted in a significant reduction of the tool life with high probability of catastrophic failure [20, 23, 24]. This effect contributed to the cutting stress concentration on the tool cutting edge where the maximum cutting temperature is located. Therefore, the machining process of Ti6Al4V is typically associated with the formation of built-up-edge (BUE). The formation of BUE has a significant drawback on the machined surface integrity and the tool life [25, 26]. Thus, adding more limitations in the aerospace production procedure [27].

Despite, the extensive to optimize separate machining process of both materials, the machining process suffers when it comes to production time, cost, and assembly positional error. Single process drilling of the CFRP and Ti6Al4V materials in-situ, also known as stacked drilling shows considerable benefits to overcome separate drilling issues [1-3, 28, 29]. However, the stack drilling of CFRP and Ti6Al4V materials represents a challenge for the aerospace industry [4]. The optimal machining parameters of each material are conflicting, and consequently, the machining process could come up with undesirable effects. For example, the accumulation of high-temperature titanium chips inside the limited evacuation space (drill flutes), results in CFRP thermal damage, high exit delamination, and chips-tool adhesion.

The experimental investigation of composite/metallic stack drilling showed contrary results, compared to the separate drilling process of each material. The average entry delamination of CFRP was increased from less than 2 mm at CFRP separate drilling to 13 mm at CFRP/Ti6Al4V stack drilling [5]. In addition, the surface roughness during stack drilling is more than double that for the separate drilling of CFRP. These increases of entry delamination and surface roughness were contributed to the effect of titanium adhesion on the drill bit margins. The poor surface roughness of CFRP and Ti6Al4V during stack drilling was confirmed in [30]. The author attributed this reduction of surface quality to the fast tool wear mechanism during stack drilling. Increasing the cutting temperature during the drilling process of Ti6Al4V resulted in a higher adhesion that leads to BUE formation [31, 32]. Consequently, the cutting edge sharpness decreased and the entry delamination increased. Tool wear has been confirmed to be much faster during the stack drilling, as reported in [4, 33].

Conversely, entry delamination showed a clear reduction during the CFRP/Ti6Al4V stack drilling [30]. Moreover, the utilization of titanium plate as a backing material for CFRP would result in a clear reduction of exit delamination. Compared to the separate drilling process of CFRP, the exit delamination was found to be much lower during the stack drilling [30, 33]. The fiber pull-out was completely extinct during the stack drilling process. In addition, stack drilling reduced the surface roughness of the CFRP, while the Ti6Al4V was rougher than separate drilling [33]. The reduction of Ti surface quality was attributed to the abrasive effect of the CFRP chip. The tool life during stack drilling increased three times compared to the separate drilling of titanium material [34]. Compared to HSS, carbide drill showed a proper machining performance with lower flank wear land [28]. This advantage was attributed to the higher hot hardness of the carbide tool.

In addition, the machining parameters such as cutting speed and feed rate showed a direct impact on the flank wear progress. Despite the limited observation of Ti adhesion during the drilling process using PCD, the cutting edge showed severe chipping compared to carbide drill [23].

Several approaches have been implemented to overcome the stack drilling machining difficulties through machining parameters optimization [2, 35, 36], two-step drilling process [3], and the utilization of an advanced lubricant ant tool coating to reduce the chip-tool friction [37]. Advanced machining process such as vibration-assisted drilling (VAD) where the axial feed is superimposed by a harmonic motion [38, 39], can be seen as a promising candidate to attain better machining quality. This is possible due to the significant benefit of changing the chips morphology from continuous to segmented [40-42], and the efficient chip evacuation mechanism [40, 43].

The experimental investigation of Low-frequency vibration assisted drilling (LF-VAD) of CFRP/Ti6Al4V showed promising results compared to the conventional drilling (CD) [38, 44]. The utilization of 1.5 cycle/rev frequency with minimum quantity lubrication (MQL), resulted in a 43% reduction on the cutting temperature with improved surface integrity [44]. Increasing the modulation frequency to 2.5 cycle/rev frequency resulted in a 56% reduction on the cutting temperature with enhanced surface integrity, significant reduction of the entry and exit delamination, and the generation of compressive residual stresses in the machined Ti6Al4V surface, as summarized in Figure 7-1 [38].

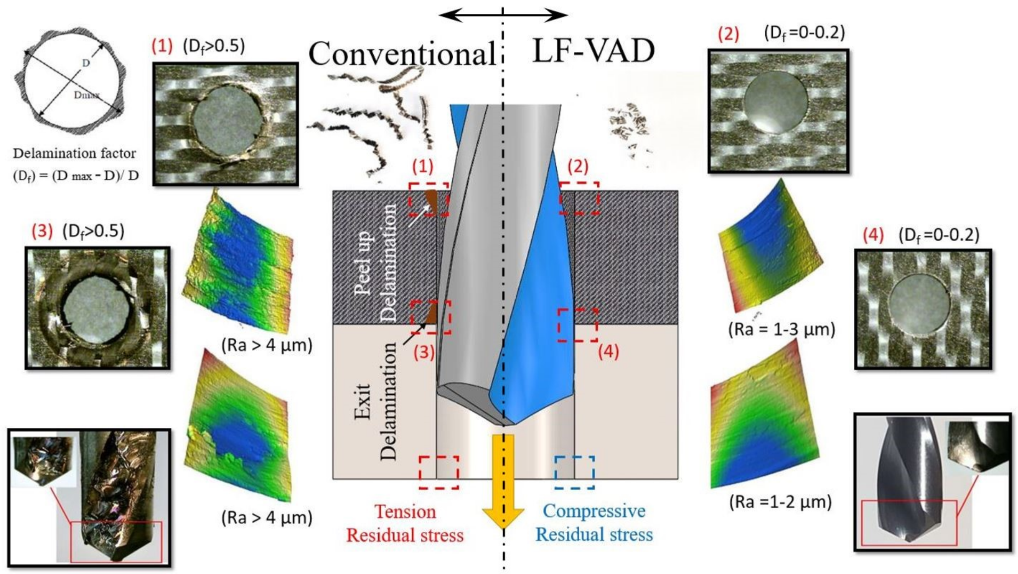


**Figure 7-1:** The effect of LF-VAD and CD on the chip morphology, surface integrity, and drill tool during the drilling process of CFRP/Ti6Al4V stack material [38].

Compared to the conventional drilling (CD), VAD showed a significant enhancement of the CFRP/Ti6Al4V stack drilling process. However, there is a limited understanding of the machining performance and tool wear progress in VAD stack drilling, in spite of its extensive possible impact in the industry. VAD using the ultra-frequency range (39KHz frequency) increased the tool life compared to CD [45]. However, as the cutting speed increased, this effect was reduced. On the other hand, the effect of LF-VAD using 1.5 oscillation/rev with a maximum of 1000 rpm cutting speed showed an apparent reduction on the tool wear as reported in [46, 47]. Despite the significant enhancement of VAD on the tool life, the available literature focused only on the thrust forces, temperature, and wear land. The effect of tool wear progression on the drilled hole quality such as delamination, and geometrical accuracy was not discussed, which represent the key factor in the aerospace industry. Our previous investigation of LF-VAD of CFRP/Ti6Al4V has mainly focused on presenting the effect of a wide range of machining parameters on the cutting forces, temperature, surface integrity, microstructure, and the induced residual stresses [38]. Based on that study, a modulation amplitude in the range of 0.1 mm to 0.25 mm was recommended to achieve proper machining quality. The current study presents the effect of the selected LF-VAD machining parameters on the tool wear mechanism and the associated influence on the machining forces, temperature, and hole quality. The hole quality parameters are presented in terms of geometrical accuracy, entry CFRP delamination, and exit CFRP delamination. In addition, the hole quality is linked to the cutting forces to generate a machining map for industrial application.

## 7.2 Experimental setup

The drilling process was conducted using a five-axis Makino A 88 machining center, as described in Figure 7-2. A special set up was designed to install the MITIS tool holder MITIS tool PG8045B3_HSK-A100_ER40, and hold the FLIR SC8000 HD Series infrared camera. The MITIS tool holder has a fixed 2.5 oscillation/rev modulation frequency, 3500 rpm speed limitation, and an adjustable amplitude of 0.01-0.48 mm. To monitor the cutting temperature, a fixed distance was set between the drilled material and dynamometer to achieve a direct view of the drill tool at the Ti6Al4V exit surface by tilting the thermo-vision infrared camera. The cutting forces were measured using a Kistler four-component dynamometer type 9272 and supported by Kistler Multichannel Charge Amplifier type 5019B.

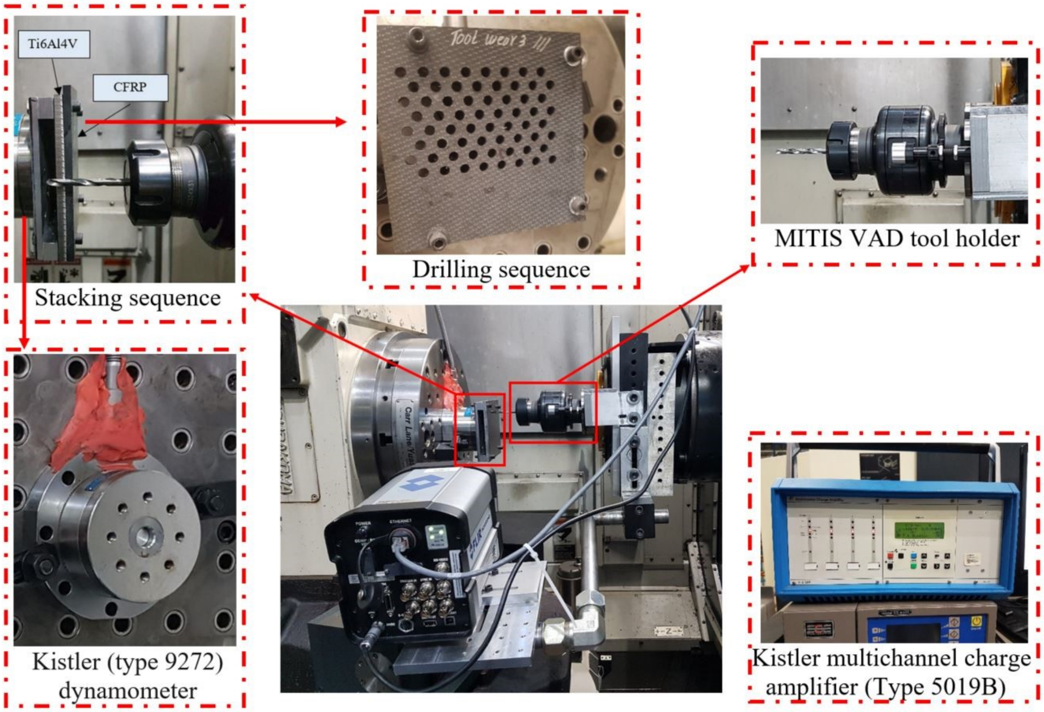


**Figure 7-2:** The experimental setup, tool holder, drilling, and stacking sequence used during the process.

Based on the typically drilled diameter in the aerospace industry, an OSG 6 mm tungsten carbide (WC) twist drill was used for the test matrix. The drill bit has a 118° point angle and a 20° helix angle. The CFRP/Ti6Al4V stacked material specimen has a 120 mm side length and a 12.55 mm thickness (5.8 ± 0.02 mm for CFRP and 6.75 ± 0.02 mm for Ti6Al4V). The CFRP has 42 x L-930(GT700) woven plies with the [[0,90]21]s configuration, and flame retardant modified epoxy prepreg (320° C decomposition temperature), while the Ti6Al4V plate was produced according to grade 5 standard. Machining parameters were selected based on the previous experimental investigation [38], where the test matrix consisted of two levels cutting speeds (37.68 and 56.52 m/min), two levels of feed rates (0.025 and 0.075 mm/rev), and three modulation amplitudes (0.1, 0.16, and 0.25 mm). To ensure a good machining productivity rate, the 37.68 m/min and

0.025 mm/rev combined machining conditions were ignored. The tool wear progress and hole quality study were conducted over a dry drilling process of 50 drilled holes. The flank wear land progress was measured at drilled hole number 5, 10, 20, 30, 40, and 50 using the Winslow engineering tool analyzer model 560. The flank surface was examined using Scanning Electron Microscopy (SEM), and the Energy Dispersion X-ray Spectroscopy (EDS) was used to identify the adhered particles chemical composition. The rounding of the cutting edge was calculated at a normal distance of 500 μm from the cutting edge margin using an Alicona microscope. While the entry and exit CFRP delamination were evaluated using a Keynece Digital Microscope. The hole diameter error was calculated by taking an average of ten points on the top and bottom surfaces for both materials using a Mitutoyo Coordinate Measuring Machine (CMM).

## 7.3 Results and discussion

### 7.3.1 Effect of tool wear on the thrust force

Drilling forces analysis is a fundamental step through which the effect of chip evacuation efficiency and tool wear progress can be predicted. Figure 7-3 shows the measured drilling forces for the investigated drilled holes for $N$= 56.52 m/min at different vibration amplitudes and feed rates. As the drilled holes number increases the cutting forces gradually increases for CD and VAD, which can be attributed to the tool wear progress. For $f$= 0.025 mm/rev, the CD thrust force and cutting torque increase rates become higher after drilled hole number 30. This observation indicates strong evidence of a change in the cutting edge geometry that resulted in high cutting and friction forces. Moreover, the high cutting torque could reflect poor chip evacuation, which has a negative effect on the machined surface integrity, as will be presented later. On the contrary, VAD showed a low thrust force and cutting torque increase rates. Compared to CD, the maximum thrust force and cutting torque showed a 25% and 45% reduction for Am= 0.1 mm, and a 15% and 25% reduction for $A_m$= 0.25 mm, respectively. This reduction can be attributed to the enhanced chip evacuation and the expected low cutting temperature [38, 46, 47], as will be explained in the next section. Consequently, the drill tool material maintained its hardness with a sharp cutting edge geometry at the low cutting temperature. Also, the low reduction percentages of cutting forces for high modulation amplitude can be attributed to the higher impact load [40]. For $f$= 0.075 mm/rev, the CD drilling process was stopped after drill hole number 2, due to the observation of the tool-chip welding process as shown in Figure 7-4 (A). This phenomenon was due to the combined effect of excessive thermal load and poor chip evacuation that resulted in tool-chips welding. In addition, this conclusion was confirmed by the significant increase of the cutting torque by 400 % (from 4 Nm to 16.9 Nm). Comparatively, the drilled holes number increased with the use of VAD. The maximum drilled a number of holes reached was 10 for $A_m$= 0.1 mm, which was doubled for Am= 0.25 mm, before the observation of tool-chips welding process as shown in Figure 7-4 (B, C). Increasing the number of holes drilled with higher amplitude can be attributed to the lower thermal load, small chip radian, and enhanced evacuation efficiency [38, 40, 41, 43].

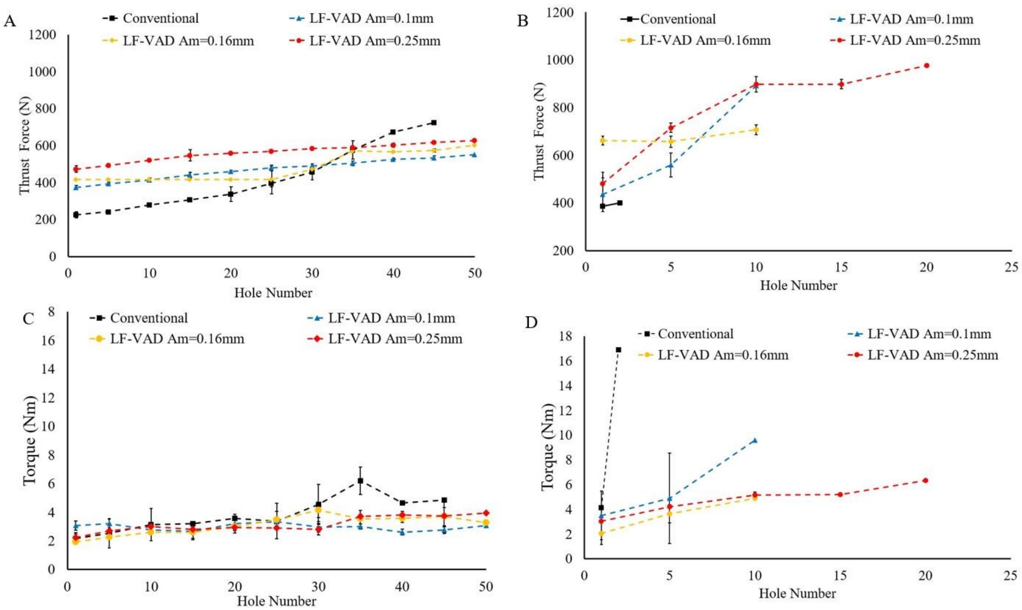


**Figure 7-3:** The effect of tool wear progress on the thrust force and cutting torque at different vibration amplitude for *N*= 56.52 m/min and (A, C) *f*= 0.025 mm/rev, and (B, D) *f*= 0.075 mm/rev.

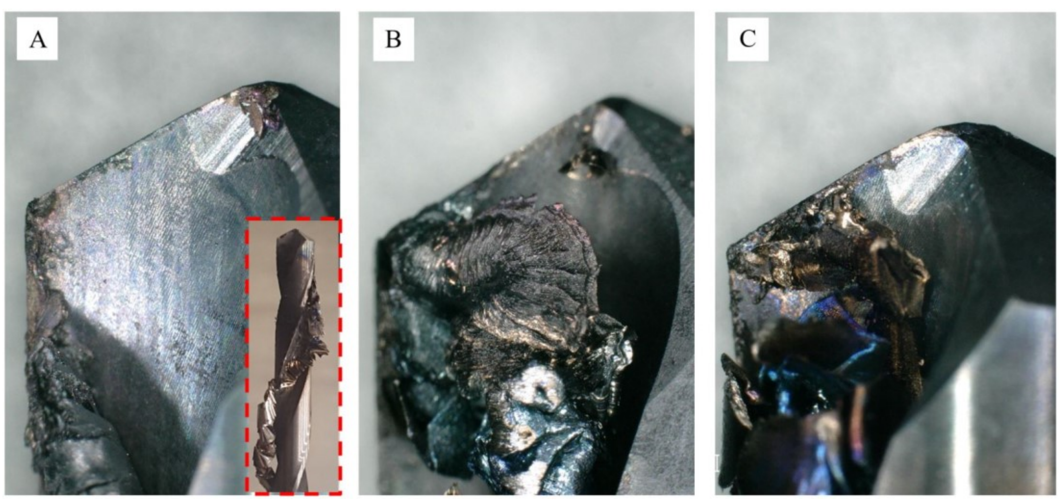


**Figure 7-4:** The effect of VAD amplitude on the tool-chip welding process at *N*=56.52 m/min and *f*=0.075 mm/rev for (A) Conventional, (B) $A_m$ = 0.1mm, and (C) $A_m$ =0.25mm.

Reducing the cutting speed to $N$= 2000 rpm resulted in a relatively low thrust force and cutting torque for both machining techniques. The measured cutting forces for VAD did not show any change over the 50 drilled holes, as shown in Figure 7-5. However, the thrust forces increased with amplitude due to the cyclic tool-workpiece impact [40]. All VAD tests at $A_m$= 0.1 mm, 0.16 mm and 0.25 mm, experienced a negligible increase of the thrust force with a number of holes. However, the test performed at $A_m$ = 0.1 mm was stopped due to the tool-chip welding, which is in agreement with the results reported previously in [38]. The cutting torque in CD increased at a high rate after drilled hole number 20, as shown in Figure 7-5 (B). This increase could indicate poor evacuation efficiency and progressive tool wear, as will be presented in the next section.

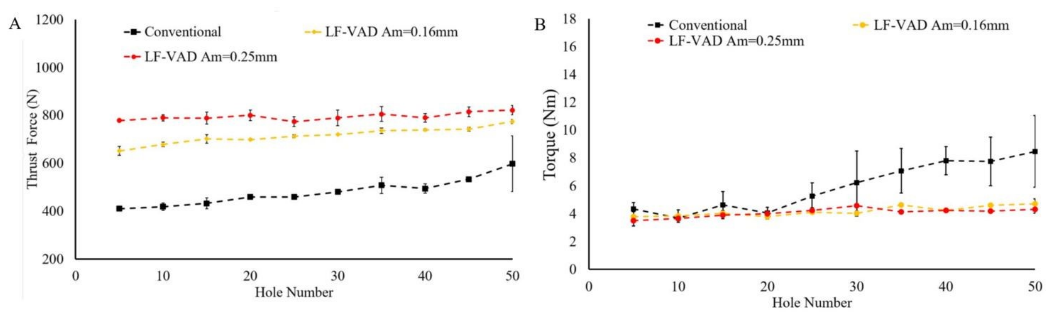


**Figure 7-5:** The effect of tool wear progress on the (A) thrust force and (B) cutting torque, at different vibration amplitude for $N$= 37.68 m/min and $f$= 0.075 mm/rev.

### 7.3.2 Effect of tool wear on the cutting temperature

Figure 7-6 shows the measured tool tip temperature at the exit machined surface for $N$= 56.52 m/min at different machining feed rates and amplitudes. For $f$= 0.025 mm/rev, the utilization of LF-VAD resulted in up to 40% reduction in the thermal load compared to CD. This reduction could be attributed to (a) the significant change of the Ti6Al4V chip morphology from a continuous spiral shape for CD to a segmented one [38, 40], (b) the enhanced chip evacuation efficiency due to the tool axial oscillation mechanism [38, 40, 43], and (c) the cyclic cooling interval during the interrupted cutting process [40]. Moreover, increasing the modulation amplitude for VAD resulted in a lower tool tip temperature. This reduction can be tracked back to the lower duty cycle and the increased cooling cycle [40]. Examining the cutting temperature across the drilled holes for CD, a relative temperature increase was observed after drilled holes number 30. This observation matches the increased cutting forces, as presented in section 7.3.1. Consequently, severe adhesion tool wear mechanism could be expected at this point. For $f$= 0.075 mm/rev, LF-VAD with $A_m$= 0.25 mm resulted in 820 °C cutting temperature after 20 drilled holes, compared to 1070 °C after the second drilled hole with CD technique. The high cutting temperature for both machining techniques resulted in tool-chip welding, which has a negative effect on the machined hole quality, as will be described in the next section. However, the benefit of VAD in reducing the machining thermal load can clearly be noticed even at high cutting speed and feed.

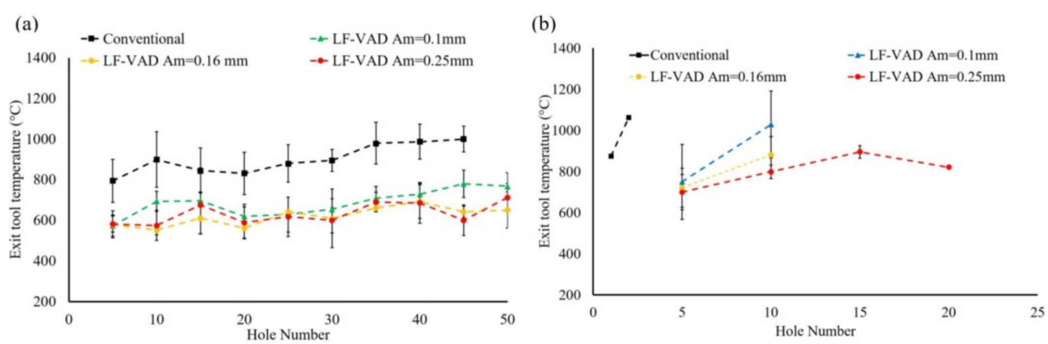


**Figure 7-6:**The effect of tool wear progress on the exit tool temperature at different vibration amplitude for $N$= 56.52 m/min and (a) $f$= 0.025 mm/rev, and (b) $f$= 0.075 mm/rev.

The machining thermal load showed a dropped relatively at the low cutting speed *N*= 37.68 m/min, compared to *N*= 56.52 m/min, as shown in Figure 7-7. This reduction resulted in a successful drilling process of 50 holes for VAD and CD without any observation of the tool-chip welding process. This enhancement could be attributed to the lower chip velocity that prevents the flute chips jamming. Therefore, the problem of the tool-chip welding process was avoided even with the observation of 1180 °C tool tip temperature for CD at drilled hole number 50.

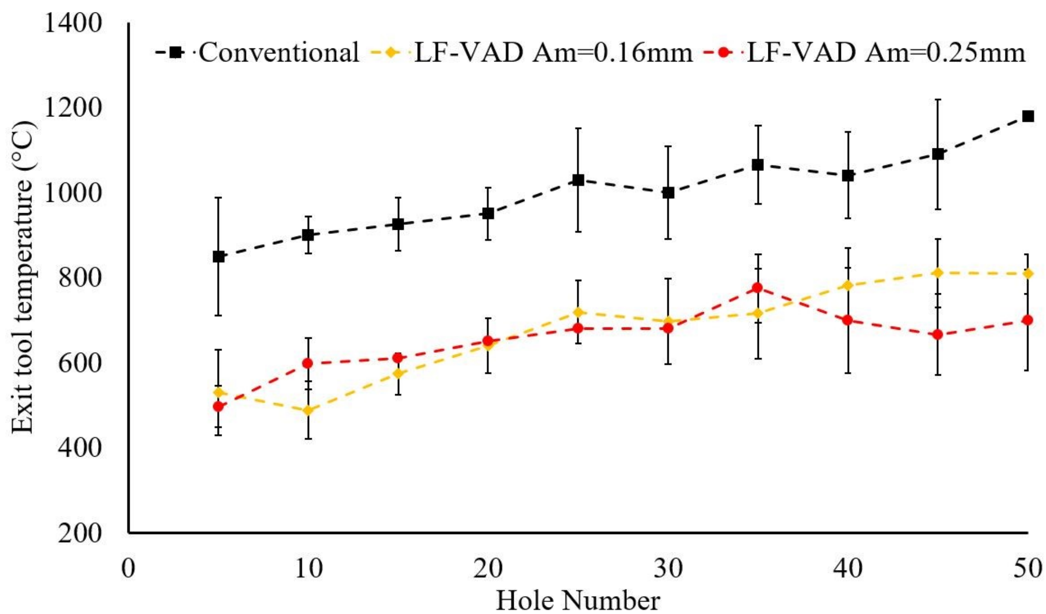


**Figure 7-7:** The effect of tool wear progress on the exit tool temperature at different vibration amplitude for *N*= 37.68 m/min and *f*= 0.075 mm/rev.

### 7.3.3 Tool wear mechanism and progression

The effect of LF-VAD modulation amplitude on the flank wear land was examined using the Winslow tool analyzer. Figure 7-8 shows the flank wear land (VB) progress for *N* = 56.52 m/min at different feed rates and vibration amplitudes. For all machining conditions, LF-VAD resulted in a lower flank wear land compared to CD. The flank wear progress passes through three distinct regions; initial wear, steady wear, and severe wear. The machining process with new cutting edge resulted in concentrated cutting forces over a narrow contact area (small cutting edge radius). Consequently, high stresses are generated and the wear progress will be high known as initial wear region (A). This process increases the tool-workpiece contact area thus reducing the generated cutting stresses on the tool cutting edges. Hence the tool wear progress will be low, also known as steady wear region (B). The continuity of the machining process with a wide tool-workpiece contact area resulted in high mechanical and thermal loads that increase the wear progress extremely, manifested in the severe wear region (C).

For CD at $f = 0.025$ mm/rev, the VB increased at a relatively higher rate compared to LF-VAD to reach 100 µm at the drilled hole number 20 representing the initial wear region. This rate declined afterward until VB reached 117 µm at drilled hole number 30 where the steady wear is located, then increased to 327 µm at the drilled hole number 40, as shown in Figure 7-8 (A). The severe wear region represents the criterion for the drilling process termination, according to ISO 3685 (VB= 300 µm) [48]. It is also noted, that transformation from steady to severe wear was recorded at the drilled hole number 30, where high mechanical (thrust force and cutting torque) and thermal loads (cutting temperature) were experienced, as described in section 7.3.1 and 7.3.2. The initial wear region for VAD took place until hole number 10 only, which is 10 holes earlier compared to CD (20 holes). This can be attributed to the excessive impact load associated with VAD process [40]. However, the maximum VB for VAD was 85 µm at drilled hole number 50, which is 75% lower than CD due to the low thermal load and proper chip evacuation.

Increasing the machining feed to 0.075 mm/rev, resulted in a severe limitation on the maximum number of drilled holes for all machining conditions, as shown in Figure 7-8

(B). This limitation was due to the observation of the tool-chip welding problem that contributed to the high cutting temperature and poor chip evacuation efficiency, as shown in Figure 7-4. For CD, the burned and welded Ti chip was observed after the second drilled hole. Conversely, increasing the vibration amplitude from 0.1 mm to 0.25 mm resulted in an increase in the total drilled holes number by 100%. This enhancement was mainly due to the lower cutting temperature and proper chip evacuation [38].

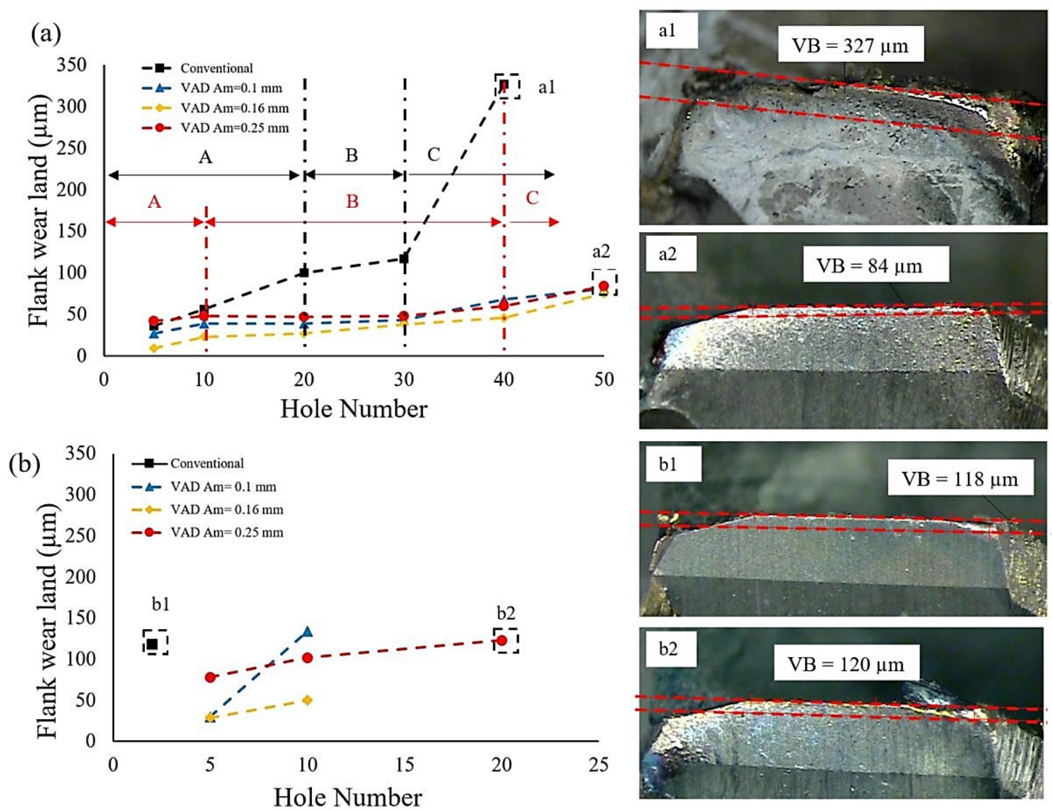


**Figure 7-8:** The effect of vibration amplitude on the tool flank land wear for *N*= 56.52 m/min at (a) *f*= 0.025 mm/rev, and (b) *f*= 0.075 mm/rev.

Figure 7-9 shows the effect of CD and VAD on the flank wear land at *N*= 37.68 m/min and *f*= 0.075 mm/rev. Based on the measured flank wear land, VAD with $A_m$= 0.25 reduced the wear progress by 45% without any observation of the tool-chip welding, as shown in Figure 7-10**.** Low thermal load and high chip evacuation efficiency were of the main factors controlling this result.

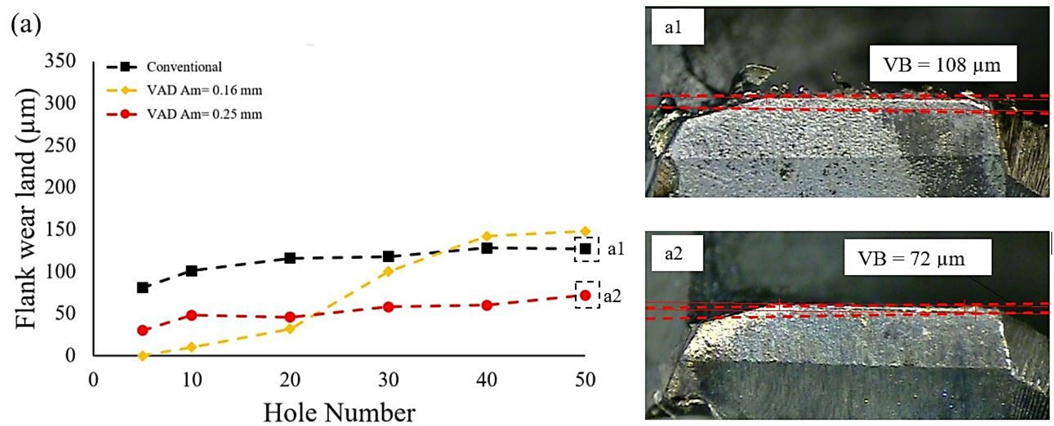


**Figure 7-9:** The effect of vibration amplitude on the tool flank land wear for $N$ = 37.68 m/min and $f$=0.075 mm/rev.

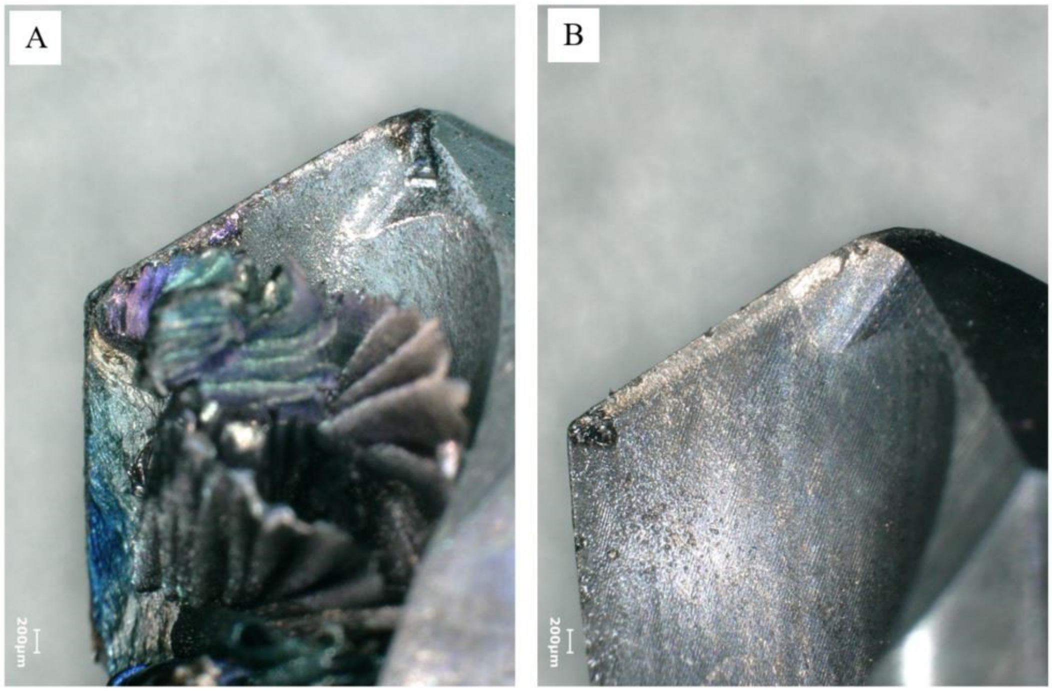


**Figure 7-10:** The effect of VAD on the tool-chip welding process at $N$=37.68 m/min and $f$=0.075 mm/rev for (A) Conventional, (B) $A_m$ =0.25mm.

To understand the different tool wear mechanisms of the tested machining conditions, Figure 7-11 shows the scanning electron microscopy (SEM) examination of CD and VAD at $A_m$= 0.25 mm at the maximum drilled hole number (40 for CD and 50 for VAD). Strong evidence of abrasion and adhesion tool wear mechanism for VAD techniques are shown in Figure 7-11 (A). Scratches on the flank face resulted from the abrasion wear mechanism, mainly caused by the tool relative motion with respect to the hard carbon fibers, broken fibers, and the powder chips particles [14, 15] during the drilling process of CFRP layer. The adhesion wear mechanism of Ti was confirmed using the Energy-dispersive X-ray spectroscopy (EDS) analysis of the selected points in Figure 7-11, as shown in Table 7-1. In the case of CD, a massive amount of adhered Ti particles with BUE formation was observed, as shown in Figure 7-11 (B). The formation of BUE has a severe drawback on the drilled hole quality and the breakage of the BUE fragments would result in tool chipping and fracture. The severe tool chipping and fracture increased the cutting edge radius (CER) to 30 µm compared to 20 µm for VAD after 50 drilled hole, as shown in Figure 7-12. Based on the observation of a large and continuous adhesion layer (Figure 7-11, (2B)) and the EDS analysis of the selected points (3-5), the adhesion wear was confirmed as the dominant wear mechanism for CD. This mechanism was developed as a result of the higher thermal load, poor cooling mechanism, continuous tool-workpiece contact, and the high affinity of Ti to chemically react with the tool material [31, 32, 49, 50].

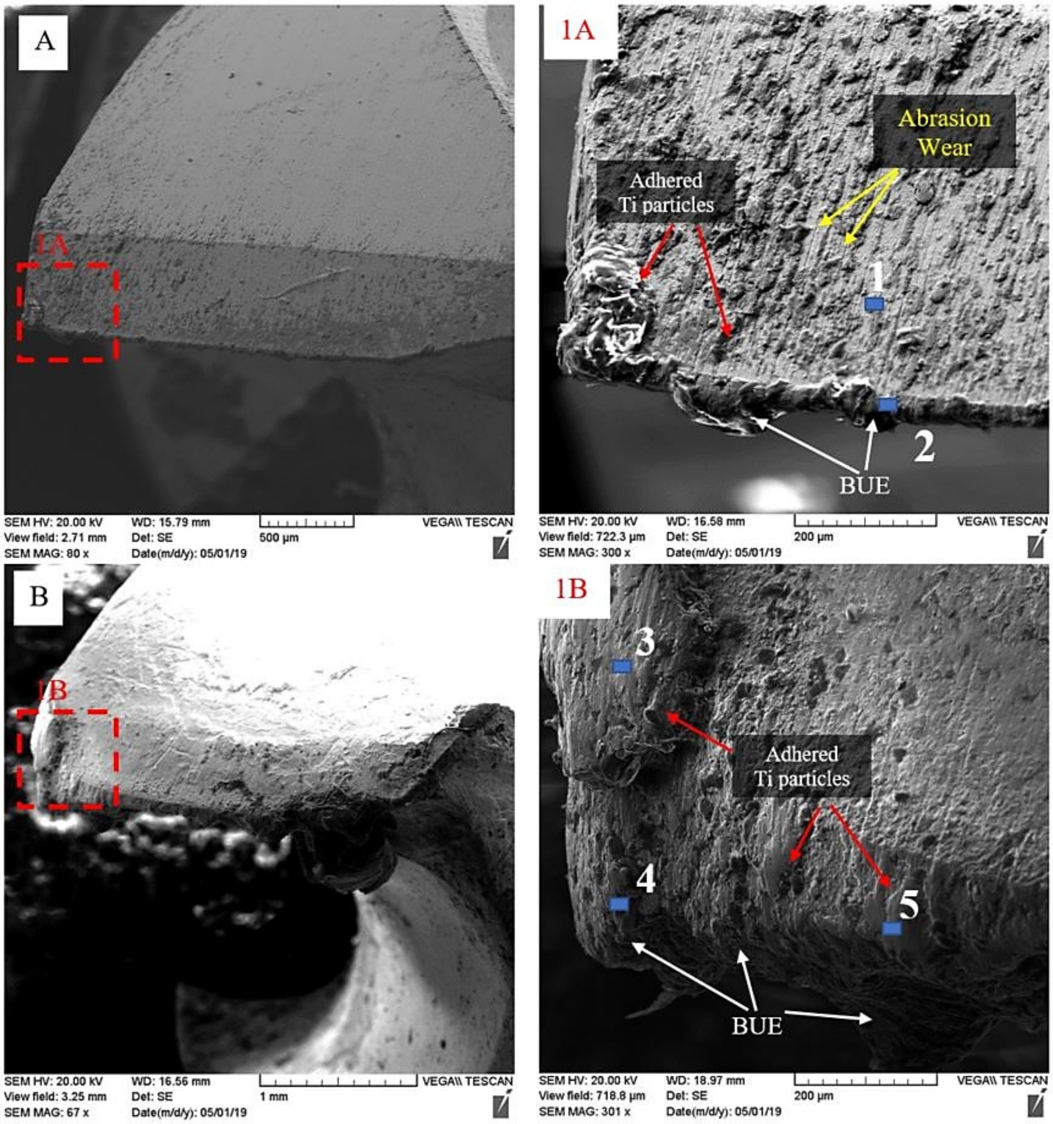


**Figure 7-11:** The SEM flank surface examination for (A) VAD at $A_m$ = 0.25 mm, and (B) conventional drilling at *N*= 56.52 m/min and *f*=0.025 mm/rev.

**Table 7-1:** EDS Element composition analysis for the selected points in **Figure 7-11**.

| | Elements by weight % | | | | | | |
|---|---|---|---|---|---|---|---|
| | C | O | Al | Ti | V | W | Total |
| **Spectrum 1** | 45.66 | 28.89 | 1.29 | 21.8 | 0.99 | 1.09 | 100.0 |
| **Spectrum 2** | 13.68 | 26.77 | 4.32 | 50.22 | 1.68 | 3.01 | 100.0 |
| **Spectrum 3** | 8.91 | 42.9 | 3.6 | 43.07 | 1.5 | 0.1 | 100.0 |
| **Spectrum 4** | 7.42 | 40.29 | 3.57 | 47.02 | 1.53 | 0.19 | 100.0 |
| **Spectrum 5** | 10.64 | 44.7 | 4 | 38.47 | 1.59 | 0.59 | 100.0 |

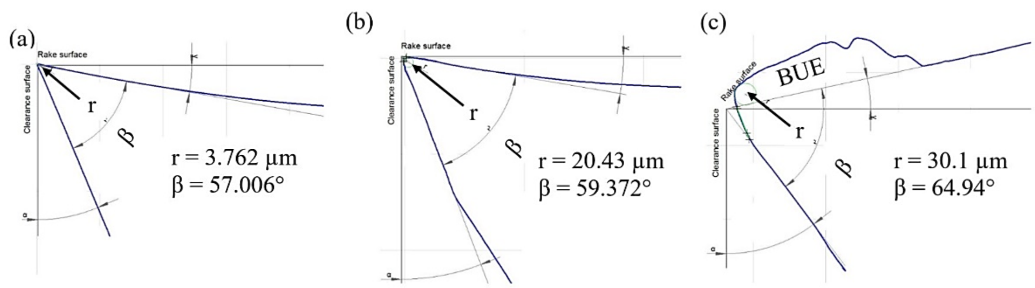


**Figure 7-12:** The effect of machining technique on the cutting edge rounding at *N*= 56.52 m/min and *f*= 0.025 mm/rev for (a) New tool, (b) VAD $A_m$= 0.25 mm, and (c) CD.

Figure 7-13 shows the SEM images of the flank surface at *N*= 37.68 m/min and *f*= 0.075 mm/rev for VAD ($A_m$= 0.25 mm) and CD. Machining process with low cutting speed reduced the adhered Ti particles for both machining technique. For VAD, abrasion and adhesion wear mechanism could obviously be identified along the flank surface. On the other hand, for CD the flank surface was covered with a continuous Ti layer with BUE formation. This could be attributed to the high thermal load during the conventional drilling process. Moreover, the CER for VAD and CD was reduced from 20 µm and 30 µm at *N*=56.52 m/min to 16.89 µm and 19.34 µm, respectively, at *N*=37.68 m/min as shown in Figure 7-14.

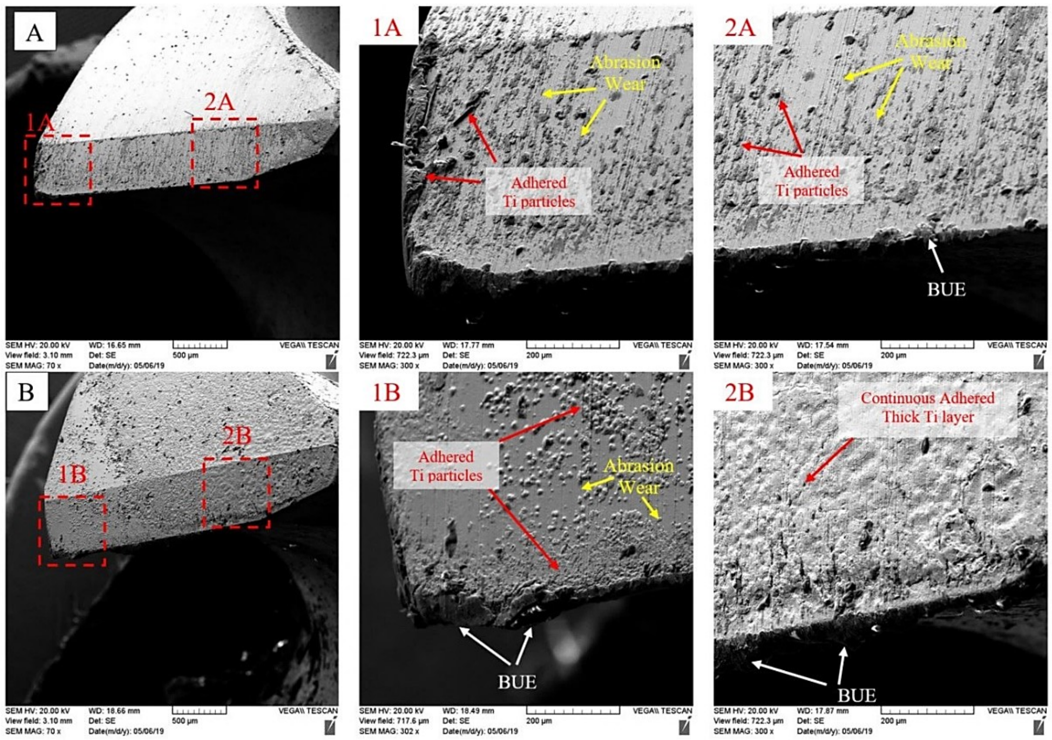


**Figure 7-13:** The SEM flank surface examination for (A) VAD at $A_m$ = 0.25 mm, and (B) conventional drilling at *N*= 37.68 m/min and *f*=0.075 mm/rev.

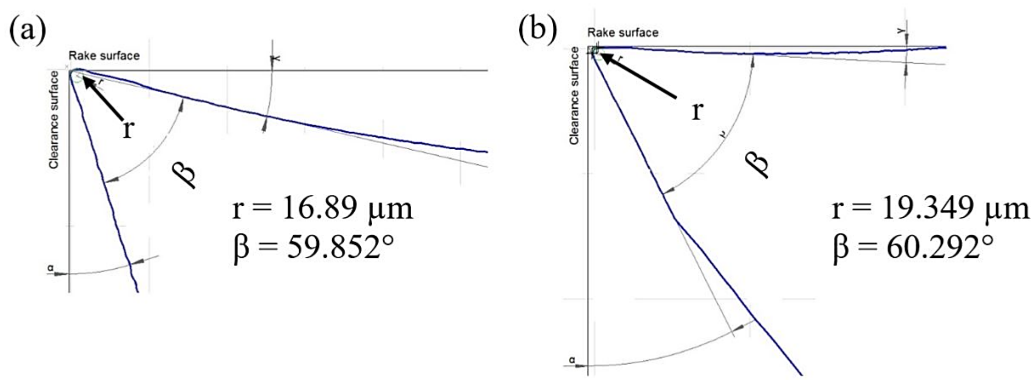


**Figure 7-14:** The effect of machining technique on the cutting edge rounding at *N*= 37.68 m/min and *f*= 0.075 mm/rev for (a) VAD $A_m$= 0.25 mm, and (b) CD.

### 7.3.4 Effect of tool wear on the drilled hole quality

#### *7.3.4.1 CFRP entry delamination*

The delamination factor (φd) for all machined parameters was calculated based on equation (7.1):

$$\varphi_d = \frac{D_{actual} - D_{nominal}}{D_{nominal}} \qquad (7.1)$$

where D actual is the diameter of a circle including the circumscribing delamination, while D nominal represents the nominal hole diameter.

For all machining conditions, VAD resulted in a lower entry delamination factor compared to CD, as shown in Figure 7-15 and Figure 7-16. Based on the defined aerospace limitation (φd ≤ 0.5) [39, 51], the delamination factor in CD was acceptable until drilled hole number 20 for *N* = 37.68 m/min, which is correlated to 460 N thrust force, as shown in Figure 7-15 (b). Increasing the cutting speed to 56.52 m/min, reducing the entry delamination for *f*= 0.025 mm/rev by an average of 50%, which remained within the acceptable limit for all tool wear levels. The maximum entry delamination value (φd =0.26) for all VAD tests was considerably less than the allowable limit. The effect of VAD compared to CD on enhancing the entry delamination was most evident at the final drilled hole, as shown in Figure 7-17.

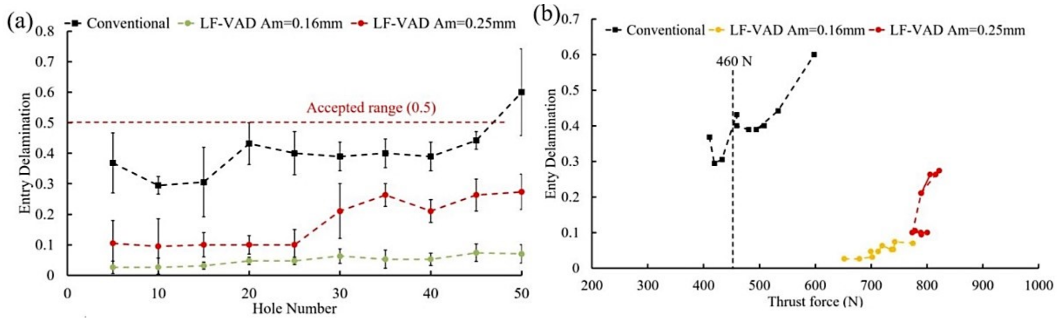


**Figure 7-15:** The effect of tool wear progress on the (a) entry delamination and (b) correlated thrust force, at *N*= 37.68 m/min and *f*= 0.075 mm/rev.

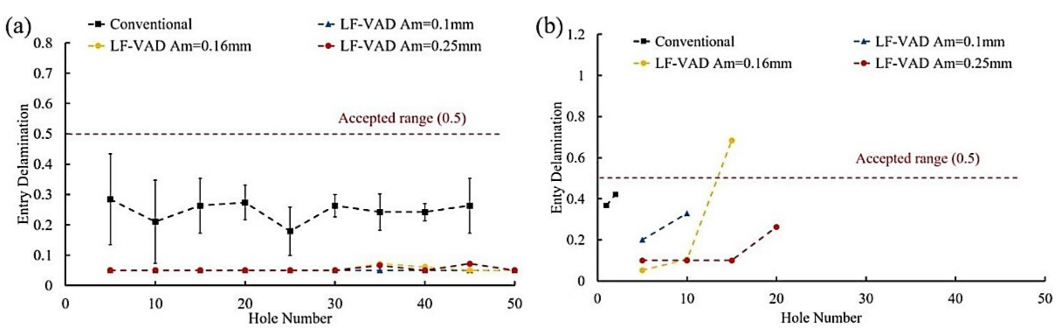


**Figure 7-16:** The effect of tool wear progress on the entry delamination at *N*= 56.52 m/min for (a) *f*=0.025 mm/rev and (b) *f*= 0.075 mm/rev.

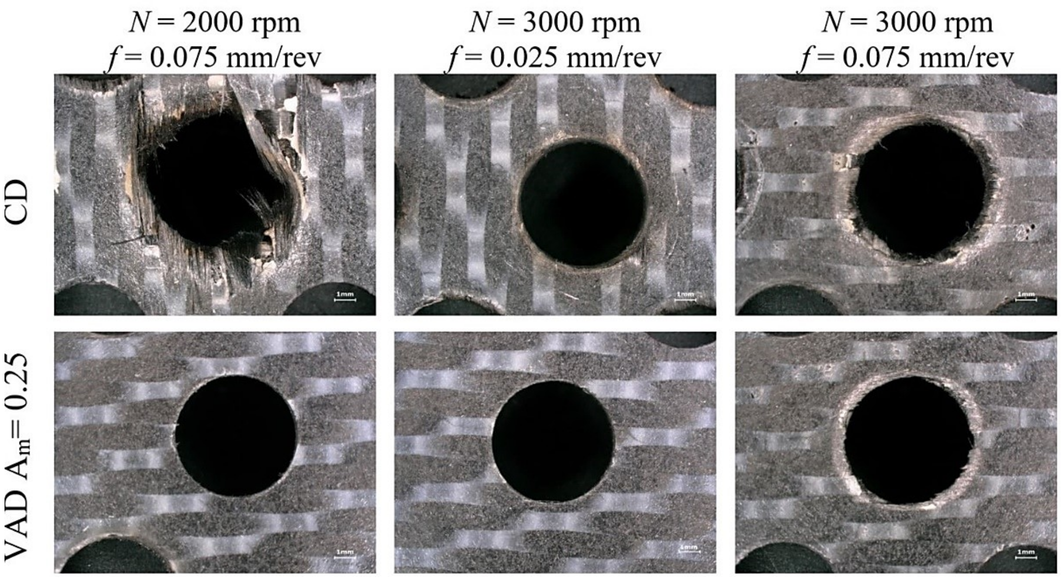


**Figure 7-17:** The effect of machining technique on the entry delamination the end of each machining parameters.

*7.3.4.2 CFRP exit delamination*

Figure 7-18 (a) and (b) shows the change in exit delamination with the increase of the number of holes and the thrust force, respectively in CD and VAD. For *N*= 37.68 m/min, CD showed acceptable delamination until the drilled hole number 20, which is corresponds to a 450 N thrust force. This interval represents the initial wear region. Increasing the flank wear resulted in a higher thermal and mechanical load, which formed larger exit delamination at the severe wear region (starting from hole number 30).

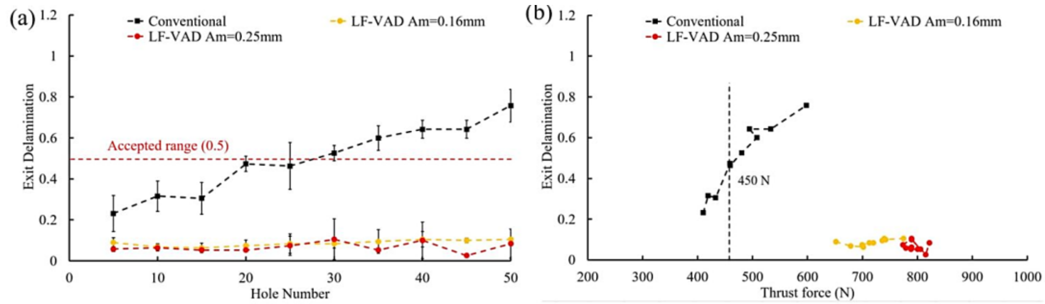


**Figure 7-18:** The effect of tool wear progress on the (a) exit delamination and (b) correlated thrust force at *N*= 37.68 m/min and *f*= 0.075 mm/rev.

For *N* = 56.52 m/min, the CD resulted in excessive exit delamination for all feed rates, as shown in Figure 7-19 and Figure 7-20. On the other hand, VAD showed acceptable delamination for all feed rates, except the final drilled hole at *f*= 0.075 mm/rev where tool-chip welding was observed.

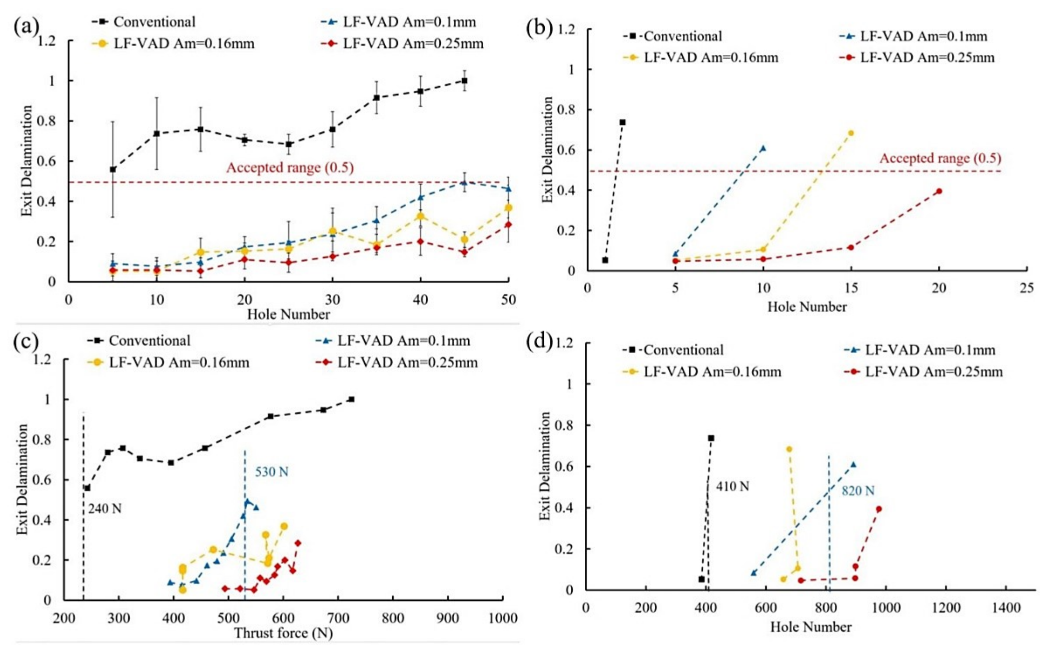


**Figure 7-19:** The effect of tool wear progress on the exit delamination and correlated thrust force at *N*= 56.52 m/min for (a, c) *f*= 0.025 mm/rev and (b, d) *f*= 0.075 mm/rev.

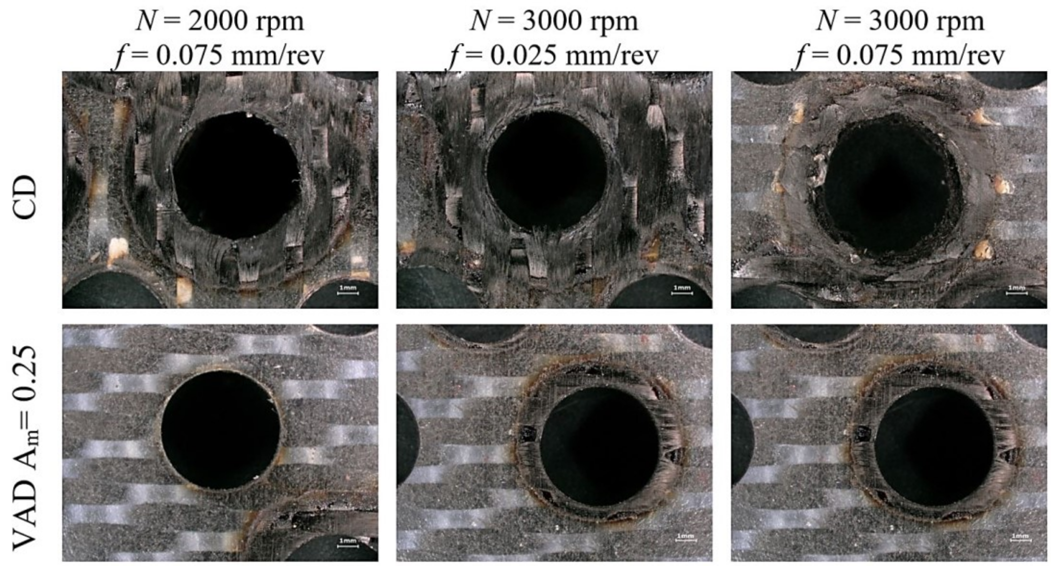


**Figure 7-20:** The effect of machining technique on the exit delamination the end of each machining parameters.

### *7.3.4.3 Hole size accuracy*

Based on the defined hole size error for aerospace limitation (-0.7 % to 0.4%) [38, 39], CD exceeds the acceptable CFRP and Ti6Al4V hole size at $N$ = 37.68 m/min, as shown in Figure 7-21. The excessive CFRP error for CD could be attributed to the poor evacuation of the continuous Ti6Al4V chip at high temperature. Additionally, the relatively higher hole size error in CFRP compared to Ti6Al4V can be attributed to the rubbing of the CFRP hole walls by the continuous Ti chips transferred to the CFRP layer in CD. On the other hand, VAD showed an acceptable hole size over the investigated drilled holes. Increasing the cutting speed to 56.52 m/min, resulted in an acceptable CFRP hole size for VAD, while the Ti6Al4V exceeded the proper range after hole number 30, as shown in Figure 7-22, as a result of tool wear. For $f$= 0.075 mm/rev, the VAD hole size was acceptable until the formation of the tool-chip welding process.

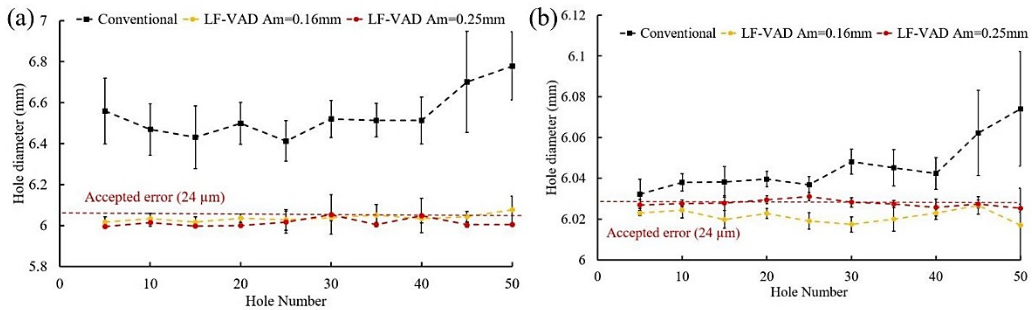


**Figure 7-21:** The effect of machining technique and wear progress on the hole accuracy at *N*=37.68 m/min for (a) CFRP, and (b) Ti6Al4V.

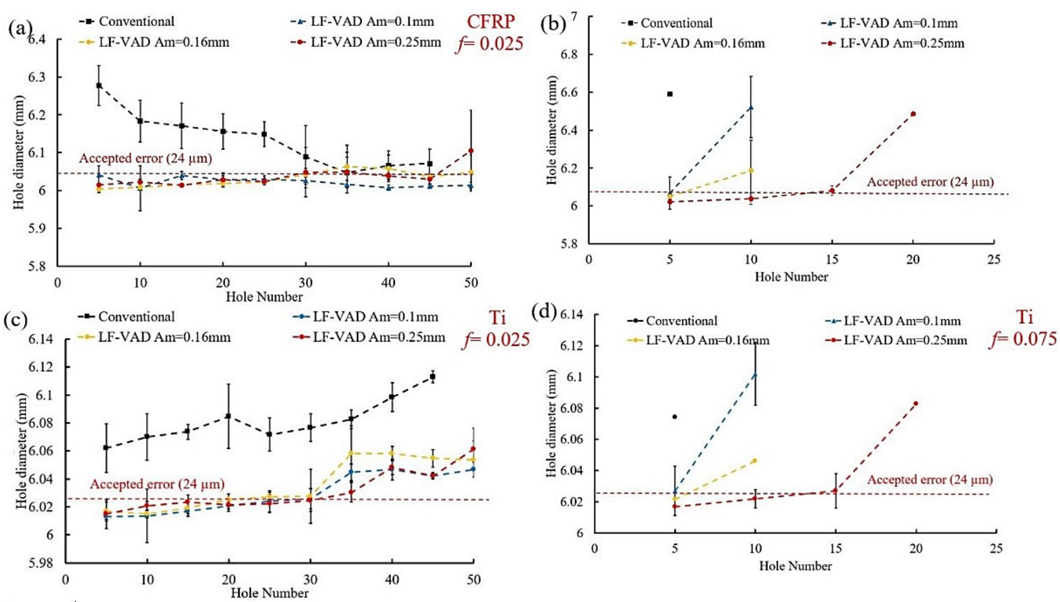


**Figure 7-22:** The effect of machining technique and wear progress on the hole accuracy at *N*=56.62 m/min and different feeds for (a, b) CFRP, and (c, d) Ti6Al4V.

## Conclusion

In this research, tool wear behavior during low-frequency vibration assisted drilling has been evaluated. The experimental investigation examined the drilling of 50 holes under various machining conditions. Three modulation amplitudes were selected based on a previous wide range study. The cutting edge examination using electron microscopy confirmed abrasion and adhesion tool wear mechanism for VAD, while the adhesion mechanism was dominant for CD. Low flank wear land, cutting edge rounding, and relatively optimum hole quality was observed at 37.68 m/min cutting speed and 0.075 mm/rev feed. Based on the experimental results, the main observations are:

- As the drilled hole number increased the cutting torque and thrust increased for both machining techniques. However, VAD resulted in up to 25% and 45 % reduction in the thrust force and cutting torque, respectively.
- For $N$= 56.52 m/min cutting speed and 0.075 feed, increasing the modulation amplitude hindered the tool-chip welding.
- LF-VAD showed a significant reduction in the machining thermal load. The exit cutting temperature was reduced by 40 %, compared to the CD.
- Up to 75% reduction on the flank wear land was achieved by VAD with high modulation amplitude. Moreover, the tool surface profile examination showed a low cutting edge roundness (CER) compared to the conventional machining process.
- Vibration-assisted drilling showed an acceptable entry and exit delamination for all the investigated machining parameters.
- The effect of tool wear progress was significant for CD at low cutting speed, while the high thermal load and poor evacuation efficiency resulted in un-acceptable delamination at the high cutting speed.
- A significant enhancement of the CFRP and Ti6Al4V geometrical accuracy has been achieved by VAD, compared to CD.

# References

[1] M. Ramulu, T. Branson, and D. Kim, "A study on the drilling of composite and titanium stacks," *Composite Structures,* vol. 54, pp. 67-77, 10// 2001.

[2] D. Kim and M. Ramulu, "Study on the drilling of titanium/graphite hybrid composites," *Journal of Engineering Materials and Technology,* vol. 129, pp. 390-396, 2007.

[3] E. Brinksmeier and R. Janssen, "Drilling of multi-layer composite materials consisting of carbon fiber reinforced plastics (CFRP), titanium and aluminum alloys," *CIRP Annals-Manufacturing Technology,* vol. 51, pp. 87-90, 2002.

[4] J. Xu, A. Mkaddem, and M. El Mansori, "Recent advances in drilling hybrid FRP/Ti composite: a state-of-the-art review," *Composite Structures,* vol. 135, pp. 316-338, 2016.

[5] K.-H. Park, A. Beal, P. Kwon, and J. Lantrip, "A comparative study of carbide tools in drilling of CFRP and CFRP-Ti stacks," *Journal of Manufacturing Science and Engineering,* vol. 136, p. 014501, 2014.

[6] E. Persson, I. Eriksson, and L. Zackrisson, "Effects of hole machining defects on strength and fatigue life of composite laminates," *Composites Part A: Applied Science and Manufacturing,* vol. 28, pp. 141-151, 1997/01/01/ 1997.

[7] W.-C. Chen, "Some experimental investigations in the drilling of carbon fiber-reinforced plastic (CFRP) composite laminates," *International Journal of Machine Tools and Manufacture,* vol. 37, pp. 1097-1108, 1997.

[8] V. Gaitonde, S. Karnik, J. C. Rubio, A. E. Correia, A. Abrao, and J. P. Davim, "Analysis of parametric influence on delamination in high-speed drilling of carbon fiber reinforced plastic composites," *Journal of materials processing technology,* vol. 203, pp. 431-438, 2008.

[9] L. Romoli and G. Dini, "Experimental study on the influence of drill wear in CFRP drilling processes," in *ICME 08*, 2008.

[10] D. Che, I. Saxena, P. Han, P. Guo, and K. F. Ehmann, "Machining of carbon fiber reinforced plastics/polymers: a literature review," *Journal of Manufacturing Science and Engineering,* vol. 136, p. 034001, 2014.

[11] D. Liu, Y. Tang, and W. Cong, "A review of mechanical drilling for composite laminates," *Composite Structures,* vol. 94, pp. 1265-1279, 2012.

[12] S. Malhotra, "Some studies on drilling of fibrous composites," *Journal of Materials Processing Technology,* vol. 24, pp. 291-300, 1990.

[13] S. Lin and I. Chen, "Drilling carbon fiber-reinforced composite material at high speed," *Wear,* vol. 194, pp. 156-162, 1996.

[14] S. Rawat and H. Attia, "Wear mechanisms and tool life management of WC–Co drills during dry high speed drilling of woven carbon fibre composites," *Wear,* vol. 267, pp. 1022-1030, 2009.

[15] R. Teti, "Machining of composite materials," *CIRP Annals-Manufacturing Technology,* vol. 51, pp. 611-634, 2002.

[16] M. Masuda, Y. Kuroshima, and Y. Chujo, "Failure of tungsten carbide-cobalt alloy tools in machining of carbon materials," *Wear,* vol. 169, pp. 135-140, 1993.

[17] J. Larsen-Basse and E. Koyanagi, "Abrasion of WC-Co alloys by quartz," *Journal of lubrication technology,* vol. 101, pp. 208-211, 1979.

[18] J. Larsen-Basse, "Abrasion Mechanisms--Delamination to Machining," *Fundamentals of Tribology,* pp. 679-689, 1978.

[19] D. Dornfeld, J. Kim, H. Dechow, J. Hewson, and L. Chen, "Drilling burr formation in titanium alloy, Ti-6AI-4V," *CIRP Annals-Manufacturing Technology,* vol. 48, pp. 73-76, 1999.

[20] P. Zhang, N. Churi, Z. J. Pei, and C. Treadwell, "Mechanical drilling processes for titanium alloys: a literature review," *Machining Science and Technology,* vol. 12, pp. 417-444, 2008.

[21] J. L. Cantero, M. M. Tardío, J. A. Canteli, M. Marcos, and M. H. Miguélez, "Dry drilling of alloy Ti–6Al–4V," *International Journal of Machine Tools and Manufacture,* vol. 45, pp. 1246-1255, 2005/09/01/ 2005.

[22] J. Pujana, A. Rivero, A. Celaya, and L. L. de Lacalle, "Analysis of ultrasonic-assisted drilling of Ti6Al4V," *International Journal of Machine Tools and Manufacture,* vol. 49, pp. 500-508, 2009.

[23] K.-H. Park, A. Beal, P. Kwon, and J. Lantrip, "Tool wear in drilling of composite/titanium stacks using carbide and polycrystalline diamond tools," *Wear,* vol. 271, pp. 2826-2835, 2011.

[24] S. Sharif and E. A. Rahim, "Performance of coated- and uncoated-carbide tools when drilling titanium alloy—Ti–6Al4V," *Journal of Materials Processing Technology,* vol. 185, pp. 72-76, 4/30/ 2007.

[25] J. I. Hughes, A. R. C. Sharman, and K. Ridgway, "The effect of tool edge preparation on tool life and workpiece surface integrity," *Proceedings of the Institution of Mechanical Engineers, Part B: Journal of Engineering Manufacture,* vol. 218, pp. 1113-1123, 2004.

[26] D. A. Stephenson and J. S. Agapiou, *Metal cutting theory and practice*: CRC press, 2016.

[27] H. Schulz and A. Emrich, "Limitations of Drilling in Difficult-to-Machine Materials such as Titanium TiA16V4, 1998," *Production Engineering,* vol. 5, p. 1, 1998.

[28] D. Kim and M. Ramulu, "Drilling process optimization for graphite/bismaleimide–titanium alloy stacks," *Composite Structures,* vol. 63, pp. 101-114, 2004/01/01/ 2004.

[29] V. Krishnaraj, R. Zitoune, and F. Collombet, "Comprehensive review on drilling of Multimaterial stacks," *Journal of Machining and Forming Technologies,* vol. 2, pp. 1-32, 2010.

[30] O. Isbilir and E. Ghassemieh, "Comparative study of tool life and hole quality in drilling of CFRP/titanium stack using coated carbide drill," *Machining Science and Technology,* vol. 17, pp. 380-409, 2013.

[31] R. Li, P. Hegde, and A. J. Shih, "High-throughput drilling of titanium alloys," *International Journal of Machine Tools and Manufacture,* vol. 47, pp. 63-74, 2007.

[32] E. Rahim and S. Sharif, "Tool failure modes and wear mechanism of coated carbide tools when drilling Ti-6Al-4V," *International Journal of Precision Technology,* vol. 1, pp. 30-39, 2007.

[33] E. Ghassemieh, "Performance and wear of coated carbide drill in machining of carbon fibre reinforced composite/titanium stack," *International Journal of Materials and Product Technology,* vol. 43, pp. 165-183, 2012.

[34] X. Wang, P. Y. Kwon, C. Sturtevant, and J. Lantrip, "Comparative tool wear study based on drilling experiments on CFRP/Ti stack and its individual layers," *Wear,* vol. 317, pp. 265-276, 2014.

[35] J. Xu and M. El Mansori, "Experimental study on drilling mechanisms and strategies of hybrid CFRP/Ti stacks," *Composite Structures,* vol. 157, pp. 461-482, 12/1/ 2016.

[36] D. Kim, C. Sturtevant, and M. Ramulu, "Usage of PCD tool in drilling of titanium/graphite hybrid composite laminate," *International Journal of Machining and Machinability of Materials,* vol. 13, pp. 276-288, 2013.

[37] N. Guibert, "Etude et modélisation de l'influence des phénomènes de coupe sur les performances du forage vibratoire," Université Joseph-Fourier-Grenoble I, 2008.

[38] R. Hussein, A. Sadek, M. A. Elbestawi, and M. H. Attia, "Low-frequency vibration-assisted drilling of hybrid CFRP/Ti6Al4V stacked material," *The International Journal of Advanced Manufacturing Technology,* vol. 98, pp. 2801-2817, October 01 2018.

[39] A. Sadek, "Vibration Assisted Drilling of Multidirectional Fiber Reinforced Polymer Laminates," Ph.D. Thesis, McGill University Libraries, 2014.

[40] R. Hussein, A. Sadek, M. A. Elbestawi, and M. H. Attia, "Surface and microstructure characterization of low-frequency vibration-assisted drilling of Ti6Al4V," *The International Journal of Advanced Manufacturing Technology,* vol. 103, pp. 1443-1457, April 05 2019.

[41] O. Pecat and I. Meyer, "Low frequency vibration assisted drilling of aluminium alloys," in *Advanced Materials Research*, 2013, pp. 131-138.

[42] Z. Deyuan and W. Lijiang, "Investigation of chip in vibration drilling," *International Journal of Machine Tools and Manufacture,* vol. 38, pp. 165-176, 1998.

[43] E. Brinksmeier, O. Pecat, and R. Rentsch, "Quantitative analysis of chip extraction in drilling of Ti 6 Al 4 V," *CIRP Annals-Manufacturing Technology,* vol. 64, pp. 93-96, 2015.

[44] O. Pecat and E. Brinksmeier, "Low damage drilling of CFRP/titanium compound materials for fastening," *Procedia CIRP,* vol. 13, pp. 1-7, 2014.

[45] A. N. Dahnel, H. Ascroft, and S. Barnes, "The Effect of Varying Cutting Speeds on Tool Wear During Conventional and Ultrasonic Assisted Drilling (UAD) of Carbon Fibre Composite (CFC) and Titanium Alloy Stacks," *Procedia CIRP,* vol. 46, pp. 420-423, // 2016.

[46] O. Pecat and E. Brinksmeier, "Tool wear analyses in low frequency vibration assisted drilling of CFRP/Ti6Al4V stack material," *Procedia CIRP,* vol. 14, pp. 142-147, 2014.

[47] C. Li, J. Xu, M. Chen, Q. An, M. El Mansori, and F. Ren, "Tool wear processes in low frequency vibration assisted drilling of CFRP/Ti6Al4V stacks with forced air-cooling," *Wear,* vol. 426, pp. 1616-1623, 2019.

[48] I. Standard, "3685," *Tool-life Testing with Single Point Turning Tools,* 1993.

[49] D. Kim, A. Beal, and P. Kwon, "Effect of tool wear on hole quality in drilling of carbon fiber reinforced plastic–titanium alloy stacks using tungsten carbide and polycrystalline diamond tools," *Journal of Manufacturing Science and Engineering,* vol. 138, p. 031006, 2016.

[50] P. Dearnley and A. Grearson, "Evaluation of principal wear mechanisms of cemented carbides and ceramics used for machining titanium alloy IMI 318," *Materials Science and Technology,* vol. 2, pp. 47-58, 1986.

[51] R. Hussein, A. Sadek, M. A. Elbestawi, and M. H. Attia, "Chip Morphology and Delamination Characterization for Vibration-Assisted Drilling of Carbon Fiber-Reinforced Polymer," *Journal of Manufacturing and Materials Processing,* vol. 3, p. 23, 2019.

# Chapter 8

## Summary and Conclusions

Minimization of the total aircraft weight is crucial to the aerospace industry to assure performance enhancement with low environmental impact. However, efficiency, high reliability, and superior quality have to be maintained. Consequently, lightweight materials such as carbon fiber-reinforced polymers (CFRP) and titanium alloys are widely used in the aerospace industry. Superior physical and mechanical characteristics such as high strength to weight ratio, low coefficient of thermal expansion, fatigue resistance and corrosion/erosion resistance, explain their widespread utilization. Moreover, the hybrid structure of CFRP/ Ti coupling (CFRP/Ti, CFRP/Ti/CFRP, and Ti/CFRP/Ti) has been identified as the typical selection in the new generation of aircraft.

The great benefits of mechanical fastening such as high reliability and maintainability resulted into making the drilling process of these materials separately or in a stacking form necessary prior to the assembly process. Drilling of CFRP is typically associated with severe surface integrity defects such as entry and exit delamination damage. This damage resulted in as much as 60 % rejection of the total CFRP machined parts. This is mainly due to anisotropic mechanical and thermal properties, and low thermal decomposition temperature range. In the case of drilling of Ti6Al4V alloy, low thermal conductivity, continuous chip morphology leading to poor evacuation, and the high tendency of burr formation pose a major challenge to the process. The research efforts reported in the available literature have focused on optimizing the drilling of CFRP and Ti-alloys separately. However, the industrial application requires the optimization of the single drilling process of CFRP/Ti stacked materials to achieve high productivity, low cost, and minimal error in assembly. Nevertheless, the optimum machining parameters of each material are conflicting and resulted in the rise of undesirable effects.

Vibration-assisted drilling (VAD) is an advanced machining process, where a harmonic motion in the axial direction is superimposed over the standard tool feed motion. This technique showed promising results that overcome the associated issues of the conventional drilling process. This enhancement was attributed to the controlled intermittent cutting status which enhances the chip evacuation and reduces the cutting temperatures.

This thesis contributes to optimization of process parameters in two VAD regimes (Low frequency/high amplitude and High frequency/low amplitude) of the widely used aerospace materials such as CFRP, Ti6Al4V, and CFRP/Ti6Al4V. The optimization criteria is based on delamination damage, microstructure, chip morphology, surface integrity, tool wear, and residual stress. In addition, this thesis contributes to understanding the effect of VAD kinematics on the uncut chip thickness, chip formation mechanism, and chip geometry in both regimes. The following conclusions can be drawn from this research:

**Low-frequency vibration assisted drilling (LF-VAD)**

1. The machining performance of LF-VAD showed a significant enhancement such as low entry and exit delamination, high geometrical accuracy, excellent surface

integrity, induced compressive stress, and long tool life. However, this process showed higher cutting forces as compared to conventional drilling 'CD' (260 % for Ti6Al4V, 120 % for CFRP) material). This increase was attributed to the effect of a relatively high modulation amplitude '$A_m$' compared to the machining feed '$f$' that increased the dynamic uncut chip thickness. Moreover, at constant modulation frequency '$W_f$' the '$A_m$' was found to have the most dominant effect on the axial tool velocity. Consequently, the axial force was increased at high '$A_m$' due to their effect on the cyclic impact load.

2. For constant '$W_f$' and '$f$', higher amplitude compared to low amplitude resulted in a positive effect on the duty cycle '$t_D$' (reduced by 45%) and cooling cycle '$t_C$' (increased by 47%). This effect resulted in up to 56 % reduction in the cutting tool temperature at the exit surface.
3. The high range of modulation amplitude ($A_m > f$) led to change the Ti6Al4V chip morphology from the typically continuous chips to be segmented. The chip radian was reduced by up to 63 % at higher '$A_m$'. This change in the chip morphology and geometry resulted in a significant enhancement in the chip evacuation efficiency and the cutting tool temperature.
4. The hypothesis that "thermo-plastic instability is the main cause of the saw-tooth chips" was investigated along the primary shear band at different '$f$' and '$A_m$'. Based on the observation of gross cracks 'GC' and more than 20 μm micro cracks 'MC' this hypothesis was rejected for LF-VAD, and consequently, the cyclic cracks theory was identified as the prevailing mechanism for saw-tooth formation.
5. For the same cutting speed '$N$' and feed '$f$', VAD could reduce the tensile residual stresses in CD or even reverse it to compressive residual stress in the case of high

‘$A_m$’ and low ‘N’. This was attributed to the low thermal load and effective chip evacuation. Consequently, a high fatigue life could be achieved with LF-VAD compared to the ‘CD’ that showed a high tensile residual stress with up to 12 μm surface cracks.

6. The cutting temperature and chip morphology have the most dominant effects on the entry and exit delamination factor ‘$\varphi_d$’. The results showed that both entry and exit delamination could be eliminated or reduced significantly below the allowable limit by using LF-VAD, while the ‘CD’ resulted in unacceptable delamination factor even with the back support of adhesive tape.
7. All the tested LF-VAD conditions improved the CFRP and Ti6Al4V geometrical accuracy and surface integrity, for the separate and stack drilling configurations. This enhancement was attributed to the low thermal load, change in chip morphology, which enhanced the chips evacuation.

**Conclusions from the High-frequency Vibration-assisted drilling study (HF-VAD)**

A new design of a HF-VAD system was presented in this research. The new design allows independent control of modulation frequency and amplitude within a wide range, The system was commissioned to stably operate at the same cutting speeds and feeds used for ‘LF-VAD’ and ‘CD’ to enable systematic analysis and benchmarking of the low and high VAD regimes compared to the CD. Such study has not been covered in the available literature. The following conclusions could be drawn the experimental investigation of HF-VAD:

8. The HF-VAD reduced the thrust force by up to 26% compared to the ‘CD’. This reduction was attributed to the effect of a relatively low ‘$A_m$’ ($A_m < f$) that resulted in reducing the dynamic uncut chip thickness.

9. For a constant frequency ‘F’, the cutting speed ‘*N*’ has the dominant effect on the cutting behavior and chip morphology based on the resultant ratio of the modulation frequency ‘$W_f$’.
10. The axial tool oscillation and low uncut chip thickness led to reducing the cutting energy and increasing the chip evacuation efficiency, which was translated to cutting tool temperature reduction by up to 37 %.
11. For all machining conditions, HF-VAD with 1500 Hz reduced the cutting energy (force and temperature) that was identified as the main causes of burr formation. Therefore, the burr height was reduced by up to 86 % compared to the ‘CD’.
12. All tested HF-VAD produced compressive residual stress, acceptable delamination, surface integrity, and geometrical accuracy.
13. For the same machining conditions, LF-VAD ($A_m > f$) showed a lower cutting temperature compared to ‘HF-VAD’ and ‘CD’. This reduction was attributed to the relatively high ‘$A_m$’ value that ensures a full tool-workpiece separation. Consequently, the proper selection of ‘$A_m$’ value has a direct positive impact on the ‘$t_C$’ and ‘$t_D$’ intervals, and the chip evacuation efficiency, that significantly reduced the cutting temperature.

**Conclusions from the Low-frequency Vibration-assisted drilling tool wear study (LF-VAD)**

Based on the wide range machining conditions investigation for LF-VAD, the optimum three modulation amplitudes and three combinations of machining conditions (speed and feed) were selected to study the effect of VAD on the tool wear and the associated hole accuracy. Modulation amplitude has shown the most dominant effect on the cutting forces, temperature, and flank wear land, over the 50 investigated holes. For the same ‘*N*’ and ‘*f*’, higher ‘$A_m$’ resulted in reducing the cutting temperature and flank wear land by 40 %, and 75 %, respectively. This was attributed to the low '$t_D$', high '$t_C$', and higher chip evacuation efficiency (small chip radian). On the other hand, the significant reduction in the thrust force was achieved at the low '$A_m$' due to the lower axial tool velocity. The LF-VAD showed a significant enhancement of the entry and exit delamination factor with low geometrical error compared to 'CD'.